Calibrating the Todd and Longstaff's Mixing Parameter Value for Miscible Finite Sized Slug WAG Injection for Application and Optimisation on a Field Scale

Zainab Imad Murtadha Al-Haboobi

BSc., MSc.

Submitted for the Degree of Doctor of Philosophy

Institute of Petroleum Engineering

School of Energy, Geoscience, Infrastructure and Society

Heriot-Watt University

March 2019

Abstract

Water alternating gas (WAG) injection is a method of controlling the viscous fingering impact in a miscible gas injection to improve the volumetric sweep efficiency and to improve the oil recovery.

Conventional reservoir simulation such as performed by a black oil simulator is too coarse to resolve the viscous fingering accurately at field scale. This is because the fingers are smaller than field scale grid blocks. Instead, empirical models are used to describe the fingers and to allow simulators to predict reliable recovery.

Todd and Longstaff (1972) model is the most commonly used among different black oil reservoir simulators to model the effects of viscous fingering on a field scale. The reason for that is it requires the selection of a single parameter, namely the mixing parameter, ω, the value of which includes all of the factors affecting fingering. Additionally, it incorporates a method to calculate the effective viscosity when mixing occurs between oil and gas phases. Todd and Longstaff (1972) recommended a choice for the ω value of ⅔ for secondary miscible gas injection to match the recovery of oil from Blackwell et al.'s (1959) experiments. They recommended ω = ⅓ for field scale simulation to account for heterogeneities.

Blunt and Christie (1993) showed that the mixing parameter needs to be calibrated for simultaneous water and gas (SWAG) injection. They calibrated the value of ω as a function of the fractional flow of water injected and showed that the value has to be increase to 1 when modelling secondary SWAG injection and to 0.92 when modelling tertiary SWAG injection, however their work did not take into account the effect of miscible finite-sized slug WAG (FSS WAG) injection.

The work in this thesis extends the work of Blunt and Christie (1993) to calibrate the value of ω taking into account the WAG ratio and slug size in miscible FSS WAG injection for both secondary and tertiary recovery. The value of ω is iteratively determined for a set of WAG ratios, slug sizes, and types of recovery.

In this Thesis, three important contributions have been made to simulate the viscous fingering impact in miscible FSS WAG injection and optimisation:

Firstly, the calibration of ω for a specific slug size and WAG ratio for both secondary and tertiary recovery for miscible FSS WAG injection using a 1D numerical model; the 1D model was checked for numerical diffusion. Then, the results of SWAG injection from the 1D model were validated against Blunt and Christie's analytical results for SWAG injection for both secondary and tertiary. Finally, the results of calibrating ω for the miscible FSS WAG injection have been compared for different viscosity ratios, number of grid blocks and variance to generate the permeability.

Secondly, the resultant values of calibrating the mixing parameter for miscible FSS WAG injection were used with a reservoir oil field using a black oil reservoir simulation. The application on a field scale was performed on two different models, a quarter five-spot model and the Watt field model, to show the reservoir performance when a specific value of ω, for a specific WAG ratio and slug size, was used for both secondary recovery. This was then compared to Todd and Longstaff's value of ⅔ and to the fully mixing value of 1. The impact of the calibrated value of ω on the WAG zone has been investigated on the quarter five-spot model. Finally, the impact of the calibrated value of ω on the oil recovery factor was investigated for both models.

Thirdly, the slug size and WAG ratio are optimised using the calibrated value of ω for both secondary and tertiary recovery to identify the impact of the calibrated value ω on the optimisation results. The results of the optimisation for the calibrated value of ω were compared with the results of the optimisation at a fixed value of $\omega = 1$. The process was extended to the optimisation of injection fluid type, so called WAG pattern injection, to further investigate the impact of the value of ω on the optimisation results. The results of the optimisation for the calibrated value of ω were compared with the results of the optimisation at a fixed value of $\omega = 1$. Furthermore, the impact of the calibrated value of ω on the optimisation results was extended to the optimisation of injection flow rate, which was added to the optimisation of WAG ratio, slug size and WAG pattern injection. The optimisation scenarios listed above were performed with the assumption of unlimited gas supply for injection. Finally, a limited gas supply scenario was examined to determine

the impact that this may have on the optimisation of WAG ratio, slug size, WAG pattern injection and the injection flow rate, using the calibrated value of ω.

Dedication

To my mom and to my husband,

You both mean the world to me

Acknowledgements

I would like to thank my Almighty Allah for his countless blessings.

I would like to acknowledge the Higher Committee for Education Development of Iraq (HCED-Iraq) for their financial support during my PhD.

I thank my academic advisor, Prof Mike Christie for giving me the opportunity of doing the PhD. He believed in my potential ability to do this research on my own with all of the obstacles I faced and his early retirement, which motivated me to do my best every day. I have learned so much since I started, and I am sure that I will continue to do so in the future.

My sincerest gratitude to Prof Sebastian Geiger for his involvement at the latest stage of my PhD.

I would like to thank my examiners Prof Eric Mackay and Prof Ann Muggeridge for making time to have my Viva on early date and to have an interesting Viva, I really enjoyed my Viva and discussing my research with you. Your feedback was very helpful.

I would like to thank the computer support team of the Institute of Petroleum Engineering for making any computer-related things smoother; the administration and finance teams are also thanked for your cooperative efforts.

I would like to thank my dearest and best friends, Prof Colin Jones, Prof Vasily Demyanov, Dr Karl Stephen, Dr Gillian Pickup, Dr Alexander Graham, Dr Ilya Fursov, Dr Junko Hutahaean, Nagoor Kani, Shing Chan, Hassan Alzayer, Bashir Alkhazmi and Muzammal Rammay. Although too many to mention by name you know who you are. You have all had an impact on me, some even positive! Your investment in me is partly responsible for this success. However, certain individuals were key to completing this research.

My sweetheart David, thank you for your endless patience, and continuous support.

My uncle Ayad, thank you for your continuous support and for teaching me valuable lessons to face life.

Finally, I would like to express my heartfelt gratitude to my Mother and Father — both of you have always set an example I would do well to emulate. Your prayer and wisdom that something good would finally come to me appear to be bearing fruit. Thanks for teaching me to do a good job for the first time, to appreciate the value of education and hard work, and especially for never giving up! I dedicate this thesis for both of you.

At the outset of my pursuit of this doctorate, it was clear to me that this attempt ought not to be purely academic in nature but should encompass the broad enrichment offered by this institution. During the past three and a half years, in the quest for this holistic experience, I took in many interesting courses, seminars, and also indulged in the pleasures of life such as traveling. With great satisfaction, I conclude that I have grown in so many respects through this journey - academically, professionally, and personally.

(This page intentionally left blank)

Table of Contents

List of Figures

List of Tables

Chapter 1

Introduction

1.1 Background and motivation

In miscible gas injection, a gas with lower viscosity is injected into the reservoir, mixing with the higher viscosity oil to produce a single-phase mixture with lower viscosity than the oil. The key advantages of miscible gas injection are that it significantly improves microscopic sweep efficiency, thus aiding recovery (Farzad, 2004, Booth, 2008). However, due to the high mobility ratio between the injected gas and the crude oil, the gas tends to finger through the oil and results in early gas breakthrough, this phenomenon is known as viscous fingering, also known as the Saffman–Taylor instability (Saffman and Taylor, 1958, Todd and Longstaff, 1972, Koval, 1963, Fayers et al., 1990, Blunt and Christie, 1993, Juanes and Blunt, 2006, Moortgat, 2016). As a result of viscous fingering, considerable quantities of gas are needed to displace the oil, making miscible gas displacement expensive and time consuming (Fayers et al., 1990, Blunt and Christie, 1993), and this is inevitably tied to the availability of injectable gas in many fields (Christensen et al., 2001, Hoffman, 2014, Muggeridge et al., 2014).

Injecting water in combination with gas is a technique known as water alternating gas (WAG) injection. This can reduce the mobility ratio at the displacement front, thereby reducing the effects of viscous fingering. WAG injection combines water injection with gas injection, whereby gas targets residual oil in previously water swept zones, as well as oil in un-swept zones, and water improves sweep efficiency and provides better mobility control of the oil displacement to stabilise the front. There are two types of WAG injection, simultaneous injection (where water and gas are injected at the same time and known as SWAG) or as finite sized slugs (where water and gas are injected in slugs alternating each other and known as finite sized slug WAG (FSS WAG)). Stalkup (1983a) suggested the use of matched velocity (MV) flooding, where gas and water travel at the same speed, to determine the optimum water alternating gas (WAG) ratio. MV decreases the apparent mobility contrast between gas and oil, which helps to minimise viscous fingering.

In the last several decades, WAG injection or miscible WAG injection schemes were the most widely used techniques to enhance oil recovery on the field scale because they lower

the oil saturation below residual oil saturation to water flooding. Examples of WAG injection on a field scale are Prudhoe Bay, Snorre, Brae South, Magnus, Rangely and Statfjord (Brodie et al., 2012, Zhang et al., 2013, Jhaveri et al., 2014, Kang et al., 2016). Originally, WAG injection was applied as a tertiary recovery method, however in more recent applications in the North Sea, this has been initiated early in the field life (Christensen et al., 2001, Awan et al., 2008, Alvarado and Manrique, 2010, Shpak, 2013, Mohagheghian, 2016). In field-scale applications, other considerations can become important – for example choosing the WAG ratio based on the availability of the gas for injection (Zahoor et al., 2011, Morais, 2012) or to allow a more efficient use of the available gas (Wilson, 2015). Therefore, it is important that the effects of viscous fingering are considered in any reservoir simulations.

Black oil reservoir simulation is commonly used in the oil industry. The objective of a reservoir study is primarily to predict the reservoir performance and to increase the oil recovery. Therefore, it is important to have a correct prediction of the oil recovery when planning miscible FSS WAG injection based on simulation models, before applying it on a field scale for field development because of the great expense and time taken to yield results (Aziz and Settari, 1979). To plan miscible WAG floods or the field-scale using a reservoir simulator, empirical models are needed to show the significances of viscous fingering within the grid blocks in a macroscopic sense (Fayers et al., 1990).

In reservoir simulation, the Todd and Longstaff model is a common approach to model (capture) the effects of viscous fingering (Todd and Longstaff, 1972, Batycky, 1997, Karacaer, 2007). This model requires the selection of one key parameter, the mixing parameter, ω. Todd and Longstaff (1972) recommended the value of ω between ⅓ and ⅔ for simulating full scale secondary miscible gas injection.

Blunt and Christie (1993) extended Todd and Longstaff's model to predict solvent fingering in oil for two -phase, three-component flow. The results were tested on a variety of injected water saturations in both secondary and tertiary displacements. They showed that the value of ω should be increased to 1 when modelling simultaneous water and gas (SWAG) injection for secondary recovery and to 0.92 for tertiary SWAG injection. However, their work was limited to simultaneous WAG injection.

There is a wide variation between the values of ω suggested by Todd and Longstaff, and Blunt and Christie. Using a value of $\omega = 1$ as suggested by Blunt and Christie (which represents a full mixing), in a reservoir simulator to plan finite slug size WAG injection for field development can lead to the oil recovery prediction being much higher than what the actual reservoir may be capable of producing. This could lead to uneconomical development of the field in question. On the other hand, if the value of $\omega = ⅔$, as suggested by Todd and Longstaff were to be used, the oil recovery may appear much lower than what the reservoir could actually produce. Leading to non-development of a reservoir, which may have great potential for oil recovery, missing opportunity and profits. The question of which value of ω should be used for finite-sized slug WAG injection for field-scale development is still open, and this gap can be filled by defining the values of the mixing parameter for finite-sized slug WAG injection by extending Blunt and Christie's approach.

1.2 Research focus

In this thesis, the research focuses on learning how to calibrate the Todd and Longstaff's mixing parameter, ω, with appropriate values for use in miscible finite-sized slug WAG injection in a reservoir simulator, at different WAG ratios, different slug sizes and with different types of recovery. Then, a workflow will be put forward to calculate the appropriate ω for any WAG setup, which can then be used in field-scale reservoir simulation models to capture the effects of viscous fingering. Then, the values of ω will be interpolated for a wide range of WAG ratio and slug size to be used in the optimisation of miscible FSS WAG injection. Finally, those values will be used in the optimisation software to optimise the WAG ratio and slug size, type of fluid to inject in each well and finally the flow rate to inject.

1.3 Research questions

The research questions, driven by several identified challenges mentioned above, are as follows:

1. How does the calibration of the mixing parameter, ω, change from the values suggested by Todd and Longstaff, and Blunt and Christie when the effect of slug

size, WAG ratio and type of recovery are taken into account for miscible FSS WAG injection?

2. How do the viscosity ratio, heterogeneity and number of grid blocks influence the calibration of ω in miscible FSS WAG injection?
3. When applying miscible FSS WAG injection on a field scale, how does the reservoir behave at calibrated values of ω in comparison to a full mixing value at $\omega = 1$ and to Todd and Longstaff's value $\omega = ⅔$? Also, how does the calibrated values of ω impact the WAG zone?
4. When optimising the slug size and WAG ratio at fixed injection rate, how does the value of ω at specific WAG ratio, slug size and type of recovery influence the optimisation results of the miscible finite-sized slug WAG injection when optimising WAG ratio and slug size using an optimisation software in comparison to a fixed $\omega = 1$?
5. If the optimisation of WAG ratio and slug size were extended to optimise the type of injection fluid (known as WAG pattern injection), how would the value of ω influence the optimisation results in comparison to a fixed ω of 1?
6. If point 5 was extended to include the optimisation of the injection rate, how would the value of ω influence the optimisation results?
7. The optimisations detailed above assume unlimited gas supply, therefore what if the gas supply was finite? The results from stage 6, with unlimited gas supply will be compared against a finite-gas to inject scenario.

1.4 Research contribution

In this thesis, three important contributions have been made to simulating the miscible finite-sized slug WAG injection and optimisation, as illustrated in Figure 1.1.

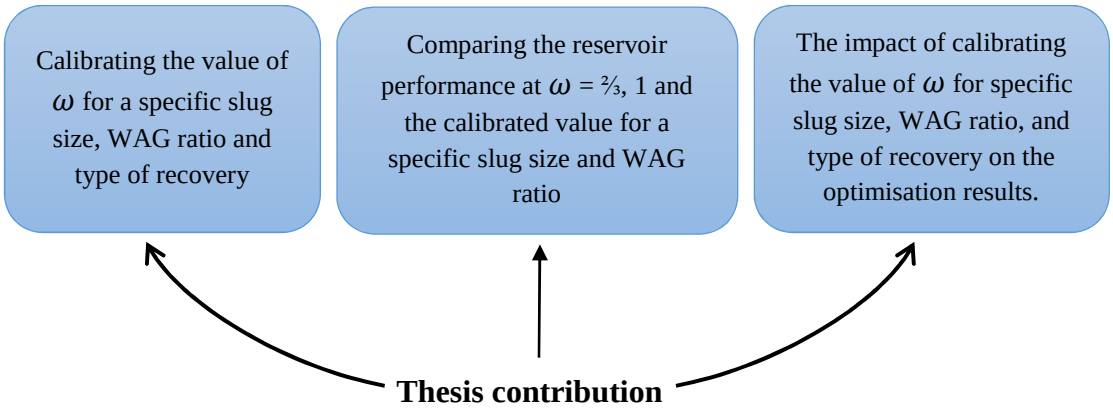

Figure 1.1 Thesis contribution to the identified challenges related to the reservoir model simulation

Each step of the diagram blocks shown in Figure 1.1. can be described as follows:

First, the value of ω is calibrated for a specific slug size and WAG ratio for both secondary and tertiary recovery for miscible FSS WAG injection using a 1D numerical model. Following this, the results of SWAG injection from the 1D model are validated against Blunt and Christie's analytical results for SWAG injection for both secondary and tertiary recovery. Finally, the results of calibrating ω for the miscible FSS WAG injection are compared for different viscosity ratios, number of grid blocks and variance to generate the permeability

Second, the resultant values of calibrating the mixing parameter for miscible FSS WAG injection were used with a reservoir oil field using a black oil reservoir simulation. The application on a field scale was performed on two different models, a quarter five-spot model and the Watt field model, to show the reservoir performance when a specific value of ω, for a specific WAG ratio and slug size, was used for both secondary recovery. This was then compared to Todd and Longstaff's value of ⅔ and to the fully mixing value of 1. The impact of the calibrated value of ω on the WAG zone has been investigated on the quarter five-spot model. Finally, the impact of the calibrated value of ω on the oil recovery factor has been investigated for both models.

Third, the optimisation of the slug size and WAG ratio using the calibrated value of ω for both secondary and tertiary recovery were used to identify the impact of the calibrated value ω on the optimisation results. The results of the optimisation for the calibrated value of ω will be compared with the results of the optimisation at a fixed value of ω=1. The

optimisation is extended to the optimisation for the type of fluid injected, so called WAG pattern injection to further investigate the impact of the value of ω on the optimisation results. Furthermore, the impact of the calibrated value of ω on the optimisation results is extended to the optimisation for the amount of flow rate injected which is added to the optimisation of WAG ratio, slug size and WAG pattern injection. The optimisation scenarios listed are performed with the assumption that there is unlimited supply of gas to inject. Finally, we investigate the impact of the calibrated value of ω on the optimisation results by adding the assumption that there is limited amount of gas to inject for the optimisation of WAG ratio, slug size, WAG pattern injection and the amount of flow rate to inject.

1.5 Thesis structure

Chapter 2 provides the theory of miscible gas injection, and how to overcome associated viscous fingering with the use of the water alternating gas (WAG) injection. Then, the factors affecting the WAG injection are addressed, followed by an introduction to the types of reservoir simulator available, with further details on the simulator that was used to simulate the miscible WAG injection in this research. Finally, the Chapter discusses the background of optimisation and some examples of the work done on optimising WAG injection using Particle Swarm Optimisation (PSO).

Chapter 3 reviews the literature on the viscous fingering experiment conducted by Blackwell et al. (1959) and the empirical models that have been developed based on this experiment to predict the viscous fingering in miscible displacement and to calibrate the mixing parameter, ω. Those models are the Peaceman and Rachford (1962) model, the Koval (1963) model, the Todd and Longstaff (1972) model, the 2D numerical simulation of viscous fingering conducted by Christie and Bond (1987) and the Analytical Calibration model by Blunt and Christie (1993).

Chapter 4 covers the 1D model for calibration of ω (including the assumptions made and the mathematical formulation), the workflow of calibrating ω against the 2D simulator (mentioned in Chapter 3), and finally discusses the results. The results cover the impact of the aspect ratio on the numerical modelling and the validation of the model by comparison of the results from the numerical model against the analytical results for both

secondary and tertiary recovery. The calibration of ω for finite-sized slug WAG injection for secondary and tertiary recovery are then presented, considering the effect of different viscosity ratio, different grid block size, and different variance to trigger the viscous fingering.

Chapter 5 covers the implementation of the calibrated value of ω for a specific slug size and WAG ratio in black oil model to check the effect on the oil recovery in comparison to Todd and Longstaff's value and Blunt and Christie's value. The chapter starts by presenting the two models under study, the fluid properties used in both models and the grid refinement study conducted on both models. Then, it provides the assumptions of applying the calibrated value of ω on a field scale. Finally, it shows the results and the impact of the calibrated value of ω on the WAG zone and the oil recovery factor.

Chapter 6 covers the interpolation of the calibrated values of ω for a wide range of slug size and WAG ratio using a python code (a program language), to enable the generation of ω value automatically for a specific slug size and WAG ratio inside the optimisation software. Then, it introduces the objective functions that are been used in the optimisation problem and the reason for selecting them. Finally, it concludes with the workflow and the results of the optimisation scenarios.

Chapter 2

Theoretical background of miscible displacement and the optimisation of WAG injection

2.1 Introduction

Crude oil is found trapped in porous geologic media (known as a petroleum reservoir rocks) up to several kilometres below the surface. This porous medium is a matrix containing pores that are interconnected and typically filled with fluids (liquid or gas), with at least several continuum paths from one side of the medium to the other over the entire porous medium domain (Bear, 1972). The fluid motion in porous media is governed by the laws of conservation (mass, momentum and energy) (Bear, 1972).

The law of mass conservation states that the inflows, outflows and change in storage of mass in a system must be in balance (when the mass is neither created nor destroyed, then the amount of mass remains constant). The mass of a fluid should be conserved when it is in motion. If the density is constant, the mass conservation equation gives a way to determine the velocity of fluid flow in a tube. If one can determine the velocity at some known area, the equation yields the velocity for any other area. For example, if there were two areas (a and b) and the area of "b" was half the area of "a", then the velocity of the fluid in "b" must be twice the velocity of the fluid in "a".

The differential form of the mass conservation equation for a single phase flow in porous media is expressed by the following equation (Nield and Bejan, 2006):

$$\frac{\partial(\varphi\rho)}{\partial t} = -\frac{\partial v}{\partial x} \tag{2.1}$$

where, φ is the porosity, which is a measure of the proportion of void space in rocks to the bulk volume of the rock, ρ is the fluid density and is a measure of the fluid mass per unit volume, t is the time, v is the fluid flux in in the x-direction and is defined as the mass rate of fluid flow (oil or water) per unit cross sectional area per unit time.

In a reservoir simulation, reservoir performance predictions are made based on the momentum equation and Darcy's equation (or Darcy's Law). Darcy was a French scientist who investigated the water flow through filter beds in 1856 (Dake, 1983, Heinemann, 2005). Darcy's equation is an empirical correlation for single-phase flow and became the basis for describing fluid flow through porous media. The volumetric flow

rate, Q, of a single fluid flowing through a porous medium can be predicted based on Darcy's equation:

$$Q = \frac{KA}{\mu}\frac{\Delta P}{L} \tag{2.2}$$

where Q is the volumetric flow rate of a fluid through porous media, A is the cross-sectional area of the porous media, K is the absolute permeability of the porous media. μ is the viscosity of the fluid, and ΔP is the pressure gradient in the L direction. Darcy's law is a 1D description of single-phase flow in a horizontal system. For the purposes of simulation, a more useful version of Darcy's equation is by the partial differential form for u, which indicates a linear relationship between the fluid velocity relative to the solid and the pressure head gradient, and an inverse proportionality to the viscosity of the fluid (Ahmed, 2006). It is given by the equation:

$$u = \frac{Q}{A} = -\frac{K}{\mu}\frac{\partial P}{\partial x} \tag{2.3}$$

where u is the Darcy velocity. The negative sign is added to the equation because the pressure gradient is negative in the direction of flow.

Petroleum reservoirs usually contain water, gas and oil. The interactions of the multiple phases must be taken into account in the flow equations. Fluids can be miscible (fluids mix perfectly together to form a solution), as in the case of oil and its solution gas, and the interactions of miscible fluids affect the fluid viscosity. Otherwise, fluids are immiscible (fluids do not mix) such as oil and water and the interaction of immiscible fluids is modelled using relative permeability ($k_{r\alpha}$) curves.

Darcy's law has been modified to take the effect of the multiphase flows in the porous media (Dake, 1983, Heinemann, 2005). It has been suitable in reservoir engineering to modify Darcy's law to describe the flows of two-phases and multiple phases by including the effect of the relative permeability as following:

$$u_\alpha = -K\frac{k_{r\alpha}}{\mu_\alpha}\frac{\partial P}{\partial x} \tag{2.4}$$

where, $k_{r\alpha}$ is the relative permeability of a phase ($\alpha = o, w \; and \; g$) that accounts for the reduced permeability of each phase due to the presence of the other phases. Relative permeability curves model the reduction in permeability due to the presence of another fluid, which is summarised in a curve of fractional values between 0 and 1, where 1 equals 100% flow of that phase, plotted against water saturation (S_w). Curves for each phase are used to calculate an effective permeability, (k_e) where $k_e = K\, k_{r\alpha}$.

Fluid saturation (S) is a fractional value representing the relative proportion of either water, gas or oil in the pore space for a given grid cell. For a single phase, the saturation is equal to 1. For multiphase flow in porous media, the sum of all the fluid saturations is equal to 1 i.e. $S_w + S_g + S_o = 1$.

Relative permeability is measured experimentally for 2 phases, but the relative permeability for 3 phase flow can be predicted by an interpolation methods between the oil–water and gas–oil–connate water saturation paths such as Stone (1973).

Based on the concept of relative permeability, Buckley and Leverett (1941) presented a theory for oil displacement by water or gas. The theory was developed for one dimensional flow (where both oil and the displacing phase flow simultaneously through the same porous section), in a linear system for immiscible, and incompressible fluids neglecting gravity, capillarity and liquid compressibility. Fractional flow is used to estimate the advance front of a fluid in the displacement process (Bear, 1972), where:

$$f_w = \frac{\lambda_w}{(\lambda_o + \lambda_w)} \tag{2.5}$$

f_w is the fractional-flow function that measures the water fraction of the total flow. λ_w, λ_o are the water and oil mobility ratio respectively, $\lambda_w = k_{rw}/\mu_w$ and $\lambda_o = k_{ro}/\mu_o$

In the context of oil recovery, the above equations that describe fluid flow through porous media are fundamental to understand production, inter-fluid interactions and resultant recovery. For real-world applications, a petroleum reservoir is initially developed and produced by using natural reservoir energy, known as primary recovery, to push the fluids from the reservoir to the wellbore. This primary recovery includes dissolved gas

expansion, gravity, change in rock volume, and aquifer influx. The primary oil recovery of the original oil in place (OOIP) has been shown to range between 5 and 20% (Verma, 2015). Field operators usually use so-called secondary recovery methods, which help to ensure higher production rates and extend the reservoir's productive life. These methods include injecting gas at the top of the reservoir or into the gas cap, and injecting water below the oil water contact. Generally, the potential for oil recovery ranges between 20 and 40% of OOIP at the end of the primary and secondary recovery processes (Sandrea and Sandrea, 2007, Verma, 2015).

The factors affecting the recovery factor (FOE) from water injection and gas injection are (Muggeridge et al., 2014):

1. The macroscopic sweep efficiency E_S which represents the proportion of the connected reservoir volume that is swept by the injected fluid(s). E_S is affected by gravitational segregation of the fluids and by geological heterogeneity in the reservoir which controls the spatial distribution of porosity and permeability.
2. The microscopic displacement efficiency E_{PS} which describes the fraction of oil displaced from the pores by the injected fluid. The typical E_{PS} from a water flood is 70% or less due to the capillary effects that traps oil in the pore space. Also, the relative mobility of the oil and water, when moving through the pore space, is controlled by the relative permeability features of the rock, which affect E_{PS}.
3. The connected volume factor E_D which represents the proportion of the total reservoir volume connected to wells. This represents the fact that sealing faults or other low-permeability barriers may result in sections of oil that are not in pressure communication with the rest of the reservoir.
4. The economic efficiency factor E_C which represents the commercial and physical constraints on field life such as life of facilities, capacity to deal with produced water and gas, reservoir energy (the fluids cannot be produced at low reservoir pressure).

Those factors can be explained using the following approximate relationship (Muggeridge et al., 2014):

$$FOE = E_{PS}.E_S.E_D.E_C \tag{2.6}$$

According to this relationship, the overall FOE would be 41% if each of the efficiency factors equalled 80%. Increasing the FOE requires that each of these factors is increased to close to 100% (Muggeridge et al., 2014).

At the end of secondary recovery, a considerable amount of residual oil remains in the reservoir, which can be accessed through enhanced oil recovery (EOR) (Lake, 1989).

EOR is an umbrella term used to describe a suite of techniques used to extend the productive life of depleted oil field by targeting the immobile oil to enhance oil displacement and restore formation pressure (Lake, 1989, Thomas, 2008). The term EOR is sometimes used interchangeably with the term Improved Oil Recovery (IOR). However, this is not the case. IOR applies to the range of improvement techniques used to achieve better oil recovery through improved engineering design and project management, for example, using seismic surveying to identify volumes of oil that have been bypassed during water flooding and drilling new wells to access those oil pockets (Muggeridge et al., 2014). EOR methods aim at increasing the macroscopic and microscopic efficiency. IOR methods are targeted at increasing connected volume factor and to some extent the macroscopic sweep efficiency. Improving the economic efficiency factor is mainly the role of the production and facilities engineers but is also affected by EOR methods if these reduce the amount of water and gas produced alongside the oil, enabling oil to be produced for longer before economic limits are reached (Muggeridge et al., 2014).

EOR is divided into four categories: (a) thermal, (b) chemical, (c) gas injection, and (d) other. The most important method of enhanced oil recovery, and which forms the basis for this thesis, is miscible gas injection.

This chapter provides the theory of miscible gas injection and discusses how to overcome the associated issue of viscous fingering with the use of the water alternating gas (WAG) injection method, as well as addressing other factors that affect the WAG injection. Following on from that, the types of reservoir simulator will be introduced alongside specific details of the simulator used to simulate the miscible WAG injection in this

research. Finally, the chapter discusses the background of optimisation and some examples of the work done on optimising WAG injection using Particle Swarm Optimisation (PSO).

2.2 Miscible gas injection

In miscible gas injection, a lower viscosity gas (solvent) is injected into the reservoir, mixing with the higher viscosity oil to produce a single-phase mixture with lower viscosity than the oil. The key advantage of miscible gas injection is that it significantly improves microscopic sweep efficiency. It improves the oil displacement because it reduces the interfacial tension (which arises from the imbalance of molecular forces at the interface between two phases) between the displacing and the displaced fluids. These fluids may now more freely displace each other within the porous medium (Stalkup, 1983b) and additionally the pressure drop around the gas injectors is reduced, thus aiding recovery (Farzad, 2004, Booth, 2008).

In the context of miscible gas injection, short-chain hydrocarbons can be used as solvents and have been used since the earliest miscible displacement processes for enhancing oil recovery. In the early days of miscible gas injection, the solvent was injected in small slugs (intermittent volumes of injected chemical) and due to the high solvent cost, it was sometimes used in small amount to form a 'pad' (a mixture with the oil) (Figure 2.1) between water and oil in a secondary oil recovery process. Later in the 1970s, due to the rise in oil price, the interest in using solvents for enhance the oil recovery increased (Lake, 1989, Booth, 2008).

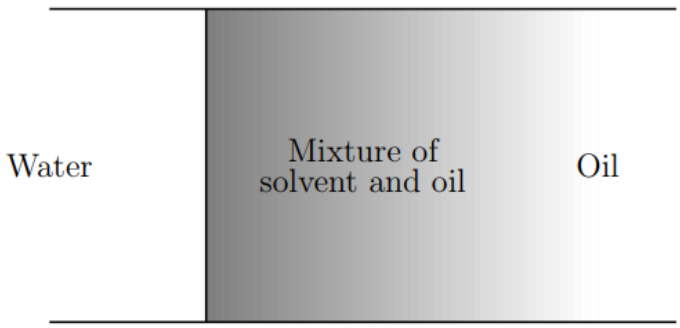

Figure 2.1 A pad of solvent between the water and oil.

Mixing of oil and gas during miscible displacements is driven by two mechanisms: diffusion and dispersion. Diffusion is the movement of molecules from a region of high concentration to a region of low concentration when two miscible fluids are in contact with each other without the presence of any porous media (Cunningham and Williams, 1980). When a porous medium is present, the solid matrix acts as a separator between streamlines of fluids and therefore is a barrier to the diffusion process. Dispersion, when two miscible fluids are in contact, is the spreading of the mass from highly concentrated areas to less concentrated areas. As the displacement progresses, the two fluids will mix due to the physical characteristics of the porous media, the fluids and the interaction with the velocity field. A transition (mixing) zone will form at the boundary between the two fluids as the front propagates. Dispersion can be differentiated from diffusion in that it is caused by non-ideal flow patterns and is a macroscopic phenomenon, whereas diffusion is caused by random molecular motions and is a microscopic phenomenon.

The partial differential form of the convection-diffusion equation was derived for homogeneous continuum conditions is given by the equation (Bear, 1972):

$$\frac{\partial c}{\partial t} = \nabla . D_h \nabla \mathrm{c} - v . \nabla \mathrm{c} \tag{2.7}$$

Here $c = c(x, t)$ is the concentration as function of space and time, v is the velocity vector. Diffusion processes show up in the first term, the second term accounts for advection of a concentration gradient. D_h is called the hydrodynamic dispersion.

There are two types of miscible gas injecting, first-contact miscible (FCM) gas and multi-contact miscible (MCM) gas. FCM describes the situation when the injection fluid mixes directly with the oil in the reservoir, in any proportion, to produce a single-phase mixture. Examples of FCM solvents are low molecular weight hydrocarbons such as methane, propane, butane, or mixtures of liquefiable petroleum gas (LPG) or heavier molecular weight hydrocarbons such as gasoline fractions (Holm, 1987, Booth, 2008).

Some injection fluids achieve miscibility by *in-situ* mass transfer of components through multiple contact between the injected solvent and the reservoir fluids and this is known

as MCM or dynamic miscibility (Stalkup, 1983a). MCM displacements require a transfer of hydrocarbon components between the injected and the reservoir fluid.

There are two types of MCM displacement, vaporizing gas drive and condensing gas drive. Vaporizing gas drives arise from injecting relatively lean gas and are therefore known as "lean" gas drives (Dumore et al., 1984, Holm, 1987). The lean gas vaporizes methane through LPG (liquefied petroleum gas) components from the reservoir oil as it travels through the reservoir, it becomes miscible with the reservoir oil when the front of the displacing gas has vaporized sufficient hydrocarbons.

Condensing gas drives arise from injecting relatively rich gas (containing hydrocarbons heavier than methane) and are therefore known as "rich" or "enriched" gas drives (Dumore et al., 1984, Holm, 1987). The gas phase composition becomes progressively leaner on contact with the reservoir oil and it gives up heavier components (as they "condense") to the oil as it travels through the reservoir. The oil becomes miscible when it becomes sufficiently enriched by the freshly injected enriched gas.

2.2.1 Disadvantages of miscible gas injection

As with any technique, miscible gas injection has disadvantages. The first disadvantage is that the availability of the gas may be limited in a field; this could be because there is no close source for the injected gas. While hydrocarbon gases in most oil fields are a by-product of production, their market value can prevent their use for injection to enhance oil recovery (Christensen et al., 2001, Hoffman, 2014, Muggeridge et al., 2014). As an example, CO_2 injection was used in the B. Kozluca field because of the availability of the CO_2 reservoir in Camurlu Field located about 10 km away (Cobanoglu, 2001). Another case, in the Ekofisk field (Jensen et al., 2000), CO_2 was removed from their consideration for WAG injection until the CO_2 price fell below $1.50/MCF at the wellhead.

The second disadvantage is the high mobility ratio between the injected gas and the crude oil. The gas tends to finger through the oil and results in early gas breakthrough, which reduces the sweep efficiency and increases gas control costs (Dutra et al., 2007, Stalkup, 1983a). This phenomenon is known as Saffman-Taylor instability (Figure 2.2) or viscous fingering (Saffman and Taylor, 1958, Blackwell et al., 1959, Perkins et al., 1965, Todd

and Longstaff, 1972, Stalkup, 1983a, Homsy, 1987, Christie and Bond, 1987, Fayers and Newley, 1988, Fayers et al., 1990, Blunt and Christie, 1993). Due to this effect, considerable quantities of gas are needed to displace the oil, making miscible gas injection expensive and time consuming (Fayers et al., 1990, Blunt and Christie, 1993).

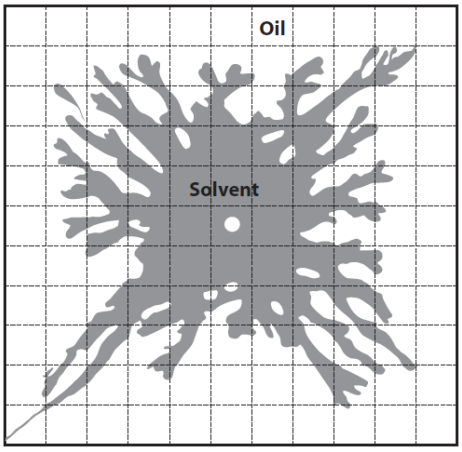

Figure 2.2 Viscous fingering due to solvent injection in a Hele-Shaw cell. Adopted from (Carlson, 2006)

2.3 Water Alternating Gas (WAG) injection

Injecting water in combination with gas is a technique that can reduce the mobility ratio at the displacement front, thereby reducing the effects of viscous fingering. This technique is known as Water Alternating Gas (WAG) injection. As the name suggests, this technique is a combination of two traditional methods, gas injection and water injection. The gas injection is used for contacting unswept zones to improve the microscopic displacement efficiency. The water injection is used to improve the macroscopic sweep efficiency and the mobility control of the displacement and for stabilising the front of the gas injection.

WAG injection is classified into different types such as miscible WAG injection which has been applied in Snorre, Brae South, and Magnus fields in the North Sea (Christensen et al., 2001, Awan et al., 2008, Mohagheghian, 2016), immiscible WAG injection, applied in Thistle field (Christensen et al., 2001, Awan et al., 2008) and SWAG injection which has been applied in Kuparuk River field in Alaska (Awan et al., 2008).

Miscible WAG injection can be either finite-sized slug WAG (FSS WAG) injection, which is the injection of a slug of water alternating with a slug of gas moving in sequence along the same route through the reservoir from injection well to production well. Or it can be simultaneous water and gas (SWAG), in which both water and gas are injected at the same time through a single injection well in the whole thickness of the reservoir, or part of it (Morais, 2012, Foroozanfar and Aminshahidy, 2013). Although both techniques can be used in field practice, miscible slug WAG injection is more widely used compared to SWAG injection because alternative miscible slug WAG injection is more convenient operationally than SWAG injection. Primarily this relates to the additional capital expenditure required to retrofit apparatus for SWAG injection, water and gas can segregate in the wellbore when injected simultaneously, and the injectivity of each fluid remaining higher when injected separately.

To achieve miscibility on the field scale between the injection gas and the reservoir oil, the miscible WAG injection is applied by injecting gas above minimum miscibility pressure (is the lowest pressure for which a gas can develop miscibility through a multi-contact process with a given reservoir oil at reservoir temperature) (Juanes and Lie, 2005). Miscible gas projects are required to bring the reservoir pressure above the minimum miscibility pressure of the fluids, though in cases of real field operation, it is difficult to maintain the reservoir pressure above minimum miscibility pressure (Christensen et al., 2001). If sufficient pressure is not maintained, miscibility will be lost, and the injection will fluctuate between miscible and immiscible gas injection during the life of oil production.

Immiscible WAG injection is the injection of gas that is not miscible with the reservoir oil and is implemented when the reservoir pressure is below the minimum miscibility pressure. This type of injection displaces the oil while maintaining its gaseous phase, with a front between the two phases (Zahoor, 2011; Fanchi, 2004).

2.4 Factors affecting WAG injecting performance

There are some factors that affect the design of WAG injection, such as three phase relative permeability effects, composition and availability of the gas, mobility and

mobility ratio, heterogeneity of permeability, injection pattern and injection parameters (Christensen et al., 2001, Zahoor et al., 2011).

2.4.1 Three phase relative permeability effects

Three phase relative permeability occurs when three different phases exist in the reservoir at the same time, and it is frequently experienced in WAG injection, an example is shown in Figure 2.3 (Shahverdi, 2012). WAG injection into an oil reservoir (with or without a gas cap) will initiate the three-phase flow and the system could experience three phase relative permeability. In two-phase flow, the saturation of one phase may either increase or decrease. The wetting phase occupies the smaller pore while the non-wetting phase occupies the larger pores with the capillary pressure controlling this mix. For three-phase flow, one of the phases becomes an intermediate wetting phase and its location in the porous medium is determined by the capillary pressure (Shahverdi, 2012). In this case, the relative permeability of three phase flow in porous media is dependent on the saturation of each phase at that position.

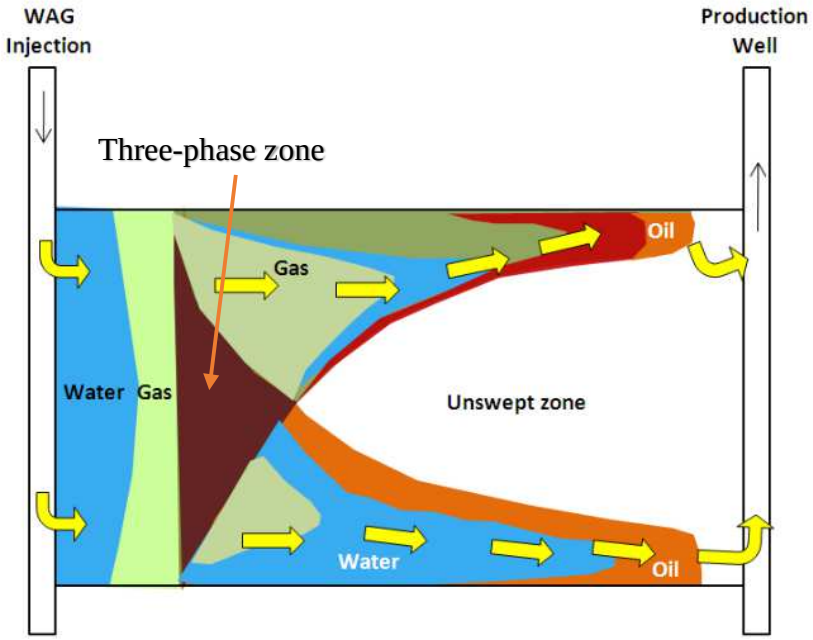

Figure 2.3 Three phase flow in WAG injection adopted from (Shahverdi, 2012)

Since, oil relative permeability is a function of all three fluid saturations, the oil, gas and water relative permeabilities from the two-phase relative permeabilities are used to

determine oil relative permeability in three-phase region. Two models have been proposed by Stone to determine the three-phase relative permeability.

In the first model, Stone defines normalised saturation as (Stone, 1970, Aziz and Settari, 1979):

$$S_o^* = \frac{S_o - S_{or}}{1 - S_{wc} - S_{or}} \qquad S_o \geq S_{or} \tag{2.8}$$

$$S_w^* = \frac{S_w - S_{wc}}{1 - S_{wc} - S_{or}} \qquad S_w \geq S_{wc} \tag{2.9}$$

$$S_g^* = \frac{S_g}{1 - S_{wc} - S_{or}} \tag{2.10}$$

where, S_o, S_w and S_g are oil, water and gas saturations, respectively. S_{wc} is the connate water saturation. S_{or} is the oil residual saturation. The oil relative permeability k_{ro} in a three-phase zone is assumed to be (Aziz and Settari, 1979):

$$k_{ro} = S_o^* \beta_w \beta_g \tag{2.11}$$

The multipliers β_w and β_g are determined from the condition that equation (2.11) reduces to two-phase data for the two cases of $S_g = S_g^* = 0$ and $S_w = S_{wc}$ (Aziz and Settari, 1979). Therefore, the multipliers β_w and β_g given by:

$$\beta_w = \frac{k_{row}(S_w)}{1 - S_w^*} \qquad \beta_g = \frac{k_{rog}(S_g)}{1 - S_g^*} \tag{2.12}$$

The second model (Stone, 1973) is modified for the mixed-wet rocks and does not require specification of S_{or} and it is able to predict it. This model is given by:

$$k_{ro} = k_{ro(cw)} \left(\left(\frac{k_{ro(w)}}{k_{ro(cw)}} + k_{rw(o)} \right) \left(\frac{k_{ro(g)}}{k_{ro(cw)}} + k_{rg(o)} \right) \right) \tag{2.13}$$

where, $k_{ro}$is the oil relative permeability on the three-phase region. $k_{ro(w)}$ is the oil relative permeability in the oil-water phase. $k_{rw(o)}$is the water relative permeability in the oil-water phase. $k_{ro(cw)}$is the oil relative permeability at connate water saturation. $k_{ro(g)}$ is the oil relative permeability in the oil-gas phase. $k_{rg(o)}$is the gas relative permeability in the oil-gas phase.

2.4.2 Composition and availability of the gas

Gas composition is an important parameter in the WAG design because it determines whether the process will be miscible or immiscible, and whether the process will be first contact miscible or multi-contact miscible under the main reservoir conditions of pressure and temperature (Zahoor et al., 2011).

The availability of the injection gas (in terms of quantity) greatly affects the economic feasibility of the choice in the WAG process design. Typically, the gas produced with the oil is separated from the oil and re-injected into the reservoir during WAG injection, therefore reducing costs (Zahoor et al., 2011).

2.4.3 Mobility and mobility ratio

Fluid mobility is defined as the effective permeability of the fluid divided by the viscosity of the fluid (Tarek, 2001). The mobility ratio is defined as the mobility of the displacing phase (injecting fluids) divided by the mobility of the displaced phase(oil) (Thomas, 2008, Romero-Zerón, 2012, Johns and Dindoruk, 2013).

$$M = \lambda_{inj}/\lambda_o \tag{2.14}$$

where, λ_{inj} is the mobility of the displacing fluid (k_{inj}/μ_{inj}), and λ_o is the mobility of the displaced fluid, i.e. oil (k_o/μ_o).

Mobility ratios are considered either "favourable" or "unfavourable." A favourable mobility ratio is less than one (≤ 1), which means that the displacing phase has a lower mobility than the displaced phase (oil). In practical terms, a favourable mobility ratio means that the displaced oil phase can move more quickly through the reservoir rock than the displacing phase. An unfavourable mobility ratio has the opposite effect where the displacing phase is moving more quickly through the reservoir rock than the displaced oil which may lead to viscous fingering.

Viscous fingering can be visualised with a simple illustration, such as that shown in Figure 2.4 (Stalkup, 1983a). In this figure, the gas is injected into a porous medium initially saturated with oil. The mobility ratio is just the ratio of oil and gas viscosities and

in the absence of heterogeneity, the front should remain a plane surface during the displacement. If part of the front comes across a more permeable region than the surrounding region, it will travel faster than the rest of the front causing a small bump to protrude a distance, ε, from the plane front.

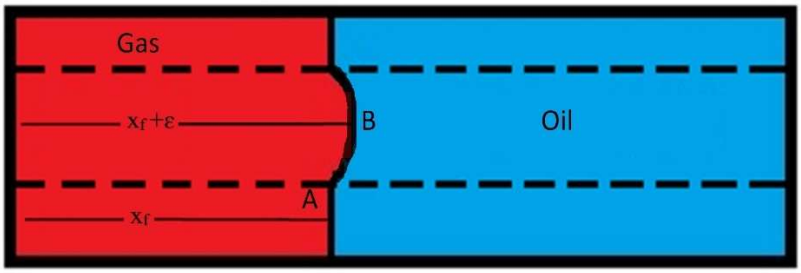

Figure 2.4 Simplified model of frontal instability. After (Stalkup, 1983a)

Let x_f be the distance from the inflow end to the undisturbed front A. The distance to the front of the bump B is $x_f + \varepsilon$. From Darcy's equation for linear flow, the velocity of the undisturbed front is (Stalkup, 1983a):

$$\frac{dx_f}{dt} = \frac{K\Delta P}{\varphi\mu_s[ML + (1-M)x_f]} \tag{2.15}$$

where $M = \mu_o/\mu_s$. The velocity of the leading edge of the perturbation is given by (Stalkup, 1983a):

$$\frac{d(x_f + \varepsilon)}{dt} = \frac{K\Delta P}{\varphi\mu_s[ML + (1-M)(x_f + \varepsilon)]} \tag{2.16}$$

By subtracting equation (2.15) from (2.16) and provided from Figure 2.4 that $\varepsilon \ll x_f$. (Stalkup, 1983a):

$$\frac{d\varepsilon}{dt} = \frac{-K\Delta P(1-M)\varepsilon}{\varphi\mu_s[ML + (1-M)x_f]^2} \tag{2.17}$$

Therefore, $\varepsilon = e^{tC}$, where C is:

$$C = \frac{-K\Delta P(1-M)}{\varphi\mu_s[ML + (1-M)x_f]^2} \tag{2.18}$$

Thus, ε initially grows exponentially with time immediately after formation of the perturbation if M > 1 but decays exponentially with time if M < 1.

Volumetric displacement efficiency is a measure of the efficiency of an EOR method that depends on the volume of the reservoir contacted by the injected fluid (Romero-Zerón, 2012). The volumetric sweep efficiency is an overall result that depends on off-pattern wells, the injection pattern selected, flow rate, position of gas-oil and oil/water contacts, fractures in the reservoir, reservoir thickness, permeability and areal and vertical heterogeneity, density difference between the displacing and the displaced fluid, and mobility ratio. When the mobility ratio decreases, the volumetric sweep efficiency increases. Consequently, when there is a large mobility ratio between the displacing fluid and the displaced fluid, it will lead to viscous fingering. High mobility ratios can be the reason for poor sweep efficiency and reducing the efficiency of oil recovery (Romero-Zerón, 2012, Kulkarni, 2003).

2.4.4 Heterogeneities of permeability

The fingering initiation process is generally attributed to the existence of variation in permeability (Stalkup, 1983a). The permeability of a field is heterogeneous if it is varying spatially and rarely reservoir rocks are homogeneous (Carlson, 2006). Some fingers are initiated from the ends of previous grown fingers similar to the limbs and twigs of a tree.

High mobility ratio (non-unit mobility ratio) or viscosity contrast make miscible gas injection sensitive to reservoir heterogeneity, as the displacing fluid will tend to flow through the zones with higher permeabilities (Carlson, 2006). As a result, large amounts of the oil may be left behind in the layers with low permeabilities because they are not effectively swept by the injected fluid (Sahimi, 2011).

The main issue of miscible gas displacements through heterogeneous porous media concerns the interaction between the intrinsic instability mechanism related to a high mobility ratio and the permeability variation. The literature reveals studies (Blackwell et al., 1959, Christie and Bond, 1987, Waggoner et al., 1990, Tchelepi et al., 1993) demonstrating that either permeability-induced channelling or viscous fingering can

dominate the displacement process, depending on the variance and correlation length of the permeability field, as well as the viscosity ratio.

Sometimes, it is difficult to distinguish the effects of the mobility ratio and heterogeneity, or channelling in high mobility ratio displacements in heterogeneous media. The term channelling is sometimes used interchangeably with the term viscous fingering because they both result in uneven displacement fronts, poor oil recovery, and early breakthrough of the injected fluid. Channelling of the injected fluid results from viscous fingering, gravity segregation (with solvent over-riding the oil zone), and permeability stratification (strata of different permeability in the reservoir). Channelling happens even for equal viscosity/density fluids in stratified sands.

2.4.5 Injection pattern

It is very important to choose the proper pattern of well spacing for WAG injection to be successful, because sweep efficiency is strongly affected by the distance between the producer and the injector wells (Christensen et al., 2001). In many cases, a five spot injection pattern is used in onshore locations with close well spacing as it can provide a superior sweep efficiency (Christensen et al., 2001, Zahoor et al., 2011). Indeed, the Judy Creek field achieved a higher recovery using a five-spot injection pattern by increasing the number of wells, thereby reducing the injection pattern size (Pritchard et al., 1990).

In offshore locations it is more challenging to select the right injection pattern because of the high cost associated with drilling additional offshore wells and well location is mostly determined by geological factors (Christensen et al., 2001). As a result, it is better to take into account the economical and geological factors for selecting the offshore injection pattern. The development of software and computer technology have made the selection of the optimum well locations and their orientation possible, through simulation studies.

2.4.6 Injection parameters (slug size, WAG Ratio, WAG cycle length and time to initiate WAG injection)

Slug size: finite sized slug WAG injection is applied by injecting a slug of the gas alternating with a slug of water into the reservoir. In some cases, the slug size of the

injected gas is in the range of 0.1 to 0.3 pore volumes (PV). In other cases, the initial slug size can be up to 40% of a hydrocarbon pore volume (HCPV) (Christensen et al., 2001). To achieve optimum recovery, the slug size of gas and water should be optimised.

WAG ratio is defined as the ratio of injected water volume to injected gas volume at reservoir conditions. In field applications, the most popular WAG ratio is 1:1 because of its simplicity. However, this ratio may not be the optimal ratio, and it will greatly affect the operational and economic conditions of the project (Christensen et al., 2001).

The WAG ratio is an important parameter and can be optimised to obtain a high oil recovery factor. If the WAG ratio is small (injecting gas more than water), WAG injection will be viscously unstable and gas may breakthrough causing the production performance to behave like gas injection (Stalkup, 1983a). Conversely, if the WAG ratio is high (injecting water more than gas), WAG injection will lead to oil trapping or may not allow sufficient gas-oil contact for a good displacement efficiency, causing the production performance to behave like water injection (Stalkup, 1983a).

To determine the optimum WAG ratio, Stalkup (1983a) suggested the use of matched velocity (MV) flooding, where gas and water travel at the same speed (full details are discussed in Chapter 4). The optimal value of WAG ratio depends on a number of different factors such as fluid viscosity, fluid density, reservoir flow rate and permeability distribution (Wu et al., 2004). In field-scale applications, other considerations can also become important e.g. choosing the WAG ratio based on the availability of the gas for injection (Zahoor et al., 2011, Morais, 2012) or to allow a more efficient use of the available gas (Wilson, 2015) by choosing the amount of injection rate and the WAG pattern.

The cycle length to switch from gas to water and how to start the cycle with either water WAG or gas WAG has an effect on the oil recovery (Christensen et al., 2001). The length of a WAG cycle under normal operational conditions could be 2 or 3 months. The initial WAG cycle at Snorre field was 3 months, which was reduced to 1 month because of gas breakthrough (Awan et al., 2008). However, the WAG cycle in some fields, such as Gullfaks, depends on the availability of the gas. While in other fields, the WAG cycle

depends on the gas market price, which is a general trend in North Sea where they inject more gas during the summer and less during the winter (Awan et al., 2008).

Time to initiate the WAG injection is another factor to consider in designing the WAG process. Two approaches include starting the WAG process at the very beginning of the reservoir development, or after flooding it with water for a period of time. Herein, these two cases are denoted as "Secondary WAG" and "Tertiary WAG", respectively. Based on simulation results, Wu et al. (2004) recommended initiating the WAG injection early in reservoir development to achieve high oil recovery and to maintain the average reservoir pressure. However, this decision should be made with reference to proper reservoir simulation studies for a specific reservoir.

To achieve optimum recovery, the injection parameters (i.e. the slug size of gas and water, WAG ratio, WAG cycle length) should be optimised. Optimising the injection parameters using a simulator is very important before applying miscible WAG injection on a field scale, as it will help to identify the oil recovery that is going to be achieved.

2.5 Simulating the WAG injection using reservoir simulator

Reservoir simulators are used to model the WAG injection and other EOR methods to predict the reservoir performance.

A reservoir simulator uses a mathematical model, i.e. a set of differential equations of a physical system that describes the physical processes active in the reservoir. In reservoir engineering, reservoir simulators are used on a daily basis in oil and gas companies to study reservoir performance, predict and optimise different scenarios, and plan reservoir management. The main reason for this, from a commercial perspective, is the ability of reservoir simulation to generate the production profiles (oil, water and gas) under several exploitation and production options that lead to different estimations of cash flow (Hutahaean, 2017).

The prediction of reservoir performance using a mathematical model is calculated by using analytical models or numerical models. The analytical models include the material balance equation (Dake, 1983), and the fractional flow curve techniques (such as the

Buckley-Leverett technique) (Buckley and Leverett, 1941) that has been mentioned previously.

The material balance equation is a fundamental of reservoir engineering. It is used to explain the behaviour of reservoir recovery mechanisms and to provide a reliable quantification of the reservoir energy sources (Dake, 1983, Dake, 2001, Eng, 2007). It is one of the basic tools in reservoir engineering and is underpineed by the principle of mass conservation. It states that for a given pressure drop, the volume of produced fluids must equal to the total expansion of the reservoir system plus any natural fluid influx (Dake, 1983). Reservoir simulators apply the material balance equation within each of their multi-dimensional cells. In its application to calculate the expected reservoir performance in terms of fluid withdrawal, the material balance uses reservoir properties, pressure data, and Pressure Volume Temperature (termed as PVT) properties to calculate the performance of the reservoir in terms of fluid withdrawal (Dake, 1983, Dake, 2001, Eng, 2007). Furthermore, material balance gives an insight into the reservoir drive mechanisms, while providing a reliable quantification of the reservoir energy sources in most cases.

On the other hand, a numerical reservoir simulation model is a more complicated technique for predicting reservoir performance. The numerical simulations of two or three phase flows in oil reservoirs use mathematical expressions in the form of partial differential equations, and use finite-difference approximation to solve the governing equations (Sahimi, 2011, Islam et al., 2016). Since the 1960, the numerical reservoir simulation has been practised and it is connected to the numerical techniques' evolution and the availability of fast digital computing machines. The numerical reservoir model includes a range of data, such as reservoir description (e.g. geological concepts), reservoir fluid (PVT data), rock properties (e.g. permeability and porosity) and their spatial distribution, dynamic data and production/injection stage and controls. The reservoir simulation model uses a gridded representation of the petroleum reservoir, where each of the grid blocks represents a local part of the reservoir and the blocks are generally connected to the adjacent blocks so fluids may flow in a block-to block manner. The reservoir simulation model integrates data on the fluids of the reservoir (PVT) and the description of the reservoir (porosities and permeabilities) and their distribution in space.

2.5.1 Discretisation methods

In mathematics, discretisation deals with the process of transferring continuous equations and models into discrete counterparts. Usually, this method is applied as a first step to make them suitable for numerical evaluation and computational implementation. The commonly used methods for discretisation are Finite Volume and Finite Difference methods, Figure 2.5 (Antoniou, 2016, Sauer, 2016), each of which are outlined below.

Finite Difference Method (FDM) is a numerical method for solving partial differential equations by using approximate spatial and temporal derivatives that are based on discrete values at spatial grid points and discrete time levels (Causon and Mingham, 2010, Kajishima and Taira, 2016). Structured grids are chosen for finite difference methods because of their simplicity. The derivative operations, such as the velocity and pressure gradients, are approximated by the difference quotients between two points that are as close as possible.

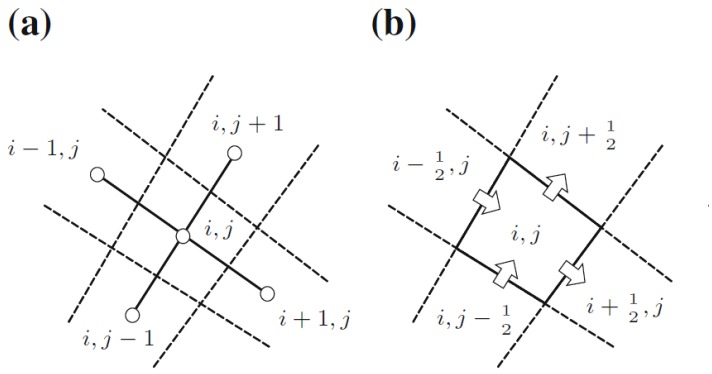

Figure 2.5 The discretisation methods (a) Finite difference method (b) Finite volume method (Kajishima and Taira, 2016)

Finite Volume Method (FVM) is a numerical method for solving the partial differential equations that arise from physical conservation laws in the form of algebraic equations. In a partial differential equation, volume integrals that contain a divergence term are converted to surface integrals by using the divergence theorem. This method is a discretisation method which is suitable for the numerical simulation of conservation laws. The conservation law is expressed as a balance of the influx and efflux from one discretisation cell to its neighbour. In addition, the FVM is formulated to allow the use of

structured and unstructured grids (Eymard et al., 2000, LeVeque, 2002, Ferziger and Peric, 2012, Kajishima and Taira, 2016).

Numerical solutions give the fluid saturations and pressure values at discrete grid blocks and at discrete times in the reservoir (Aziz and Settari, 1979, Satter et al., 2008, Islam et al., 2016). The grid block size should allow the use of average properties throughout the grid block. A partial differential equation is written for a given point in space at a given time level to carry out discretisation. The time level choice leads to the explicit, or implicit, method for solving the equation. The explicit methods solve the equations at a later time from equations at the current time, while implicit methods find a solution by solving an equation at a later time from equations at both the current and the later time. (Satter et al., 2008, Islam et al., 2016).

The discretisation (grid block and time) leads to errors in the model from the approximation of the conservation equations with discrete analogues in relation to the chosen grid block size. Numerical diffusion, known as truncation error, limits the use of numerical finite-difference approximations to solve partial differential equations (Lantz, 1971). In the solution of partial differential equations, such as those that occur in miscible displacement, truncation error results in an artificial dispersion term often denoted as numerical diffusion. Many users of numerical programs recognize that the degree of the numerical diffusivity for differential equations can depend on both gridblock size and time step.

2.5.2 Types of reservoir simulators models

Reservoir simulators that are typically used in the petroleum industry are usually one of two types, black oil models (such as Eclipse E100) or compositional models (such as Eclipse E300).

The black oil model (miscible flood option in E100) assumes multi-phase flow of fluids (oil, gas and water) where the fluids are homogeneous. The assumption is that the gas can dissolve in any proportion in the oil to avoid the problem of computing the detailed phase diagrams of the mixture that requires the thermodynamic equation of state (Sahimi, 2011). The black oil model is able to model the miscible gas injection (Geoquest, 2014). The

black oil model consists of a three-component system, stock tank oil together with the associated solution gas, injection gas (solvent) and water (Geoquest, 2014). The black oil model has the implementation of Todd and Longstaff's mixing parameter, which describes the mixing between the solvent and oil within a grid block and describes the degree of gas fingering through the oil within each grid cell (Geoquest, 2014). In the E100 miscible flood option to control the numerical diffusion of oil and solvent gas, a two-point upstream algorithm operating only on the miscible component relative permeabilities is available for use and it is illustrated in Figure 2.6 (Geoquest, 2014). To calculate the flow of component C between cells i and j which are aligned along the x-axis, suppose that cell i is the upstream cell for the flow of component C between i and j. Let cell k be the second upstream cell to cell j and K_{ck}, K_{ci} and K_{cj} represent the component relative permeabilities in cells k, i and j respectively. DX_k, DX_i and DX_j are the x-direction cell sizes. The equation for single point upstream weighting, the flow rate of component C across the i-j cell interface is $F_{ij,c}$:

$$F_{ij,c} = T_{ij} \frac{K_{\mathrm{ci}}}{B_{\mathrm{ci}}\, \mu_{\mathrm{ci}}} DP_{ij,c} \tag{2.19}$$

where, $DP_{ij,c}$ is the potential difference for component C between cells i and j, T_{ij} is the transmissibility between cells i and j, and $\mu_{\mathrm{c}}, B_{\mathrm{c}}$ are the viscosity and formation volume factor of component C.

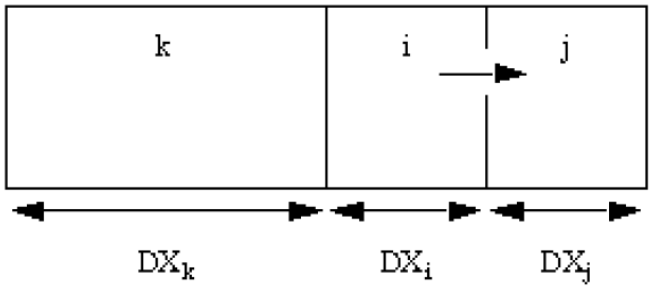

Figure 2.6 Represents the two-point upstream projection technique. Adopted from (Geoquest, 2014)

On the other hand, compositional models assume multi-phase flow with mass transfer between the phases (Carlson, 2006, Sahimi, 2011). They are more complicated than the black oil models because they take into account the effects of the phase behaviour and compositionally dependent properties, for example viscosity, phase density and

interfacial tension. Moreover, such models have to ensure that the initial saturations are in compositional equilibrium and it considers the thermodynamic equilibrium between phases. However, the compositional models do not have the implementation of Todd and Longstaff's mixing parameter (Carlson, 2006).

Overall, compositional models are more complicated than black oil models because they calculate the fluid properties for the equations of flow at every time step, while black oil models read the fluid properties from input tables. In addition, compositional models need more time and resources for compositional fluid flow, which could also translate into significant computational requirement. As a result of the advantages that the black oil models offer compared to compositional models, this approach to modelling the miscible finite-sized slug WAG injection will be taken for applying the Todd and Longstaff's mixing parameter on a field scale and then the optimisation study detailed herein.

2.6 Optimisation of the WAG injection and the optimisation algorithm

In order to achieve a better oil recovery, optimising WAG injection parameters (such as slug size, WAG Ratio, WAG cycle length and time to initiate WAG injection) became recognized as a practical technique for controlling gas mobility and achieving high recovery (Mehos and Ramirez, 1989, Chen et al., 2010, Panjalizadeh et al., 2015, Chen and Reynolds, 2016, Chen and Reynolds, 2018, Mohagheghian et al., 2018).

Optimisation is the search for an optimal value in which one has to minimise or maximise one or more objectives that are functions of some real or integer values (Mohamed, 2011, Bandyopadhyay and Saha, 2012, Hutahaean, 2017). It can be done using numerical optimisation methods to reduce the computation time (Agada et al., 2017), and it can effectively and systematically evaluate many solutions. Particle swarm optimisation (PSO) algorithm has been widely used by researchers for the optimisation of WAG injection.

John (2015) used the particle swarm optimisation (PSO) algorithm to run an optimisation study to evaluate the optimum injection rate and WAG ratio in SWAG injection to maintain the pressure of the reservoir for as long as possible for improved oil recovery. The optimal WAG ratio selected from the available result was 2:3, then an optimisation

of the injection rate at this WAG ratio was conducted and the oil recovery was 68% of oil in place in the reservoir. Caetano (2017) used the PSO algorithm to run an optimisation study to evaluate the optimum water and Liquefied petroleum gas (LPG) injection rates. LPG is a by-product of processing the associated gas in the field, which has no local market nor nearby facilities to allow being sold or consumed. The main goal was to maximise the oil recovery using water alternated with LPG injection. The PSO algorithm optimised the injection rates of both fluids and Caetano (2017) found that the higher the LPG injection rate was, the higher is the cumulative oil production because LPG has a first contact miscibility with the reservoir oil, which helps to decrease its viscosity and increase the microscopic sweep efficiency. Mohagheghian et al. (2018) used the PSO algorithm to run an optimisation study at the field scale to optimize the operating parameters of WAG injection, which include water and gas injection rates, bottom-hole pressures of the oil production wells, cycle ratio, cycle time, the composition of the injected hydrocarbon gas and the total WAG period. In their study, they increased the problem complexity by increasing the number of decision-making variables, while potentially improving the efficacy of the WAG process. They optimised the incremental recovery factor (IRF) within a fixed total WAG simulation time. Also, they highlighted the distinctions between the WAG parameters found by optimising Net present value (NPV) and oil recovery. They found that PSO converged to the same optimal solution in all the trials for each case study they made.

The PSO algorithm is a population-based stochastic sampling algorithm that has been developed to simulate the social behaviour observed in bird flocks looking for the best place for food in nature (Kennedy and Eberhart, 1995). PSO is a swarm intelligence method that has been used for optimisation and history matching in the oil industry for an optimum solution. In PSO each particle is a single solution in the search space. Each particle has a random position in the search space at the beginning, then the position of each particle is changed according to the velocity of the particle's value and the memory of the previous best position $pbesti$. The $pbest$ vector of the particle with the best fitness in the neighbourhood is denoted as $gbest$.

The PSO algorithm computational workflow is performed by the following steps (Mohamed, 2011, Hutahaean, 2017):

1. Initialise a set of models (particles) with a random locations and velocities in the search space.
2. Solve each model and obtain the relevant objective function value for each model (particle).
3. Update the position and the value (*pbest*) of each model (particle) with the best solution the particle has seen. If the current objective function value of one particle is better than its *pbest* value, then the current objective function value and position will replace its *pbest* value and position, respectively.
4. Find the value and the corresponding best position *gbest* of the global best objective function across the whole swarm's *pbest*.
5. Update all the particles' positions and velocities
6. Those steps 2 – 5 will be repeated until a stopping criterion is achieved (e.g. a sufficiently good objective function value or the maximum number of iterations is reached).

PSO is relatively straightforward, computationally efficient, easy to implement (has a small number of parameters to adjust) and has been applied successfully to solve a variety of optimisation problems. There are studies showing the efficiency of the PSO algorithm in comparison to other optimisation algorithms, see for example (Hassan et al., 2004, Mohagheghian et al., 2018). There are many studies, especially in the oil industry, that have shown PSO to be an effective optimisation algorithm (Hassan et al., 2004, Kathrada, 2009, Mohamed, 2011, Arnold et al., 2016, Hutahaean, 2017). It has been applied to well placement optimisation (Onwunalu and Durlofsky, 2010), history matching (Mohamed, 2011, Fernández Martínez et al., 2012, Vazquez et al., 2015), drilling (Self et al., 2016) and WAG injection optimisation (John, 2015, Caetano, 2017, Mohagheghian et al., 2018) as mentioned earlier.

There are two concepts in the optimisation, single and multi-objective optimisation. Single-objective optimisation is the task of optimising one objective function. It aims to find the best solution that agrees to the minimum or maximum value of a single objective function (Mohamed, 2011, Hutahaean, 2017). Single objective optimisation does not trade different objectives against each other (Savic, 2002, Hutahaean, 2017). This challenge can be rectified using multi objective optimisation.

Multi-objective (MO) optimisation is the task of optimising two or more objectives simultaneously with respect to a set of certain limitations to find diverse solutions (Hutahaean, 2017). This diversity in the solutions is achieved through the trade-offs the objectives by improving one objective over the other. Multi-objective optimisation yields several optimal solutions, instead of having a single best solution. Later, a decision maker can pick which optimal solution(s) to use based on their preference (Hutahaean, 2017).

The general form of the multi-objective optimisation as the following (Hutahaean, 2017):

$$\begin{aligned} &\text{Maximise/ Minimise} && f_m(x), && \text{m}= 1,2,\dots,M; \\ &\text{subject to} && g_j(x) \geq 0, && \text{j}= 1,2,\dots,J; \\ & && h_k(x) = 0, && k = 1,2,\dots,K; \\ & && x_i^{(L)} \leq x_i \leq x_i^{(U)}, && i = 1,2,\dots,N; \end{aligned} \tag{2.20}$$

where, $f_m(x)$: $\mathbb{R}^N \rightarrow \mathbb{R}^M, x = (x_1, x_2, \dots, x_K, \dots, x_N)$ is the vector of the N parameters, M is the number of objective functions, h_k and g_j are the equality and inequality constraints, respectively, with K and J are the number of equality and inequality constraints that the solution must satisfy, respectively. The last set of constraints are the parameter bounds restricting each parameter x_i to take a value within an upper bound $x_i^{(U)}$ and a lower bound $x_i^{(L)}$. If the solution of x satisfies all of the (K and J) constraints and the parameter bounds, it is known as a feasible solution, otherwise, it is known as an infeasible solution (where at least one of the constraints is violated).

In multi-objective optimisation algorithms, two solutions are compared on the basis of whether one dominates the other solution or not and they are known as *dominance* and *Pareto optimality* (Hutahaean, 2017). Figure 2.7 shows the concept of the dominance for a two-objective minimisation problem, where solution x_2 strongly dominates solutions x_5 and x_6 as it is better in both objectives. A solution x_1 dominates a solution x_2 (denoted $x_1 \leq x_2$, if and only if it satisfies two conditions (Hutahaean, 2017):

1. The solution x_1 is no worse than the solution x_2 in all objectives.
2. The solution x_1 is strictly better than the solution x_2 in at least one objective.

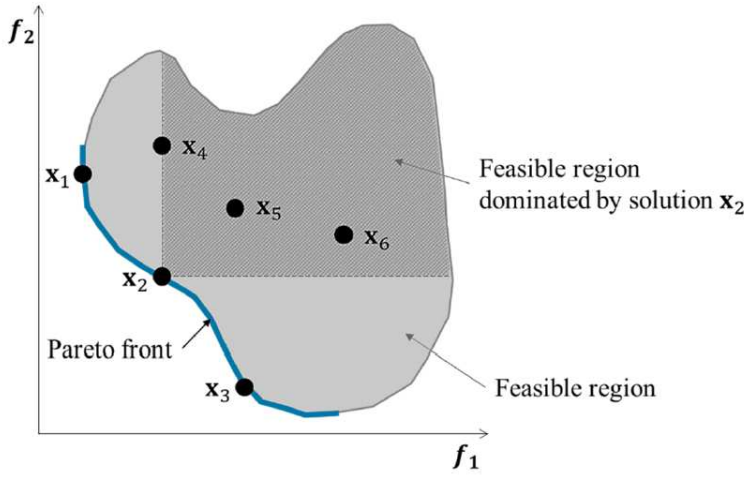

Figure 2.7 Represents the Pareto optimality and Dominance of hypothetical two objective minimisation problem. Striped area is the feasible region dominated by solution x_2. Adopted from (Hutahaean, 2017).

Pareto optimal set is a set of non-dominated solutions Ṕ (called the Pareto front) amongst a set of solutions P (called remainders) and not dominated by any member of the set P (Khu and Madsen, 2005, Fonseca et al., 2003). Solutions x_1, x_2 and x_3 in Figure 2.7 are the non-dominated (Pareto optimal) set of solutions. While, Pareto optimal front or sometimes called as Pareto front is shown as in Figure 2.7 as the blue line. One of the main goals in multi-objective optimisation is to find the set of Pareto-optimal solutions. Solutions in multi-objective approaches are the set of results on the Pareto Front, i.e. the non-dominated solutions.

Using MOPSO has been shown to be more efficient because of the faster convergence (is to obtain the solutions as close as possible to the Pareto front) speed (Mohamed, 2011) and obtain solutions as diverse as possible along the Pareto front (a variety of optimal solutions which trades off the objectives differently) when comparing it to the single objective PSO (Mohamed, 2011).

2.7 Summary of the chapter

This chapter provides the theory of miscible gas injection and discusses how to overcome the associated issue of viscous fingering (which arises from the high mobility ratio between the injected gas and the crude oil) with the use of the water alternating gas (WAG) injection method. As the name suggests, this technique is a combination of two traditional methods, gas injection and water injection. The gas injection is used for contacting unswept zones to improve the microscopic displacement efficiency. The water injection is used to improve the macroscopic sweep efficiency and the mobility control of the displacement and for stabilising the front of the gas injection. The chapter addresses other factors that affect the WAG injection such as three phase relative permeability effects, composition and availability of the gas, mobility and mobility ratio, heterogeneity of permeability, injection pattern and injection parameters.

Following on from that, the types of reservoir simulator will be introduced alongside specific details of the black oil models (such as Eclipse 100) simulator as it was used to simulate the miscible WAG injection in this research.

Finally, the chapter discusses the background of optimisation and some examples of the work done on optimising WAG injection using multi-objective Particle Swarm Optimisation (MOPSO) algorithm. PSO is relatively straightforward, computationally efficient, easy to implement (has a small number of parameters to adjust) and has been applied successfully to solve a variety of optimisation problems. There are many studies, especially in the oil industry, that have shown PSO to be an effective optimisation algorithm. It has been applied to well placement optimisation, history matching, drilling and WAG injection optimisation as mentioned earlier.

Chapter 3

Review of the Blackwell experiment and the empirical models predicting the viscous fingering and calibration of the mixing parameter based on this experiment

3.1 Introduction

Viscous fingering generally refers to the onset and developing of instabilities that occur in miscible gas displacement in porous media. In most but not all cases, the mechanism of the instability is intimately linked to the mobility difference between two phases. Viscous fingering represents one of the most important properties in multiphase flow that exists in most of the displacement cases for enhanced oil recovery because it lowers the oil recovery due to gas breakthrough. To-date, reservoir simulators such as black oil model are unable to model this phenomenon because the fingers are too small and it's difficult to resolve them using conventional field scale reservoir simulation models (Jamaloei et al., 2011, Islam et al., 2016).

Empirical models have been developed in order to understand the formation and evolution of viscous fingering and to predict the degree of viscous fingering by estimating the average flow behaviour of solvent and phase mobility on a field scale reservoir simulation (Fayers et al., 1990, Blunt et al., 1994). Those models have been calibrated against an experimental study performed by Blackwell et al. (1959) and are Koval (1963) model, Todd and Longstaff (1972) model, and the analytical Calibration model by Blunt and Christie (1993), which is an extension of both Koval's model and Todd and Longstaff's model. Peaceman and Rachford (1962) developed a mathematical model of partial differential equations for a numerical simulation of unidirectional miscible displacement and matched the results with Blackwell et al. (1959). Christie and Bond (1987) developed a 2D numerical simulation to simulate viscous fingering and matched the results with Blackwell et al. (1959).

A review of the literature reveals a great wealth of studies on the effect of viscous fingering in porous media, research that has been ongoing for many decades (Saffman and Taylor, 1958, Blackwell et al., 1959, Koval, 1963, Perkins et al., 1965, Todd and Longstaff, 1972, Christie, 1987, Homsy, 1987, Fayers, 1988, Fayers and Newley, 1988, Fayers et al., 1990, Tan and Homsy, 1992, Araktingi and Orr Jr, 1993, Blunt and Christie, 1993, Christie et al., 1993, Tchelepi et al., 1993, De Wit and Homsy, 1997, Juanes and Blunt, 2006, Moortgat, 2016). However, it is not possible to examine and encompass every study in detail and so for this thesis it was chosen to focus on the Blackwell et al.

(1959) experiment and the models that have been calibrated against this experimental study as they represent the basis of this research. Expanding upon the previous research in this area.

This chapter will focus on the experiment conducted by Blackwell et al. (1959) and the models that have been calibrated against this experimental study to predict the viscous fingering in miscible displacement and to calibrate the mixing parameter, ω.

3.2 Blackwell et al. (1959) experiment

Blackwell et al. (1959) performed an experimental study to investigate the factors that control the efficiency with which oil is displaced by a miscible displacement in heterogeneous porous media. These factors include mobility ratio, flow rate, system size (model dimension), gravity segregation and permeability heterogeneities on the recovery of horizontal and vertical linear floods. The purpose of this experiment was to clarify the relevant processes both on a macroscopic level (within a large sand body) and on a microscopic level (within individual or between neighbouring pore spaces).

Blackwell et al. (1959) studied the factors that determining the viscous fingering behaviour in miscible displacement at adverse mobility ratio, which demonstrated that diffusion will not be effective in preventing the formation and growth of fingers in reservoirs of realistic widths even in homogeneous sands. They extended their study to fluids of equal viscosity-unequal density and to fluids of unequal viscosity-equal density and verified that the mixing amount in a single straight capillary can be predicted. In addition, they showed that molecular diffusion is important in providing complete displacement of the oil by solvent at rates and capillary sizes comparable to reservoir rates and pore sizes.

Blackwell et al. (1959) used gases whose molecular diffusivities are many times greater than those of the reservoir liquids they simulate. To make it possible to investigate in the laboratory the microscopic flow phenomena for flow rates and pore sizes characteristic of reservoir conditions in a practical time. Argon was used to displace a mixture of 10% helium and 90% argon from a 120 ft stainless steel tube with an inside diameter of 0.53 in. They packed the tube with 60- to 80-mesh silica sand to achieve a porosity of 33.9%

and a permeability of 15 D. They made thirty-six displacements at rates from 0.023 to 0.72 cm/s. In a typical reservoir, these velocities for miscible liquids correspond to field rates of 0.32 to 10.2 ft/day. The lengths of the mixing zones corresponding to the 10 and 90% concentration levels of the solvent were determined by thermal conductivity measurements of the effluent.

Blackwell et al. (1959) studied the effect of channelling by a low viscosity solvent on the resident fluid with fluids of equal densities. Channelling of the injected solvent results from viscous fingering, gravity segregation (with solvent over-riding the oil zone), and permeability stratification (strata of different permeability in the reservoir). Channelling happens even for equal viscosity/density fluids in stratified sands. To study the channelling of low-viscosity solvents in homogeneous sands, Blackwell et al. (1959) used four models in this experiment and one of the model's dimensions were: 3/8×1/2×72 in. in thickness, width and length, respectively. They performed a number of displacements covering a wide range of both fluid viscosity and flow rate. They packed the models uniformly with 20 to 30, 30 to 70, or 100 to 140 mesh Ottawa sand for a given series of experiments. An example of viscous fingering is shown in Figure 3.1 for a viscosity ratio of 20 after injection 0.15 PV. Figure 3.1 shows a number of large fingers of approximately similar shapes and equal length.

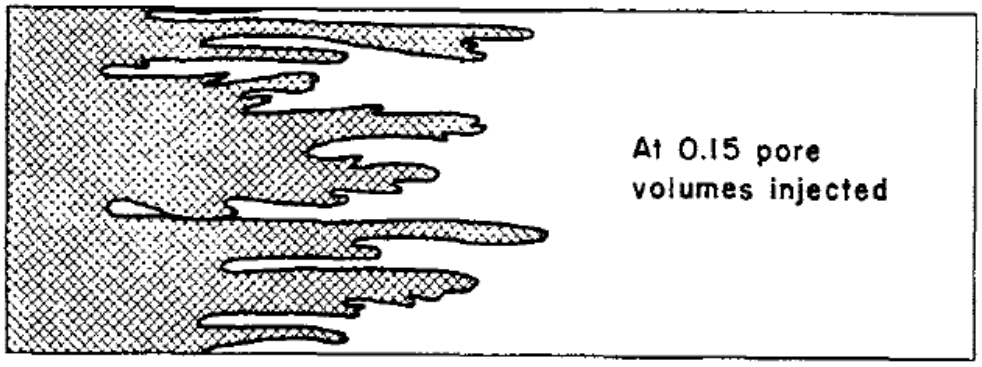

Figure 3.1 Viscous fingering for a viscosity ratio of 20. After Blackwell et al. (1959)

To investigate the flow behaviour in parallel strata having different permeabilities, a 3/8 × 6×72-inch model was packed with two 3-inch wide communicating sand strata. The permeabilities of the two strata were 190 and 43 D, giving a permeability ratio of 4.4. They conducted three experiments for mobility ratios of 1, 4.6 and 75. To investigate a

second type of stratification a ¼×3×72-inch model was packed with 12 segments. Each segment was 6-inches long and contained six ½-inch wide strata. Six sands with permeabilities of 56, 41, 33, 16, 9 and 6 D were arranged in each segment so that the permeability of each layer of the segment was different from the permeabilities of the corresponding layers in adjacent segments. Three experiments were conducted for mobility ratios of 1, 4.6 and 23.1 with flow rates ranging from 41 to 72 ft/day. Blackwell et al. (1959) found that channelling of a low viscosity solvent increases the size of the solvent bank required. Fingering through permeable strata increase the interface area between the oil and the solvent through which diffusion can disperse the solvent. In reservoirs having uniform sand the optimum bank size may be quite small, 3 to 5 per cent of a pore volume.

Blackwell et al. (1959) found that the maximum oil recoveries obtained from homogeneous horizontal reservoirs by injecting low-viscosity solvents with similar density as oil. the recovery at solvent breakthrough in horizontal reservoirs being flooded with solvents can be expected to decrease as the mobility ratio increases. Therefore, as the mobility ratio increases, amount of solvent required for complete recovery increases. In addition, fingering caused by permeability variation will cause poor recovery.

Blackwell's et al. (1959) experiment (as they provided all the input parameters and results) later became the main reference of many numerical works such as Peaceman and Rachford (1962), Koval (1963), Todd and Longstaff (1972) and Christie and Bond (1987). The data they used in their experiment were taken under conditions simulating low flow rates and small sand particle sizes comparable to those in the reservoir. This is particularly important as the data in the literature does not identify how much mixing occurs between solvent and oil in the reservoir. Most of the laboratory data were taken at high flow rates in models packed with large sand particles-conditions under which the effects of mixing are dominant.

3.3 Peaceman and Rachford (1962) Model

Peaceman and Rachford (1962) developed a mathematical model of partial differential equations for a numerical simulation of unidirectional miscible displacement. The model

combines the transport equation of solvent with Darcy's law for the fluid flow through the porous media. The model takes into account the effect of gravity, the spatial distribution of permeability, diffusion, fluid densities and fluid viscosities.

The Peaceman and Rachford (1962) model assumed that the fluids were an incompressible, two-component system with constant diffusivity, where the viscosity is dependent on the solvent concentration i.e. the solvent volume fraction in the oil-solvent mixture. The model is given by:

$$\nabla . u = 0, u = \frac{K}{\mu}(\nabla P + \rho g \nabla \mathrm{h}), \tag{3.1}$$

and the conservation equation is:

$$\varphi \frac{\partial c}{\partial t} = KX \frac{\partial^2 c}{\partial x^2} + KY \frac{\partial^2 c}{\partial y^2} + \nabla . \frac{cK}{\mu}(\nabla P + \rho g \nabla \mathrm{h}) \tag{3.2}$$

where c is the concentration of solvent, u is the total volume flux of fluid per unit area, K is the permeability of the rock, D is the effective diffusion of the solvent, $\mu(c)$ is the viscosity of the mixture which is a function of c, ρ is the density of the mixture, and φ is the porosity of the medium.

Peaceman and Rachford (1962) solved equations (3.1) and (3.2) numerically using a "leap-frog" method. The pressure distribution in the flow field is obtained at each time step. With this pressure distribution the new flow field can be determined, that is, the velocity at each point can be computed. Using these velocities, the new concentration distribution for the next time step may be determined from the convective dispersion equation (Peaceman and Rachford, 1962)

The model had been validated by comparing the results from the simulation of horizontal two-dimensional displacements with Blackwell et al. (1959) experiments. Good agreement was obtained for the miscible displacement for cumulative oil recovery. Viscous fingering was generated using small, random variations of permeability. Even though development of early fingers was more complex than could be practically computed with a uniform grid, the propagation rate of the fingers was in close agreement with that observed in experiments.

The Peaceman and Rachford (1962) approach to predict viscous fingering in miscible gas displacements was applied to relatively homogeneous sand packs. According to Homsy (1987), the Peaceman and Rachford (1962) pioneering attempt at such a simulation failed as it was dominated by numerical errors and also their approach has led to a misconception in the literature of petroleum engineering that fingering instabilities are caused because of permeability heterogeneities only (Homsy, 1987, Sahimi, 2011). However, Christie and Bond (1987) were able to trigger the viscous fingering by mobility ratio difference as well as by the permeability heterogeneity.

3.4 Koval Model

Koval (1963) developed an empirical solution to predict the behaviour of unstable miscible displacement in porous media taking into account heterogeneity of permeability. This model can predict the oil recovery and solvent cut as a function of the pore volumes of solvent injected. The solvent fractional flow equation is derived from the Buckley Leverett equation. In his model, Koval's factor replaced the function of the fractional flow in the Buckley-Leverett's equation and is given by:

$$f_{Koval}(c) = c \Big/ \left(c + \left(\frac{1-c}{K_G} \right) \right) \tag{3.3}$$

where K_G is Koval factor and can be obtained from the system heterogeneity index (H-factor, H_k) is given by:

$$K_G = H_k M_{eff} \tag{3.4}$$

H_k was back-calculated by first estimating K_G factor and then calculating H_k. The resultant H_k depends only on the rock and not on the viscosity ratio of the test.

$$F_S' = \frac{1}{V_{pi}} = \frac{K_G}{\left(1 + S(K_G - 1)\right)^2} \tag{3.5}$$

where F_S' is the fractional flow equation of oil recovery and solvent injected, V_{pi} is the pore volume injected and S is the water saturation. Since, Koval had difficulty in obtaining the saturation data, S in Equation (3.5) is usually eliminated by using the

fractional flow equation to describe miscible gas displacement $F_S = (K_G\, S)/\big(1 + S(K_G\, - 1)\big)$, which leads to:

$$V_{pi} = \frac{K_G}{\big(K_G - F_S(K_G\, - 1)\big)^2}$$
$$F_s = \frac{K_G - (K_G/V_{pi})^{1/2}}{K_G\, - 1} \tag{3.6}$$

The effective viscosity ratio, M_{eff}, is defined as the ratio between the viscosity of the oil and the mixture viscosity of oil and solvent in which the solvent volume fraction is c. Koval (1963) chose the effective viscosity M_{eff} such that the model results will match Blackwell experimental results and given by:

$$M_{eff} = (0.78 + 0.22\, M^{0.25})^4 \tag{3.7}$$

where, M is the viscosity ratio μ_o/μ_s. Equation (3.7) was derived by determining an appropriate composition and viscosity for the effective displacing solvent. This was accomplished by examining experimental data in which the effects of dispersion were minimal. In this way, the effects of viscosity ratio were isolated. From the data of Blackwell et al. (1959) a reasonable composition for the effective displacing solvent was found to be 78% oil and 22% solvent. Equation (3.7) can be estimated reliably by the fourth root mixing rule used extensively in refinery calculations and given by:

$$\frac{1}{(\mu_{o+s})^{1/4}} = \frac{vol.fraction\ solvent}{(\mu_s)^{1/4}} + \frac{vol.fraction\ oil}{(\mu_o)^{1/4}} \tag{3.8}$$

Equation (3.8) is the general form of the viscosity mixing rule (Koval, 1963).

Interfacial tension is absent when the solvent is miscible with the oil in all proportions. Moreover, there will be no effect of heat or volume on mixing, if the fluids are treated as ideal. Another assumption is a total lack of interaction between oil and solvent, then oil relative permeability $k_o = kS_o$ and solvent relative permeability $k_s = kS_s$ or $k_o/k_s = (1 - S)/S$ (Koval, 1963).

The Koval model produced a good agreement with the laboratory results of Blackwell et al. (1959) for secondary miscible displacements. Fayers (1988) stated that there is no physical justification for the good agreement between the results of Koval model with Blackwell et al. (1959) measurements for a range of viscosity ratios using the fixed expression for μ_{eff}.

3.5 Todd and Longstaff model

In comparison to Koval's (1962) model, the Todd and Longstaff (1972) model has a single adjustable parameter that measures the degree of mixing between the gas and oil within a gridblock and describes the degree of fingering of solvent through the oil. The model computes effective viscosities for both gas and oil using a mixing parameter, ω value to blend between the original viscosities and the fully mixed viscosity by using the effective viscosity.

The mixing parameter ω is used to determine the properties of the fluid (viscosity μ and density ρ) in the mixing zone between solvent and oil. The mixing parameter can be used in black oil reservoir simulators to model the effect of the viscous fingering (Todd and Longstaff, 1972, Okandan, 1984).

A value of ω = 1 refers to complete mixing within a gridblock of oil and injected gas (solvent). In this case, the injection will be similar to piston like displacement. ω = 0 means that there is no mixing at all or negligible dispersion because the effects of viscous fingering are severe in the system, which is similar to immiscible displacement. When the value of ω is between 0 and 1, it is known as partial mixing. In this case the solvent effective viscosity will be less than the oil effective viscosity (Todd and Longstaff, 1972, Batycky, 1997, Karacaer, 2007). In this case, solvent will travel faster and finger through the oil which create viscous fingering.

The effective viscosity allows the connection of the two phases together by using the mixing parameter, ω (Todd and Longstaff, 1972):

$$\mu_{oe} = {\mu_o}^{1-\omega} * {\mu_m}^{\omega} \tag{3.9}$$

$$\mu_{ge} = {\mu_g}^{1-\omega} * {\mu_m}^{\omega} \tag{3.10}$$

where, μ_{oe} and μ_{ge} are the effective viscosity of the oil and gas respectively. The fully mixed viscosity μ_m is given by the quarter power mixing rule (Todd and Longstaff, 1972):

$$\mu_m = \left(\frac{S_g}{\mu_g^{1/4}} + \frac{1 - S_g}{\mu_o^{1/4}} \right)^4 \tag{3.11}$$

The Todd and Longstaff (1972) model assumes first contact miscibility in a black oil simulator taking into account the effect of viscous fingering. Todd and Longstaff (1972) recommended ω = ⅔ to model viscous fingering in secondary miscible gas injection and to match Blackwell laboratory experiments. Stalkup (1983a) suggested a range of ω values of between 0.5 to 0.7. However, high values of ω as high as 0.8 to 1 have been used (Carlson, 2006). The exact value of ω depends on the size of the gridblock, the mobility of the fluids, and the mobility ratio.

Todd and Longstaff (1972) recommended a value for ω of ⅓ to account for heterogeneity in field scale applications (approximately 10 to 40 acres/well) and relatively low injection rates of secondary miscible displacement.

3.6 2D Numerical simulation of viscous fingering

Christie and Bond (1987) developed a high resolution 2D simulator to simulate the viscous fingering behaviour in two phases, three component flow. The simulator is a higher order finite difference, implicit-pressure explicit-saturation simulator capable of simulating laboratory to kilometre scale secondary and tertiary displacement processes on a detailed enough scale to resolve the growth of viscous fingering (Christie and Bond, 1987, Christie, 1989).

The flow equations in the 2D simulation are based on the following assumptions (Christie, 1987, Christie and Bond, 1987, Christie, 1989):

1. Two-phase flows of water and hydrocarbon.
2. Three components of water, gas and oil.

3. Incompressible fluids.
4. First contact miscibility between solvent and oil
5. Solvent is present in the hydrocarbon phase only.
6. Ideal mixing for oil and solvent densities
7. Quarter power mixing rule for viscosities.

The fluid flow equations in the simulator are solved internally in a dimensionless form using the finite difference method to discretise this system of dimensionless equations. Accuracy and speed are the main requirements for solving the fluid flow equations. The conservation equations are written using the total velocity formulation described by Peaceman and Rachford (1962).

Pressure equation (Christie and Bond, 1987):

$$\nabla.\lambda(c)\nabla\bar{P} + Q_t = 0 \tag{3.12}$$

where $\bar{P}$ is the average pressure $(P_o + P_w)/2$, $\lambda(c) = 1/\mu(c)$ is the mobility, c is the concentration, and $v_t = v_o + v_w$ is the total velocity

Conservation of solvent (Christie and Bond, 1987):

$$\frac{\partial c}{\partial t} + \nabla.vc = \nabla.D\nabla c \tag{3.13}$$

where D is the diffusion/dispersion tensor.

A Flux Corrected Transport (FCT) algorithm is used in the 2D simulator to ensure that the concentration profiles calculated are sharp but non-oscillatory.

To ensure that the simulator can model miscible gas displacements, Christie and Bond (1987) compared the predictions of the simulation with the experiments of Blackwell et al. (1959). Good agreement was obtained for the miscible gas displacement at different mobility ratios. Christie (1989) showed that the percentage of oil recovery against pore volume injected at ω =2/3 was in good agreement with secondary miscible gas experiments. The ability of the simulator to predict viscous fingering in miscible gas displacements has been validated by comparing its predictions with the results from numerous well characterised experiments (Christie and Bond, 1987, Christie, 1989,

Christie et al., 1993, Muggeridge et al., 2002, Al-Shuraiqi, 2005). Christie (1989) also showed that the mixing parameter, ω, needs to be calibrated for water alternating gas (WAG) injection.

3.7 Analytic calibration of ω for SWAG injection

Blunt and Christie (1993) developed an analytical model to calibrate the value of ω for SWAG injection for both secondary and tertiary recovery. They extended the models of Koval (1962), and Todd and Longstaff (1972) to account for viscous fingering in two phase, three component flow. This model was validated by comparison with 2D detailed simulation.

Blunt and Christie (1993) modified the conservation equation to account for viscous fingering in two-phase, three component flow and it is given by (Blunt and Christie, 1993):

$$\emptyset \frac{\partial S_h(x)}{\partial t} + \frac{\partial F(S,c) v_t}{\partial x} = 0 \tag{3.14}$$

where, $S_h(x)$ is the hydrocarbon phase saturation and v_t is the total velocity. The conservation equation of solvent is given by (Blunt and Christie, 1993):

$$\emptyset \frac{\partial S_h(x) c(x)}{\partial t} + \frac{\partial c(x) F(S,c) v_t}{\partial x} = 0 \tag{3.15}$$

where, $c(x)$ is the solvent concentration in the hydrocarbon phase. $F(S,c)$ is the hydrocarbon phase fractional flow and given by the equation (Blunt and Christie, 1993):

$$F(S,c) = \frac{\lambda_h(S,c)}{\lambda_h(S,c) + \lambda_w(S)} \tag{3.16}$$

where λ_h and λ_w are the mobility of the hydrocarbon and water phase respectively, it is defined as the phase relative permeability divided by the phase mobility, and given by the equation (Christie, 1987, Christie, 1989, Blunt and Christie, 1993):

$$\lambda_h(S,c) = k_{ro(S)}/\mu_h \tag{3.17}$$

$$\lambda_w(S) = k_{rw}(S)/\mu_w \tag{3.18}$$

The hydrocarbon phase viscosity μ_h is determined by the quarter power mixing rule (Christie, 1987, Christie, 1989, Blunt and Christie, 1993):

$$\mu_h = \left(\frac{1-c}{\mu_o^{0.25}} + \frac{c}{\mu_s^{0.25}}\right)^{-4} \tag{3.19}$$

They used Todd and Longstaff's solvent fractional flow $f^{TL}(c)$ given by:

$$f^{TL}(c) = \frac{c}{c + (1-c)/M_{eff}} \tag{3.20}$$

In this case, the effective viscosities of oil and solvent will change gradually with the solvent concentration variation. This fractional flow means that the leading edge of the fingering moves at a speed $v = df/dc|_{c=0} = M_{eff}$, while the trailing edge has a speed $v = df/dc|_{c=1} = 1/M_{eff}$

The spreading of the solvent front is controlled by the mobility difference between the injected and the displaced fluid compositions. The mobility ratio contrast is caused by the composition of the injected fluids, as well as the viscosities of the solvent, water and oil. They generated a special graph (Figure 3.2) by plotting μ_{eff} as a function of the saturation on the right-hand side S_{right}, when the solvent concentration $c = 0$ and for various saturation on the left-hand side S_{left} when $c = 1$ using the following equation:

$$M_{eff} = \frac{S}{F(S,0)} \left.\frac{\partial F(S,0)}{\partial S}\right|_{S=S_{right}} \tag{3.21}$$

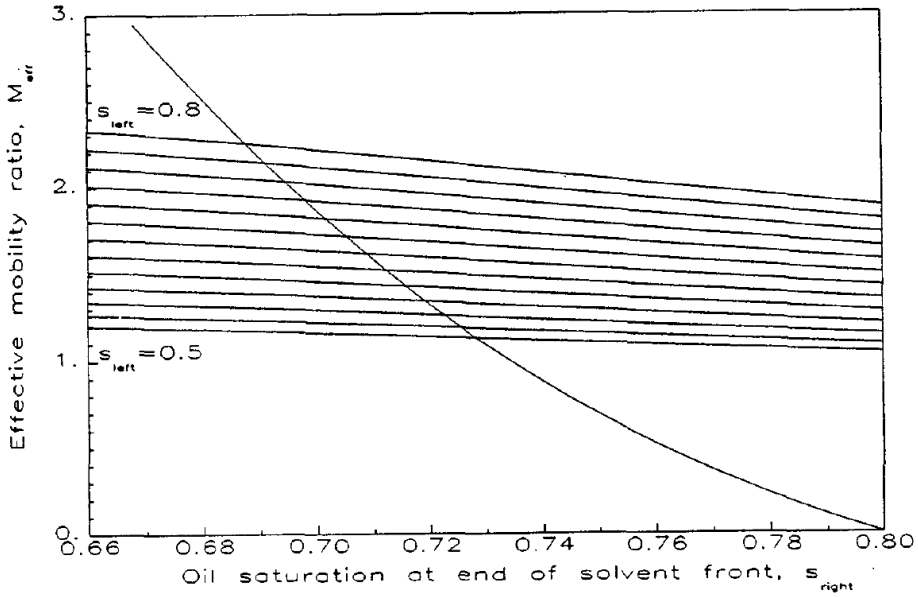

Figure 3.2 Two expressions for the effective mobility ratio for three component flow. μ_{eff} as a function of S_{right} when the solvent concentration is equal to zero. μ_{eff} as a function of S_{left} when the solvent concentration is equal to 1. After (Blunt and Christie, 1993)

Equation (3.22) gives the value of M_{eff} that is consistent with the spreading front of solvent. Therefore, the solution to this equation is calculated by replacing the mobility ratio in the Koval's equation with the following:

$$M_{eff} = \left(0.78 + 0.22\left(\frac{\lambda_t(S_{left}, c=1)}{\lambda_t(S_{right}, c=0)}\right)^{0.25}\right)^4 \tag{3.22}$$

where λ_t is the total mobility $\lambda_t = \lambda_h + \lambda_w$, and λ_h, λ_w is the hydrocarbon and water mobility respectively. S_{left} is the oil saturation at the trailing edge of the solvent front where the solvent concentration is equal to 1, $\lambda_t(S_{left}, c=1) = (k_{rw}/\mu_w) + (k_{ro}/\mu_s)$ and S_{right} is the oil saturation at the leading edge of the solvent front where the solvent concentration is equal to zero, $\lambda_t(S_{right}, c=0) = (k_{ro}/\mu_o)$ (Blunt and Christie, 1993).

Multiple values of M_{eff} are possible depending on the saturation of the oil before or after the solvent front. ω is analytically calculated by using the equation:

$$\omega = 1 - (log\ M_{eff}/log\ M) \tag{3.23}$$

where M is the viscosity ratio $M = \mu_o/\mu_s$.

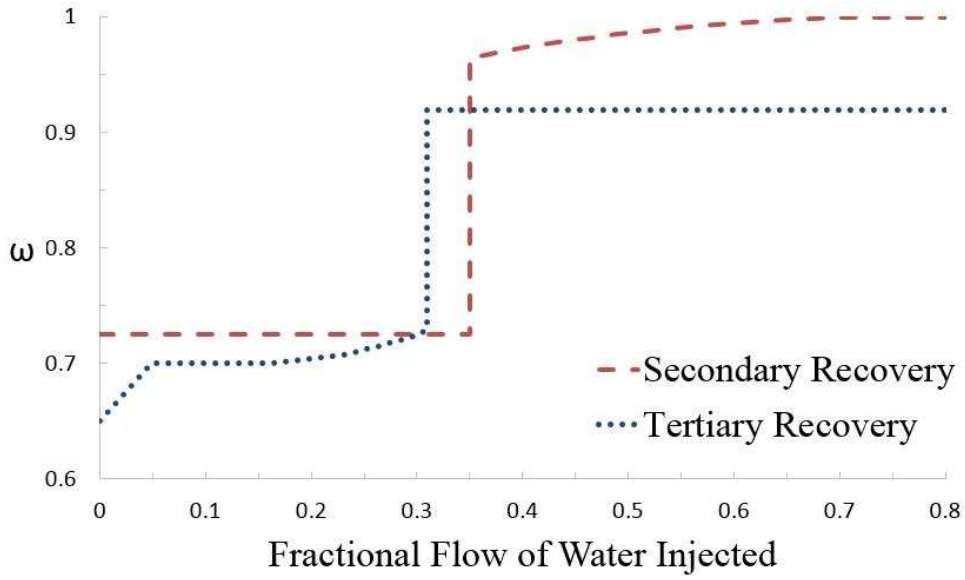

Figure 3.3 Recalibration of ω of SWAG injection for secondary and tertiary displacement (Blunt and Christie, 1993)

Blunt and Christie (1993) showed analytically for SWAG injection that ω varies depending on the fractional flow of injected water for both secondary and tertiary displacement as shown in Figure 3.3. The calibration of ω was limited to SWAG injection because it is difficult to perform analytical solutions for periodic WAG injection. As this work was limited to SWAG injection only, there is a need to calibrate the value of ω for finite-sized slug WAG injection for field-scale application.

3.8 Summary of the chapter

This thesis focused on reviewing the Blackwell et al. (1959) experiment and the models that have been calibrated against this experimental study as they represent the basis of this research and it is not possible to examine and encompass every study in detail.

Blackwell's et al. (1959) experiment has become the main reference for many of the key numerical works on miscible gas injection such as Peaceman and Rachford (1962), Koval (1963), Todd and Longstaff (1972), Christie and Bond (1987) and Blunt and Christie (1993) as the study provides a complete set data for the input parameters and results.

Peaceman and Rachford (1962) developed an initial mathematical model of partial differential equations for numerical simulation of unidirectional miscible displacement.

However, their pioneering attempt at such a simulation failed as it was dominated by numerical errors and also led to a misconception in the literature of petroleum engineering that fingering instabilities were caused because of permeability heterogeneities only. Christie and Bond (1987) later showed the triggering of viscous fingering by mobility ratio difference in addition to the permeability heterogeneity.

Koval (1963) developed an empirical solution to predict the behaviour of unstable miscible displacement in porous media taking into account heterogeneity of permeability. This model can predict the oil recovery and solvent cut as a function of the pore volumes of solvent injected. Koval chose the effective viscosity such that the results from the model matched those of the Blackwell experiment, which have been used by Blunt and Christie to calibrate the value of the Todd and Longstaff mixing parameter.

The Todd and Longstaff (1972) model assumes first contact miscibility in a black oil simulator taking into account the effect of viscous fingering. They recommended a value for the mixing parameter, $\omega = ⅔$ to model viscous fingering in secondary miscible gas injection and they recommended a value for ω of ⅓ to account for heterogeneity in field scale applications and relatively low injection rates of secondary miscible displacement.

Christie and Bond (1987) developed a high resolution 2D simulator to simulate the viscous fingering behaviour in two phases, three component flow. The simulator type is a higher order finite difference, implicit-pressure explicit-saturation simulator capable of simulating laboratory to kilometre scale secondary and tertiary displacement processes on a detailed enough scale to resolve the growth of viscous fingering. This 2D simulator has been used in this research to initiate viscous fingering for finite sized slug WAG injection.

Blunt and Christie (1993) developed an analytical model to calibrate the value of ω for SWAG injection for both secondary and tertiary recovery. They showed analytically that for SWAG injection the ω value varies depending on the fractional flow of injected water for both secondary and tertiary displacement. The calibration of ω was limited to SWAG injection because it is difficult to perform analytical solutions for periodic WAG

injection. As their work was limited to SWAG injection only, their work is extended here to calibrate the value of ω for finite-sized slug WAG injection for field-scale application

Chapter 4

Calibration the mixing parameter’s value for viscous fingering for varying WAG ratios, slug sizes and recovery type

4.1 Introduction

This chapter presents the results for the calibration of the mixing parameter, ω, value using a 1D numerical model. This is a refinement and extension of previous work on the recalibration of ω for SWAG injection by Blunt and Christie (1993), accounting for finite-sized slug WAG injection.

The ω value can be used to represent sub grid block viscous fingering in a reservoir simulator that has an explicit permeability field. Here it is hypothesized that the Todd and Longstaff model can describe the viscous fingering of the solvent in two-phase, three-component flow. The theory is based on the construction of a numerical solution to the system of component conservation laws in one dimension, which include empirical expressions for the mixing parameter value.

This chapter covers the 1D model for calibration of ω (including the assumptions made and the mathematical formulation), the workflow of calibrating ω against the 2D simulator (mentioned in section 3.6), and finally discusses the results. The results cover the impact of the aspect ratio on the 1D numerical modelling and the validation of the model by comparing the results from the 1D numerical model against the analytical results for both secondary and tertiary recovery. The results for the calibration of ω for finite-sized slug WAG injection for secondary and tertiary recovery are then presented and compared with the effect of different viscosity ratio, different grid block size, and different variance to trigger the viscous fingering.

4.2 1D Numerical model assumptions and mathematical formulation

This is a refinement and extension of previous work on the recalibration of the mixing parameter ω for SWAG injection (Blunt and Christie, 1993). The theory is based on the construction of a numerical solution to the system of component conservation laws in one dimension, which include empirical expressions for the ω value to be calibrated for miscible finite sized slug WAG (FSS WAG) injection.

The flow equations have been solved numerically in a 1D model to take into account the Todd and Longstaff mixing parameter, using the following assumptions (Christie, 1989):

1. Two-phase flows of water and hydrocarbon.
2. Three components of water, gas and oil.
3. Incompressible fluids (the fluid density is constant).
4. First contact miscibility between solvent and oil, and they are present in the hydrocarbon phase only.
5. Rule of quarter power mixing for viscosities.
6. Gravity effects are ignored.
7. Capillary pressure between the phases is neglected or zero.
8. There is no physical diffusion or dispersion.
9. The effect of relative permeability hysteresis is ignored (hysteresis appears in changes of the relative permeability curve's shape and values of residual fluid saturation. It arises due to continuous saturation changes of the injection fluids in three-phase flows and leads to gas entrapment).
10. The relative permeability curves are a function of water saturation

Darcy's law has been modified empirically by including the relative permeability to describe how one phase flows in the presence of another phase (Aarnes et al., 2007). If two immiscible fluids flow through a porous medium, then the ability of one phase to move depends on the environment at that location, which is the relative permeability of one phase that depends on the saturation of the phases at that specific location. Relative permeability is defined as a quantity (fraction) that describes the impairment amount to flow of one phase on another. In the two-phase Darcy law, it depends on the water

saturation S_w (since $S_w + S_o = 1$). If one interprets the fluid relative permeabilities to be a function of the normalised water saturation *S*, given by the equation:

$$S^* = \frac{S_w - S_{wc}}{1 - S_{or} - S_{wc}} \tag{4.1}$$

where S_w is the water saturation, S_{wc} is the connate water saturation and S_{or} is the residual oil saturation. The relative permeabilities are given by the equations (Christie, 1989):

$$k_{ro}(S) = k_{ro}^{'}(1 - S^*)^2 \tag{4.2}$$

$$k_{rw}(S) = k_{rw}^{'}(S^*)^2 \tag{4.3}$$

where $k_{ro}(S)$ and $k_{rw}(S)$ is the oil and water relative permeability with respect to water saturation. k'_{ro} and k'_{rw} are the end point of oil and water relative permeability respectively. $S^*$is the normalised water saturation and is given by the equation (Christie, 1989, Li and Horne, 2006):

11. The effects of permeability variations are neglected. The empirical fractional flow could be used to represent sub grid block viscous fingering in a reservoir simulator which has an explicit permeability field.
12. Simplified thermodynamical systems (the injected gas mixes with oil in all proportions to form a single hydrocarbon phase) that can be approximated by a first contact miscibility model. Because modelling multi-contact miscibility involves calculations of the thermodynamic phase equilibria for the mixture of the reservoir fluids and the injected gas. This scenario can be achieved in practice if the gas is injected above the minimum miscibility pressure (Juanes and Lie, 2005).

The physical instability causing viscous fingering in the 1D model is driven by the adverse viscosity ratio across a fluid front. This viscosity contrast is affected by the oil and solvent viscosities. It is hypothesized here that the Todd and Longstaff model can describe the viscous fingering of the solvent in two-phase, three component flow.

The oil and solvent effective viscosities and the fully mixed viscosity are given by the equations (Todd and Longstaff, 1972, Christie, 1987, Christie, 1989, Blunt and Christie, 1993):

$$\mu_m = \left(\frac{c}{\mu_s^{0.25}} + \frac{1-c}{\mu_o^{0.25}}\right)^{-4} \tag{4.4}$$

$$\mu_{oe} = {\mu_o}^{1-\omega}\, {\mu_m}^{\omega} \tag{4.5}$$

$$\mu_{se} = {\mu_s}^{1-\omega}\, {\mu_m}^{\omega} \tag{4.6}$$

An effective equation of fractional flow of solvent:

$$f^{TL}(c) = \frac{c}{c + ((1-c)/M_{eff})} \tag{4.7}$$

M_{eff} is calculated using the equations (4.5) and (4.6) to take the effect of the Todd and Longstaff's mixing parameter as follows:

$$M_{eff} = \frac{\mu_{oe}}{\mu_{se}} = \frac{{\mu_o}^{1-\omega}\, {\mu_m}^{\omega}}{{\mu_s}^{1-\omega}\, {\mu_m}^{\omega}} = \left(\frac{\mu_o}{\mu_s}\right)^{1-\omega} \tag{4.8}$$

Therefore, the effective equation of fractional flow that considers the effect of the mixing parameter is given by:

$$f^{TL}(c) = \frac{c}{c + ((1-c)/(\mu_o/\mu_s)^{1-\omega})} \tag{4.9}$$

In this case, the viscosities of oil and solvent will change gradually with the mixing parameter variation. By adding $f^{TL}(c)$ to the conservation equation to account for the mixing parameter value as follows:

$$\varphi \frac{\partial S(i)\, c(i)}{\partial t} + v_t \frac{\partial f^{TL}(c)\, F(S,c)}{\partial x} = 0 \tag{4.10}$$

In this equation, the physics are changed to account for solvent viscous fingering into the oil in the hydrocarbon phase, and to take the effect of the mixing parameter. Therefore, the WAG ratio and the slug size in the numerical solution will change the viscosity ratio and thus affect the value of ω.

4.3 Workflow of calibrating ω value using the 1D Numerical

The 2D simulator (Christie, 1987) (section 3.6) is used to model the viscous fingering in a line drive and to calibrate the values of ω from the 1D model. The numerical methods

used in this simulator have been fully described by Christie (1989) and have been mentioned in chapter three and will not be described here.

The outputs from the 2D simulations in a line drive are the solvent concentration and the water saturation profiles. To allow comparison between the 1D model and the 2D simulation, the average 1D response from the 2D simulation is calculated by averaging the 2D profiles along *y*-direction (perpendicular to the flow direction). The average profile is fairly smooth as a factor of distance and is taken over several fingers in the system. The finger region spread linearly with time and the spreading rate increased with the mobility ratio.

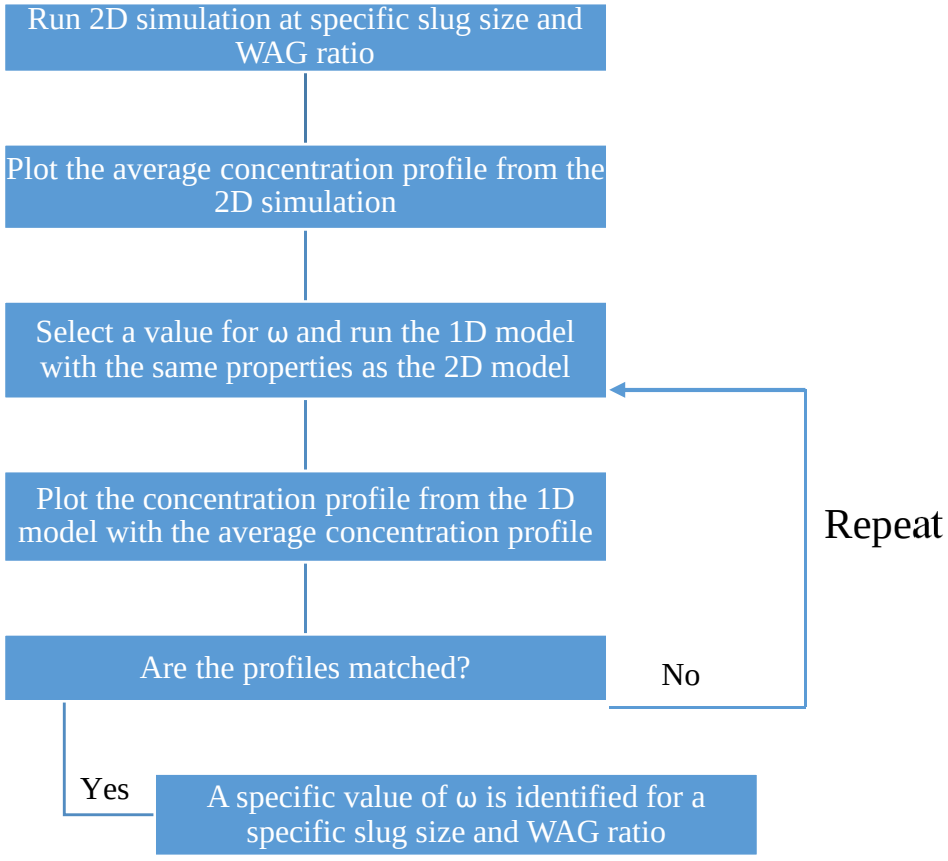

Figure 4.1 The workflow *ω* value calibration for finite slug size WAG ratio

Figure 4.1 shows a simple flow chart describing how *ω is calibrated in the 1D model for finite-sized slug WAG ratio against the 2D simulator.*

1. The value of *ω* in the 1D model is adjusted to achieve the best match between the solvent concentration profiles obtained from the 1D model and the average solvent

concentration profile obtained from the 2D simulation in a line drive.

2. The profile from the 1D model was plotted with the profile from the 2D simulation and the sample standard deviation is calculated between the two profiles using the equation $\sqrt{\frac{1}{N-1}\sum_{i=1}^{N}(x_2 - x_1)^2}$

3. If the profiles matched with the least error (sample standard deviation), then a value of ω is identified for a specific WAG ratio, slug size and type of recovery. If the profiles were not matched, then a new value for ω is selected and the process is repeat from step 2.

4.4 Results from the 1D Model

The 2D simulations were performed using a 375×150 grid, while the 1D simulations were performed using 375 grid blocks with a grid aspect ratio of 1:1. The distance and time in both models are dimensionless.

The fluid properties and relative permeability are given in Table 4.1 (Blunt and Christie, 1993, Al-Haboobi et al., 2017). The oil-solvent viscosity ratio was 10:1. The permeabilities in the 2D simulation were chosen from uncorrelated stochastic Log-Normal distribution with a variance of 1%, which is appropriate to trigger the viscous fingering within a few grid blocks of the injector. Figure 4.2 shows the permeability distribution in the *x*- and *y*-direction and the wells location.

Table 4.1 Fluid properties that has been used in the calibration of the value of ω

Oil Viscosity, μ_o	4 cp
Water Viscosity, μ_w	1 cp
Solvent Viscosity, μ_g	0.4 cp
Connate water saturation, S_{wc}	0.2
Residual oil saturation, S_{orw}	0.4
Oil relative permeability	$k_{ro}(s) = \left(\frac{1 - S - S_{or}}{1 - S_{wc} - S_{or}}\right)^2$
Water relative permeability	$k_{rw}(s) = \left(\frac{S - S_{wc}}{1 - S_{wc} - S_{or}}\right)^2$

In the 2D simulator, the injector well was located and completed in the grid blocks (BLX=1, BLY=1 to BLX=1 and TRY=NY=150) and the producer was located and completed in the grid blocks (TRX= NX=375, BLY= 1 to TRX= NX=375 and TRY=NY=150), = (375, 1 to 375, 150).

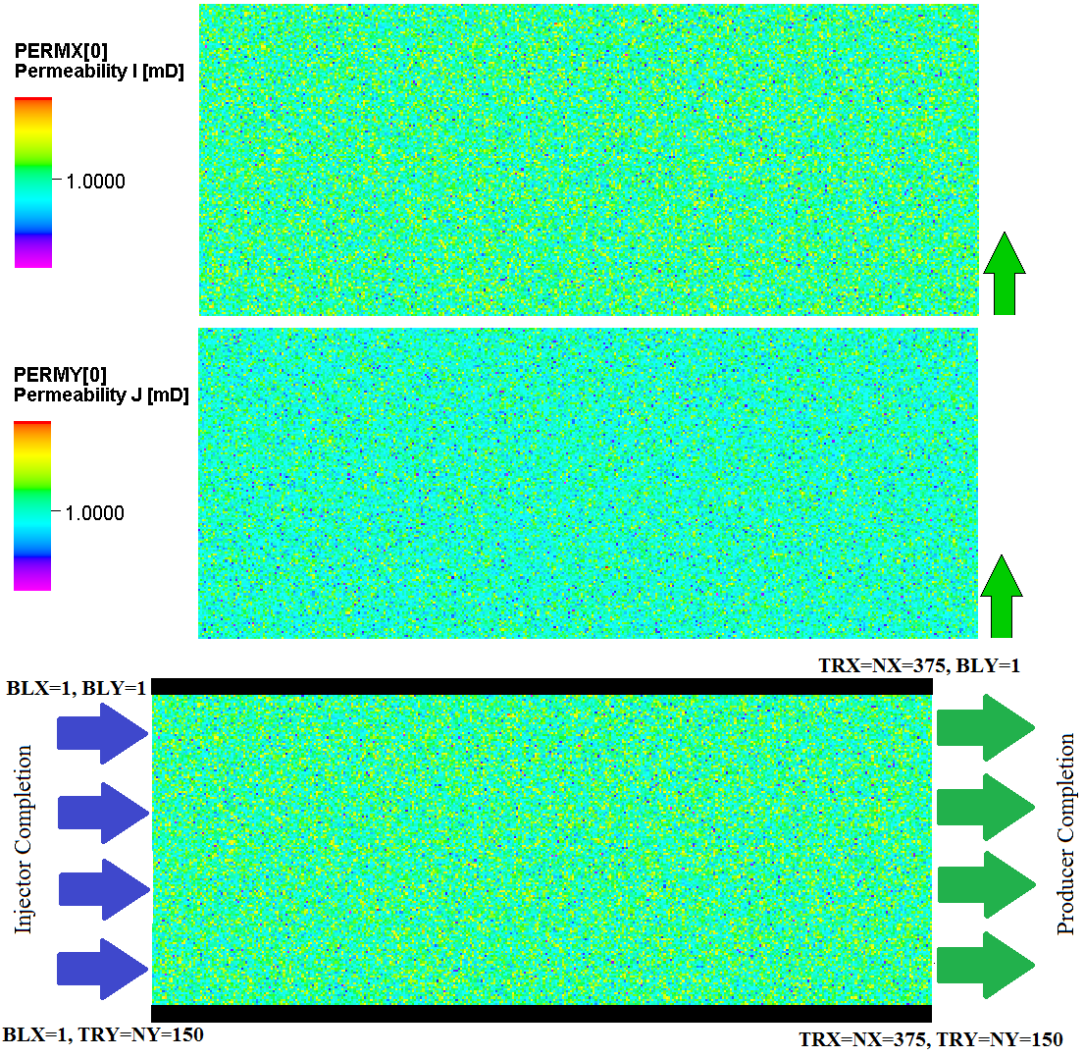

Figure 4.2 Permeability distribution in the *x*- and *y*-direction using uncorrelated stochastic Log-Normal distribution with a mean of 1 and a standard deviation of 1% to trigger the viscous fingering

4.5 The effect of the number of grid blocks on the calibration of ω

A grid refinement study was performed to observe the effect that the number of grid blocks has on the calibration of ω. This was done for a secondary miscible gas displacement. This is performed to determine the effect of numerical diffusion in the 1D model because of the grid discretisation. It is necessary to ensure that the numerical

diffusion is small in the 1D model and that the viscous fingering is triggered due to physical instability rather than numerical diffusivity, otherwise, it would have an effect on the calibration of ω for the finite-sized slug WAG injection.

For the results presented here, a large number of grid blocks ranging from 100×50 to 1000×500 were used, with an aspect ratio of 2:1 over the same area. Using a uniform finite difference scheme the solution is recovered from the numerical equations and the error became smaller as the grid size is refined (Lax and Richtmyer, 1956). As the grid size decreased (became finer), the value of ω decreased until it stabilised on one value.

Figure 4.3 shows the average solvent concentration profile after 0.3 PVI for different grid sizes along the *x*-direction. As the gridblock size is refined, the average 2D solvent concentration profiles started to converge to each other and became consistent.

The value of ω is calibrated for each average 2D solvent concentration profile at their specific grid block size. It is found that the average 2D solvent concentration profiles converged under fine grid blocks and had the same value of $\omega = 0.67$, meaning that under grid refinement, the mixing parameter's value returned to the Todd and Longstaff value and there is no effect of the numerical diffusion in the 1D model. Therefore, viscous fingering in the 1D model is triggered due to the viscosity difference between the solvent and oil. Figure 4.4 shows the average 2D solvent concentration profile that converged under grid refinement with the 1D solvent concentration profile where the value of the mixing parameter $\omega = 0.67$.

Figure 4.5 plots the calibrated ω value for secondary miscible displacement against grid size. The value of ω decreased as the grid refinement increased in the *x*-direction until it stabilised on the value 0.67. Under this level of refinement where the average 2D solvent concentration profile converges, the size of the fine grid blocks no longer has a significant effect on the value of ω.

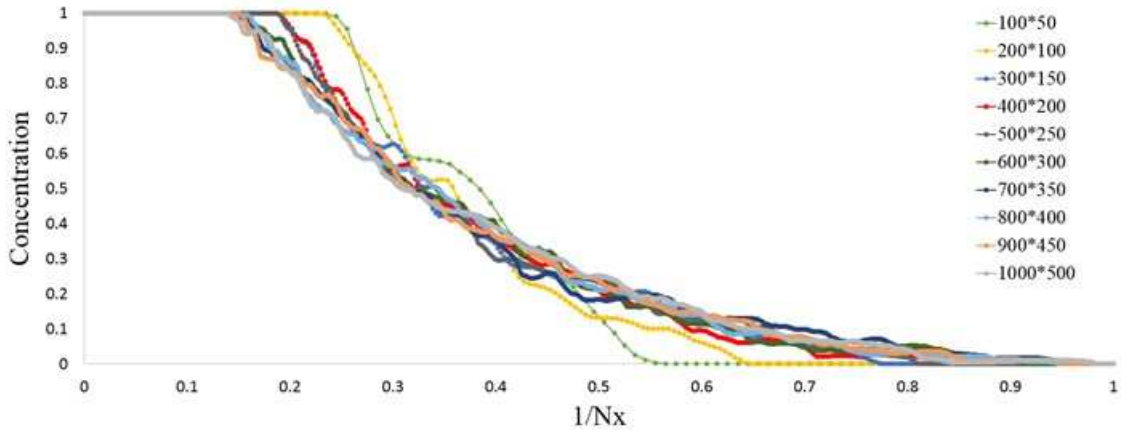

Figure 4.3 The average solvent concentration profile after 0.3 PVI at different grid sizes, where 1/Nx is the number of grid blocks along the *x*-direction in a one unit dimension, to make the comparison at different grid sizes comparable. As the grid size is made finer, the average 2D solvent concentration profiles started to converge under this grid refinement.

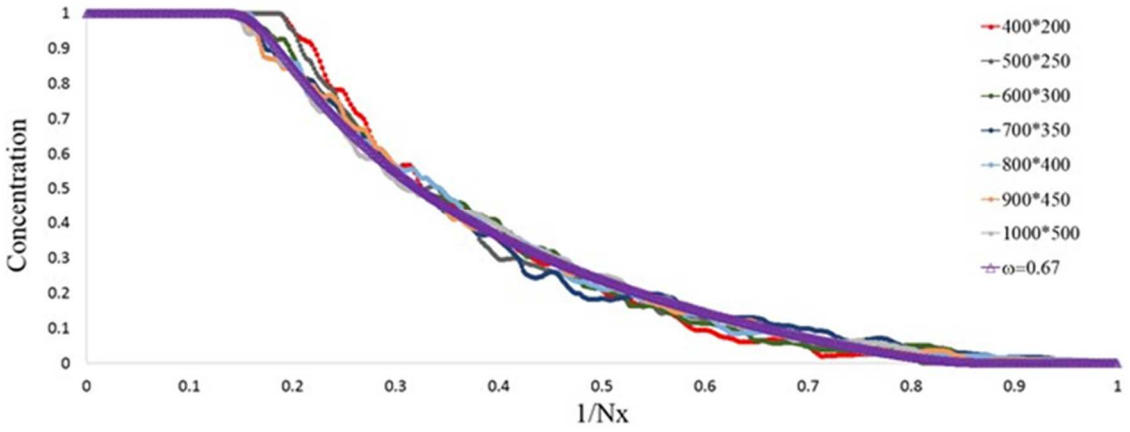

Figure 4.4 The average 2D solvent concentration profile convergence under grid refinement with the 1D solvent concentration profile where the value of the mixing parameter ω = 0.67. When the value of ω is calibrated for each solvent concentration profile at their specific grid size, it is found that the solvent concentration profiles that converged under the grid refinement had the same value of ω = 0.67.

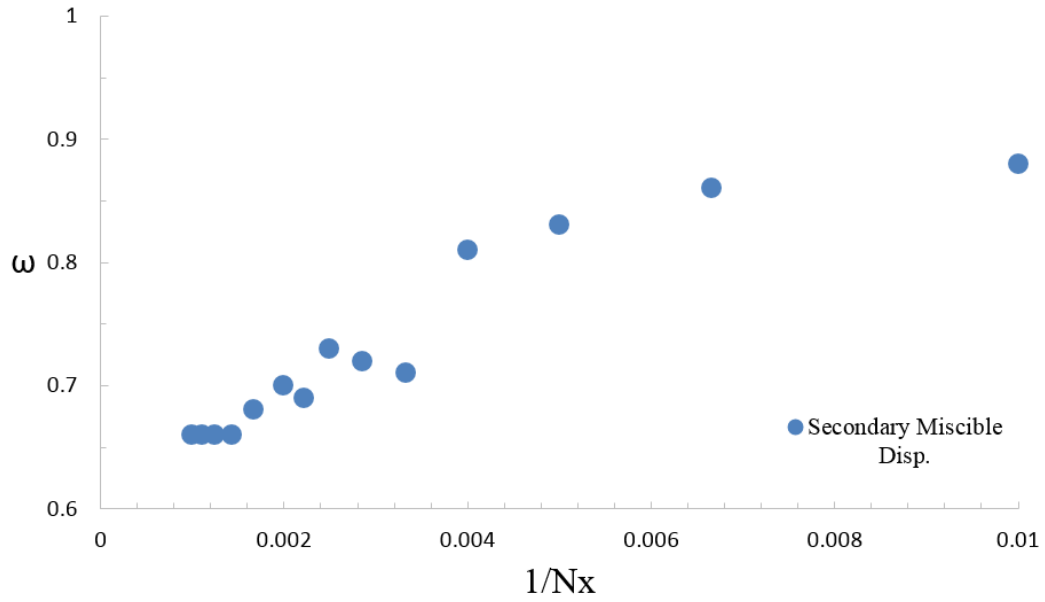

Figure 4.5 The effect of grid size on ω for secondary miscible injection, where Nx is the number of gridblocks along the *x*-direction. The value of ω decreased as the grid size is getting finer until it stabilised at 0.66. At this level of refinement, where the solvent concentration profiles converge, a fine sized grid no longer has a significant effect on the value of ω.

4.6 Matching the analytical calibration of ω for SWAG injection

Both analytical and numerical results can be significant, and the extent of the significance is measured by their reliability. Analytical solutions are exact, but may be impossible to find, and numerical solutions are approximate but can be determined more readily via computational methods. Numerical solutions, if formulated appropriately, should converge to the analytical solution under the same conditions. Analytical results are deterministic, while numerical model results may vary and can't be taken as a fundamental for further research. Therefore, in general, fundamental research in any domain is based on analytical results. In practice every numerical model should be tested against an analytical solution where the answer is known, to validate that the numerical model is functioning as intended. A well validated numerical model gives more confidence in later applications against partial differential equations where there are no analytical results. Therefore, the results obtained from the 1D numerical model, and presented herein, were validated against Blunt and Christie's analytical results.

Since Blunt and Christie performed their analytical calibration using a grid size 375×150, which is the largest grid size they could simulate at that time, the current numerical

calibration is carried out on the same grid size to make it possible to compare the results from the 1D numerical model with the analytical results. It is possible to use the same assumptions in a manner to compare results obtained in two different ways. The fluid properties used were the same as those used in the previous work and are summarized in Table 4.1.

Provided herein are different examples of ω calibration for SWAG injection. The examples start with matched velocity SWAG injection for both secondary and tertiary recovery, followed by secondary 1:1 SWAG injection and tertiary 1:9 SWAG injection. These examples were chosen because the numerical calibration for ω value is exactly the same as the value of ω from the analytical calibration of Blunt and Christie (1993). The fact that the value ω from the numerical calibration did not match the analytical calibration will be explained separately.

4.6.1 Secondary matched velocity (MV) SWAG injection

The optimum stabilization of fingering is obtained when water and solvent travel at the same speed by using the matched velocity of water and solvent, as shown in Figure 4.6 (Stalkup, 1983a). MV decreases the apparent mobility contrast between solvent and oil, which helps to minimise the viscous fingering so that a good displacement and high sweep can be achieved.

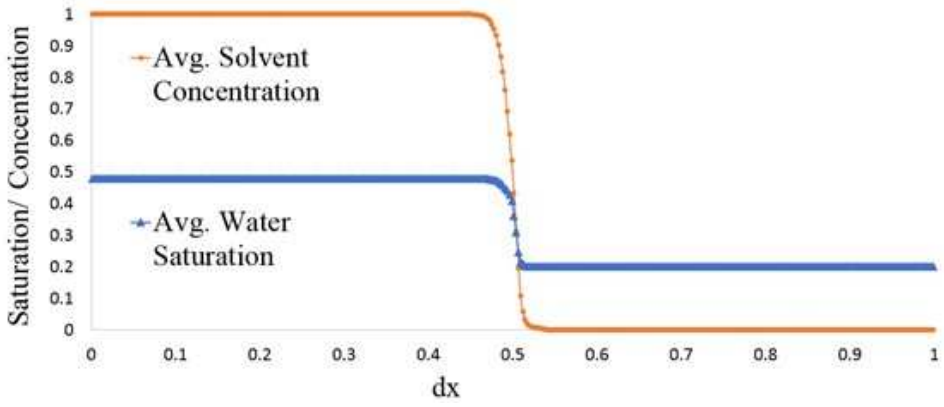

Figure 4.6 Matched velocity WAG ratio where solvent and water travels at the same speed. dx is a dimensionless distance (Nx/L)

Stalkup (1983a) used many simplifying assumptions in his model: a homogenous reservoir, simultaneous injection of gas and water, solvent-water and oil-water relative

permeabilities were the same, and no gravity segregation took place during the displacement. He proposed the following equation for solvent and water injection to travel at the same speed:

$$\frac{f_w^* - f_{wi}}{S_w^* - S_{wi}} = \frac{1 - f_w^*}{1 - S_w^*} \tag{4.11}$$

where, f_w^* = water fractional flow in the solvent/water region. S_w^* = water saturation in the solvent/water region, fraction PV. f_w is calculated using the equation:

$$f_w = \frac{\lambda_w}{\lambda_w + \lambda_h} \tag{4.12}$$

where, $\lambda_h = k_{ro}/\mu_s$. Stalkup (1983a) solved this equation graphically, as shown in Figure 4.7, by plotting f_w against S_w and then drawing a line from point A (at $f_w = 1, S_w = 1$) to the initial point B (at f_{wi}=0 and $S_w = S_{wi}$). Therefore, the solution for f_w^* and S_w^* will be the intersection of the solvent/water fractional flow curve with the straight-line AB. The MV WAG ratio is given by ($f_w^*/(1 - f_w^*$)).

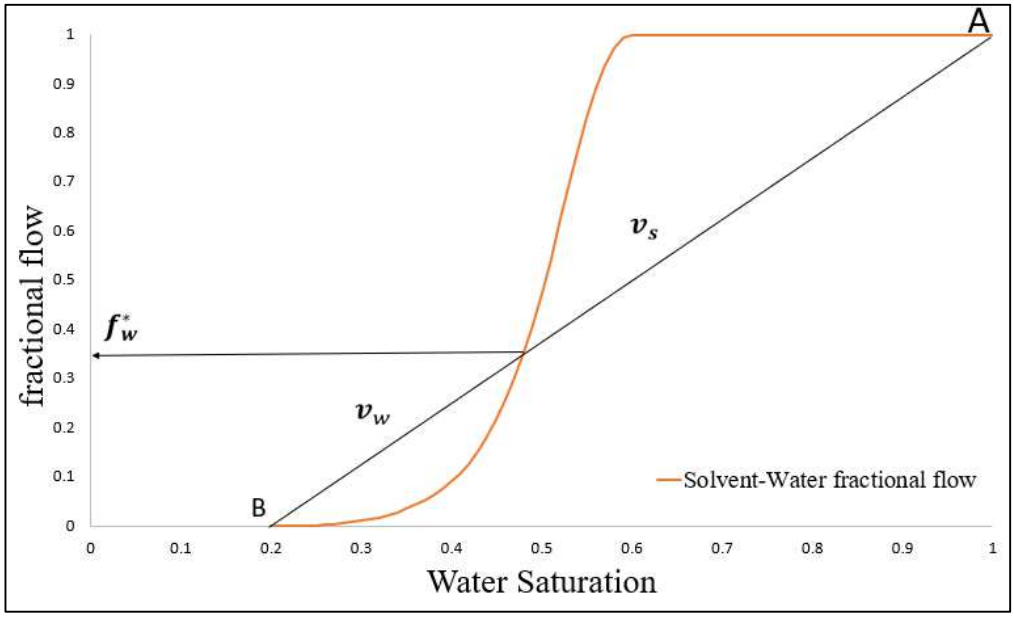

Figure 4.7 An example of Stalkup's method to estimate the matched velocity WAG ratio using Table 4.1. f_w^* is the fraction of water at which the water velocity v_w matching the solvent velocity v_s.

The reasons to select matched velocity flow (Stalkup, 1983a) are:

1. If the water is injected at a low rate, the solvent front will travel faster than the water front, which leads to solvent bank ahead of the solvent/water zone. The mobility ratio of the solvent/oil bank is the viscosity ratio between oil and solvent, and leads to solvent fingers through the oil, as shown in Figure 4.8.

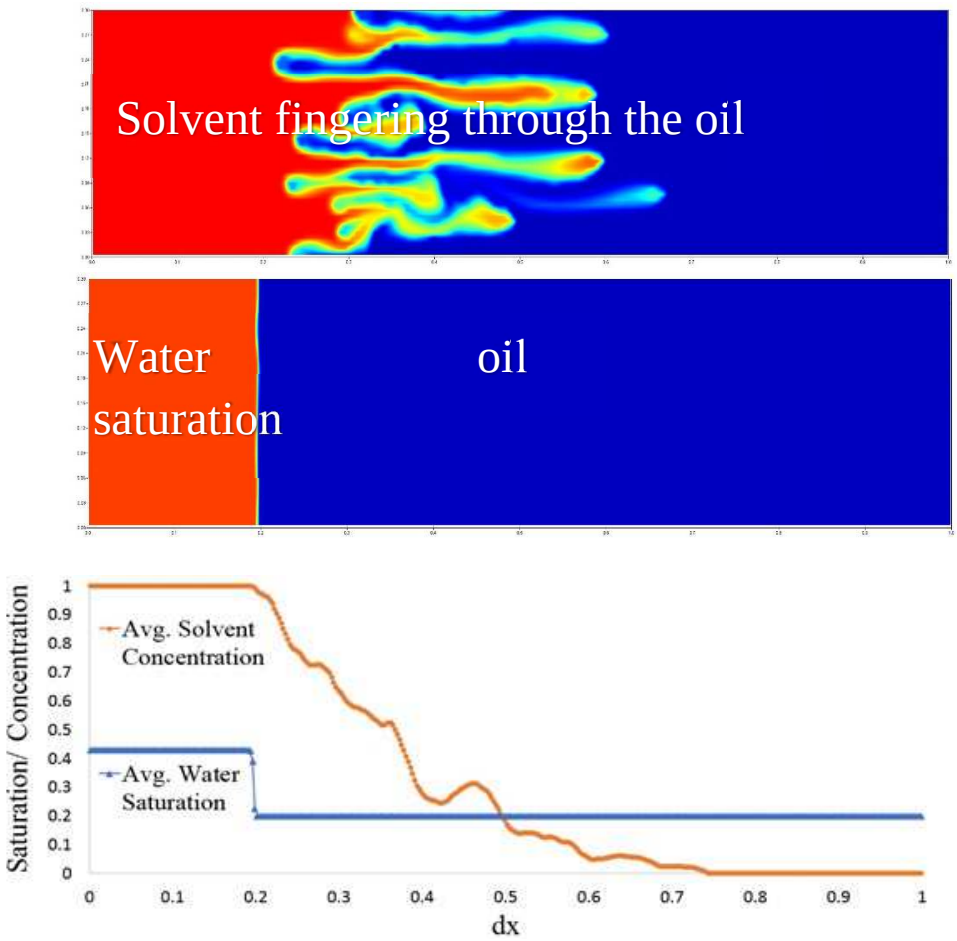

Figure 4.8 Average 2D water saturation and solvent concentration profiles of under-injecting water. The solvent is traveling faster than the water and it is fingering through the oil. dx is a dimensionless distance (Nx/L)

2. If the water is injected at high rate, the water front will travel faster than the solvent. This leads to a high-water saturation at the solvent/oil front, as shown in Figure 4.9. This water can trap some of the oil at the oil bank.

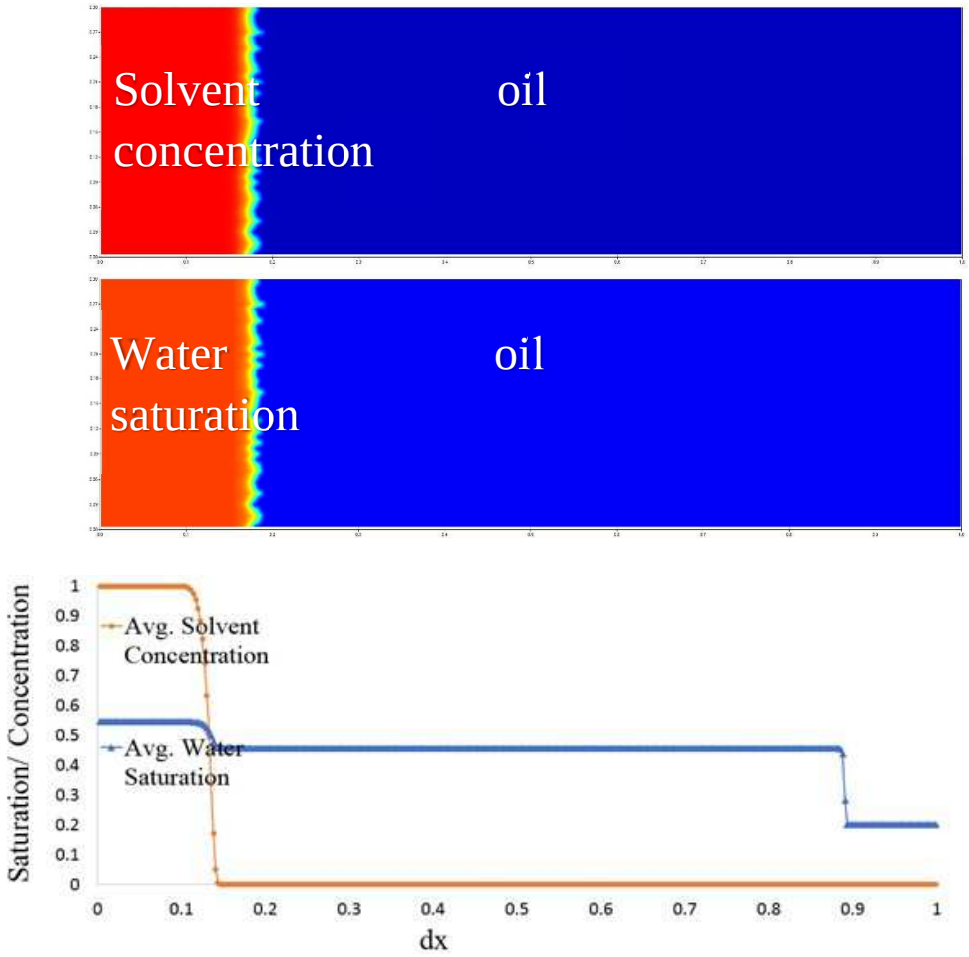

Figure 4.9 Average 2D water saturation and solvent concentration profiles of over-injecting water. The water is travelling faster than the solvent and leads to a high-water saturation at the solvent/oil front. dx is a dimensionless distance (Nx/L)

For the fluid properties in Table 4.1 and from Figure 4.7, the matched velocity of water and solvent has a fractional flow of 0.35. Figure 4.10 shows a high stabilisation of viscous fingering for the secondary MV SWAG injection in the 2D simulations. The value of ω from the 1D model was calibrated against the 2D simulation, by adjusting the value of ω to get a good match between the profiles from the 1D and the 2D (Figure 4.11). Since there is a high stabilisation of the fingering by MV SWAG injection, the numerical calibration of ω is equal to 1. Figure 4.11 is the 2D simulation of water saturation distribution of MV SWAG after 0.4 PVI and Figure 4.12 represents the best match between the water saturation profiles computed from the 1D model and the average water saturation profiles from the 2D simulation for secondary displacement for MV SWAG after 0.4 PVI .

The value of ω is checked at different realisations by generating five different realisations to the one that is used in the calibration to confirm that the results were not due to stochastic variability. The numerical calibration of ω for five different realisations resulted in the same value of ω = 1.

However, the value of ω for secondary MV SWAG injection from the numerical calibration is slightly higher than the value of ω from the analytical calibration (where ω = 0.97) by about 0.03. If the value of ω is calculated analytically using the Blunt and Christie (1993) method:

1. Calculate the mobility ratio in the left-hand side $\lambda_t(S_{left}, c = 1) = (k_{rw}/\mu_w) + (k_{ro}/\mu_s) = 0.35$
2. Calculate the mobility ratio in the right-hand side $\lambda_t(S_{right}, c = 0) = (k_{ro}/\mu_o) = 0.25$
3. Calculate M_{eff} using the equation $M_{eff} = \left(0.78 + 0.22\left(\frac{\lambda_t(S_{left}, c=1)}{\lambda_t(S_{right}, c=0)}\right)^{0.25}\right)^4 =$ 1.079
4. Then, using the equation $\omega = 1 - (log\ M_{eff}/log\ M)$ a value for ω of 0.97 is obtained.

which is the same value as Blunt and Christie (1993) analytical calibration for the secondary MV SWAG injection. By plotting the solvent concentration profile at ω = 1 with the solvent concentration profile at ω = 0.97 against the 2D average solvent concentration profile, it can be seen that ω = 1 gave a better match than ω = 0.97 between the solvent concentration profile from the 1D and the 2D as shown in Figure 4.11

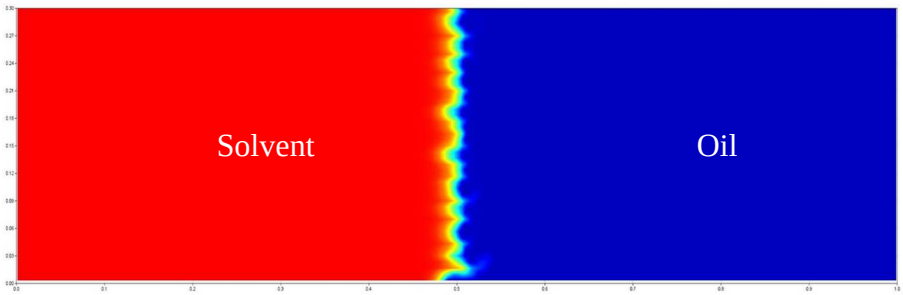

Figure 4.10 2D simulation of solvent concentration distribution for MV SWAG after 0.4 PVI

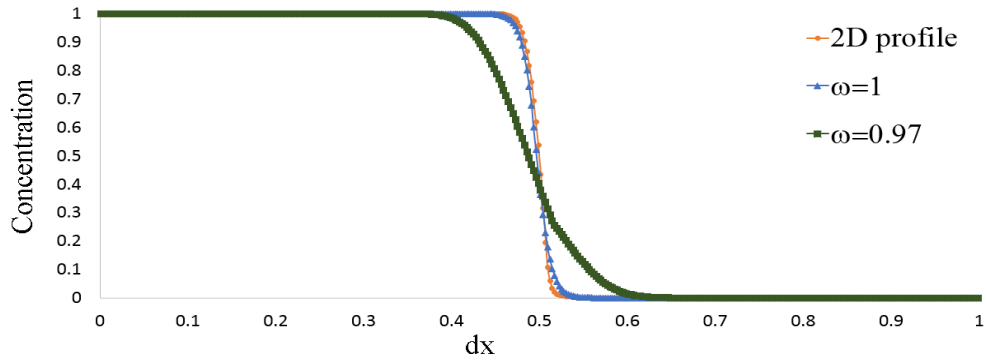

Figure 4.11 The solvent concentration profiles computed from the 1D model at ω = 1 and ω = 0.97, and the average solvent concentration profiles from the 2D simulation for secondary displacement for MV SWAG after 0.4PVI. The figure shows clearly that there is a better match between the 1D solvent concentration profile and the average 2D solvent concentration profile at ω = 1 than at ω = 0.97. dx is a dimensionless distance (Nx/L)

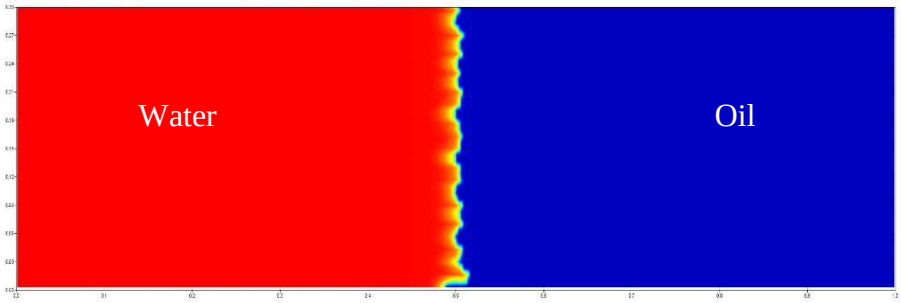

Figure 4.12 2D simulation of water saturation distribution of MV SWAG after 0.4 PVI

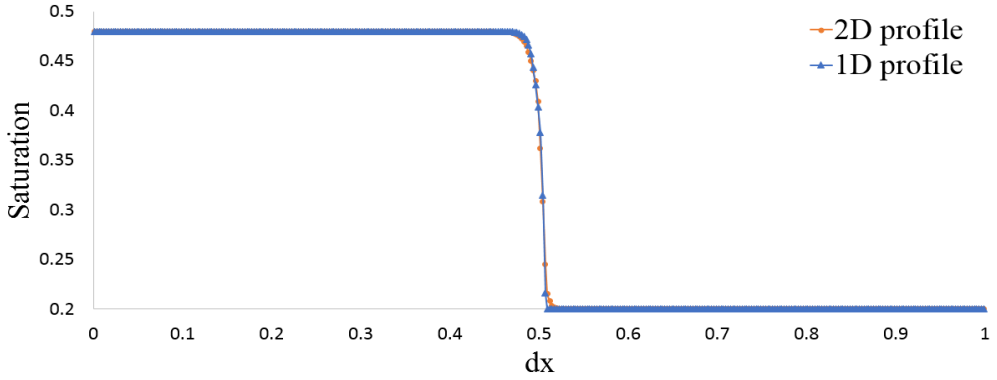

Figure 4.13 The best match between the water saturation profiles computed from the 1D model and the average water saturation profiles from the 2D simulation for secondary displacement for MV SWAG after 0.4 PVI

4.6.2 Tertiary Matched Velocity (MV) SWAG injection

The tertiary WAG recovery is when water and solvent are injected into the reservoir which has already been flooded with water. Therefore, the initial saturation in the tertiary recovery is 1-S_{or}, while the initial saturation in the secondary recovery is S_{wc}.

The front of tertiary MV SWAG (fractional flow of 0.35) injection is unstable compared to secondary MV SWAG injection, as shown in Figure 4.14. The fingers in the system have an effect on the mixing between the solvent and the oil, which resulted in a ω of 0.92 to yield the best match between the 1D solvent concentration profile and the average 2D solvent concentration profile (Figure 4.15). This is very low compared to secondary MV SWAG injection, but it is the same value as that calibrated analytically by Blunt and Christie. Figure 4.16 is the 2D simulation of water saturation distribution of tertiary MV SWAG after 0.3 PVI and Figure 4.17 is the best match between the water saturation profiles computed from the 1D model and the average water saturation profiles from the 2D simulation for tertiary displacement for MV SWAG after 0.3 PVI

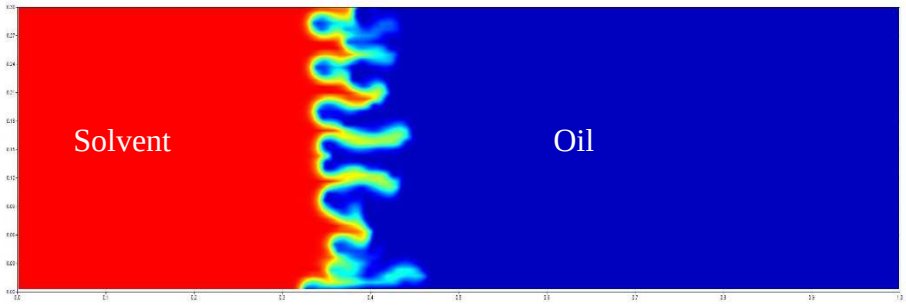

Figure 4.14 2D simulation of solvent concentration distribution of tertiary MV SWAG after 0.3PVI

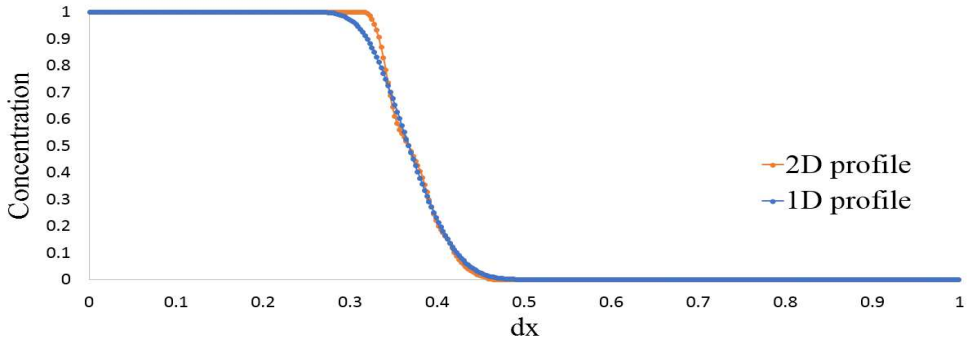

Figure 4.15 The best match between the solvent concentration profiles computed from the 1D model and the average solvent concentration profiles from the 2D simulation for tertiary MV SWAG injection after 0.3 PVI

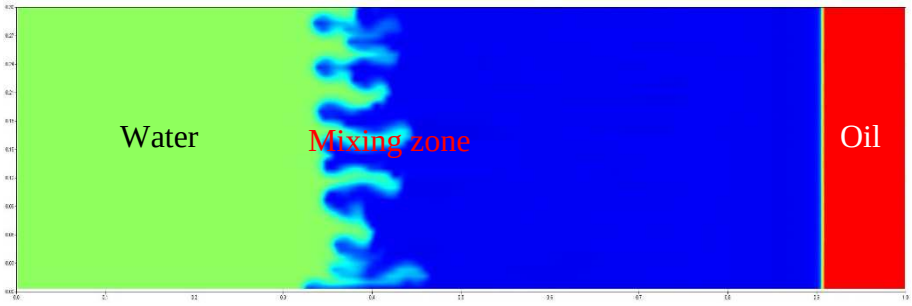

Figure 4.16 2D simulation of water saturation distribution of tertiary MV SWAG after 0.3 PVI

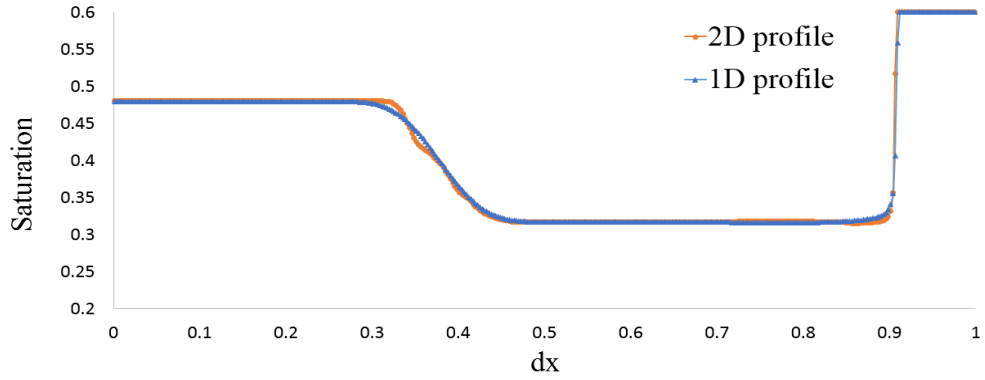

Figure 4.17 The best match between the water saturation profiles computed from the 1D model and the average water saturation profiles from the 2D simulation for tertiary displacement for MV SWAG after 0.3PVI

4.6.3 Secondary 1:1 SWAG injection

Another example of ω calibration for secondary 1:1 SWAG injection is detailed below. 1:1 SWAG injection (fractional flow of water injected is 0.5) is an over injection of water compared to MV SWAG injection (the fractional flow of water injected is 0.35) and did not completely stabilize fingering (Figure 4.18). This viscous fingering affected the mixing between solvent and oil and reduced the value of ω to 0.985 for the best match between the 1D profile and the average 2D profile (Figure 4.19). Figure 4.20 is the 2D water saturation profile of secondary 1:1 SWAG injection after 0.4 PVI and Figure 4.21 is the best match between the water saturation profiles computed from the 1D model and the water saturation profiles from the 2D simulation for secondary displacement of 1:1 SWAG at ω = 0.985.

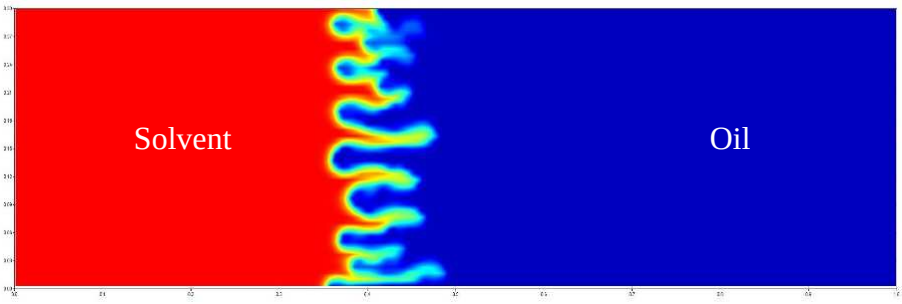

Figure 4.18 2D solvent concentration of secondary 1:1 SWAG injection after 0.4 PVI

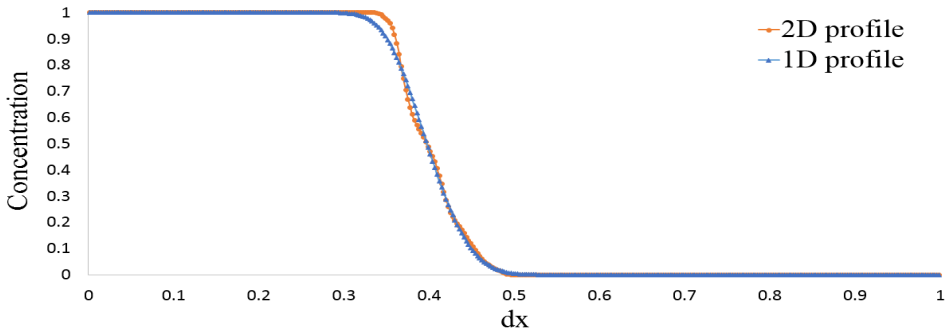

Figure 4.19 The best match between the solvent concentration profiles computed from the 1D model and the solvent concentration profiles from the 2D simulation for secondary displacement of 1:1 SWAG where ω = 0.985

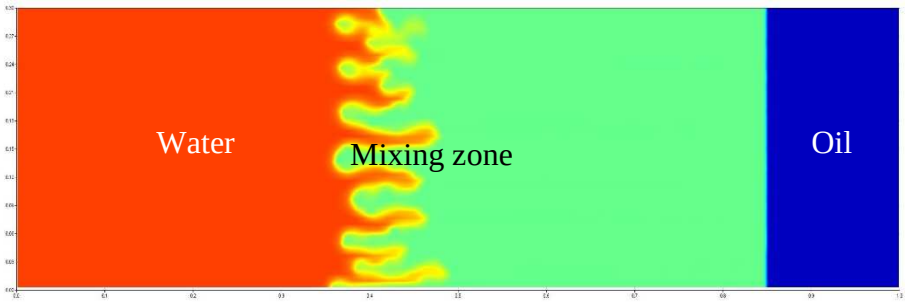

Figure 4.20 2D water saturation of secondary 1:1 SWAG injection after 0.4 PVI

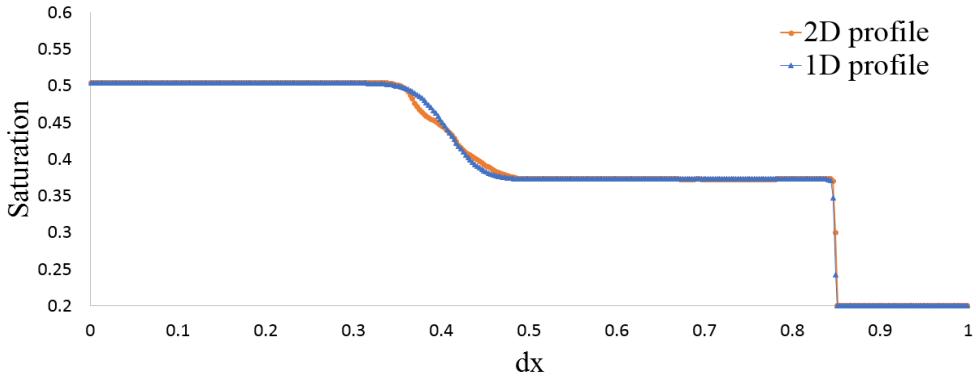

Figure 4.21 The best match between the water saturation profiles computed from the 1D model and the water saturation profiles from the 2D simulation for secondary displacement of 1:1 SWAG at ω = 0.985

4.6.4 Tertiary 1:9 SWAG Injection

The calibration of ω for tertiary 1:9 SWAG injection is detailed below as an example for the tertiary recovery. 1:9 SWAG injection is an over injection of gas and there were lots of fingers in the system at 0.3 PVI, as shown in Figure 4.22. Those fingers reduce the mixing parameter value to 0.7 (Figure 4.23). Figure 4.24 is the 2D water saturation profile

of tertiary 1:9 SWAG injection after 0.3 PVI and Figure 4.25 is the 1D water saturation profile at ω = 0.7 with the average 2D water saturation profile.

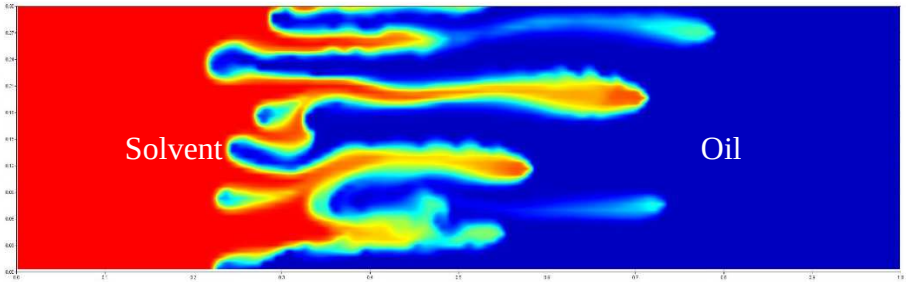

Figure 4.22 2D solvent concentration of tertiary 1:9 SWAG injection after 0.3 PVI

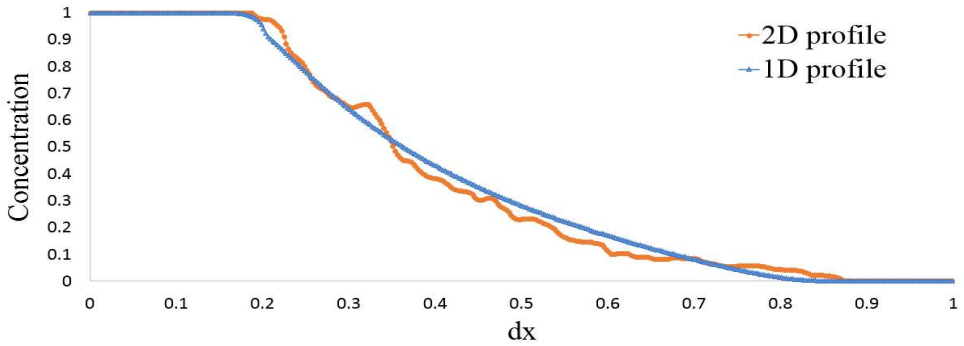

Figure 4.23 The best match between the solvent concentration profiles computed from the 1D model and the solvent concentration profiles from the 2D simulation for tertiary displacement of 1:9 SWAG where ω = 0.7

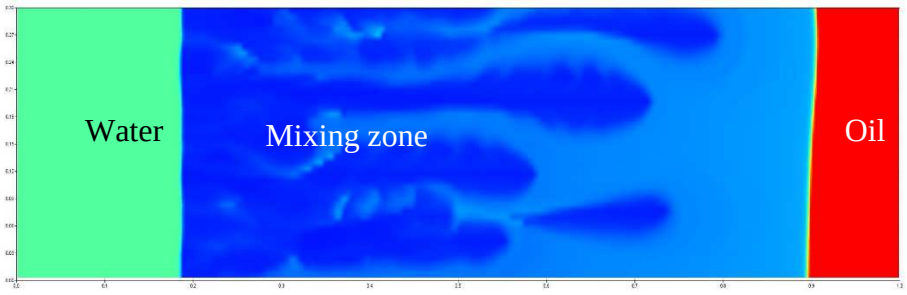

Figure 4.24 2D water saturation of tertiary 1:9 SWAG injection after 0.3 PVI

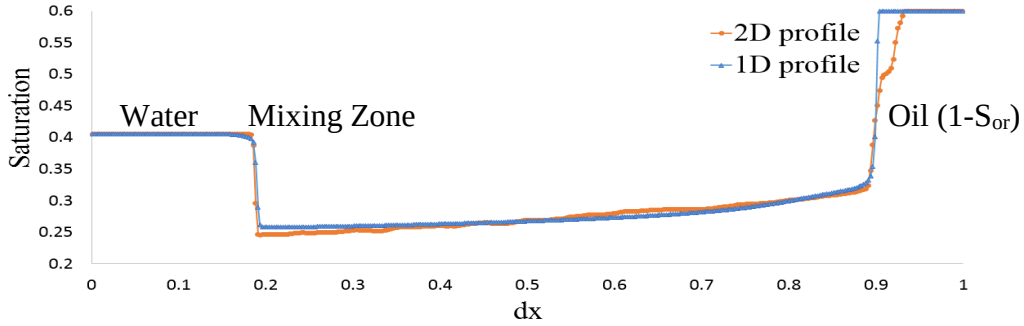

Figure 4.25The best match between the water saturation profiles computed from the 1D model and the water saturation profiles from the 2D simulation for tertiary displacement of 1:9 SWAG at ω = 0.7

4.7 Results from numerical calibration of ω for different SWAG ratios for both secondary and tertiary recovery

The results of ω calibration for SWAG injection from the numerical model were validated against the analytical results of Blunt and Christie (1993) for SWAG injection for both secondary and tertiary recovery (Figure 4.26). The numerical results were in good agreement with the analytical results for different SWAG injection for both secondary and tertiary displacement. This gave confidence in the results from the numerical model by comparing them to known and understood results from an analytical study, before moving onto the calibration of ω for finite-sized slug WAG injection.

There are some points from the numerical results that did not have a good match with the analytical results as shown in the highlighted points in Figure 4.26, the reasons for which are given in the next section.

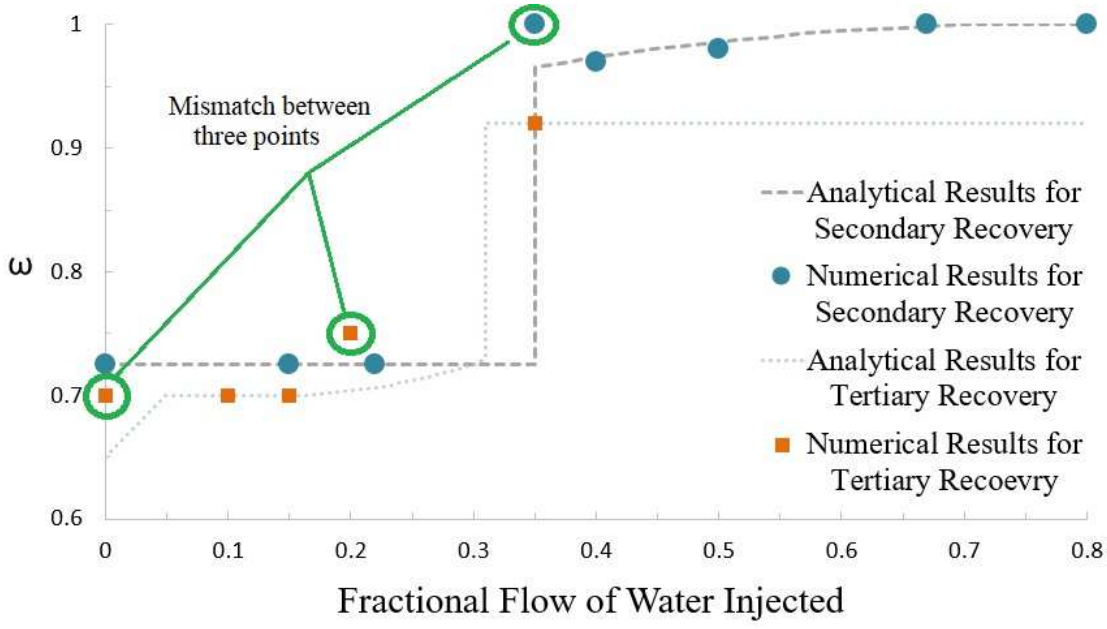

Figure 4.26 The predicted values of ω as a function of SWAG ratio for secondary and tertiary displacement on grid size 375×150. The numerical results showed a good match with Blunt and Christie analytical results for SWAG at different FWINJ.

4.8 The mismatch of ω value between the numerical calibration and the analytical calibration for SWAG injection

From Figure 4.26, there were 3 points in the numerical calibration that did not match the analytical calibration. Those points were secondary MV SWAG injection, tertiary miscible gas injection (fractional flow of water injected 0) and tertiary 1:4 SWAG injection (fractional of water injected 0.2).

The mismatch between the values of ω from the numerical results and the analytical results for secondary MV SWAG injection have been discussed previously (section 4.6.1).

For tertiary miscible gas injection, Figure 4.28 shows clearly that there is a better match between the 1D solvent concentration profile and the average 2D solvent concentration profile (computed from Figure 4.27) at ω = 0.7 than at ω = 0.65, as is suggested by Blunt and Christie. It is similarly the case with tertiary 1:4 SWAG injection.

Figure 4.30 shows a better match between the 1D solvent concentration profile and the average 2D solvent concentration profile (computed from Figure 4.29) at ω = 0.76 than at ω = 0.7, again suggested by Blunt and Christie.

This mismatch in the tertiary recovery results comes from the assumption of how to calculate μ_{eff} for a tertiary SWAG ratio less than the tertiary MV SWAG ratio. Blunt and Christie calculated μ_{eff} for the tertiary SWAG ratio (which is tertiary 1:4 SWAG injection with f_w = 0.2 and tertiary miscible gas injection with f_w = 0) less than the tertiary MV SWAG ratio (which has f_w = 0.35) from the special graph they created in their paper (Figure 3.2). It is believed that this is the reason why there are discrepancies in some of the values of ω between the numerical values and the analytical values for tertiary recovery.

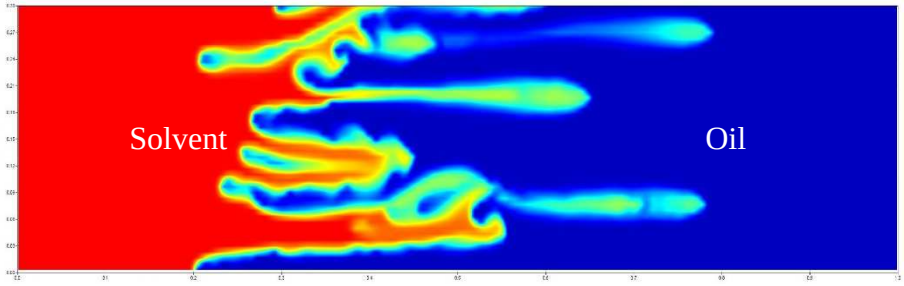

Figure 4.27 2D water saturation of tertiary miscible gas injection after 0.3 PVI

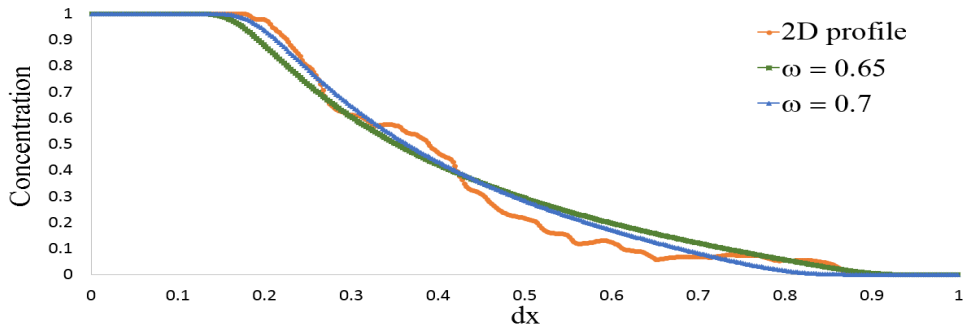

Figure 4.28 The solvent concentration profiles computed from the 1D model at ω = 0.7 and ω = 0.65, and the average solvent concentration profiles from the 2D simulation for tertiary miscible gas injection. The figure shows that there is a better match between the 1D solvent concentration profile and the average 2D solvent concentration profile at ω = 0.7 than at ω = 0.65.

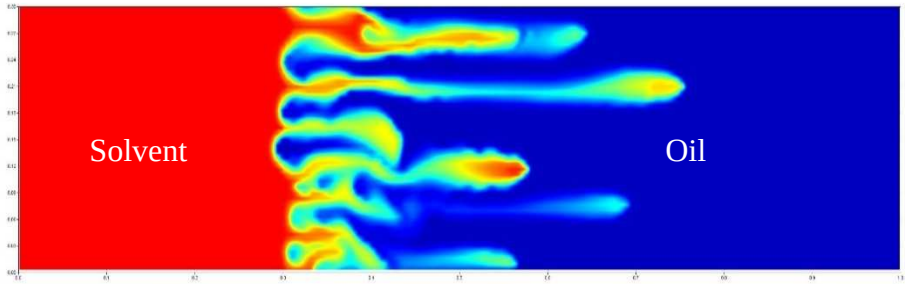

Figure 4.29 2D water saturation of tertiary 1:4 SWAG injection after 0.3 PVI

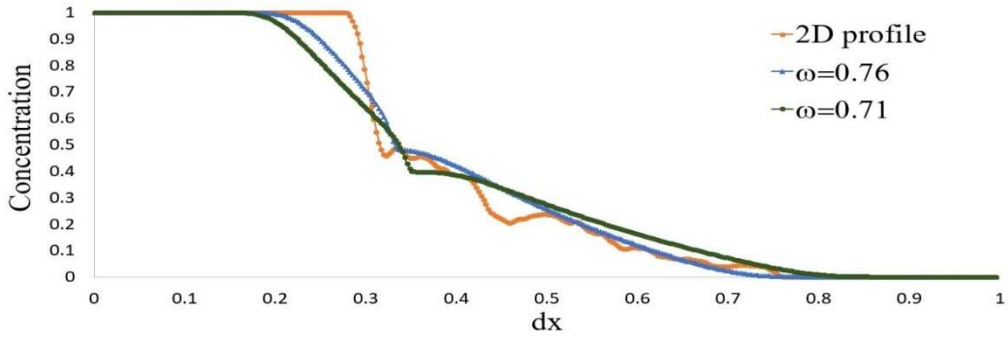

Figure 4.30 The solvent concentration profiles computed from the 1D model at ω = 0.76 and ω = 0.71, and the average solvent concentration profiles from the 2D simulation for tertiary 1:4 SWAG injection. The figure shows that there is a better match between the 1D solvent concentration profile and the average 2D solvent concentration profile at ω = 0.76 than at ω = 0.71.

4.9 Tertiary SWAG ratio higher than the MV SWAG ratio

For tertiary recovery, Blunt and Christie assumed that the ω value for any SWAG ratio higher than the MV SWAG ratio will be the same value as that for the MV SWAG ratio *i.e.* $\omega = 0.92$. This assumption is derived from the fact that the tertiary MV SWAG ratio gave a very small amount of fingering in the examples they considered (Figure 4.31). Figure 4.32 shows the best match at the value of $\omega = 0.92$ between the solvent concentration profiles computed from the 1D model and the average solvent concentration profiles from the 2D simulation for tertiary displacement of tertiary MV SWAG injection.

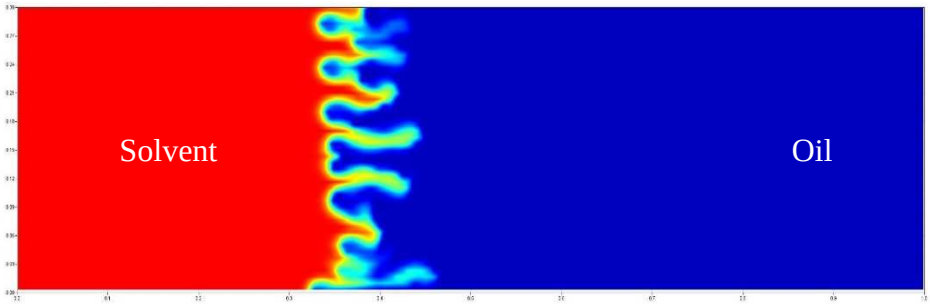

Figure 4.31 2D solvent concentration of tertiary MV SWAG injection after 0.3 PVI.

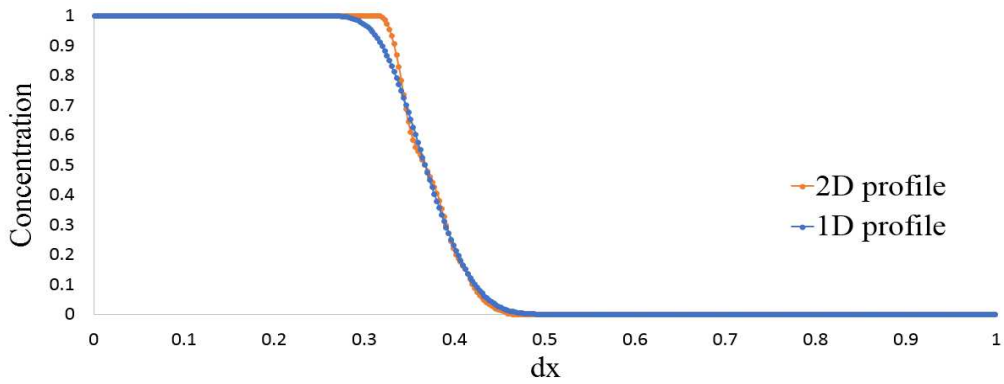

Figure 4.32 The best match between the solvent concentration profiles computed from the 1D model and the average solvent concentration profiles from the 2D simulation for tertiary displacement of MV SWAG where the value of ω is 0.92

It is suggested by Blunt and Christie that one could attempt an iterative procedure to find the values of ω for any SWAG injection higher than the MV SWAG injection and that attempted here.

Herein are some examples of tertiary SWAG injection with a fractional flow higher than the MV SWAG injection with fractional flow of 0.35.

4.9.1 Tertiary 1:1 SWAG injection

Tertiary 1:1 SWAG injection (fractional flow 0.5) is an over injection of water compared to tertiary MV SWAG injection (fractional flow 0.35). Figure 4.33 and Figure 4.35 show that there is less viscous fingering in this system compared to tertiary MV SWAG injection. The ω for tertiary 1:1 SWAG injection is 0.96, higher than the ω value of tertiary MV SWAG injection *i.e.* 0.92. On the other hand, if ω = 0.96 and ω = 0.92 are plotted with the average solvent concentration, as shown in Figure 4.34 and Figure 4.36, it is possible to see that there is a good match between the solvent concentration profile and the average solvent concentration at these values of ω.

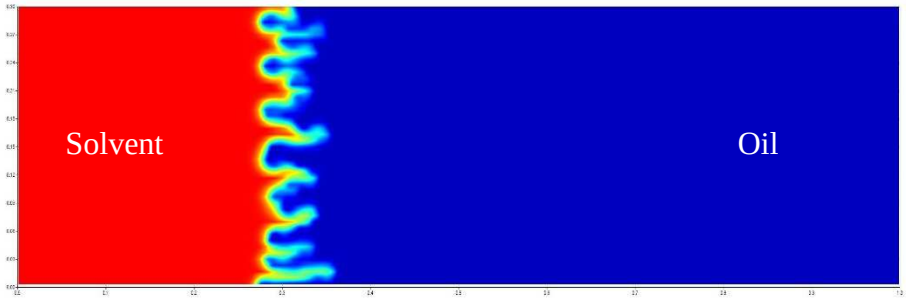

Figure 4.33 2D solvent concentration of tertiary 1:1 SWAG injection after 0.3 PVI.

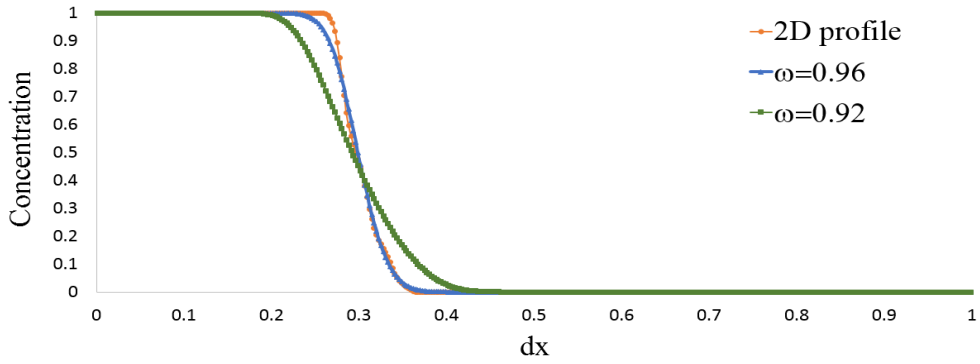

Figure 4.34 The best match between the solvent concentration profiles computed from the 1D model and the average solvent concentration profiles from the 2D simulation for tertiary 1:1 SWAG injection. ω = 0.96 gave a better match between the 1D solvent concentration profile and the average 2D solvent concentration profile than ω = 0.92.

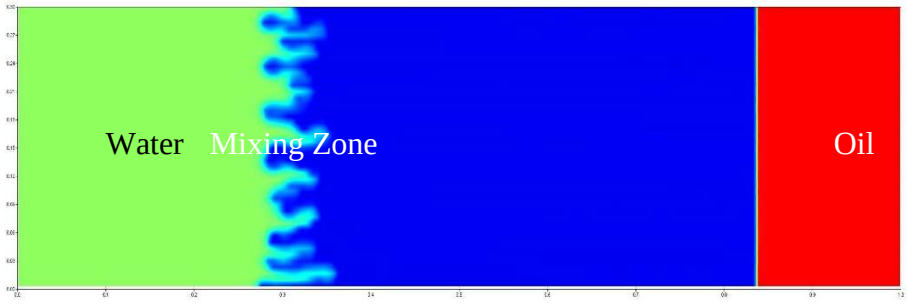

Figure 4.35 2D water saturation of tertiary 1:1 SWAG injection after 0.3 PVI.

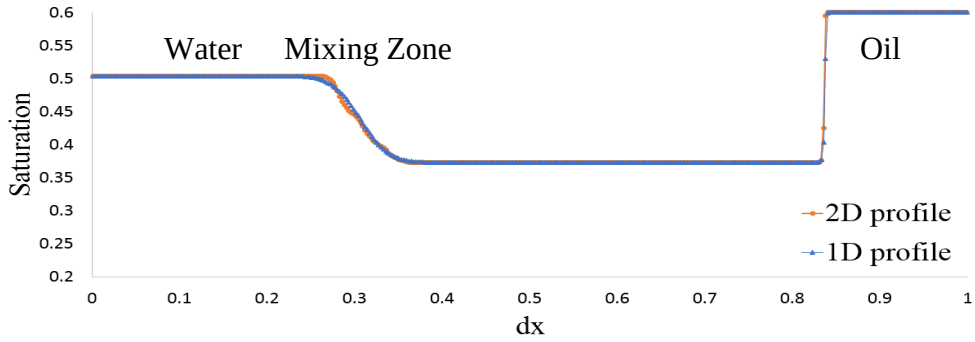

Figure 4.36 The best match between the water saturation profiles computed from the 1D model and the average water saturation profiles from the 2D simulation for tertiary 1:1 SWAG injection

4.9.2 Tertiary 2:1 SWAG injection

Another example of tertiary 2:1 SWAG injection (fractional flow 0.65), which is higher than tertiary MV SWAG injection (fractional flow 0.35), is presented. Figure 4.37 shows that there is less fingering in the system compared to tertiary MV SWAG injection. Even though there are tiny fingers in the system, the value of ω is equal to 1. Again, if ω = 1 and ω = 0.92 are plotted with the average solvent concentration (Figure 4.38), there is a better match between the solvent concentration profile and the average solvent concentration at ω = 1 than at ω = 0.92.

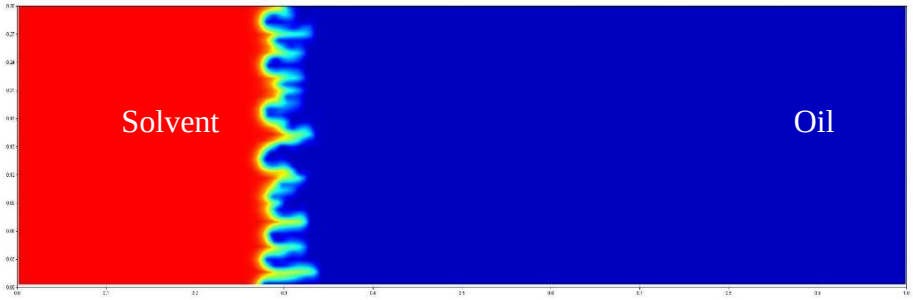

Figure 4.37 2D solvent concentration of tertiary 2:1 SWAG injection after 0.4 PVI

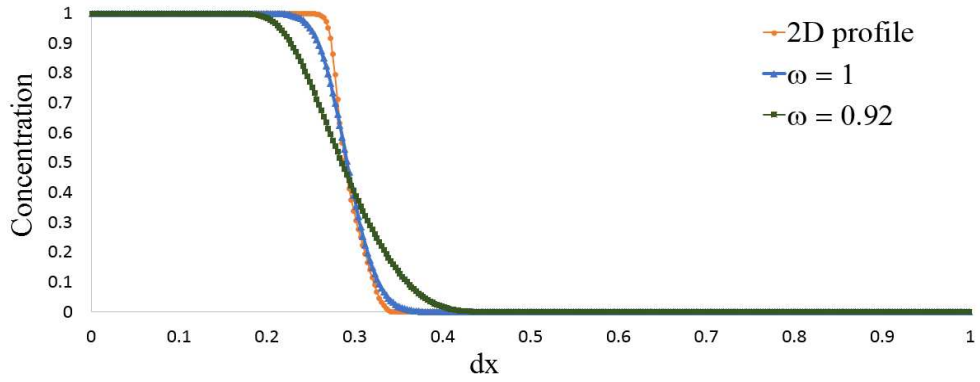

Figure 4.38 The best match between the solvent concentration profiles computed from the 1D model and the average solvent concentration profiles from the 2D simulation for tertiary 2:1 SWAG injection. ω = 1 gave a better match between the 1D solvent concentration profile and the average 2D solvent concentration profile.

4.9.3 Tertiary 4:1 SWAG injection

The final example of comparison is between tertiary 4:1 SWAG injection (fractional flow 0.8) and tertiary MV SWAG injection (fractional flow 0.35). Figure 4.39 shows that the fingers were completely suppressed in the tertiary 4:1 SWAG injection system compared to tertiary MV SWAG injection and to tertiary 2:1 SWAG injection. The value of ω is 1 and there is a complete match between the 1D solvent concentration profile and the 2D solvent concentration profile (Figure 4.40).

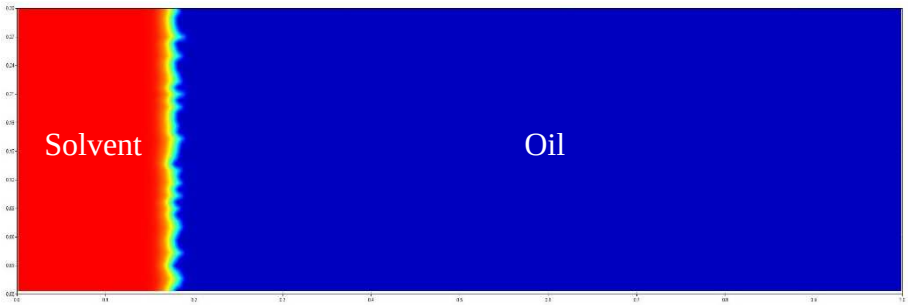

Figure 4.39 2D solvent concentration of tertiary 4:1 SWAG injection after 0.4 PVI

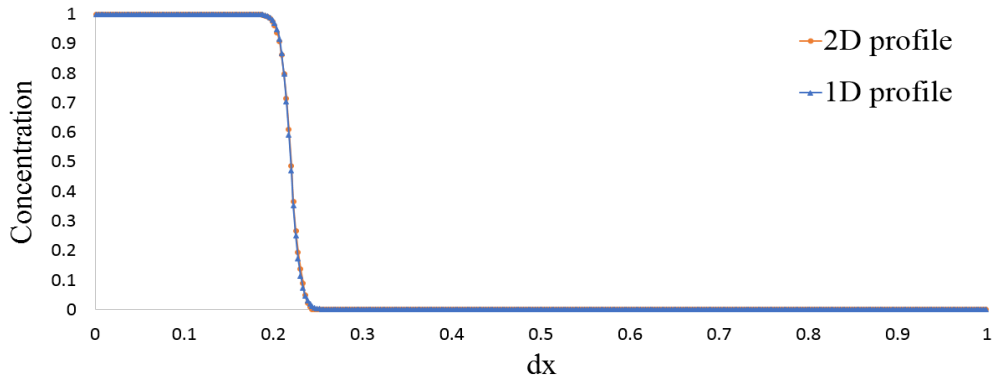

Figure 4.40 The best match between the solvent concentration profiles computed from the 1D model and the average solvent concentration profiles from the 2D simulation for tertiary 4:1 SWAG injection. ω = 1 gave a better match between the 1D solvent concentration profile and the average 2D solvent concentration profile.

4.9.4 Results from different tertiary SWAG injection

The results of calibrating ω for tertiary SWAG injection with a fractional flow higher than the tertiary MV SWAG injection (fractional flow of water injected = 0.35) are shown in Figure 4.41. The values of ω increased beyond the value of ω = 0.92 for the tertiary MV SWAG ratio that Blunt and Christie suggested. Even though the MV SWAG ratio gave a very small amount of fingering in the examples they considered, the viscous fingering decreased as the fractional flow increased. As a result, the values of ω increased as the fractional flow of water injected increased until the value of ω reached 1 for 2:1 SWAG injection (fractional flow of water injected = 0.67) and the value of ω stabilised at 1 beyond that.

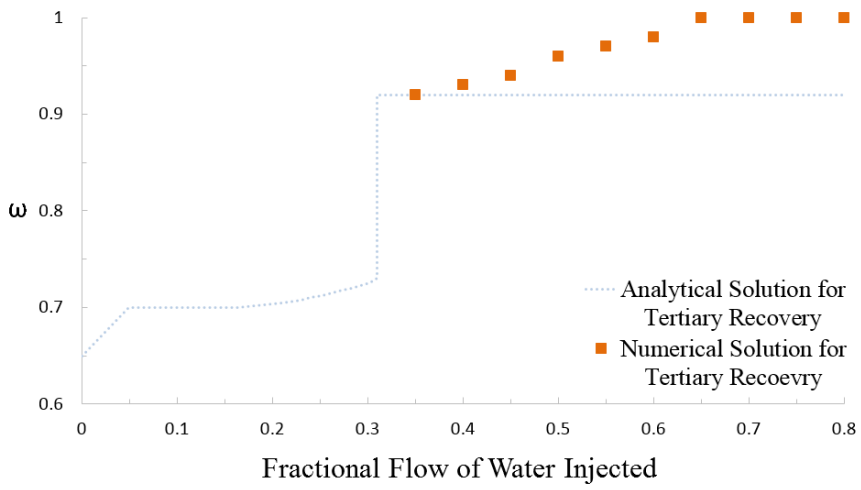

Figure 4.41 Tertiary recovery of SWAG injection higher than MV SWAG on grid size 375×150.

4.10 Relationship between ω and slug size at different WAG ratios

The WAG ratio has been varied to study the effects of over and under injection of water (compared to the MV WAG ratio) to understand the impact of the slug size on calibrating the value of ω for different WAG ratios and slug sizes. This is intended to capture the effect of different WAG ratios on the stabilisation of viscous fingering at different slug sizes.

Some examples are provided of the work conducted on different WAG ratios to calibrate the value of ω at different slug sizes for both secondary and tertiary recovery. The same steps of calibrating ω for SWAG injection to calibrate the value of ω for finite-sized slug WAG injection were repeated. The value of ω in the 1D is adjusted to get the best match between the solvent concentration and water saturation profiles obtained from the 1D model and the average solvent concentration and water saturation profiles obtained from the 2D simulation.

4.10.1 Secondary MV WAG Injection

Compared to secondary MV SWAG injection (fractional flow 0.35), secondary finite-sized slug MV WAG injection (fractional flow 0.35) showed considerably less stabilisation with a slug size of 0.1 PV (Figure 4.42). To achieve the best match between the 1D solvent concentration profile and the average 2D solvent concentration profile obtained from 2D simulator for secondary MV WAG injection at slug size 0.1 PV (Figure 4.43), the value of ω value is 0.81. Figure 4.43 shows that the value of ω holds at different PVI. Figure 4.44 shows the 2D simulation of water saturation distribution for secondary finite-sized slug MVWAG injection at slug size 0.1 PV and after 0.4 PVI and Figure 4.45 is the best match between the water saturation profiles computed from the 1D model and the average water saturation profiles from the 2D simulation for secondary MVWAG injection at slug size 0.1 PV where ω is 0.81.

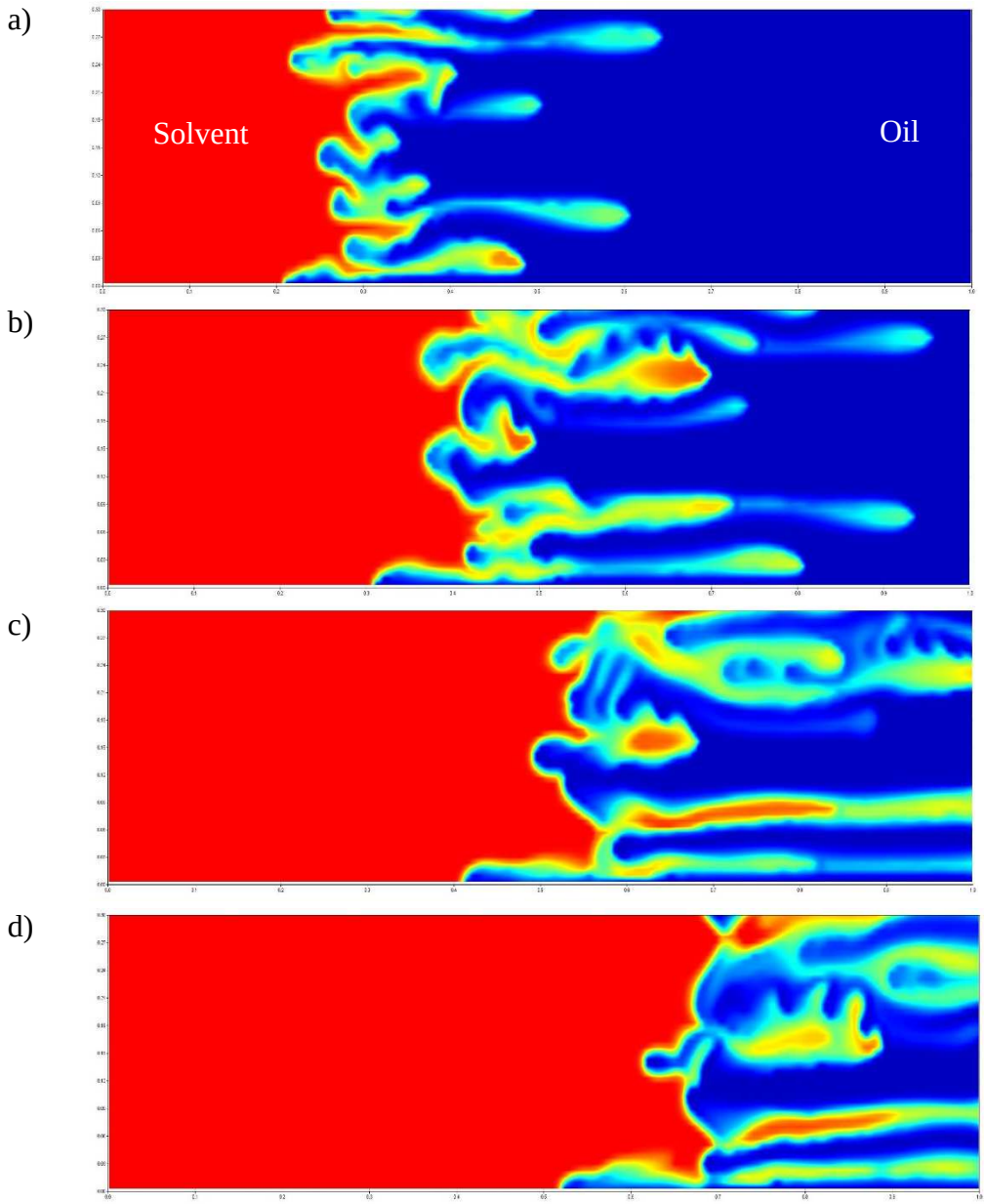

Figure 4.42 2D simulation of solvent concentration distribution of secondary MV WAG injection at slug size 0.1 PV and after: a) 0.27 PVI, b) 0.4 PVI, c) 0.54 PVI, d) 0.675 PVI

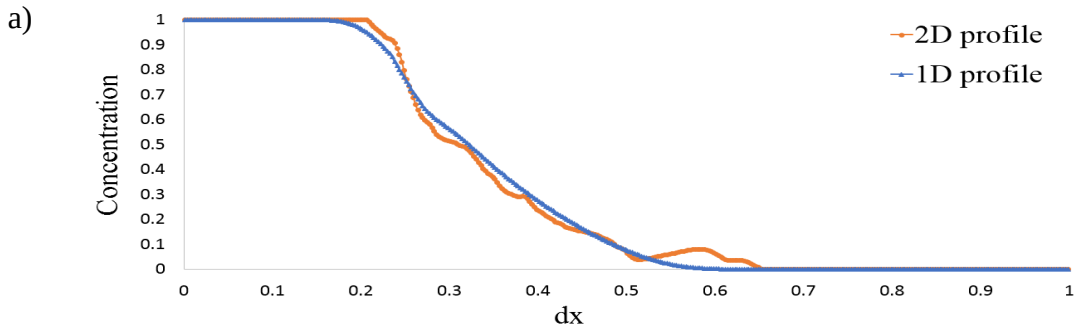

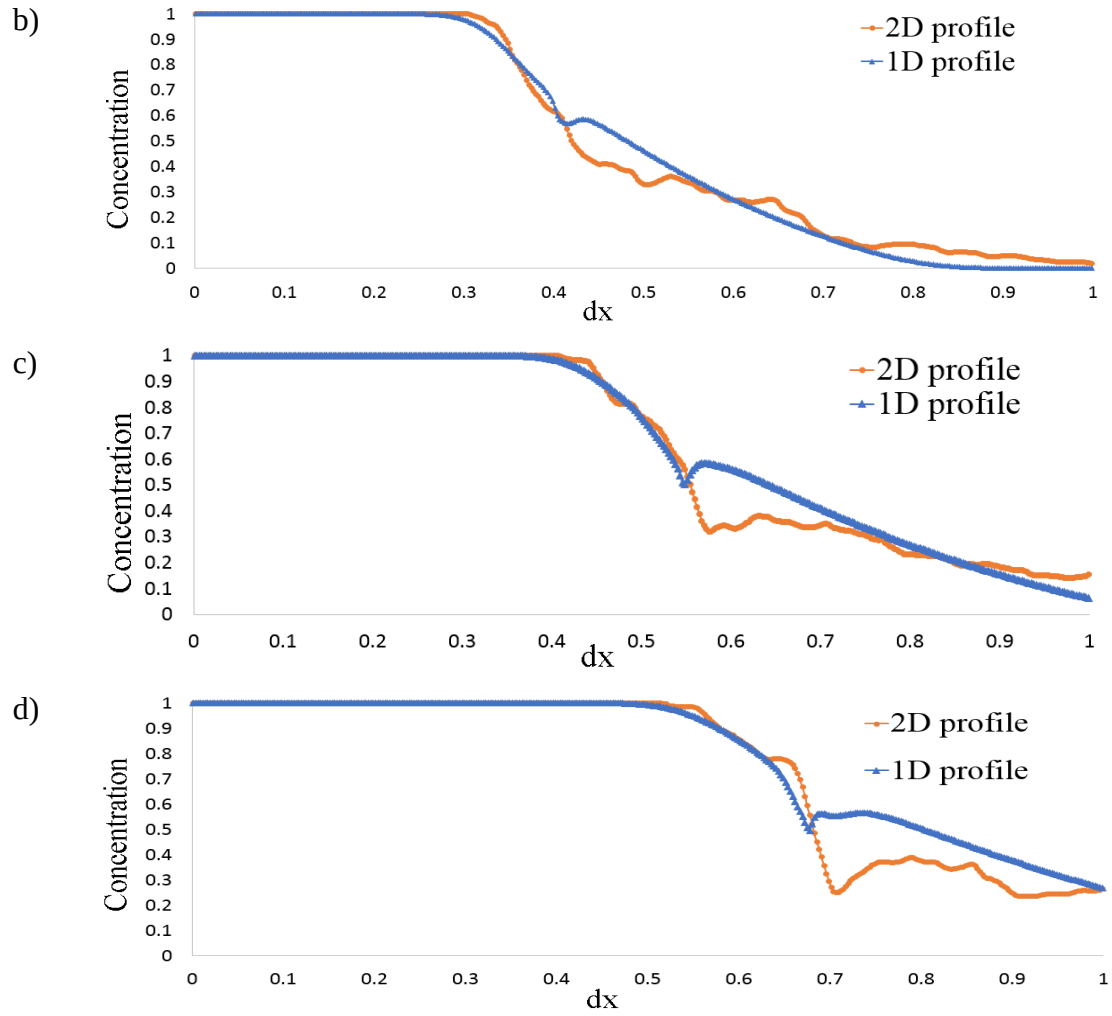

Figure 4.43 The best match between the solvent concentration profiles computed from the 1D model and the average solvent concentration profiles from the 2D simulation for secondary MV WAG injection at slug size 0.1 PV and after: a) 0.27 PVI, b) 0.4 PVI, c) 0.54 PVI, d) 0.675 PVI where the value of ω is equal to 0.81. Therefore, the value of ω holds at different PVI.

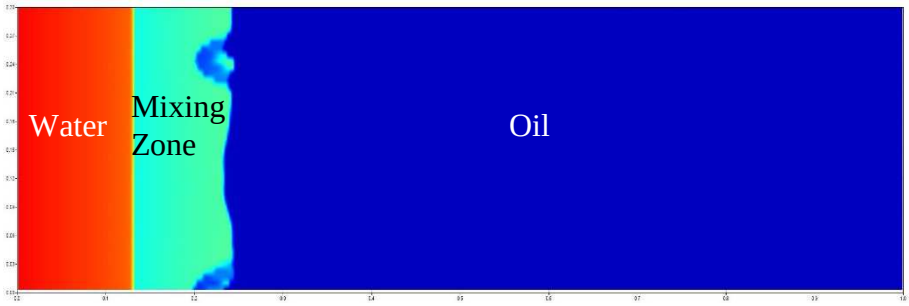

Figure 4.44 2D simulation of the water saturation of secondary MV WAG injection at slug size 0.1 PV and after 0.4 PVI. The mixing zone is very small compared to MV SWAG injection.

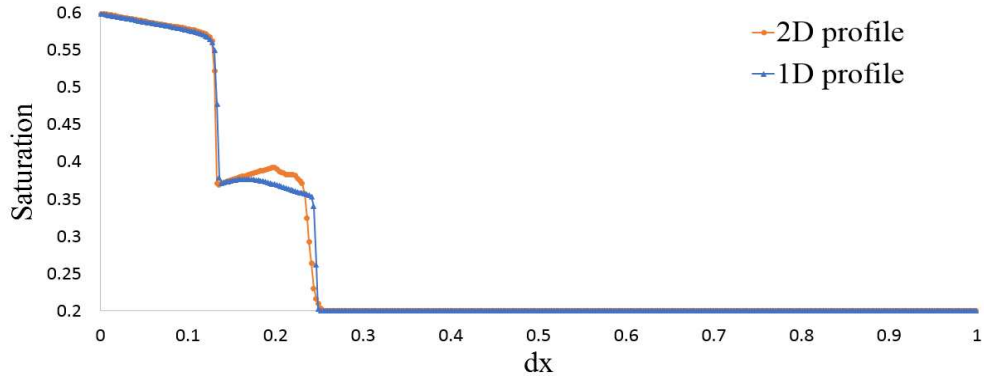

Figure 4.45 The best match between the water saturation profiles computed from the 1D model and the average water saturation profiles from the 2D simulation for secondary MV WAG injection at slug size 0.1 PV where the value of ω is 0.81

4.10.2 Calibrating ω for secondary 1:1 WAG injection

From Figure 4.46, a 1:1 WAG ratio with a slug size 0.1 PV and after 0.4 PVI had a significant number of fingers in the system compared to 1:1 SWAG injection. Figure 4.47 shows the best match between the 1D solvent concentration profile and the average 2D solvent concentration profile obtained from a 2D simulator for secondary 1:1 WAG injection at slug size 0.1 PV with an ω value of 0.84. Figure 4.48 shows a 2D simulation of the water saturation of 1:1 WAG injection at slug size 0.1 PV and after 0.4 PVI and Figure 4.49 shows the best match between the water saturation profiles computed from the 1D model and the average solvent concentration profiles from the 2D simulation for secondary 1:1 WAG injection for a slug size of 0.1 PV where ω = 0.84.

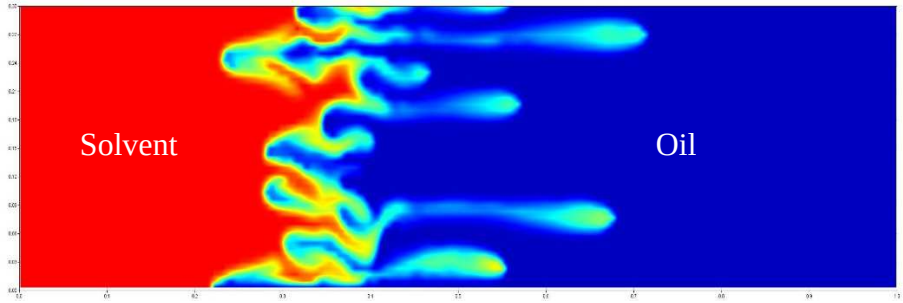

Figure 4.46 2D simulation of solvent concentration distribution of 1:1 WAG injection at slug size 0.1 PV and after 0.4 PVI

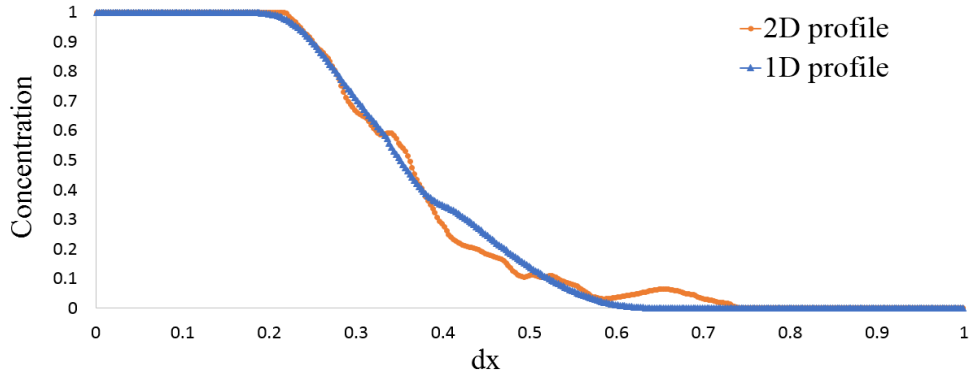

Figure 4.47 The best match between the solvent concentration profiles computed from the 1D model and the average solvent concentration profiles from the 2D simulation for secondary 1:1 WAG injection with a slug size of 0.1 PV where ω = 0.84

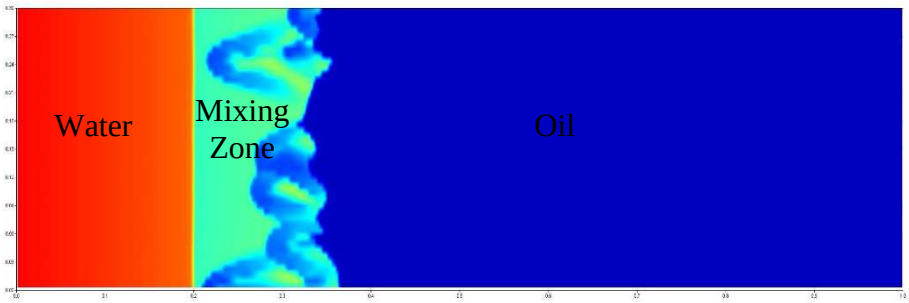

Figure 4.48 2D simulation of the water saturation of 1:1 WAG injection with a slug size of 0.1 PV and after 0.4 PVI

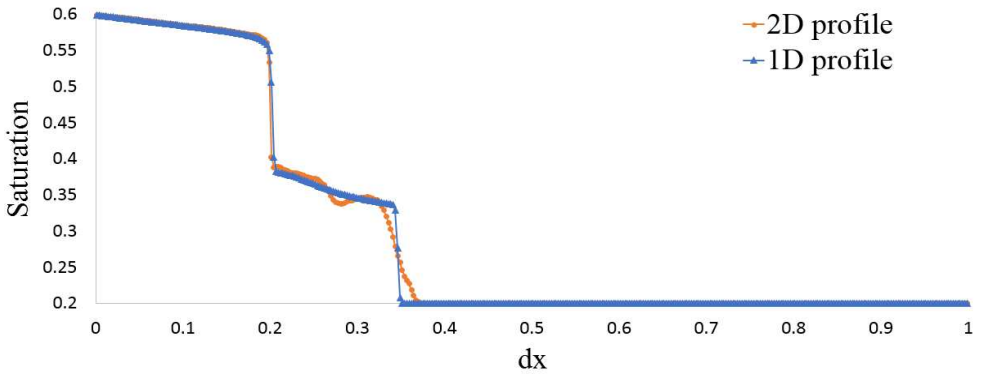

Figure 4.49 The best match between the water saturation profiles computed from the 1D model and the average water saturation profiles from the 2D simulation for secondary 1:1 WAG injection at slug size 0.1 PV where the value of ω = 0.84

4.10.3 Results of different WAG ratios, slug sizes and type of recovery on the calibrating value of ω

The results for calibrating the value of ω from the 1D model against the 2D simulator for different slug sizes and WAG ratios are given in Figure 4.50 for secondary recovery and

Figure 4.51 for tertiary recovery. From those figures, as the slug size increased the value of ω decreased, and the relationship depended on the WAG ratio and type of recovery.

Figure 4.50 shows that the value of ω for secondary finite-sized slug WAG injection changes smoothly depending on the slug size and WAG ratio between the Koval (1963) calibration value (0.72) using equation ($M_{eff} = (0.78 + 0.22\, M^{0.25})^4$) and Todd and Longstaff (1972) value (0.67) for secondary miscible gas injection and between Blunt and Christie's (1993) calibration for secondary SWAG injection. For secondary miscible gas injection, Todd and Longstaff suggested a mixing parameter value of 0.67 (line with stars in the bottom of the Figure 4.50), while the Koval calibration is 0.72 (line with triangles in the bottom of the Figure 4.50), and none of these values is seen to applicable for SWAG injection nor finite-sized slug WAG injection. Blunt and Christie showed that the mixing parameter value changes for secondary SWAG injection (circle points on the *y*-axis, because SWAG injection assumed to have zero slug size). The value of ω returns to the Koval (1963) calibration for a secondary miscible FSS WAG injection for high slug sizes (0.25 to 0.3 PV) and for a WAG ratio 1:6.5 (Figure 4.50).

Even though that the MV showed a high stabilisation of viscous fingering in SWAG injection, this was not the case with WAG injection. It can be seen from Figure 4.50 that the values of ω at the MV are less than the values of ω at 1:1 WAG ratio, and the difference is equal to 0.17 at slug size 0.01 PV. Therefore, MV does not work for WAG injection and 1:1 WAG ratio at small slug sizes has a better apparent mixing between the solvent and the oil than at MV WAG ratio.

The value of ω for tertiary finite-sized slug WAG injection (Figure 4.51) decreased as the slug size increased and this change depended on the WAG ratio. The Blunt and Christie (1993) calibration for tertiary SWAG injection are the circle points on the *y*-axis, because SWAG injection assumed to have zero slug size. Also, it can be seen that the value of ω at the MV WAG ratio and at 1:1 WAG ratio has the same value at the same slug size. Therefore, MV does not work for tertiary WAG injection.

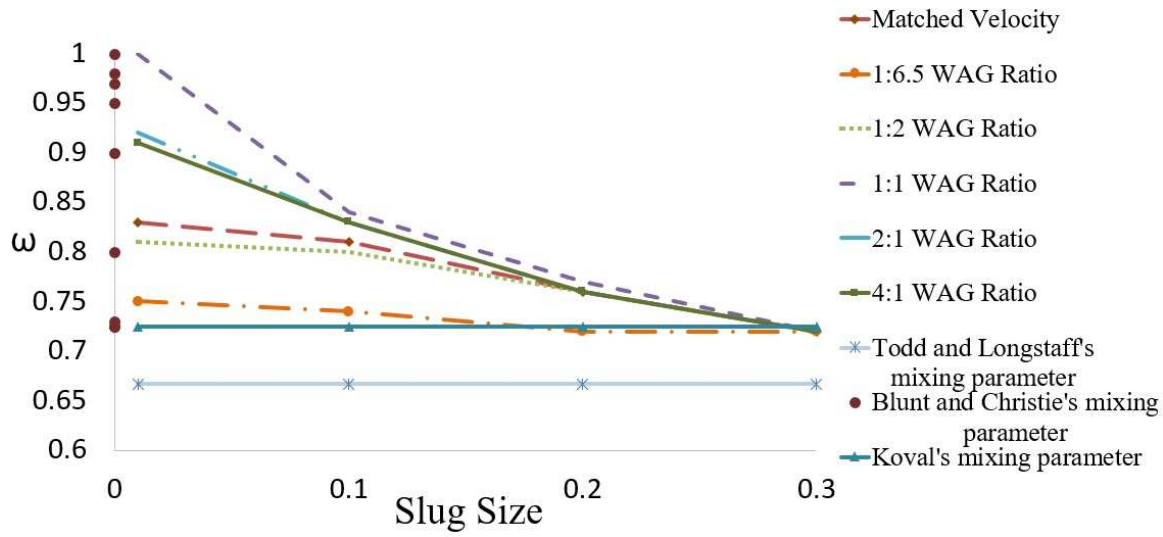

Figure 4.50 The relationship between ω and slug size for different WAG ratio for secondary recovery using grid size 375×150 and viscosity ratio=10.

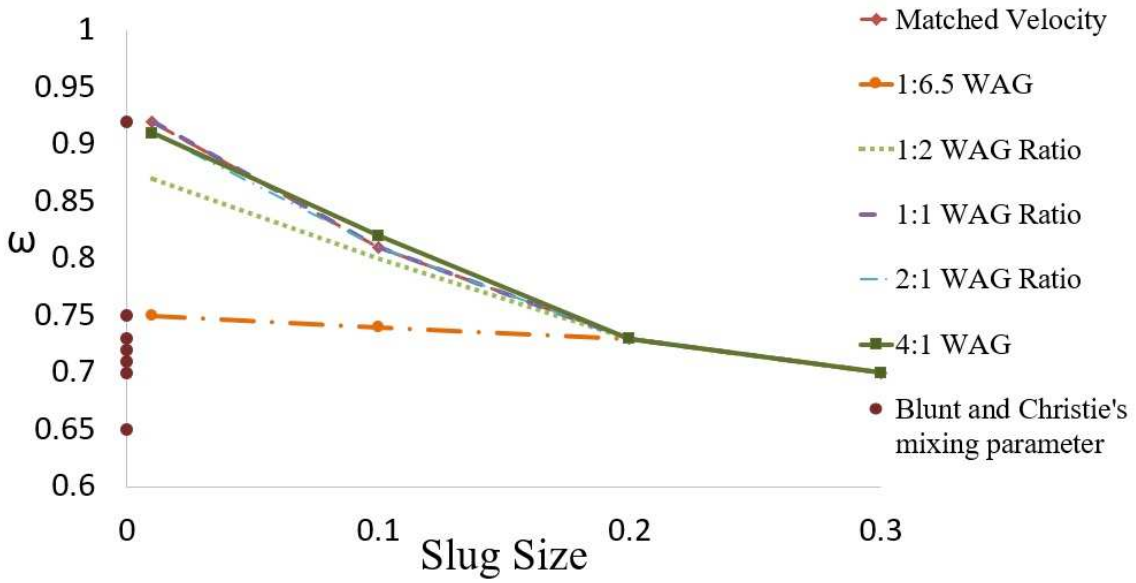

Figure 4.51 The relationship between ω and slug size for different WAG ratio for tertiary recovery using grid size 375×150 and viscosity ratio=10.

4.11 Relationship between ω and WAG Ratio for different slug sizes for both secondary and tertiary recovery

The values of ω were plotted at different slug sizes for finite-sized slug WAG injection as a function of the fractional flow of water injected (f_w), along with the values of ω for SWAG injection for both secondary and tertiary recovery, where WAG ratio = $f_w/(1-f_w)$. This can be considered as another way of looking into the results of calibrating the value of ω for finite-sized slug WAG injection.

There is a significant difference between the ω value obtained using the numerical calibration method for finite-sized slug WAG injection and Blunt and Christie's analytical results for SWAG injection as shown in Figure 4.52 for secondary recovery and Figure 4.53 for tertiary recovery. For small slug sizes, the values of ω for finite-sized slug WAG injection were less than SWAG injection, except the value of ω for the 1:1 secondary finite-sized slug WAG injection at slug size 0.01 PV was higher than SWAG injection. While, the values of for the tertiary finite-sized slug WAG injection were close to SWAG injection at slug size 0.01 PV, therefore, the mixing between the injected gas and oil at 0.01 PV for WAG injection tends to act like SWAG injection. Overall, as the slug size increased the apparent mixing between solvent and oil decreased. At a slug size of 0.3 PV, there is no change in the value of ω at all for both secondary and tertiary displacement and for different WAG ratios.

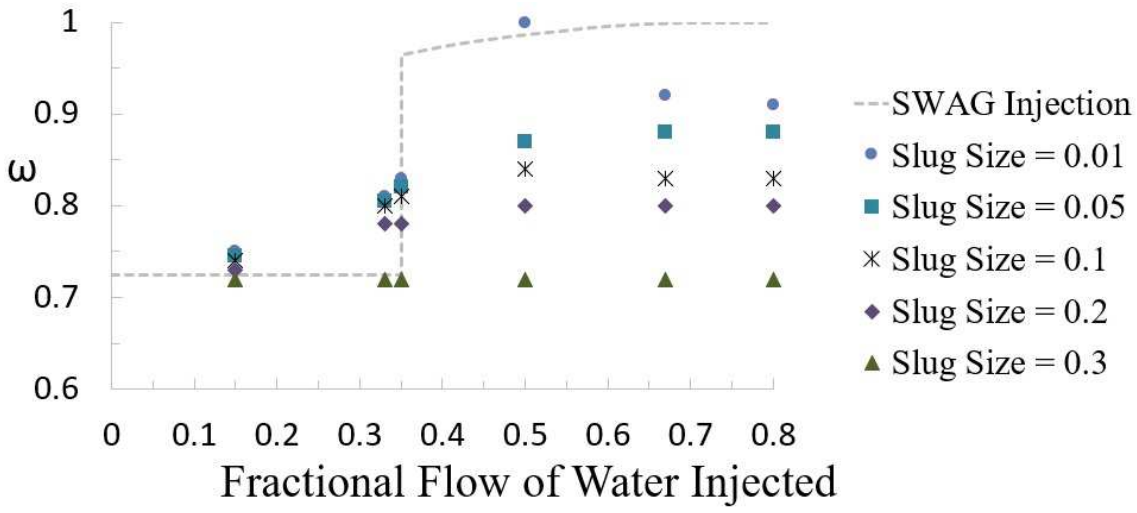

Figure 4.52 ***The calibrated values of ω as a function of the slug size vs WAG ratio for secondary recovery on grid size 375×150.***

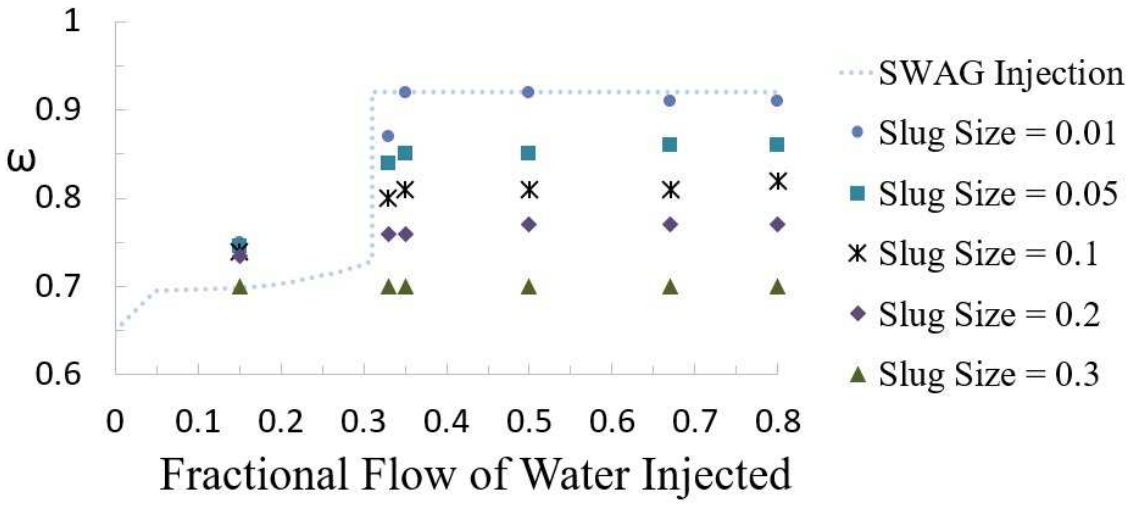

Figure 4.53 The calibrated values of ω as a function of the slug size vs WAG ratio for tertiary recovery on grid size 375×150.

4.12 Comparing the results of the calibrated values of ω at different viscosity ratio, grid size and variance to generate the permeability

In order to check if the results presented previously hold, the value of ω was calibrated at different viscosity ratio, grid size and variance to generate the permeability field.

4.12.1 Calibrating the values of ω at different viscosity ratio

The work was extended to observe the effect of high viscosity ratio on the calibration of ω. The oil viscosity in this case was 20 cP; the rest of the properties are the same. This make the viscosity ratio equal to 50. Our previous work is applicable for reservoirs where the viscosity ratio between the oil and the injected gas is 10.

The same steps were repeated, as described earlier, of calibrating ω in the 1D model against the 2D simulator where the viscous fingering triggered by the same permeability that previous resulted had been triggered.

One example of calibrating the value of ω from the 1D model against the 2D simulator for secondary MV WAG injection is detailed below. The viscous fingering of the solvent in the oil is shown in Figure 4.54, the calibration of ω from the 1D model against the 2D simulator is shown in Figure 4.55 and the resultant value of ω is 0.74, which is very low compared to the value of ω for secondary MVWAG injection at a viscosity ratio = 10.

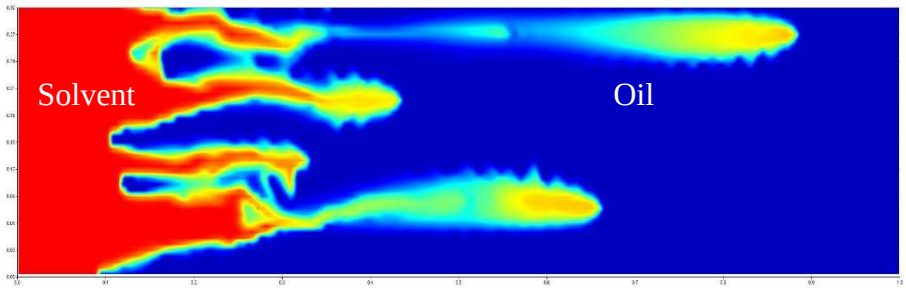

Figure 4.54 2D solvent concentration of secondary MV WAG injection at slug size 0.1 PV and after 0.3 PVI for a viscosity ratio of 50

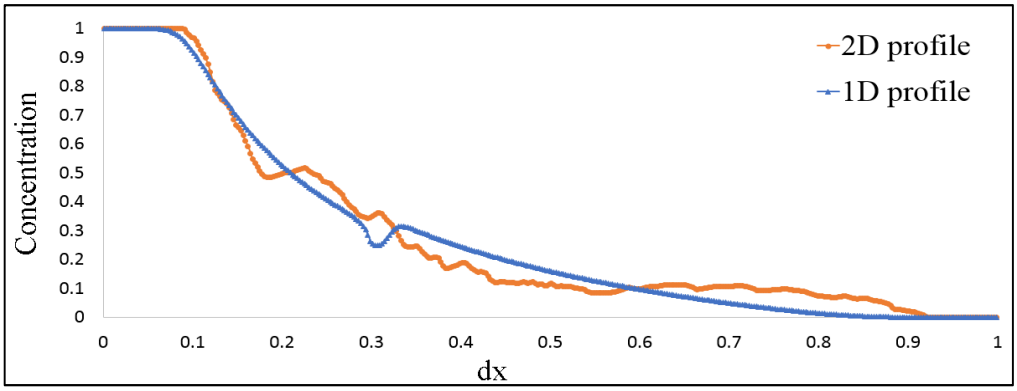

Figure 4.55 The best match between the solvent concentration profiles computed from the 1D model and the average concentration profiles from the 2D simulation for secondary MV WAG injection at slug size 0.1 PV and after 0.3 PVI. The value of ω is 0.74.

The results for calibrating ω for finite-sized slug WAG injection for a viscosity ratio of 50 are given in Figure 4.56. Figure 4.57 shows a comparison between the results for viscosity ratios of 10 and of 50 for a secondary finite-sized slug WAG injection. There is a significant difference between the calibrated values of ω, and the trend of the values are different at the same WAG ratio and slug size. Therefore, to use the values of the calibrated ω on a field scale, the values of ω should be calibrated considering the viscosity ratio.

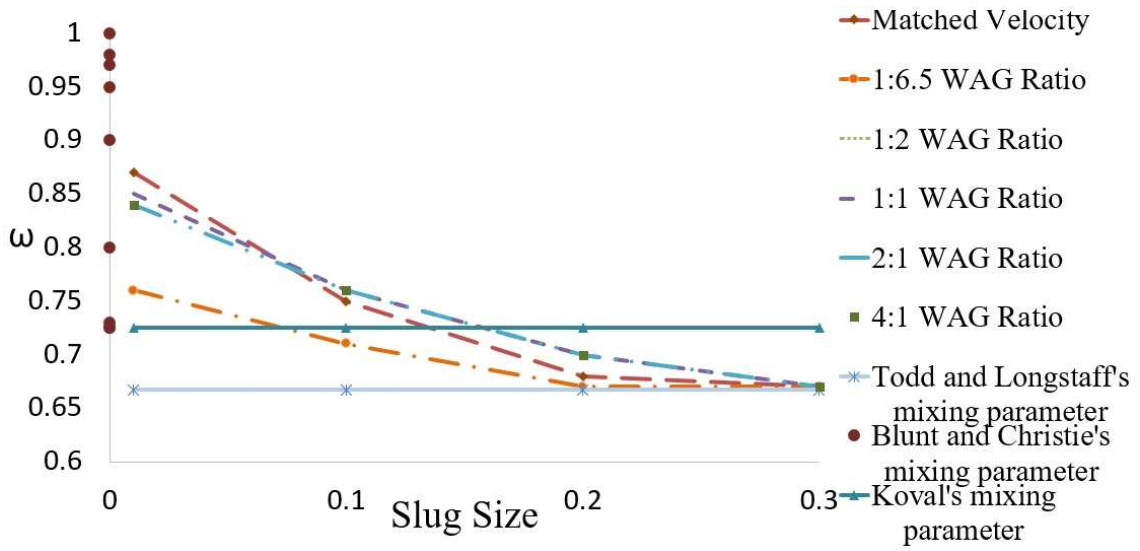

Figure 4.56 The relationship between *ω* and the slug size at different WAG ratios for a secondary recovery on grid size 375×150 for a viscosity ratio = 50.

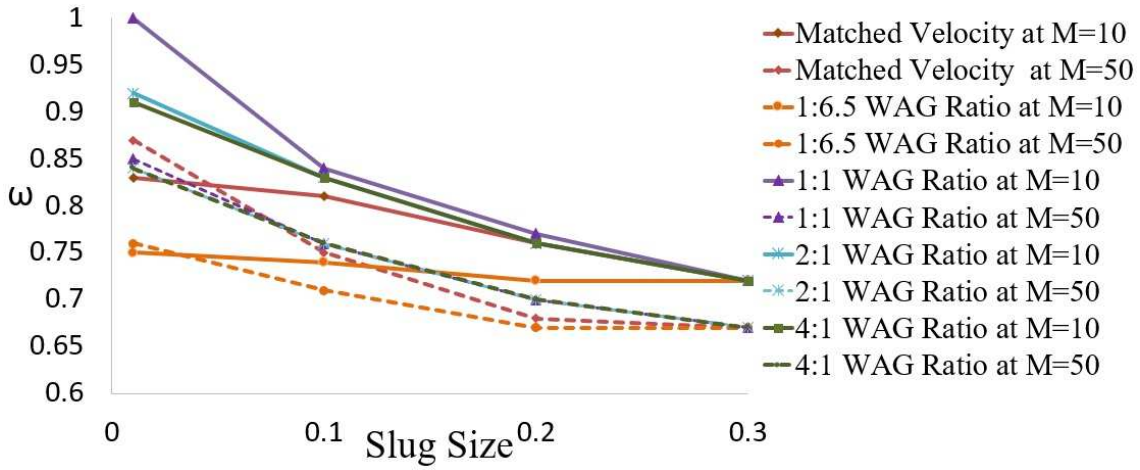

Figure 4.57 Comparison between the values of *ω* for viscosity ratios of 50 and 10.

4.12.2 Calibrating the values of ω for different grid size

The work was extended to examine the effect of fine grid blocks on the calibration of ω. The properties were the same as for a viscosity ratio of 10. The grid size tested here was 750×300, with an aspect ratio of 2:1 compared to 375×150.

The same steps described above for calibrating ω in the 1D model against the 2D simulator were repeated, whereby the viscous fingering is triggered by using the same mean and standard deviation to generate the permeability that is used for the grid blocks of 375×150.

One example of calibrating the value of ω from the 1D model against the 2D simulator for secondary MV WAG injection is shown. The viscous fingering of the solvent in the oil is shown in Figure 4.58, the calibration of ω from the 1D model against the 2D simulator is shown in Figure 4.59 and the resulting value of ω is 0.75, which is approximately 6% lower than the value of ω = 0.81 using a 375×150 grid.

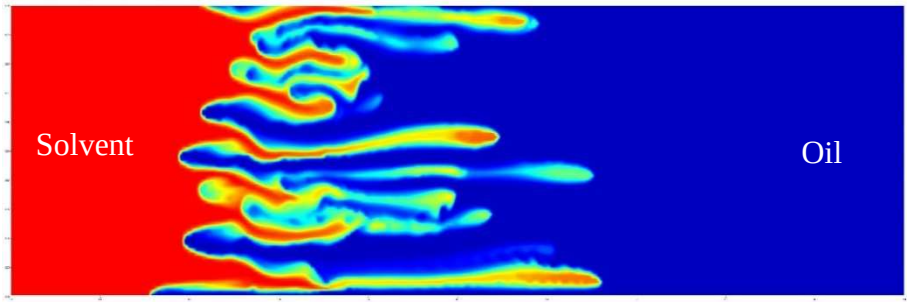

Figure 4.58 2D solvent concentration profile of secondary MV WAG injection at slug size 0.1 PV and after 0.3 PVI for a viscosity ratio = 10

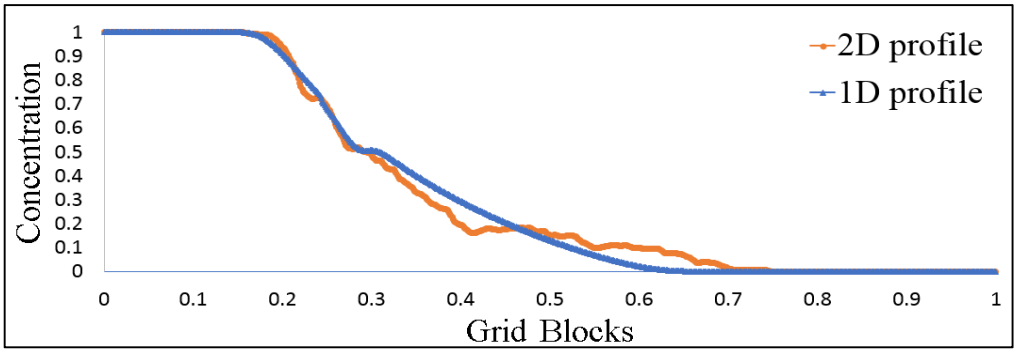

Figure 4.59 The best match between the concentration profiles computed from the 1D model and the average concentration profiles from the 2D simulation for secondary MV WAG injection at slug size 0.1 PV and after 0.4 PVI. The value of ω is 0.75.

The results for calibrating ω for finite-sized slugs WAG injection for a grid size = 750×300 are presented in Figure 4.60. Comparing between the results in Figure 4.61 using 750×300 grid and a 375×150 grid for a secondary finite-sized slug WAG injection, revealed that there is a difference in the calibrated values of ω. The values of ω for a 750×300 grid was less than the values of ω for a 375×150 grid by about 5 to 7%, but the trend is the same. Therefore, it is the author's opinion that the values of ω at 375×150 are applicable for a wide range of grid blocks since the difference is not big.

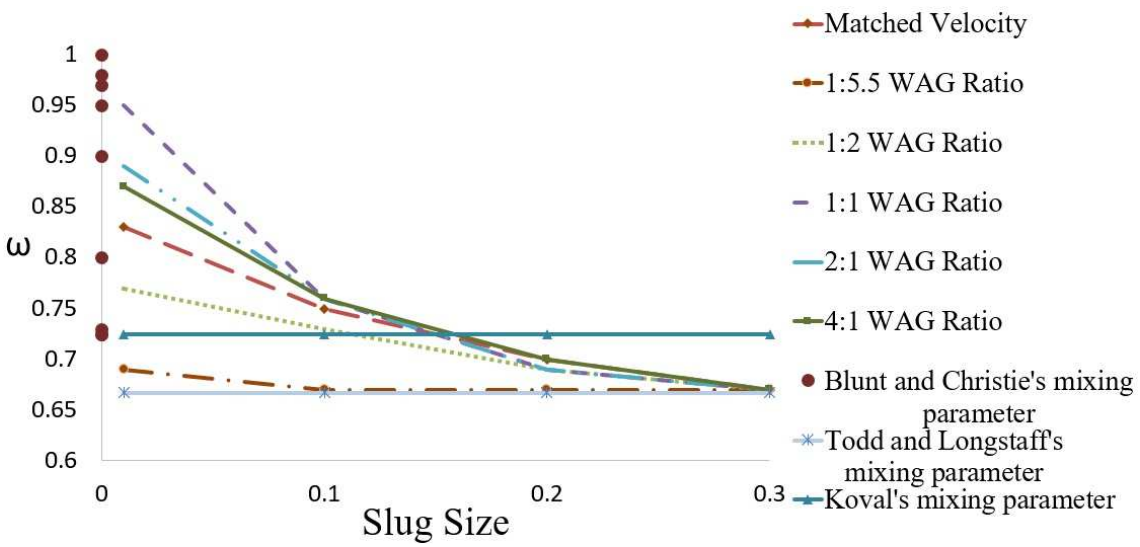

Figure 4.60 The relationship between ω and the slug size at different WAG ratio for a secondary recovery finite-sized slug WAG injection at grid block=750×300

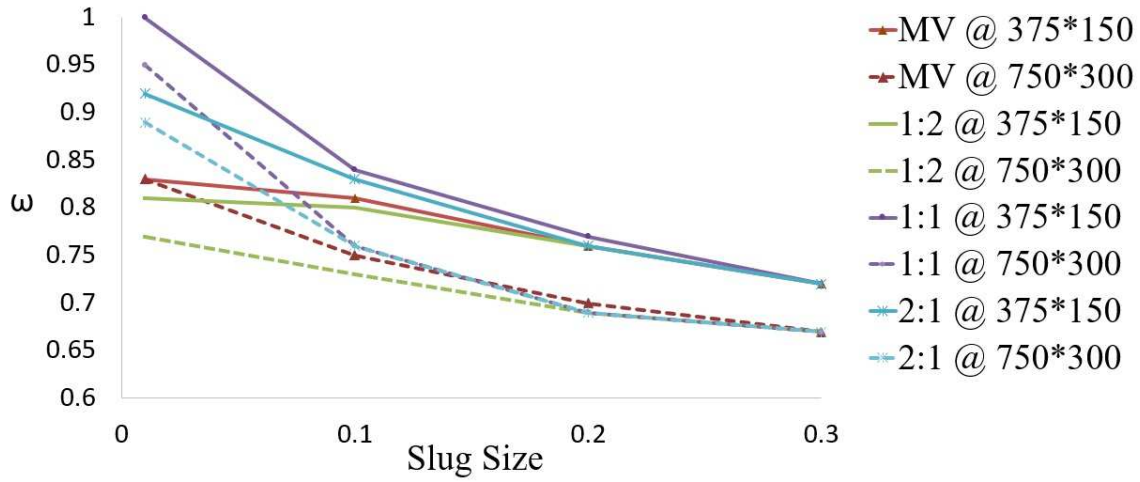

Figure 4.61 Comparison between the values of ω or a 750×300 grid and a 375×150 grid

4.12.3 Effect of different variance to generate the permeability on the calibration of mixing parameter value

To test the effect of different variances to generate the permeability (heterogeneity) distribution on the calibration of ω's value, uncorrelated permeability distribution was generated with a mean of 1 and a standard deviation of 0.1% as shown in Figure 4.62 and a standard deviation of 10% as shown in Figure 4.63.

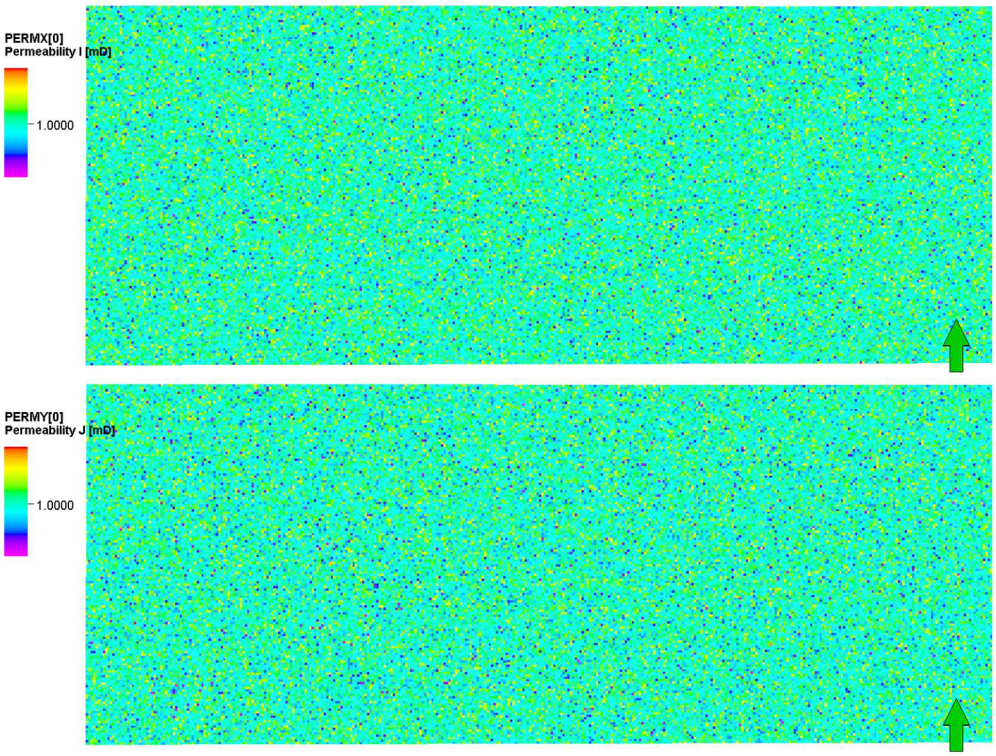

Figure 4.62 Permeability distribution in the *x*- and *y*-direction using uncorrelated stochastic Log-Normal distribution with a mean of 1 and a standard deviation of 0.1% to trigger the viscous fingering.

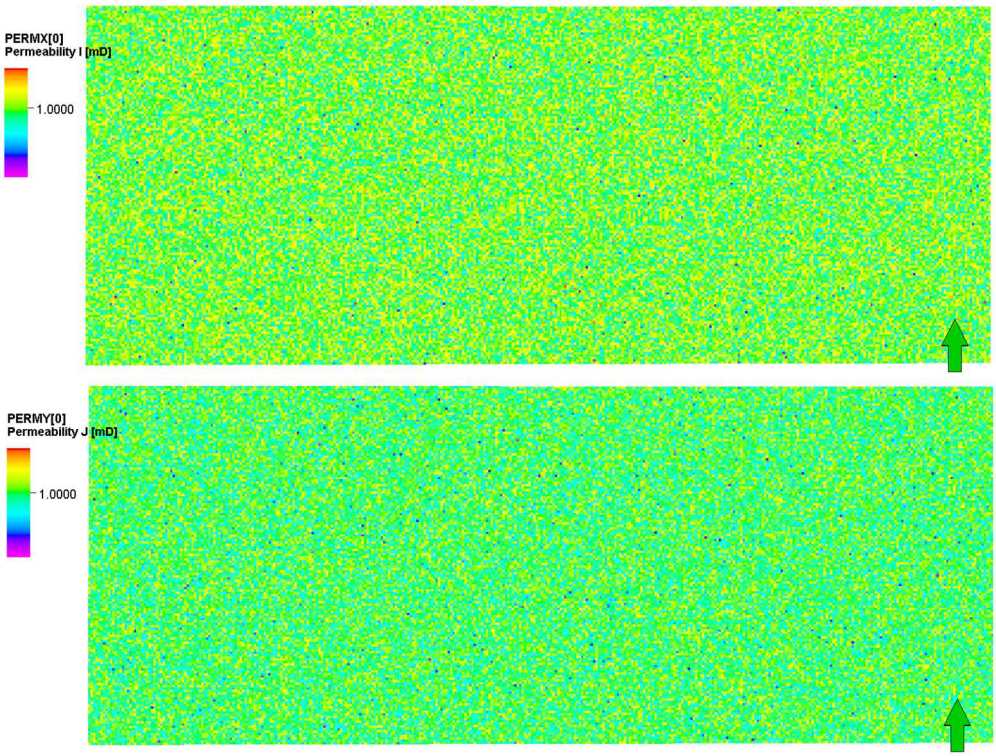

Figure 4.63 Permeability distribution in the *x*- and *y*-direction using uncorrelated stochastic Log-Normal distribution with a mean of 1 and a standard deviation of 10% to trigger the viscous fingering.

The same steps as described earlier, of calibrating ω in the 1D model against the 2D simulator were repeated in a scenario where the viscous fingering triggered by different variation in permeability.

Two examples of calibrating the value of ω from the 1D model against the 2D simulator for secondary MV WAG injection are presented, where the viscous fingering in the 2D model triggered by the variation in permeability for a standard deviation of 0.1 and 0.001. The apparent mixing between solvent and oil in the system, where the permeability is generated with a mean of 1 and a standard deviation of 0.1, is shown in Figure 4.64. The calibration of ω from the 1D model against the 2D simulator is shown in Figure 4.65 and the value of ω is 0.77. While the mixing between solvent and oil in the system where the permeability is generated with a mean of 1 and a standard deviation of 0.001 is shown in Figure 4.66. The calibration of ω from the 1D model against the 2D simulator is shown in Figure 4.67 and the value of ω = 0.8.

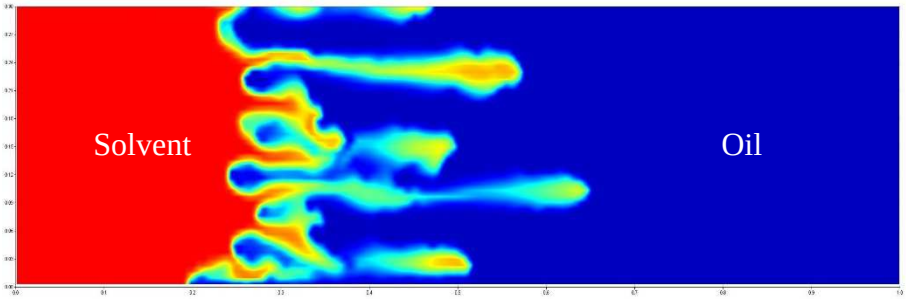

Figure 4.64 2D solvent concentration profile of secondary MV WAG injection for a slug size of 0.1 PV, after 0.4 PVI with permeability generated with a mean of 1 and a standard deviation of 0.1

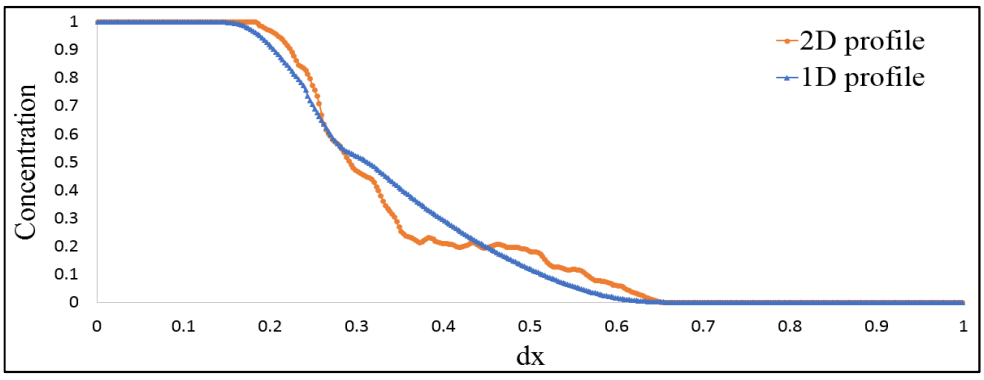

Figure 4.65 The best match between the concentration profiles computed from the 1D model and the average concentration profiles from the 2D simulation in Figure 4.56 for secondary MV WAG injection at slug size 0.1 PV and after 0.4 PVI with permeability generated with a mean of 1 and a standard deviation of 0.1. The value of ω is 0.77.

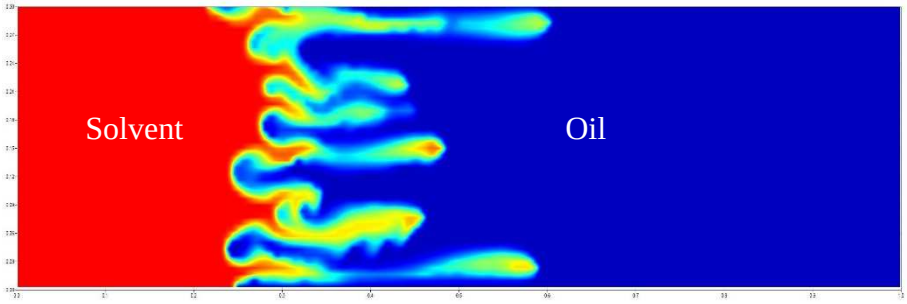

Figure 4.66 2D solvent concentration profile of secondary MV WAG injection at slug size 0.1PV and after 0.4 PVI with permeability generated with a mean of 1 and a standard deviation of 0.001

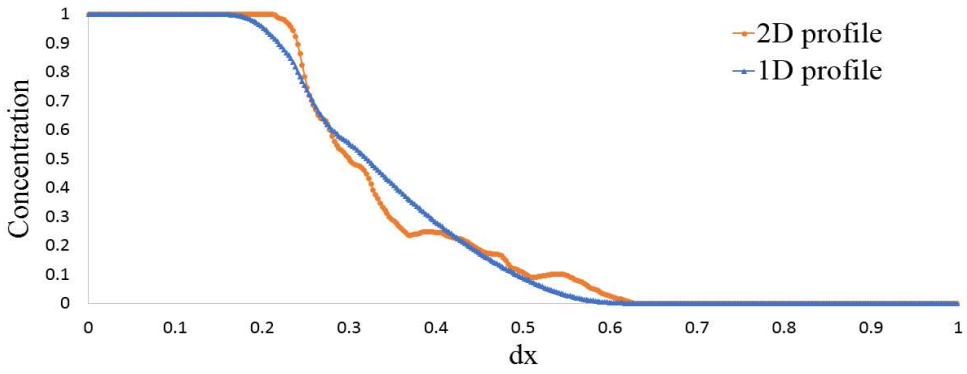

Figure 4.67 The best match between the concentration profiles computed from the 1D model and the average concentration profiles from the 2D simulation, Figure 4.58, for secondary MV WAG injection at slug size 0.1 PV and after 0.4 PVI with permeability generated with a mean of 1 and a standard deviation of 0.001. The value of ω is 0.8.

Figure 4.68 shows the results for the standard deviation of 10% and Figure 4.69 the standard deviation of 0.1%. Figure 4.70 represents a comparison between the calibrated values of ω for a standard deviation of 0.1% and a standard deviation of 1%, where the difference between the values of ω range from 0-5%, as shown in the figure. Figure 4.71 shows a comparison between the calibrated values of ω at the standard deviation of 10% and the standard deviation is 1% where the difference between the values of ω range from 0-4%, as shown in the figure. From those figures, there is a slightly change in the value of ω under the effect of different variations (heterogeneity), and this change depends on the heterogeneity in the system. Therefore, the values of ω generated in Figure 4.50 is reasonable for different types of variance to generate the permeability.

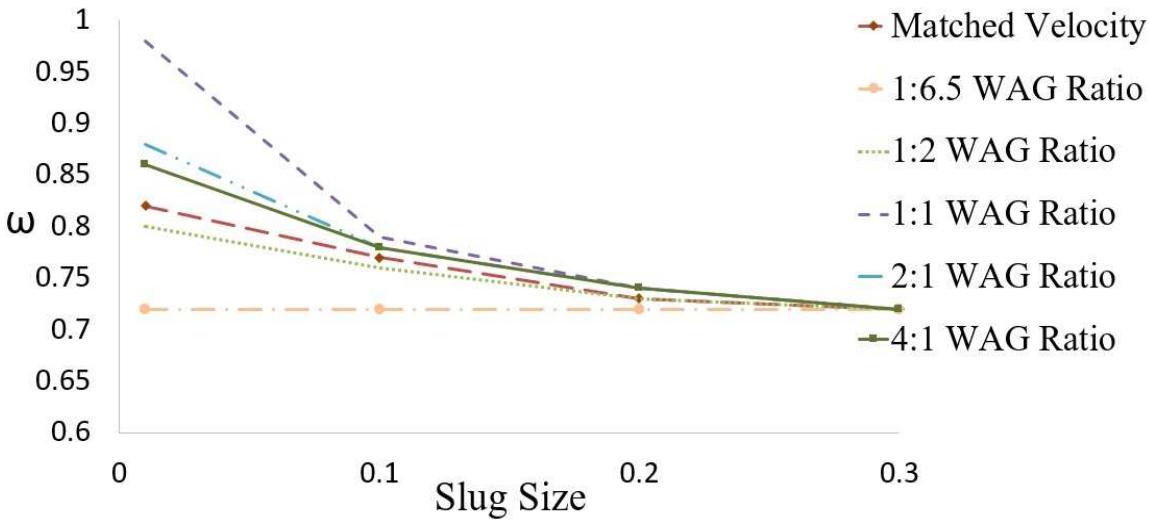

Figure 4.68 The relationship between *ω* and the slug size at different WAG ratio for a secondary recovery with permeability distribution with a mean of 1 and a standard deviation of 10%

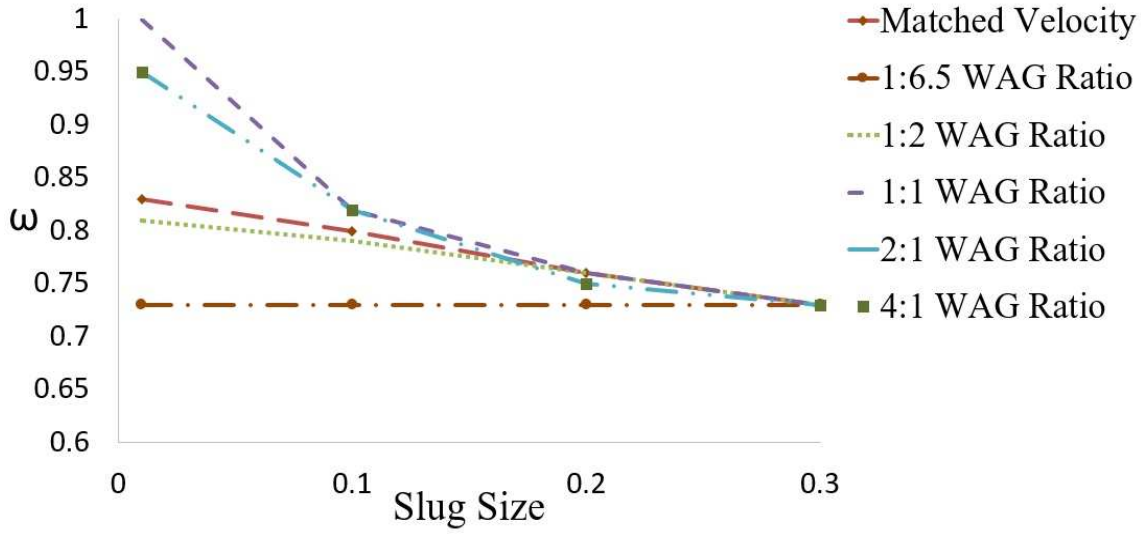

Figure 4.69 The relationship between *ω* and the slug size at different WAG ratio for a secondary recovery with permeability distribution with a mean of 1 and a standard deviation of 0.1%

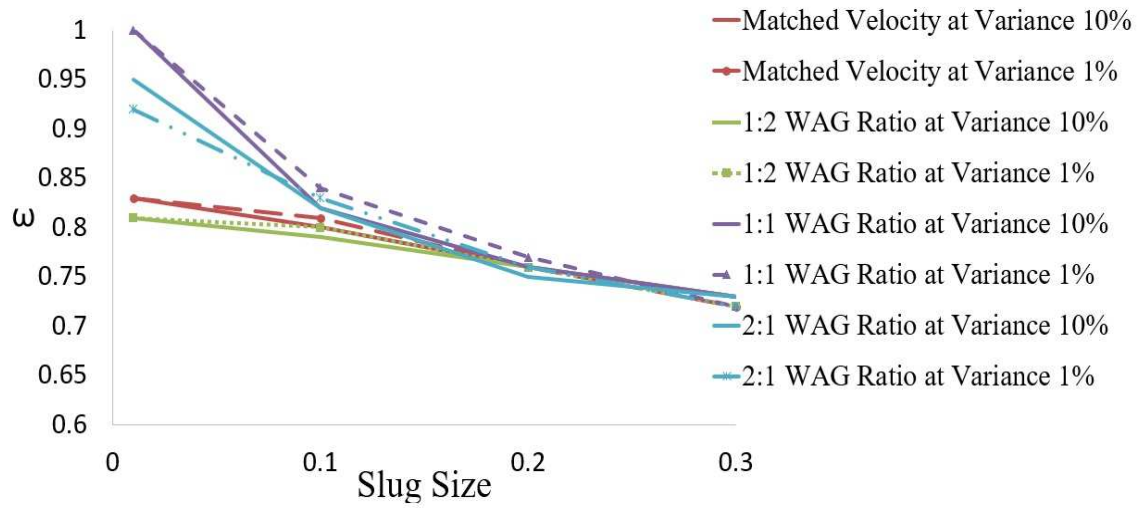

Figure 4.70 Comparison between the calibrated *ω*'s values for a secondary miscible FSS WAG injection with permeability distribution with a mean of 1 and a standard deviation of 10% and a standard deviation of 1%

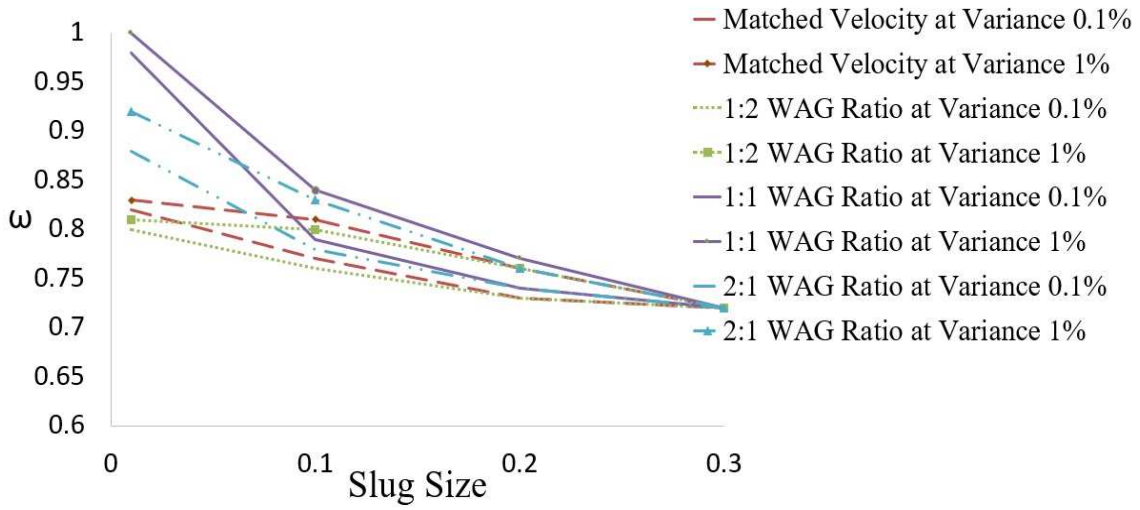

Figure 4.71 Comparison between the calibrated *ω*'s values for a secondary miscible FSS WAG injection with permeability distribution with a mean of 1 with a standard deviation of 0.1% and a standard deviation of 1%

4.12.4 Effect of different initialisation to generate the permeability on the calibration of mixing parameter value

To test the effect of different initialisations for the generation of the permeability (heterogeneity) distribution on the calibration of *ω*'s value, an uncorrelated permeability distribution was generated six times with a mean of 1 and a standard deviation of 1%.

Two examples of calibrating the value of ω from the 1D model against the 2D simulator for secondary MV WAG injection and 1:1 WAG injection is presented. The same steps as described earlier, of calibrating ω in the 1D model against the 2D simulator were repeated in a scenario where the viscous fingering is triggered by variations in permeability.

Figure 4.72 and Figure 4.73 show the impact of different initialisations for the same mean and standard deviation to generate the permeability on triggering the viscous fingering for secondary MV WAG injection at slug size 0.1 PV and secondary 1:1 WAG injection at slug size 0.1 PV, respectively. From these figures, there can be seen to be a slight change in the value of ω under the effect of different initialisations to generate the permeability.

The average calibration of ω from the 1D model against the 2D simulator over 6 initialisations is the value of 0.81 for secondary MV WAG injection at slug size 0.1 PV and a value of 0.84 for secondary 1:1 WAG injection at slug size 0.1 PV. These values are in agreement with the values obtained previously using a single random initialisation to generate the permeability. Therefore, it is reasonable to infer that the values of ω generated in Figure 4.50 are a reasonable representation for different initial initialisations points to generate the permeability.

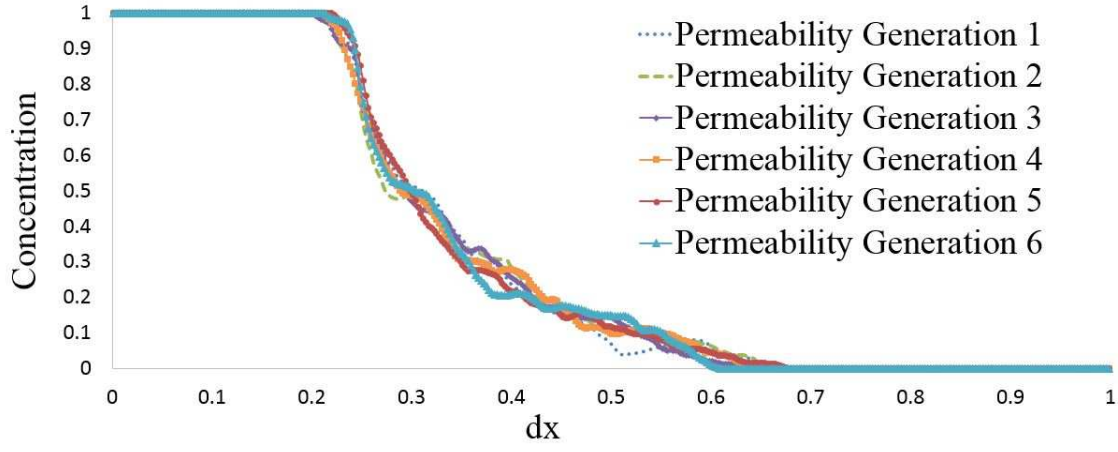

Figure 4.72 The average concentration profiles from the 2D simulation using different initialisations to generate the permeability with a mean of 1 and a standard deviation of 1%. For secondary MV WAG injection at slug size 0.1 PV, the average value of calibrating ω= 0.81

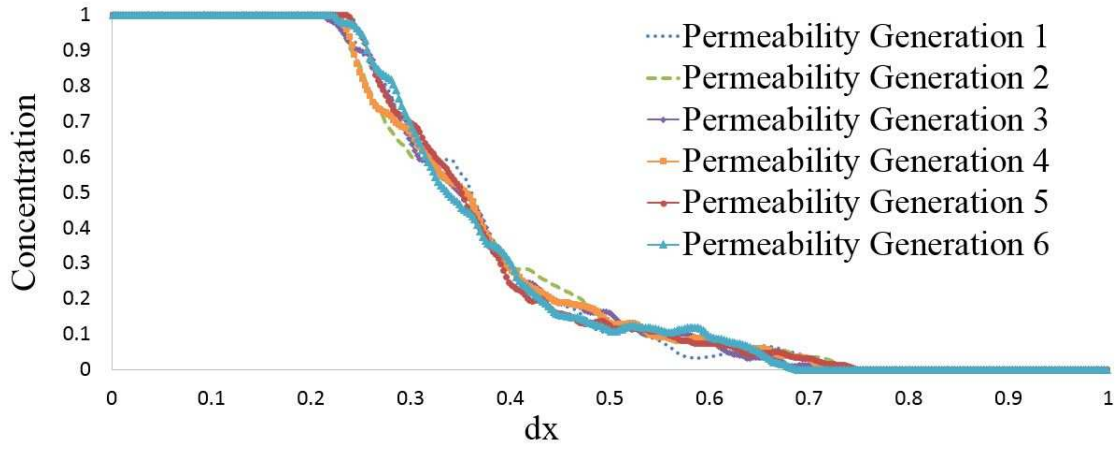

Figure 4.73 The average concentration profiles from the 2D simulation using different initialisations to generate the permeability with a mean of 1 and a standard deviation of 1%. For secondary 1:1 WAG injection at slug size 0.1 PV, the average value of calibrating ω=0.84

4.13 Summary of the chapter

This chapter presented the results from the calibration of the mixing parameter, ω, using a 1D numerical model compared against 2D detailed simulation. This represents a refinement and extension of previous work on the recalibration of ω for SWAG injection by Blunt and Christie (1993), accounting for finite-sized slug WAG (FSS WAG) injection. Its innovation is the calibration of the mixing parameter ω for a set of WAG ratio, slug size, and different types of recovery.

The value of ω can be used to represent sub grid block viscous fingering in a reservoir simulator that has an explicit permeability field. Herein it was hypothesized that the Todd and Longstaff model could describe the viscous fingering of the solvent in two-phase, three-component flow. The theory was based on the construction of a numerical solution to the system of component conservation laws in one dimension, which included empirical expressions for the ω value.

The results show that ω decreases as the slug size increases and this change depends on the WAG ratio for both secondary and tertiary FSS WAG injection. The value of ω for secondary FSS WAG injection changed smoothly between the Koval (1963) value and Todd and Longstaff (1972) value for secondary miscible gas injection and between Blunt and Christie's (1993) calibration for secondary SWAG injection. The value of ω returns

to Koval (1963) calibration for a secondary miscible gas injection at high slug sizes (0.25 – 0.3 PV) and at WAG ratio 1:6.5.

Even though that the matched velocity (MV) showed a high stabilisation of viscous fingering in secondary SWAG injection, this was not the case with secondary FSS WAG injection. The values of ω at the MV are less than the values of ω at 1:1 WAG ratio, and the difference is equal to 0.17 at slug size 0.01 PV. Therefore, MV does not work for WAG injection and 1:1 WAG ratio at small slug sizes has a better mixing between the solvent and the oil than at MV WAG ratio. 1:1 WAG ratio will be used on field scale application to test the results of the calibrated ω.

Plotting the values of ω at different slug sizes for FSS WAG injection as a function of the fractional flow of water injected (f_w) along with the values of ω for SWAG injection for both secondary and tertiary recovery, where WAG ratio = $f_w/(1-f_w)$ can be considered as another way of considering the results of calibrating of ω. There was a significant difference between the ω using the numerical calibration method for FSS WAG injection and Blunt and Christie's analytical results for SWAG injection for secondary and tertiary recovery. As the slug size increases the mixing between solvent and oil decreases. For secondary recovery at small slug sizes, the values of ω for finite-sized slug WAG injection were less than SWAG injection, except the value of ω for the 1:1 secondary finite-sized slug WAG injection at slug size 0.01 PV was higher than SWAG injection. While, the values of for the tertiary finite-sized slug WAG injection were close to SWAG injection at slug size 0.01 PV, therefore, the mixing between the injected gas and oil at 0.01 PV for WAG injection tends to act like SWAG injection. At a slug size of 0.3 PV, there was no change in the value of ω at all for either secondary or tertiary displacement or for different WAG ratios.

Chapter 5

Applying the calibrated value of the mixing parameter at its specific WAG ratio and slug size on the field scale

5.1 Introduction

The aim of this chapter is to show the application of the calibrated values of the mixing parameter, ω, for miscible finite-sized slug WAG (FSS WAG) injection presented previously in Chapter 4. The application on a field scale was through the use of a black oil simulator, Eclipse E100, and was designed to show the reservoir performance obtained using the calibrated values of ω for 1:1 WAG ratio at different slug sizes. Also, to compare the reservoir performance at the calibrated value with a full mixing ω =1 and with Todd and Longstaff's value = ⅔ that has been established earlier in chapter 4. Todd and Longstaff recommended a value of ⅓ to be applied on a field scale to take into account the effect of heterogeneity. However, the value of ⅔ is used in this comparison, because this comparison was established in previous work (Chapter 4).

Two case studies were used to test the reservoir performance, a synthetic quarter five spot model and a semi-synthetic model (Watt field model). The quarter five-spot model allowed the demonstration of some of the key features of FSS WAG injection in a 3D model without the additional complexity of multiple wells, horizontal producers, faults, and complex permeability and porosity distributions, such as those in the Watt field model.

This chapter starts by presenting the models under study, their fluid properties and the grid-refinement study conducted on both models. Then, it provides the assumptions of applying the calibrated value of ω on a field scale. Finally, it shows the results and the impact of the calibrated value of ω on the WAG zone and the oil recovery factor.

5.2 Quarter five-spot model

To conduct a reservoir performance analysis, it is common practice to study a representative unit element or a confined pattern such as a quarter five-spot (one injection well at one corner of a square and one production well at the other corner of the square). Studies of quarter five-spot models have focused on both immiscible and miscible displacements, in heterogeneous as well as homogeneous porous media because of their practical importance in enhanced oil recovery. The quarter five-spot has served for seven decades as the model pattern for exploring the physical dynamics governing a

displacement, to gain an understanding of the dynamics at a fundamental level and to support the development of more accurate models, which in turn should allow better performance predictions of large reservoirs (Chen and Meiburg, 1998).

A quarter five-spot injection model was used to simulate the performance of the miscible FSS WAG injection using the calibrated value of ω for different slug sizes of secondary 1:1 WAG ratio. The modelled system used (Figure 5.1), was a box-shaped reservoir with a horizontal area of 500×500 ft and a vertical thickness of 100 ft. The model had a homogeneous porosity of 0.3, and homogeneous permeability of 100 mD in Nx and Ny, and 10 mD in Nz. The model total pore volume PORV = 1.335×10^6 RB (reservoir barrel) and oil original in place is 1.084×10^6 STB (stock tank barrel). Another model has a heterogeneous permeability Figure 5.2 and heterogeneous porosity.

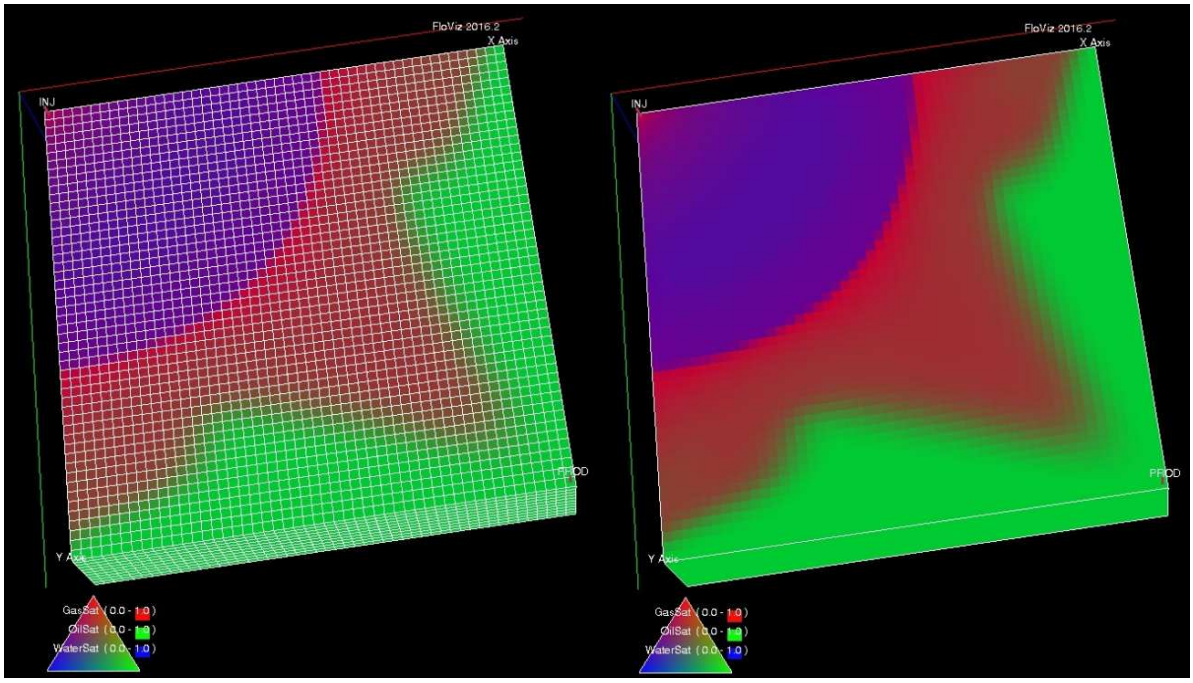

Figure 5.1 The quarter five-spot (homogeneous) model with and without the grid lines for a grid size of 100×100×20

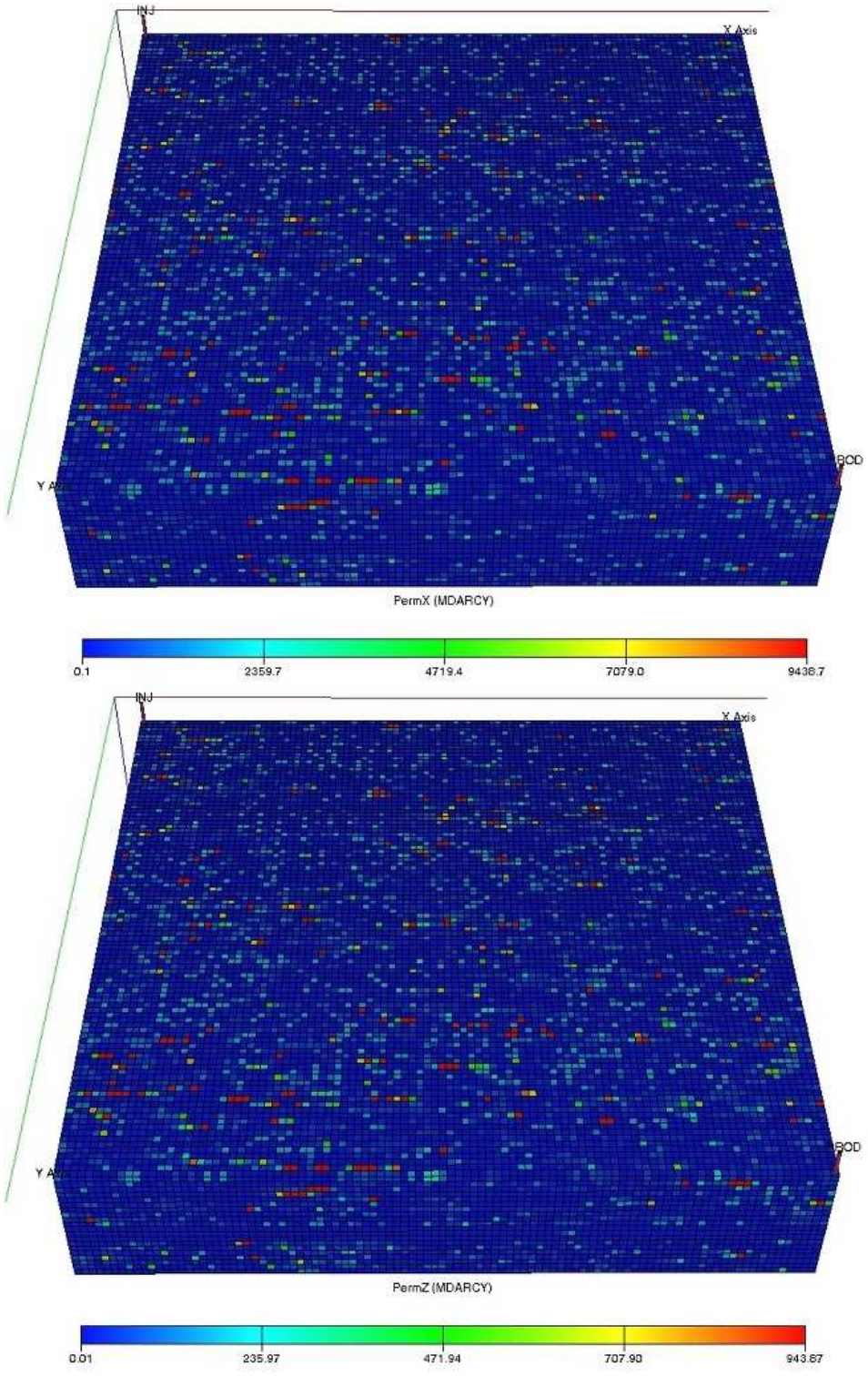

Figure 5.2 The permeability distribution in the x, y and z-direction of a (heterogeneous) quarter five-spot model for a grid size of 100×100×20

5.3 Watt field model

The Watt field is a semi–synthetic case study based on a mixture of real field (seismic data to interpret the faults and top structure) and synthetic data (the fluid properties, relative permeability, and capillary data) to describe a realistic field example (Arnold et al., 2013). The model provides the complexity of multiple wells, horizontal producers, faults, and complex permeability and porosity distributions, such as those in a real field and is therefore an appropriate evaluation for examining the effect of ω calibration.

The reservoir spans an area of 12.5 km by 2.5 km elongated in the East/West direction and has a thickness of about 190 m, much of which is below oil water contact (OWC) (1635 m below subsurface). The reservoir simulation model for this study has 8 injector wells and 21 producer wells.

There are nine faults in the model as shown in Figure 5.3 and they are permeable. Figure 5.4 is the permeability distribution of the Watt field in the directions x, y and z.

The model was originally saturated with oil and water and there was no free gas in the reservoir; the water was in the bottom part of the model. The model has a heterogeneous porosity that ranges between 0.03 and 0.266, and heterogeneous permeability. The model total pore volume PORV= 2.030×10^9 RB (reservoir barrel) and the original oil in place was 1.664×10^9 STB (stock tank barrel).

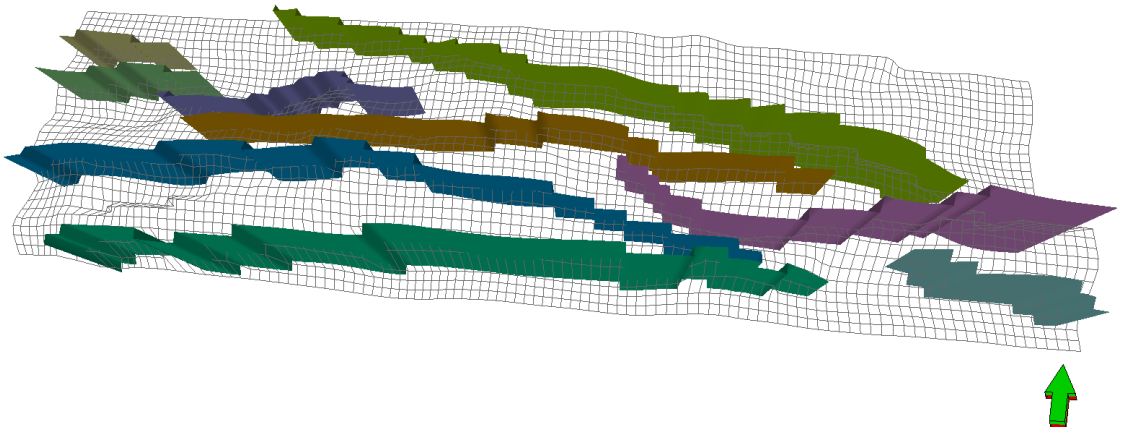

Figure 5.3 The fault distribution in the Watt Field with the grid cells of a grid size of 112×30×40

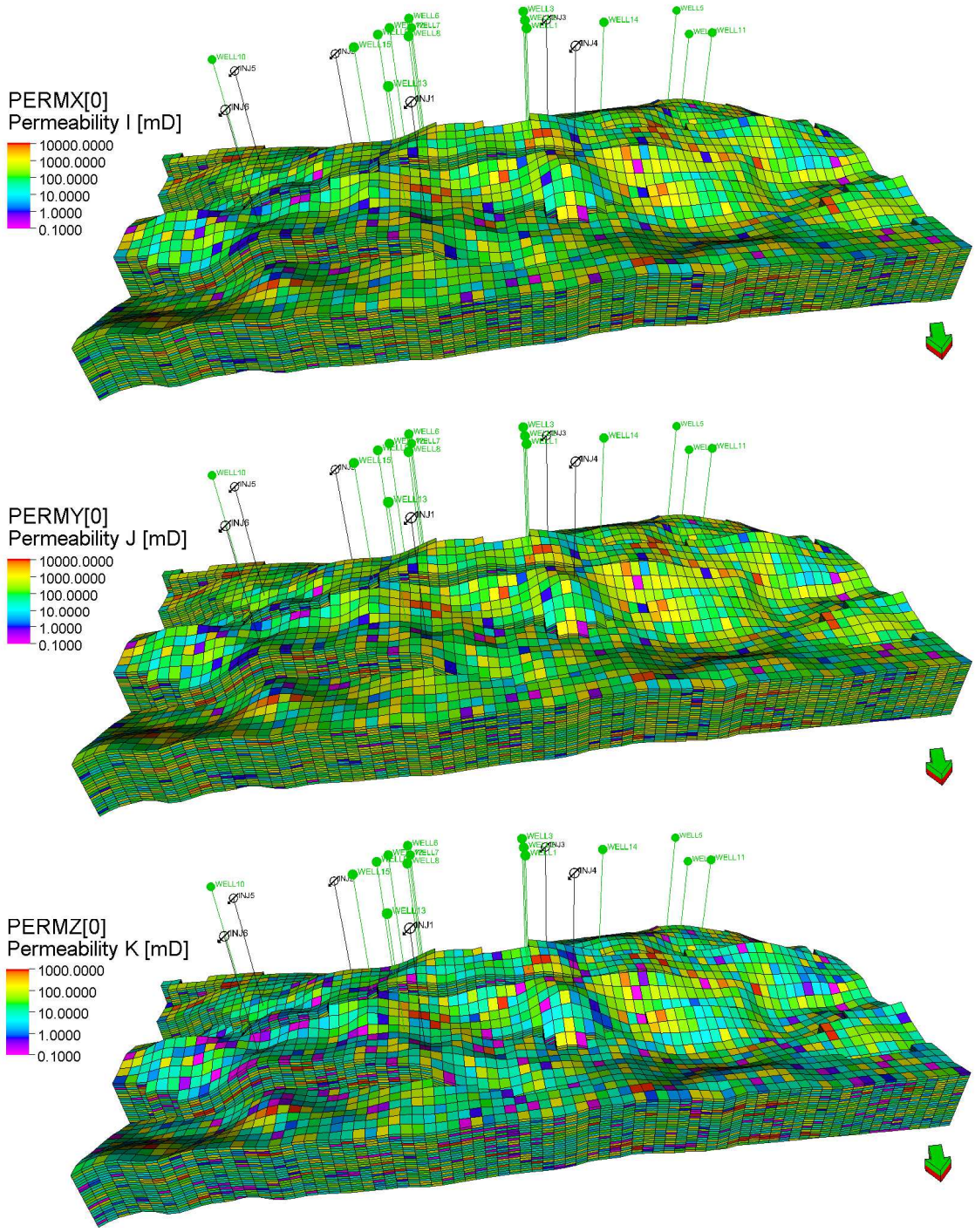

Figure 5.4 The permeability distribution in the x, y and z-direction of a Watt Field, the black wells are injectors and the green wells are producers.

5.4 Fluid properties used in the models under study

To implement miscible finite sized slug WAG injection in the quarter five-spot and Watt field models, the fluid properties (synthetic data) were taken from the files provided by Schlumberger with the Eclipse 100 package for first contact miscible gas injection (Figure 5.5). The properties were for under saturated oil reservoir with live oil properties and no gas cap (the average reservoir pressure was 6000 psia and the bubble point pressure was 1200 psia, where gas solution versus the change in depth is equal to 0.5). The gas viscosity had been modified so that the viscosity ratio of oil to gas would equal 10 to implement the previously calibrated values of ω.

The oil and water relative permeability curves in Figure 5.6 were used based on the equations that have been given in Chapter 4, while the gas relative permeability was the same as the one provided by the Eclipse 100 package. The capillary pressure was assumed to be zero.

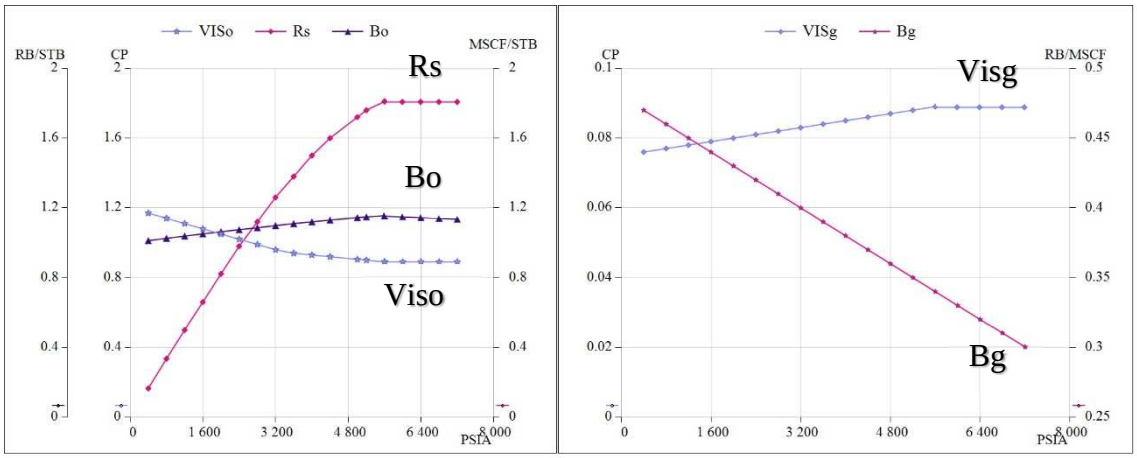

Figure 5.5 Properties of live oil (with dissolved gas) on the left-hand side picture and the properties of dry gas (no vaporized oil) on the right-hand side picture

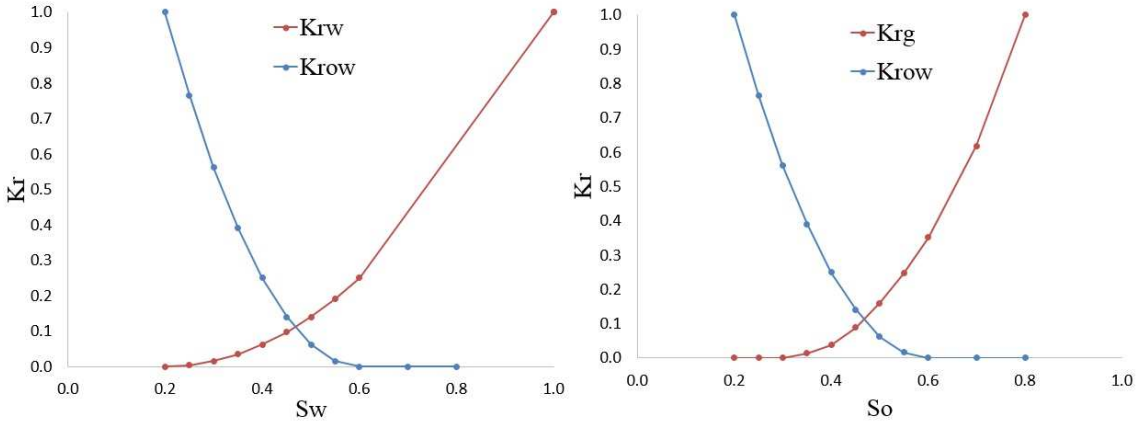

Figure 5.6 The relative permeability curves for water/oil system and gas/oil system.

5.5 Grid refinement study

To find the optimum grid size for this study, a grid refinement study was conducted on the quarter five-spot and Watt field. The grid refinement was considered for all the directions (Nx, Ny and Nz).

The difference between the incremental recoveries for the refined grids for both models was used to examine the impact of grid refinement. Figure 5.7 shows the effect of both horizontal and vertical grid size refinement in the quarter five-spot model on the oil recovery for miscible FSS WAG injection for a WAG ratio 1:1, and a slug size of 0.01 PV because the value of ω =1. The results show that there was not a significant change in the oil recovery efficiency (FOE) with increasing grid refinement.

Figure 5.8 shows the impact of the grid refinement on the field water cut (FWCT) and on the field gas production (FGPR). Grid refinement was seen to have no impact on the field water cut, however a significant rise in FGPR was noted for the 100×100×20 grid.

For quarter five-spot model, the grid size of 100×100×20 was found to be suitable for this study to capture the details as further grid refinement resulted in little change in the curve of the field gas production and the oil recovery. Also, the computational time of this grid size was reasonably fast (2 days).

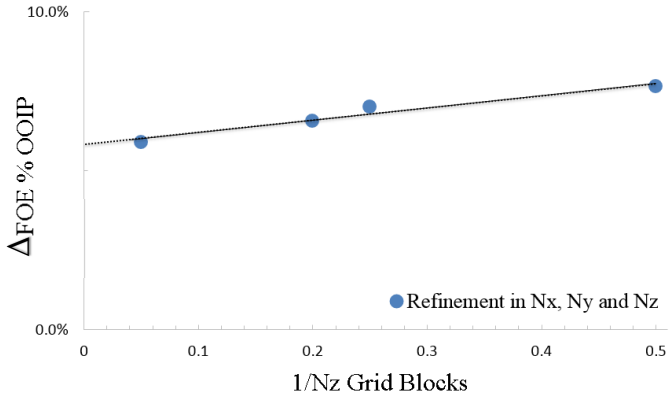

Figure 5.7 The effect of horizontal and vertical grid refinement on the efficiency of oil recovery (FOE) in miscible finite sized slug WAG injection in quarter five-spot model

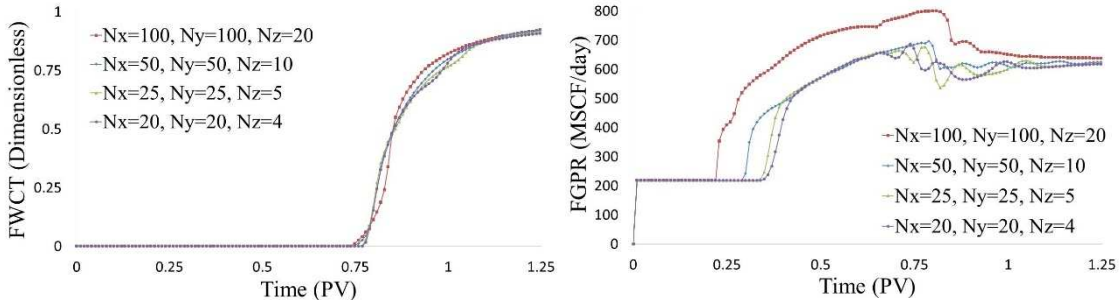

Figure 5.8 The effect of horizontal and vertical grid refinement on field gas production (FGPR) and field water cut (FWCT) in miscible finite sized slug WAG injection in a quarter five-spot model

Due to the complexity of the Watt field model and the computation time required to finish the run, only three points were conducted for the grid refinement. The grid refinement was conducted on a 336×90×120 (grid refinement of 112×30×40 multiplied by 3, which took 7 days to finish the run), a 560×150×200 (grid refinement of 112×30×40 multiplied by 5, which took 12 days to finish the run) and a 784×210×280 (grid refinement of 112×30×40 multiplied by 5, which took 4 weeks to finish the run).

Similarly, the difference between the incremental recoveries for different grids was used to examine the impact of the grid refinement. Figure 5.9 shows the effect of both horizontal and vertical grid size refinement in the Watt field model on the oil recovery for miscible FSS WAG injection for a WAG ratio 1:1, a slug size of 0.01 and $\omega = 1$. From the results it can be seen that there is little difference between the recoveries as a result of the grid refinement. The point ΔFOE=7.57 is the difference between FOE obtained from

grid size 784×210×280 and FOE obtained from 112×30×40. Similarly, is the case with the other points.

Figure 5.10 shows the impact of the grid refinement on the field water cut (FWCT) and on the field gas production (FGPR). The difference is small between FWCT and FGPR for the different grid refinements.

For, the Watt field model, the grid size of 112×30×40 was found to be suitable for this study as further grid refinement resulted in little change in the oil recovery, field gas production and field water cut. Also, the computational time of this grid size is reasonably fast if it is to be used later in the optimisation.

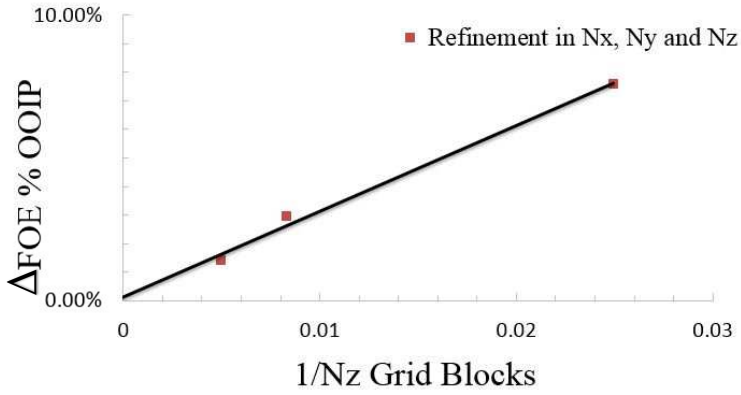

Figure 5.9 The effect of horizontal and vertical grid refinement on efficiency of oil recovery (FOE) in miscible finite sized slug WAG injection in a Watt field model

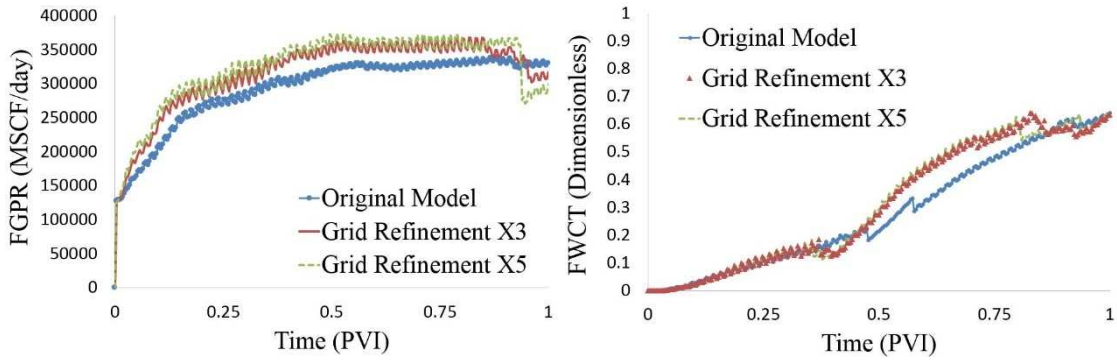

Figure 5.10 The effect of horizontal and vertical grid refinement on the field gas production (FGPR) and on the field water cut (FWCT) in miscible finite sized slug WAG injection in a Watt field model

5.6 Assumptions of applying the calibrated ω's value on the field scale

The value of ω is the key parameter influencing the reservoir model behaviour during miscible finite sized slug WAG injection in a black oil model. To demonstrate that the calibrated values of ω for a specific WAG ratio and slug size work, the values need to be applied on the field scale.

The assumptions for applying ω on the field scale are:

1. Gravity effects are included in the field simulations but not used in calibrating ω.
2. Capillary pressure is zero
3. The effect of relative permeability hysteresis is ignored (hysteresis appears in changes of the relative permeability curve's shape and values of residual fluid saturation. It arises due to continuous saturation changes of the injection fluids in three-phase flow and leads to gas entrapment).
4. Viscosity ratio of oil to solvent equal to 10
5. First contact miscible gas injection
6. The effects of permeability variations are neglected. The value of ω could be used to represent sub grid block viscous fingering in a reservoir simulator which has an explicit permeability field.

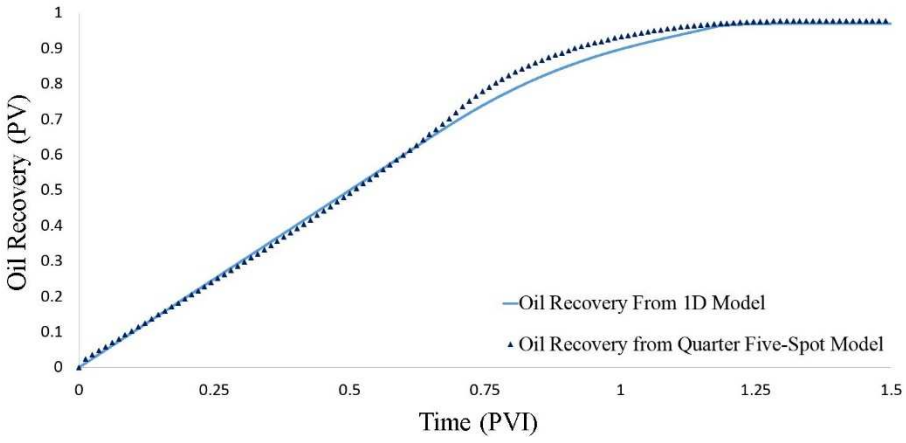

Figure 5.11 A good match between the oil recoveries obtained from the 1D model and the quarter five-spot model.

In order to implement the calibrated value of on a field scale, the recovery from the 1D model and from the Eclipse E100 are compared. Figure 5.11 shows there is a good match

between the oil recovery obtained from the 1D model and from the quarter five-spot model. This step was for a research purpose and it is not necessary with different models. Therefore, with the assumptions provided earlier, the ω's values are implemented on the field scale.

5.7 Reservoir oil recovery at different types of injection

The results of calibrating ω are tested first on the quarter five-spot model to allow the demonstration of some of the key features of FSS WAG injection in a 3D reservoir model without the additional complexity of multiple wells, horizontal producers, faults, and complex permeability and porosity distributions that exists in the Watt field model. It also enabled the question of how the calibration of ω impact the reservoir performance if the reservoir system (i.e. geometry/heterogeneity/wells) becomes more complex to be addressed.

AWAG ratio of 1:1 has been put forward as the most popular ratio for field-scale application (Christensen et al., 2001, Al-Shuraiqi, 2005) and it is stated that a slug size of between 0.1 and 0.3 PV is common practice in the industry. According to Minssieux and Duquerroix (1994), under operational conditions, an injection approaches SWAG injection at a slug size smaller than 0.03 PV. Therefore, a slug size of 0.01 PV would be considered as being similar to SWAG injection, however there remain fundamental differences in capital expenditure associated with SWAG that impact operational decisions and the facility design. Since the more popular slug sizes, 0.1 to 0.3 PV, were shown above to have a low mixing parameter (Chapter 4), the scenarios tested in this section used slug sizes of 0.01, 0.05 and 0.1 PV.

A WAG ratio of 1:1 and a slug sizes of 0.01 PV (ω = 1), 0.05 PV (ω = 0.87) and 0.1 PV (ω = 0.84) were used to show the reservoir performance (FOE % OOIP) of secondary FSS WAG injection compared with SWAG injection, miscible gas injection (at ω = ⅔ and 1) and water injection.

The reservoir volume production rate was set using minimum BHP equal to 2000 psia. The reservoir injection rate was fixed during the whole period of injection and was equal to the reservoir production rate of 250,000 RB/day at reservoir volume rate to maintain

the reservoir pressure, to compare between the different types of injection and to show the impact of ω on the results. The injection was carried out for 30 years (1.3 PVI).

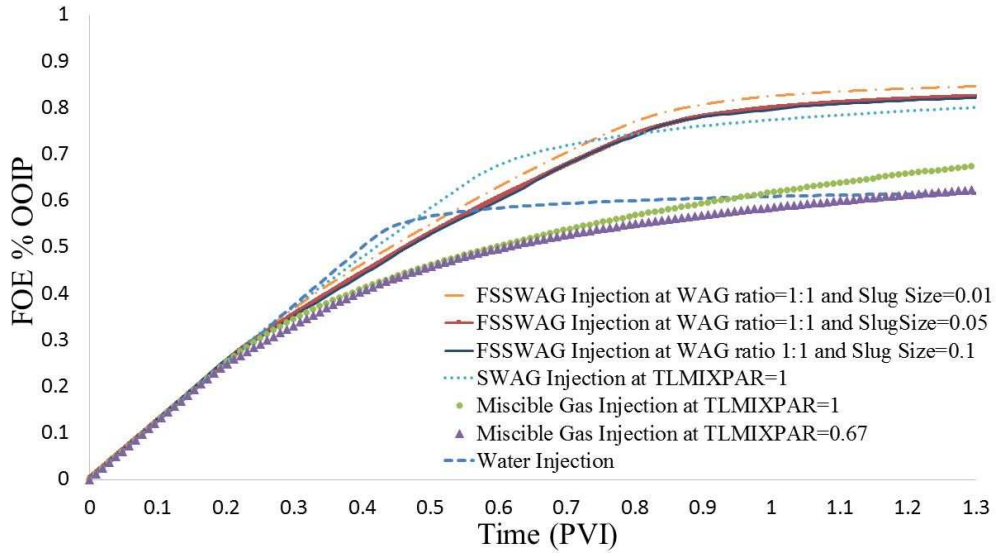

Figure 5.12 Comparison between the oil recoveries for different types of injection for quarter five-spot model. Where, FOE means the field oil recovery (%, percentages refer to the original oil in place), TLMIXPAR means the mixing parameter value ω and FSS WAG means finite sized slug WAG injection.

Figure 5.12 shows the oil recovery for different types of injection conducted on a quarter five-spot model. As the slug size of secondary miscible FSS WAG injection increased the oil recovery decreased slightly. The oil recovery for the FSS WAG injection at different slug sizes was greater than for the secondary SWAG injection, the secondary miscible gas injection and the water injection. As can be seen, the oil recovery for the water injection method showed the highest recovery at earlier injection time (until 0.4 PVI) compared to the other types of injection, however, in the long term the oil recovery obtained was lower compared to the other methods. Secondary SWAG injection achieved almost the same recovery as secondary FSS WAG injection at slug size of 0.05 and 0.1 PV but was still lower than the FSS WAG injection for the slug sizes shown. This suggests that miscible FSS WAG injection improves oil recovery to a greater extent compared with the other types of injection.

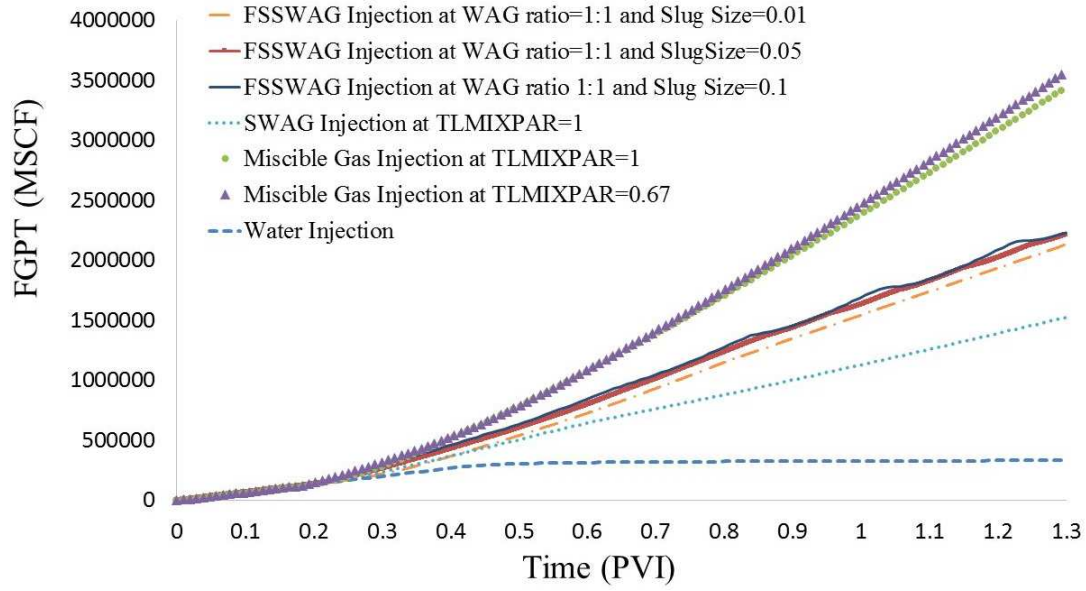

Figure 5.13 Comparison between the total gas productions (FGPT) for different types of injection for quarter five-spot model. Where, TLMIXPAR means the mixing parameter value ω and FSS WAG means finite sized slug WAG injection.

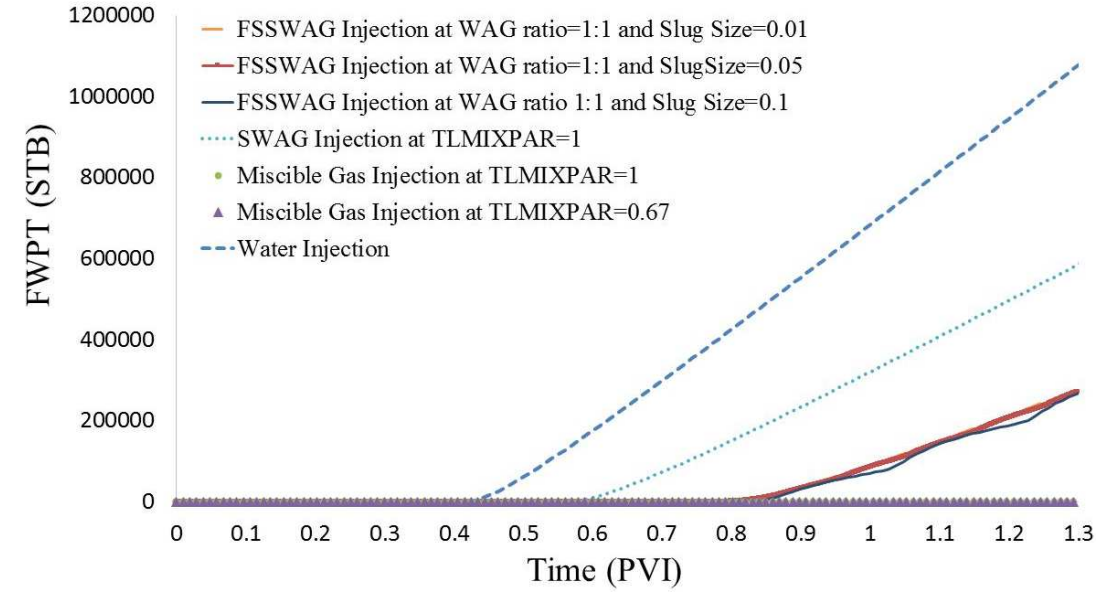

Figure 5.14 Comparison between the total water productions (FWPT) for different types of injection for quarter five-spot model. Where, TLMIXPAR means the mixing parameter value ω and FSS WAG means finite sized slug WAG injection

Figure 5.13 and Figure 5.14 show the total gas production (FGPT) and the total water production (FWPT) respectively, for different types of injection conducted on a quarter five-spot model. From Figure 5.13, it can be seen that the total gas production for miscible gas injection at both ω=1 and ω=0.67 is the highest while from Figure 5.14 the total water

production for this method was equal to zero. The opposite behaviour is observed during the water injection. It can be seen from Figure 5.13 that the total gas production during water injection is the lowest (gas solution) while from Figure 5.14 the total water production for this method was the highest. Additionally, it can be seen that the total gas production during SWAG injection is higher than the total gas production during water injection and is less than the total gas production during the other types of injection. The opposite behaviour is observed in Figure 5.14 with the total water production during SWAG injection as it can be seen that the total water production during SWAG injection is less than the total water production during water injection and higher than the total water production during the other types of injection. As for miscible FSS WAG injection, it can be seen that as the total gas production increases as the slug size increases. However, for the total water production there is no notable difference with changes of slug sizes.

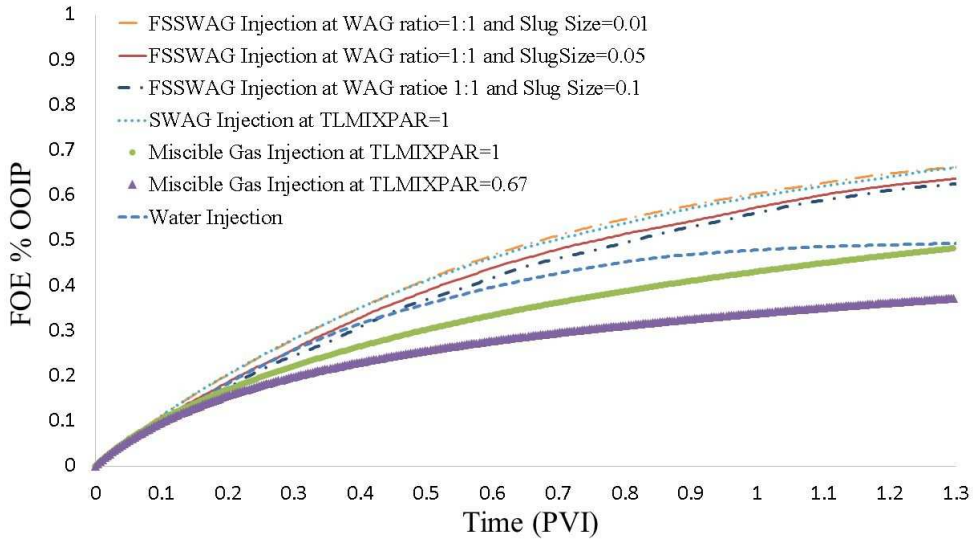

Figure 5.15 Comparison between the oil recoveries at different types of injection for Watt field model. Where, FOE means the field oil recovery (%, percentages refer to the original oil in place), TLMIXPAR means the mixing parameter value ω and FSS WAG means finite sized slug WAG injection.

Figure 5.15 represents the oil recovery obtained for different types of injection on the Watt field model. Using the same injection techniques as previously used in the quarter five-spot model, it can be seen that the oil recovery from the Watt field model behaves differently. The oil recovery was the highest for the FSS WAG injection with a slug size 0.01 PV and for the SWAG injection (both recoveries were equal). While the SWAG and FSS WAG showed equal oil recovery, miscible FSS WAG was the preferred method as

SWAG has an operational complexity for implementation on a field scale (as mentioned in Chapter 2). The oil recovery for the FSS WAG injection increased as the slug size decreased, which is similar to that observed in the quarter five-spot model. The oil recovery from the water injection and the miscible gas injection at $\omega = 1$ were almost the same at the end of injection, with both being lower than the FSS WAG injections.

Figure 5.16 and Figure 5.17 show the total gas production (FGPT) and the total water production (FWPT) respectively, for different types of injection conducted on a Watt field model. Similar behaviour is observed in the total gas and water production on the Watt field model using the different types of injection compared with what has been seen using the quarter five spot model. From Figure 5.16, it can be seen that the total gas production is highest for the miscible gas injection at both ω=1 and ω=0.67, while from Figure 5.17 the total water production for this method was equal to zero. The opposite behaviour is observed during the water injection. It can be seen from Figure 5.16 that the total gas production during water injection is the lowest (gas solution) compared with all other injection methods, while from Figure 5.17 the total water production for this method was the highest. In addition, it can be seen that the total gas production during SWAG injection is higher than the total gas production during water injection and is less than the total gas production during the miscible gas injection but is similar to the total gas production using miscible FSS WAG injection. The opposite behaviour is observed in Figure 5.17 with the total water production during SWAG injection. It can be seen that the total water production during SWAG injection is less than the total water production using water injection and higher than the total water production using the other types of injection. As for miscible FSS WAG injection, it can be seen that as the total gas production increases as the slug size increases however, they are similar. While it can be seen that the total water production increases as the slug size decreases, the difference between the values is negligible.

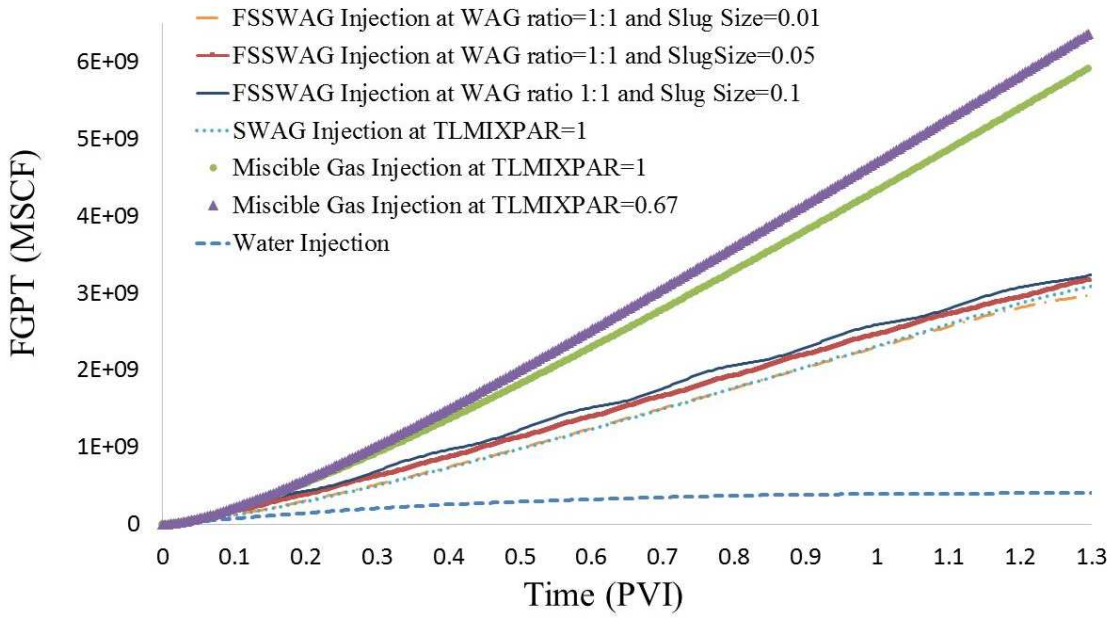

Figure 5.16 Comparison between the total gas productions (FGPT) at different types of injection for Watt field model. Where, TLMIXPAR means the mixing parameter value *ω* and FSS WAG means finite sized slug WAG injection

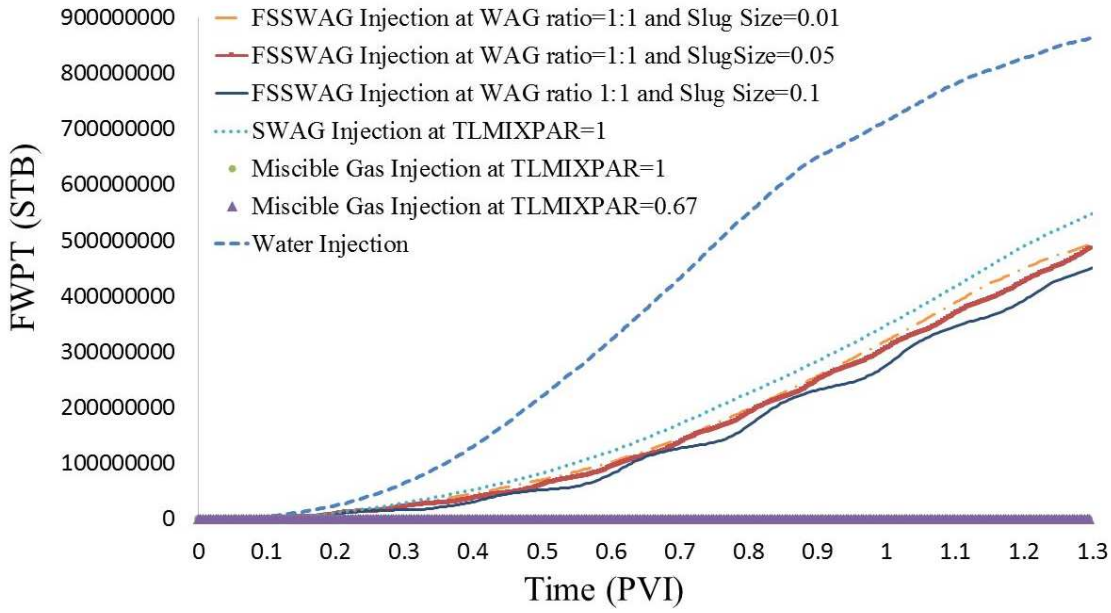

Figure 5.17 Comparison between the total water productions (FWPT) at different types of injection for Watt field model. Where, TLMIXPAR means the mixing parameter value *ω* and FSS WAG means finite sized slug WAG injection

5.8 The impact of ω's value on the reservoir performance

Complete oil sweep during an injection process is unlikely to be achieved on the field scale even under perfectly miscible conditions with first contact miscibility. There will be some remaining oil left that is quantified by the residual oil saturation value, S_{or} (Ahmed, 2006). The term residual oil saturation is usually associated with the oil, when it is being displaced gas or water.

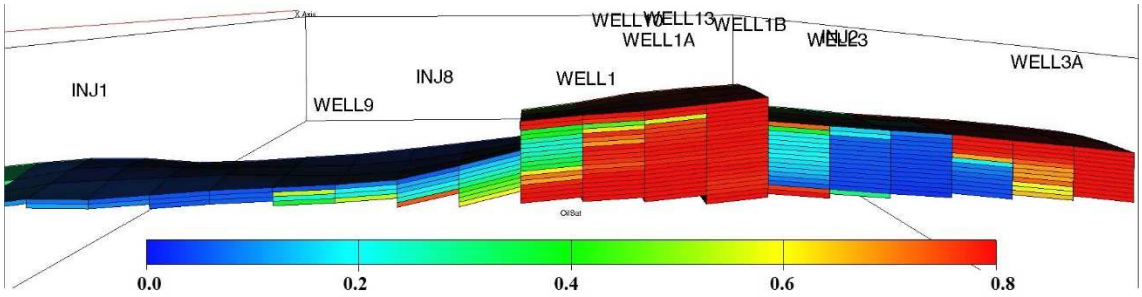

Figure 5.18 shows distribution of oil saturation on the Watt field model for miscible FSS WAG injection at WAG ratio 1:1 and a slug size of 0.05 PV.

Figure 5.18 shows the distribution of oil saturation in the Watt field model for miscible FSS WAG injection at WAG ratio 1:1 and a slug size of 0.5 PV. Due to the complexity of the Watt Field, it is hard to capture the details on a well level compared to the quarter five-spot model.

Figure 5.19 shows the distribution of oil saturation in the quarter five-spot model for different types of injection. For miscible gas injection, it can be seen that the two-phase region (the green area in which gas and oil exist at the same time) at ω = 1 was smaller than the two-phase region when ω = 0.67. By using ω = 1, the gas mixes completely with the oil and there will be no viscous fingering in the system like the case with ω = 0.67. This was similarly the case with water flooding, in which the two-phase region was even smaller than the miscible gas injection at ω = 1. However, the residual oil saturation after water flooding (S_{orw}= 0.3) was higher than the residual oil saturation after miscible gas injection (S_{org}= 0.0).

Alternatively, in the FSS WAG injection there was a three-phase region where gas, water and oil existed at the same time/place (the green area still represents a two-phase region of water and oil since gas is first contact miscible with the oil).

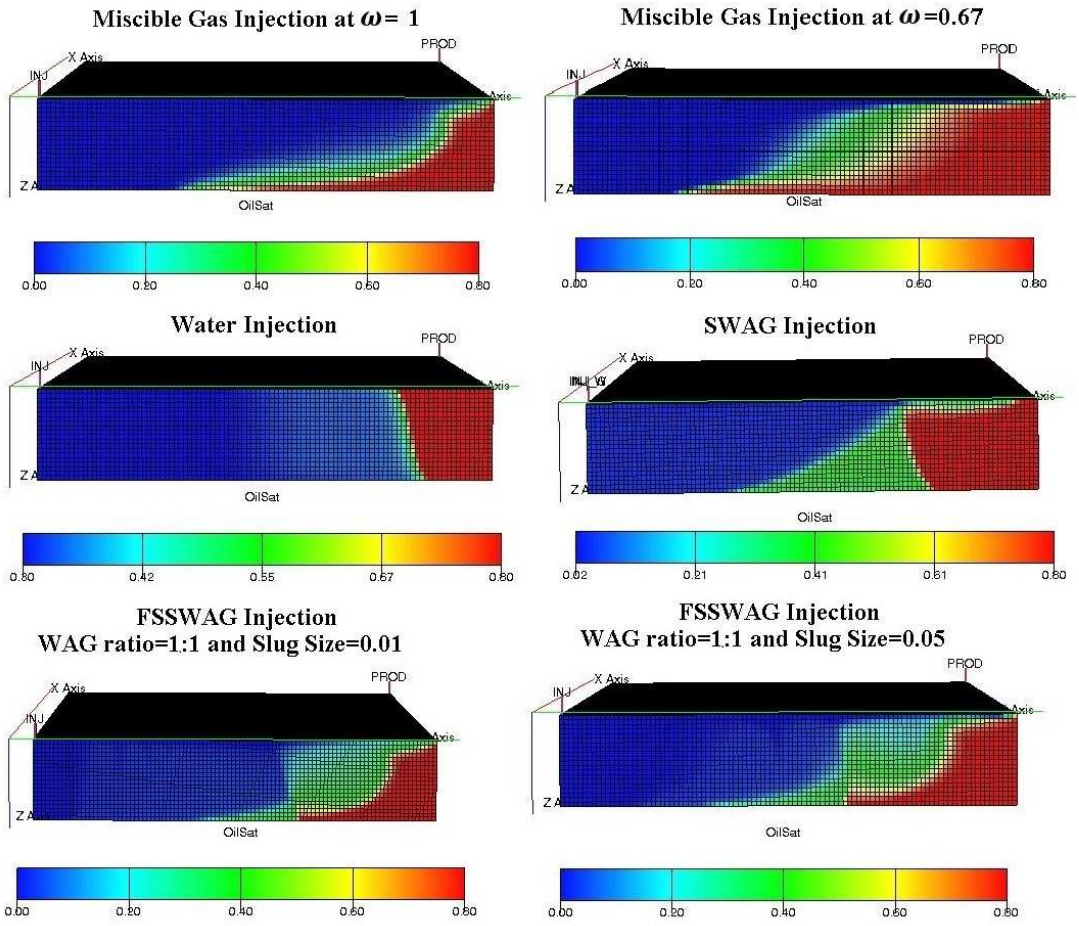

Figure 5.19 Distribution of oil saturation in the quarter five-spot model (homogeneous model) at the same time of gas breakthrough. Where, TLMIXPAR stands for Todd and Longstaff's mixing parameter. The residual oil saturation after water injection was S_{orw}=0.3, after miscible FSS WAG injection was S_{org}=0 and after miscible gas injection was S_{org}==0.

When three phases are flowing at the same time, three-phase relative permeabilities are required to account for the interaction of flow among the different phases. They are often interpolated from two-phase relative permeability data. Specifically, gas-oil and oil-water relative permeability (at connate water saturation) are used to compute the three-phase relative permeability through three-phase models (Zuo et al., 2014). The reason for this is that three-phase flow occurs when the saturation of water is higher than the irreducible water saturation, while oil and gas also exist in the same place as mobile phases.

The three-phase zone is usually represented by the ternary diagram to illustrate the changes in the relative permeability values as shown in Figure 5.20. The three corners of the ternary diagram represent 100% oil saturation S_o, 100% gas saturation S_g, and 100% water saturation S_w, whereas the sides of the triangle (opposite ends) of these corners represent 0% saturation of that phase (Dandekar, 2013).

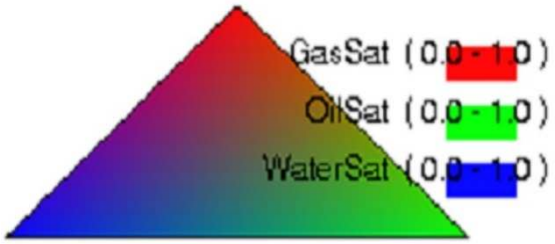

Figure 5.20 Represents the ternary diagram of the phase distribution where green, blue and red represents oil, water and gas, respectively

Due to the complexity of the Watt Field model, it is difficult to capture the three-phase region and the impact of ω on the miscible FSS WAG injection as shown in Figure 5.21, which represents the saturation distribution in the Watt field model using the ternary diagram. The three-phase region was observed at field-resolution at a grid size of 112×30×40, on a well level (Injector 1) for the grid size 112×30×40 and on a well level after a grid refinement (336×90×120). In those three cases, it was difficult to observe the impact of ω on the three-phase region, therefore the three-phase region was examined in further detail on the quarter five-spot model

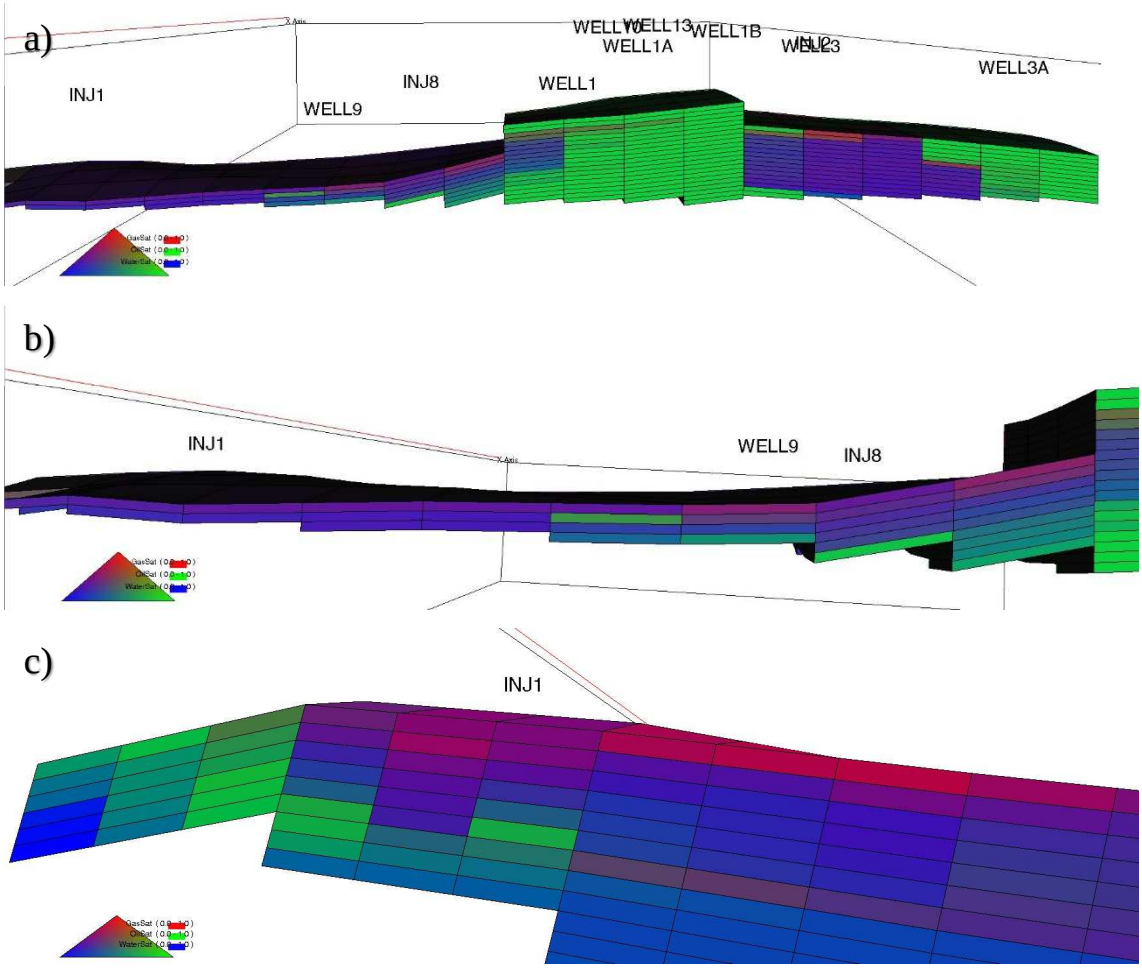

Figure 5.21 Three-phase distribution in the Watt field model using the ternary diagram. a) represents the saturation distribution on a grid size 112×30×40, b) represents the saturation distribution on a well level (Injector 1) and c) represents the saturation distribution on a well level after a grid refinement (336×90×120)

Figure 5.22 represents the three-phase distribution using the ternary diagram for both homogeneous (righ-hand side) and heterogeneous (left-hand side) versions of the quarter five-spot model. The three-phase region was examined for a WAG ratio of 1:1 and a slug size of 0.05 PV or 0.1 PV. Those slug sizes allowed for the comparison between the calibrated value of ω with the full mixing ω =1, and Todd and Longtsaff's value of 0.67.

It can be seen that considerable three-phase flow occurred in the WAG processes and that the gas significantly fingered through the oil in the heterogenous model. Additionally, it can be seen that the value of ω impacted the three-phase zone in the heterogeneous model, because at the same grid block and time, the saturations varied significantly. On the other

hand, the homogeneous model yielded similar three phase regions for the different values of ω, but the spread of gas from the injector did vary considerably between the examples.

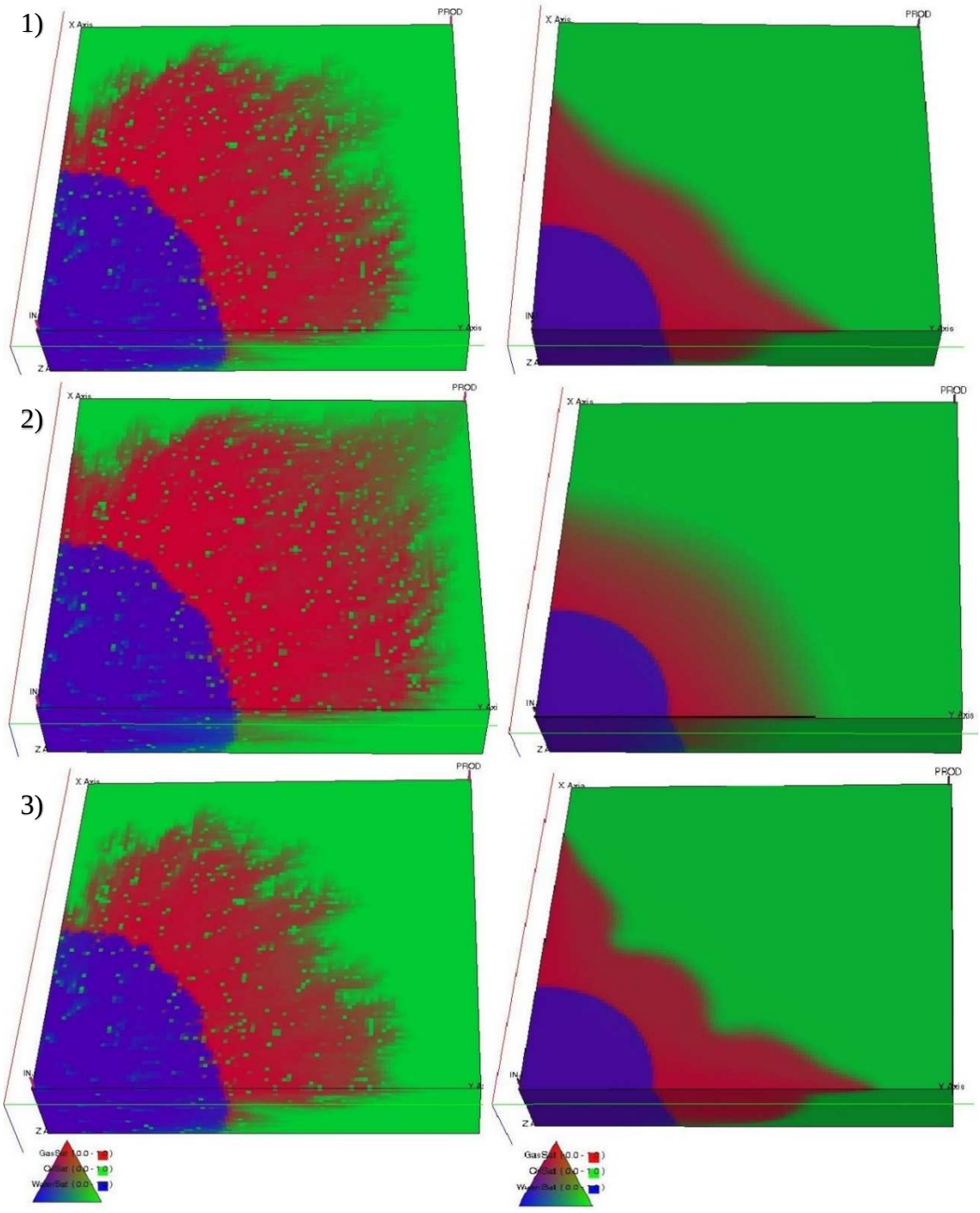

Figure 5.22 Represents the three-phase distribution using the ternary diagram for the WAG ratio 1:1 and a slug size of 0.05 PV at the time of gas breakthrough for both homogeneous (righ-hand side) and heterogeneous (left-hand side) of the quarter five-spot model. where 1) is at the calibrated value of ω, 2) is at $\omega = 1$ and 3) is at $\omega = 0.67$. The purple region is where all the three phases exist at the same time.

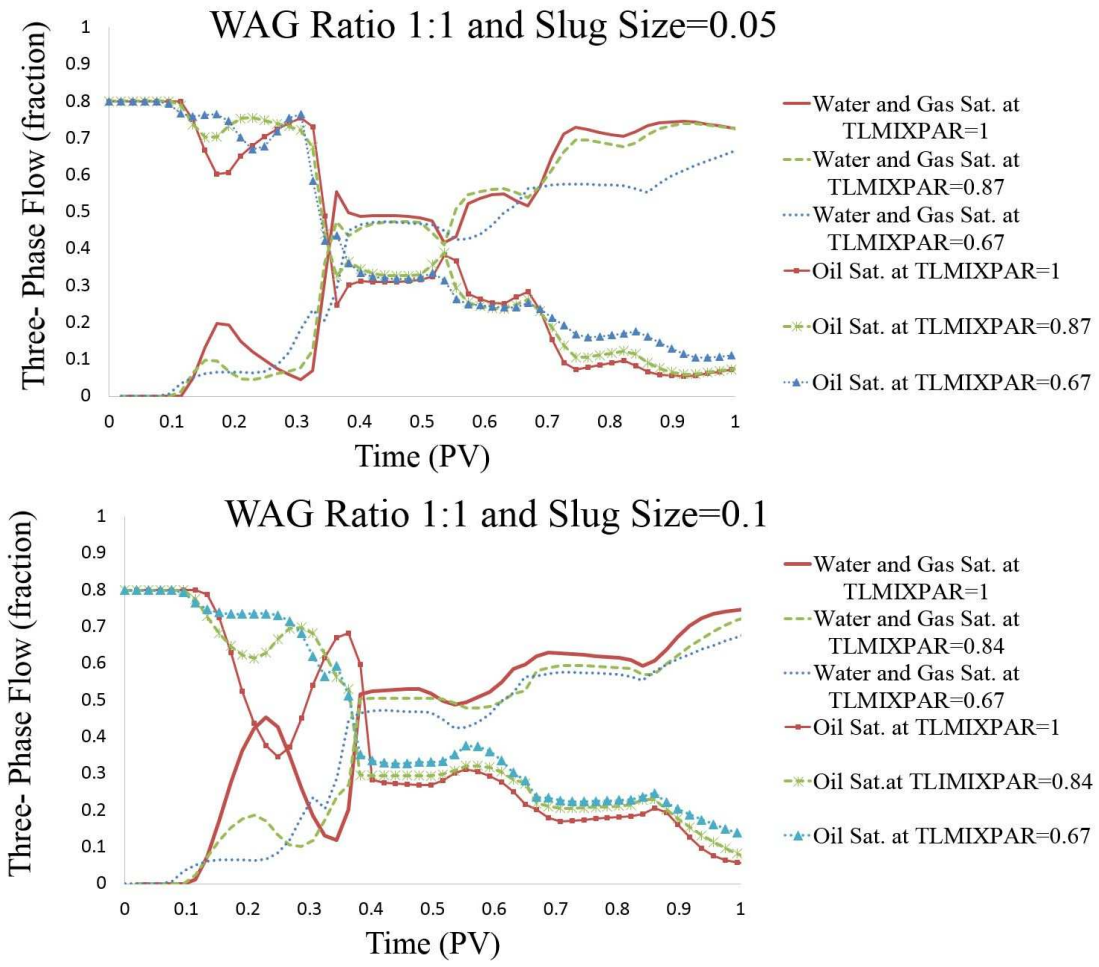

Figure 5.23 Fractions of three-phase-flow region (S_{or}=0.2) at different values of the mixing parameter (TLMIXPAR) during 1:1 WAG injection at grid block 50, 50, 10.

Figure 5.23 shows the evolution of the percentage of three-phase fraction with time at grid block (50, 50, 10) for 1:1 WAG ratio and at slug size 0.05 PV and 0.1 PV. This grid block (50, 50, 10) is in the middle of the quarter five-spot model and within the three-phase zone. The average reservoir pressure was maintained at the original reservoir pressure, so the results were due to the effect of ω alone. From Figure 5.23, it can be seen that the fraction of three-phase-flow was considerably higher at ω = 1 than at ω = 0.67. It is also evident that the percentage of three-phase zone was higher at slug size 0.05 PV than at 0.1 PV. Whilst the three-phase zone was equal at the end of the 0.05 PV slug size for ω = 1 and the calibrated value of ω, it can be seen that there was a difference at the end of the injection for a slug size 0.1 PV. The three-phase zones at slug size of 0.05 PV is bigger than the three phase zones at slug size of 0.1 PV.

5.9 Reservoir oil recovery at different values of ω

Based on the results of the previous section, the miscible FSS WAG injection at a slug size of 0.05 PV was chosen to compare the values of ω at the fully mixing value (ω = 1) and at the Todd and Longstaff's value (ω = 0.67). The reason for choosing this slug size was that at a slug size of 0.01 PV the value of ω was 1 based on the calibration in chapter 4, so it will not give a chance for a comparison at two different values. In addition, the slug size of 0.05 PV gave a better recovery than the 0.1 PV in both models, as shown previously.

Figure 5.24 shows a comparison between the oil recovery obtained from secondary miscible FSS WAG injection at a WAG ratio of 1:1 and a slug size of 0.05 PV at the calibrated value of ω = 0.87 and ω = 1 and 0.67. The reservoir pressure was maintained at the original average reservoir pressure, so that all the results obtained were due to the effect of ω. From Figure 5.24, 1), it has been observed that the different values of ω have no impact on the reservoir performance in the homogeneous model (where permeability and porosity are the same across the model) of the quarter five-spot model. This means that, for homogeneous models, the mixing parameter value has no impact on the reservoir performance, and the recovery will be almost equal at the end of the injection period. As a result, the value of ω is tested on a heterogeneous model of the quarter five-spot model. From Figure 5.24, 2), it is observed that the values of ω has an impact on the oil recovery. The oil recovery at ω = 1 was the highest, while the oil recovery at ω = 0.67 was the lowest and the oil recovery at ω = 0.87 comes in between. This represents the reliable, achievable oil recovery. Similar results were obtained from the Watt field model as shown in Figure 5.24 (3). The oil recovery at ω = 1 was the highest, while the oil recovery at ω = 0.67 was the lowest and the oil recovery at ω = 0.87 comes in between. The impact of ω on the oil recovery is very clear. For longer injection periods, the difference in the oil recovery would be even greater.

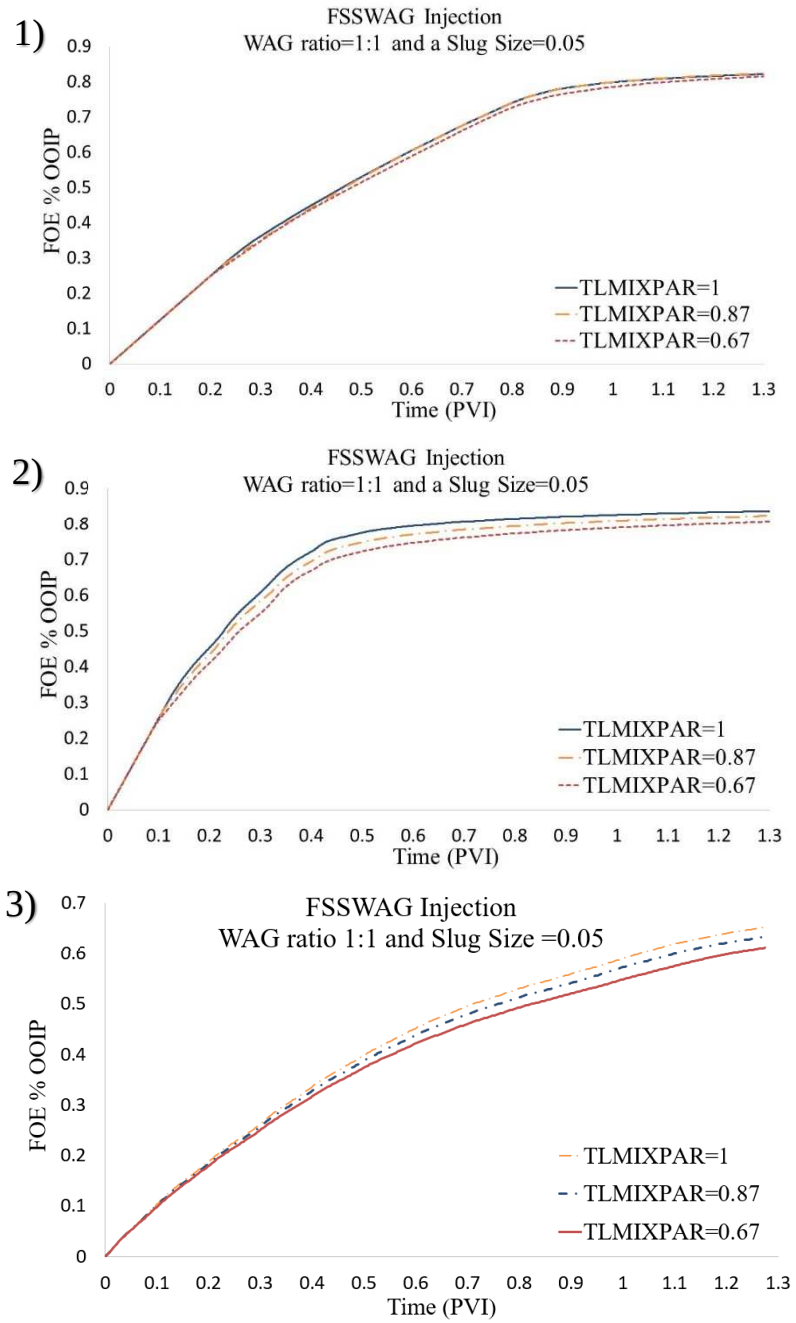

Figure 5.24 the oil recovery obtained using different ω (TLMIXPAR) values for secondary FSS WAG injection for a WAG ratio 1:1 and a slug size of 0.05 PV. The grid size is 100×100×20. 1) a quarter five-spot model (homogeneous model) the grid size is 100×100×20. 2) a quarter five-spot model (heterogeneous model). 3) Watt field model (heterogeneous model) the grid size is 112×30×40

5.10 Summary of the chapter

This chapter shows the application of the results of calibrating the mixing parameter, ω, for miscible finite sized slug WAG (FSS WAG) injection presented previously in Chapter

4. The reason of the application on the field scale was to show the reservoir performance obtained when using the calibrated value of ω at its specific WAG ratio and slug size for both secondary and tertiary recovery. Also, to compare the reservoir performance at the calibrated value with Todd and Longstaff's value = ⅔ and with a full mixing $\omega = 1$.

Two case studies were used to test the reservoir performance, a synthetic quarter five spot model and a semi-synthetic model (Watt field model). Both models used the same properties mentioned earlier in this chapter. The quarter five-spot model allowed for the demonstration of some of the key features of FSS WAG injection in a 3D model without the additional complexity of multiple wells, horizontal producers, faults, and complex permeability and porosity distribution like the one in the Watt field model.

The results showed that as the slug size increases the oil recovery decreases and it achieved better recovery than SWAG injection.

The results showed that the values of ω had an impact on the three-phase zone and on the oil recovery. It was observed that the fraction of three-phase-flow was considerably higher at $\omega = 1$ than at $\omega = 0.67$. This resulted in the highest oil recovery for ω=1, followed by ω=0.87, with ω=0.67 giving the lowest recovery. Whilst the three-phase zone was equal at the end of the 0.05 PV slug size for $\omega = 1$ and the calibrated value of ω, it can be seen that there was a difference at the end of the injection for a slug size 0.1 PV. The three-phase zones increase as the slug size decreases which means that the oil recovery increases as the slug size decreases.

Chapter 6

Optimisation of miscible finite sized slug WAG (FSS WAG) injection

6.1 Introduction

In order to achieve a better oil recovery, optimising WAG injection parameters (such as slug size, WAG Ratio, WAG cycle length and time to initiate WAG injection) became recognized as a practical technique for controlling gas mobility and achieving high recovery (Mehos and Ramirez, 1989, Chen et al., 2010, Panjalizadeh et al., 2015, Chen and Reynolds, 2016, Chen and Reynolds, 2018, Mohagheghian et al., 2018).

In order to identify the impact of the calibrated value of ω on the optimisation of miscible FSS WAG injection, the optimisation of the slug size and WAG ratio for both secondary and tertiary recovery are used. The optimisation is extended to the optimisation of the type of fluid to inject, so called WAG pattern injection to further investigate the impact of the value of ω on the optimisation results. Furthermore, the impact of the calibrated value of ω on the optimisation results is extended to the optimisation for the flow rate injected which is added to the optimisation of WAG ratio, slug size and WAG pattern injection. The optimisation scenarios listed are performed with the assumption that there is an unlimited supply of gas to inject. Finally, the impact of the calibrated value of ω on the optimisation results has been investigated by adding the assumption that there is a limited amount of gas to inject for the optimisation of WAG ratio, slug size, WAG pattern injection and the amount of flow rate to inject. The results of the optimisation scenarios listed for the calibrated value of ω will be compared with the results of the optimisation at a fixed value of ω=1.

The optimisation has been accomplished using a multi-objective particle swarm optimisation (MOPSO) algorithm, which is implemented in Epistemy's Raven (www.epistemy.com) and it is combined with Schlumberger's Eclipse 100 (Geoquest, 2014), as a fluid flow simulator.

This chapter covers the interpolation of the calibrated values of ω for a wide range of slug size and WAG ratio using a Python code (a programming language), to enable the generation of ω values automatically for a specific slug size and WAG ratio inside the optimisation software. Next, it introduces the objective functions that are used in the optimisation problem and the reason for selecting them. Finally, it concludes with the workflow and the results of the optimisation cases.

6.2 Interpolating the Mixing Parameter, ω Values

In Chapter 4 (Figure 4.50 and Figure 4.51), the value of the mixing parameter, ω, was calibrated as a function of slug size and WAG ratio, as shown in Figure 6.1 for secondary recovery. The values of ω (TLMIXPAR) can be plotted as a function of fractional flow of water injected (FWINJ) at different slug sizes, where:

$$FWINJ = wat/(wat + gas), \\ if FWINJ = 0.5, then\ the\ WAG\ ratio\ will\ be\ 1:1 \tag{6.1}$$

It can be seen from Figure 6.1 that as the slug size increases the value of ω (TLMIXPAR) decreases. While this data set gave an idea of what occurs as the parameters were varied, it did not represent a complete data set for all the points and the parameter variations. For example, for FWINJ = 0.5 and a slug size = 0.03 PV, the value of ω (TLMIXPAR) has not been calculated. The reason for this is due to the computation expense and time needed to run the simulations necessary to generate the values required. Instead a number of values covering the search area of interest were studied and they were interpolated to generate the remaining data need for the optimisation of slug size and WAG ratio.

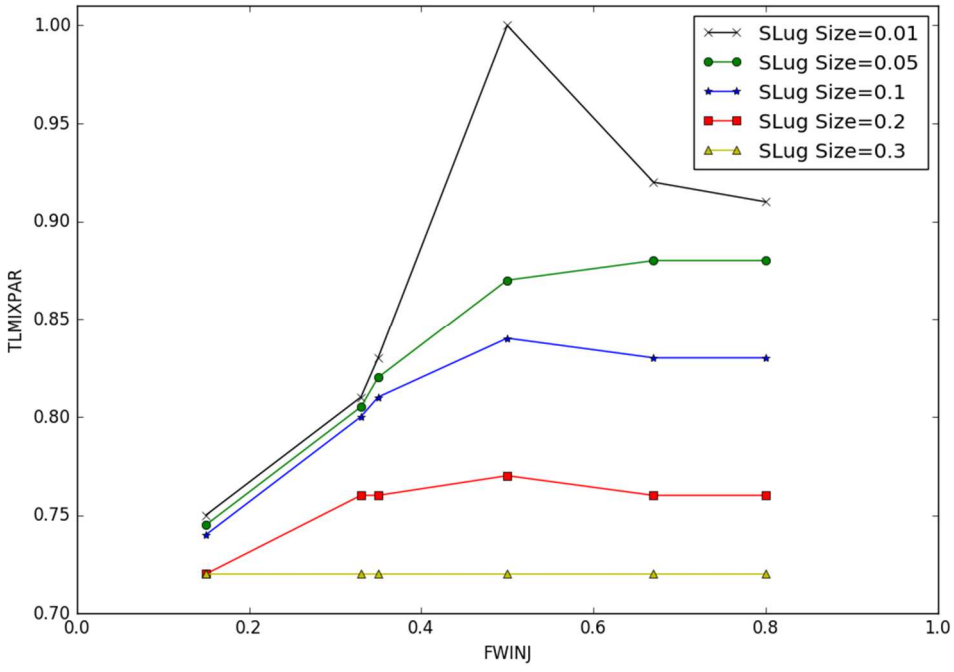

Figure 6.1 2D plot of the calibrated values of ω (TLMIXPAR) and WAG ratio at different slug sizes for secondary recovery (Figure 4.50).

In numerical analysis, interpolation is a method of filling gaps between existing points (Lepot et al., 2017). A Python code was developed to interpolate the missing values for the mixing parameter, slug size and WAG ratio from the existing data as shown in Figure 6.2, which shows the data after the interpolation, plotted in three-dimensions. A three-dimensional plot was required to display the data as the number of values has increased significantly, giving a wider number of points of slug size and WAG ratio values available for use by the optimiser.

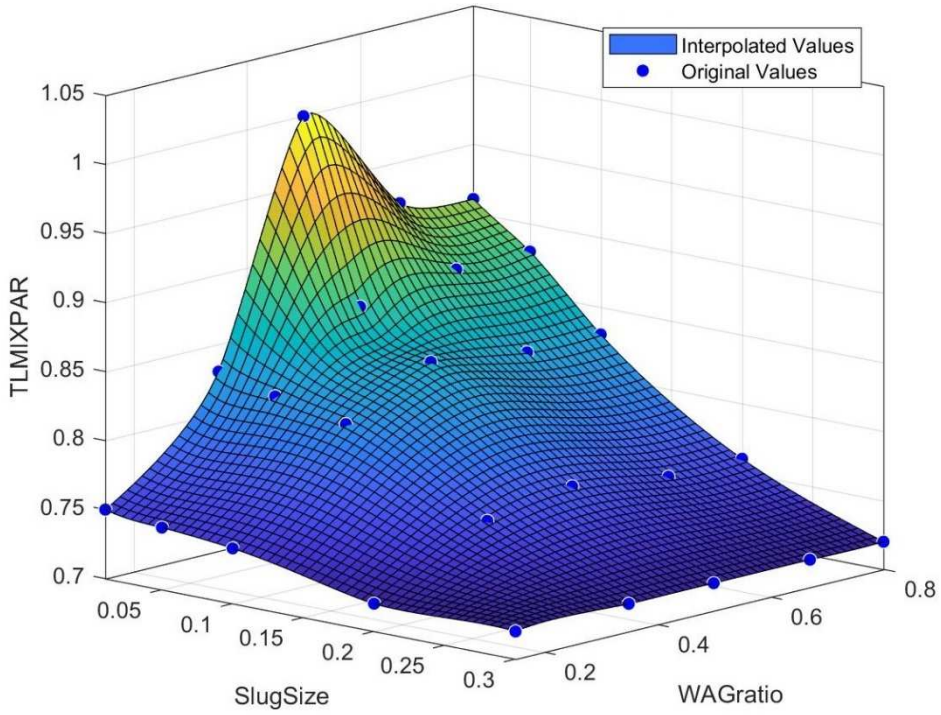

Figure 6.2 3D plot of the interpolated values of the mixing parameter (TLMIXPAR) as a function of slug size and WAG ratio. The highlighted points are the original values from Figure 6.1.

The interpolated values from the code were checked by selecting three random points, then manually calibrating ω for each of these and comparing with the results of the interoplation. These agreed well with each other.

This code was used in the optimisation scenarios that will be mentioned later.

6.3 Reservoir model used in the optimisation problem

The Watt field model (explained in Chapter 5) was used in the optimisation because this model is a semi-synthetic field. It has the complexity of a real field such as multiple wells

(21 producers and 8 injectors), some producers are horizontal wells, faults (Figure 5.3), and complex permeability (Figure 5.4) and porosity distribution. The model does not have aquifer support. The properties in this model were the same properties used in Chapter 5. The original oil in place was 1.664×10^9 STB.

A grid size of 112×30×40 was used for this study as the computational time using this grid size was reasonably fast (2-3 hours) meaning it could be used in the optimisation.

6.4 Objective function that will be used in the optimisation problem

As outlined in Chapter 2 (section 2.6), multi-objective optimisation is the task of optimising two or more objectives simultaneously with respect to a set of certain limitations to find different solutions (Hutahaean, 2017). The objective function expresses the main aim of the optimisation problem, which is either to be maximised or minimised.

In this research, the objective functions to optimise were:

1. Field Oil Production Total (FOPT).
2. Field Water Production Rate (FWPR).
3. Field Gas Production Rate (FGPR).

The objective of this research was to increase the cumulative oil production and to minimise both water and gas production, which will contribute to the sustainable development of producing fields. The reasons for selecting these objective functions are that they are the main indictors for the profitability and viability of the oil field. A primary objective for oil recovery is to maximise the oil production while minimising any additional outputs from the process (i.e. water and gas), as this directly impacts the profitability of the field. Excess production of water represents an important cost and liability to the oil and gas producer because of its high handling cost, while reduction in the produced gas (vented and flared) has become a governmental objective with the imposition of a carbon tax in some countries. The full details are outlined below.

Field Oil Production Total (FOPT): Optimising oil production is defined as the process of maximising the production of oil to achieve the optimum profitability from the well or field (Izadmehr et al., 2018). The focus of oil companies today is to maximise the

recovery factor (FOE) as well as maintaining an economic oil rate from their oilfields because it is difficult to discover new oil fields (Muggeridge et al., 2014).

Field Water Production Rate (FWPR): Oil fields typically produce a larger volume of water than oil (Davies, 2016). Separating water from oil usually occurs near to the production well to minimise unnecessary expense from pumping large volumes of water over large distances. Excess production of water represents an important cost and liability to the oil and gas producer because of its high handling cost, and its environmental impact, even though water often drives secondary production and assists in primary recovery. Water production may eventually increase, even with the best field-management techniques, to the point that it represents more than 90% of liquid volume brought to the surface. Surface-handling systems become overloaded, influencing the productivity and efficiency. Ultimately, the cost of dealing with produced water reduces field profitability and eventually leads to the abandon most of oil and gas wells, leaving large volumes of hydrocarbons behind (Khatib and Verbeek, 2003, Arnold et al., 2004).

Field Gas Production Rate (FGPR): Gas production mainly depends on the field whether it is an oil field or gas field. If the field is an oil field. The produced gas has to be exported, used or otherwise disposed of at the same time as it is produced. Alternatives to pipeline export are compressed natural gas or liquefied natural gas which require very capital-intensive facilities and very large volumes of gas to be economic. If a local market exists, then smaller volumes of gas can be used for electrical power generation. The remaining gas must be disposed of by burning the gas (flaring), released to the atmosphere without consumption (venting) or underground disposal. Reduction in the produced gas (vented and flared) has become a governmental requirement with the imposition of a carbon tax in some countries. If the field is a gas field, then the produced fluid will be mainly gas accompanied by small volumes of water and condensate, also known as natural gas liquids or natural gasoline. Offshore separation disposes the water to the sea and exports the gas/condensate to the coast via multiphase pipelines.

In this thesis, the assumption is that the field is an oil field and that the surface facility cannot handle excessive gas and water production.

6.5 Results of optimisation

It is important to determine the impact of the calibrated value of ω on the optimisation results and to compare these results against the optimisation results of the fixed value of $\omega = 1$.

The optimisation's scenarios were:

1. Optimisation of WAG ratio and slug size assuming unlimited gas supply.
2. Optimisation of WAG ratio, and slug size during the optimisation of WAG pattern assuming unlimited gas supply.
3. Optimisation of WAG ratio, and slug size during the optimisation of WAG pattern and injection fluid volume assuming unlimited gas supply.
4. Optimisation of WAG ratio, and slug size during the optimisation of WAG pattern and injection fluid volume assuming limited gas supply.

500 simulations were run to provide the optimiser with a large number of points to analyse and to find the optimal solution to meet the objective function. This number of simulations was chosen to provide the best balance of computational cost and simulation time while providing an adequate number of points for meaningful results.

The assumptions used in the optimisation were:

1. The production well was set using minimum BHP equal to 2000 psia.
2. The reservoir injection rate was fixed during the whole period of injection and was equal to the reservoir production rate of 250,000 RB/day at reservoir volume rate to maintain the reservoir pressure and to show the impact of ω on the results.
3. Secondary FSS WAG injection was carried out for 30 years of alternating miscible gas with water, while tertiary FSS WAG injection was carried out by flooding the reservoir with water first for 10 years then alternating miscible gas with water for another 30 years.
4. During the scenario in which there were limited gas volumes for injection, the assumption was that the amount of the gas available to inject was 5,000 MM RB.

The constraints in the optimisation are:

1. The maximum time to inject was 30 years (1.3 PVI) for secondary recovery and 30 (1.3 PVI) years for tertiary recovery after flooding the model with water for 10 years (0.45 PV).
2. The reservoir volume injection rate (FVIR in reservoir barrel RB) was stable during the injection and equal to the reservoir volume production rate (FVPR in RB) to maintain the reservoir pressure. The simulation run should be terminated once the FVPR began to decline and the pressure started to increase above the original average reservoir pressure by about 30 psi to avoid fracturing the reservoir and to maintain the results due to effect of the value of ω.
3. During the scenario of optimising the flow rate, the total amount of flow rate to inject should not exceed 300,000 RB/day, as this would lead to fracturing the reservoir. The reservoir volume production rate was updated according to total injection rate to maintain the average reservoir pressure and to show the impact of ω on the results.

6.5.1 Optimisation of WAG ratio and slug size while there is unlimited gas available to inject

Optimising the WAG ratio and slug size is very important in order to achieve a higher recovery of oil before applying the miscible FSS WAG injection on a field scale. Since the values of ω were calibrated based on the WAG ratio, slug size and type of recovery, optimising the WAG ratio and slug size for both secondary and tertiary recovery helps to identify the impact of the calibrated value ω on the optimisation results. The results of optimisation using the calibrated values of ω were compared with the results of the optimisation using a fixed value of $\omega = 1$.

Optimising the slug size with respect to pore volume should specify the times at what gas was injected and water was injected. The time was calculated using the equation:

$$t_{inj}(months) = int(ss\ (PV) * PORV\ (RB)/Q_{inj}(RB/months)) \quad (6.2)$$

where, t_{inj} is the time required to inject gas or water, ss is the slug size in PV, $PORV$ is the reservoir pore volume in (RB) and Q_{inj} is the amount of fluid to inject ($RB/months$). Optimising the WAG ratio specifies the length of gas injected with respect to water

injected. The WAG ratio was optimised using the fractional rate of water injected (FWINJ), and was calculated using the equation:

$$FWINJ(fraction) = wat/(wat + gas) \quad (6.3)$$

If it is assumed that the time to inject gas at a slug size of 0.01 PV is two months, and the optimisation software selected the value of 0.5 for FWINJ, then the WAG ratio will be 2 months to inject water and two months to inject gas i.e. the WAG ratio will be 1:1, while if the optimisation software selected the value of 0.25 for FWINJ, then the WAG ratio will be two months of injecting water to six months of injecting gas i.e. the WAG ratio will be 1:3. If the WAG ratio increases, it means water is injected more than gas (FWINJ>0.5). If the WAG ratio decreases, gas is injected more than water (FWINJ<0.5).

Finally, the number of cycles refer to how many times that the gas injection will alternate the water injection. It was calculated using the following equation:

$$no.of\ cycles = integer(years\ of\ injection/(t_{inj}(gas) + t_{inj}(water))) \quad (6.4)$$

If the number of cycles equals 10, then the gas injection will alternate with water injection ten times. Gas injection always precedes water injection.

The optimisation parameters are:

1. FWINJ (fraction): distribution between (0.3 - 0.8).
2. Slug size (PV): distribution between (0.005 - 0.15).

The workflow of the optimisation using MOPSO algorithm is shown in the diagram below, Figure 6.3, and it was implemented as follows:

1. The optimisation software (Raven) provided the Python code 1 (Appendix C.1) with the optimisation parameters, which is in this case was FWINJ (WAG ratio) and the slug size.
2. The Python code 1 was developed to interpolate the values of ω for different slug sizes and WAG ratios, then find the equivalent value of ω for a given slug size and WAG ratio and put this value into the Eclipse deck under the Todd and Longstaff mixing parameter (TLMIXPAR) value. The Python code does not change the value of ω when optimising the WAG ratio and slug size at ω = 1.

Hence, the models will not have a single value of ω like in the case of the fixed value of ω=1, instead the value of ω will change from model to model depending on the optimised slug size and WAG ratio input.

3. The Python code updated the time step of injection and the number of cycles.
4. The optimiser then ran the Eclipse deck and returned the results of the objective function values.

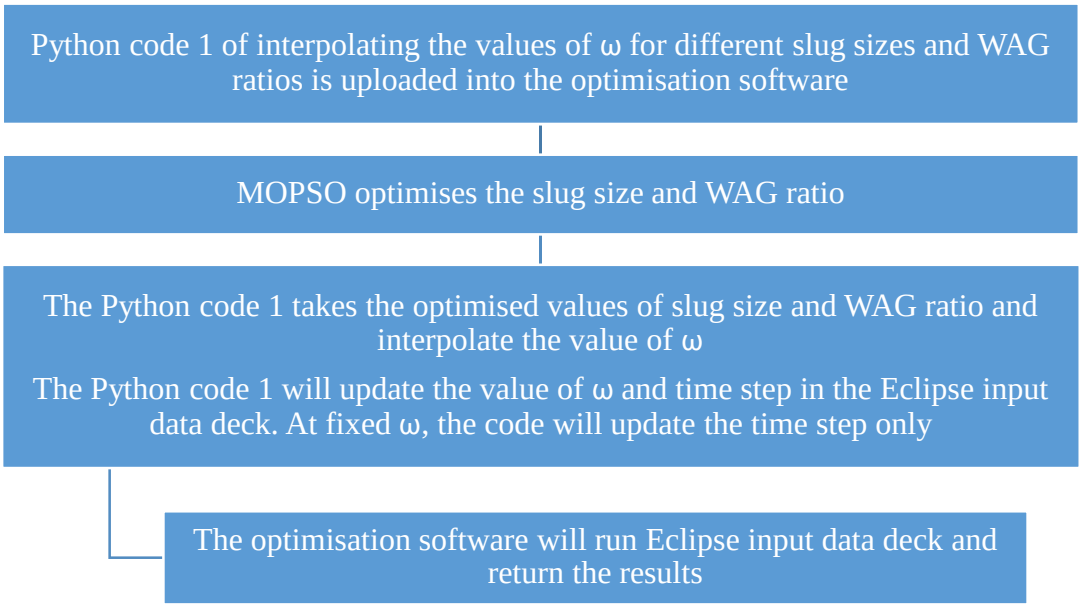

Figure 6.3 A diagram to show workflow of the WAG ratio and slug size optimisation

6.5.1.1. Results of optimising the WAG ratio and slug size

The optimisation results were obtained for both secondary and tertiary recovery of miscible FSS WAG injection for two cases, the calibrated value of ω and at the fixed value of ω. The aim was to compare the optimisation results that were obtained for the calibrated value of ω (modified in the Eclipse data file according to the value of the slug size and WAG ratio) with the optimisation results at a fixed value of ω = 1 (in the Eclipse data file).

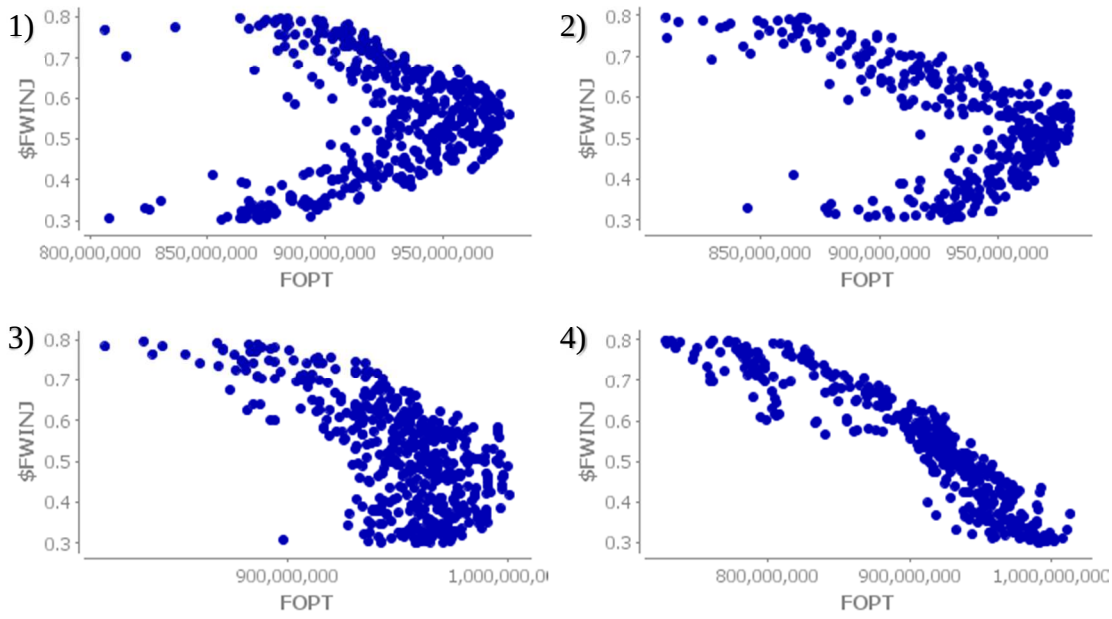

Figure 6.4 The optimisation results for the WAG ratio (i.e. FWINJ) vs the total oil production (FOPT), for: 1) secondary recovery using the calibrated value of ω, 2) secondary recovery using fixed value of ω = 1, 3) tertiary recovery using the calibrated value of ω, 4) tertiary recovery using fixed value of ω = 1.

Figure 6.4 shows the optimisation results for the WAG ratio (FWINJ) versus the total oil production (FOPT) for both secondary and tertiary recovery using the calibrated value of ω and the fixed value of ω. For secondary recovery (examples 1 and 2 in the figure) the total oil recovery was consistent between the scenarios i.e. the highest values were obtained when water injection was equal to or slightly above gas injection (FWINJ = 0.5 to 0.6). For tertiary recovery, the oil recovery was maximised when the WAG ratio ranged between FWINJ = 0.4 to 0.6 for the calibrated value of ω but tended towards lower WAG ratio (FWINJ = 0.3 to 0.4) for the fixed value of ω. This shows that the value of ω influences the optimisation results for the tertiary recovery but not for the secondary.

The gas production (FGPR) increased as the WAG ratio decreased (injecting gas more than water) for all the cases (Appendix D. 1). While, the water production (FWPR) increased as the WAG ratio increased (injecting water more than gas) for all the cases (Appendix D. 2).

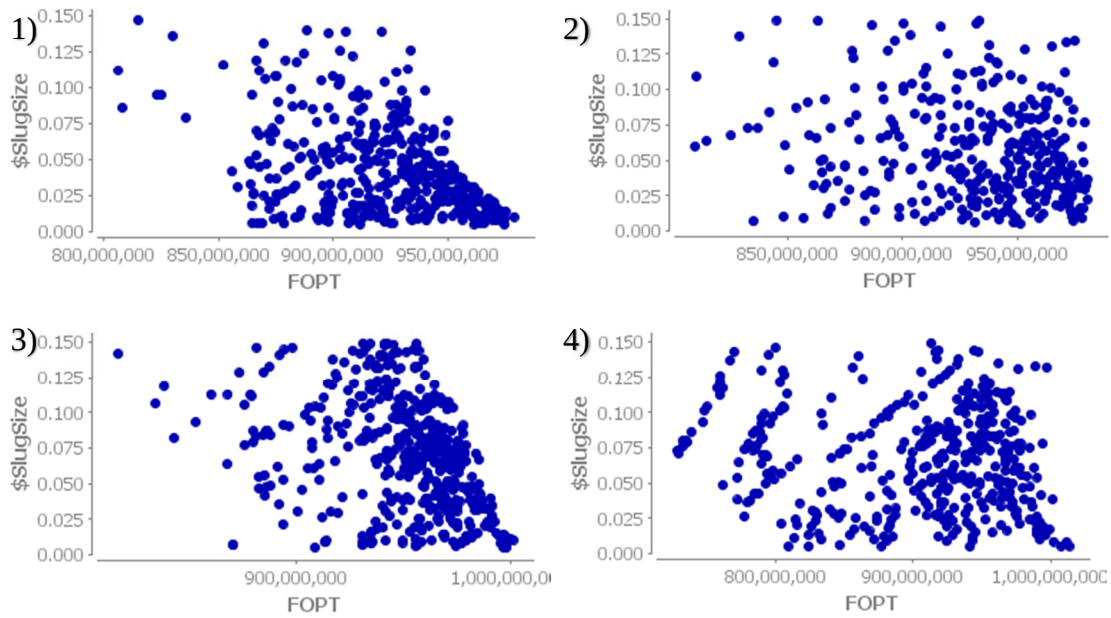

Figure 6.5 The optimisation results for the slug size vs the total oil production (FOPT), for: 1) secondary recovery using the calibrated value of ω, 2) secondary recovery using fixed value of ω = 1, 3) tertiary recovery using the calibrated value of ω, 4) tertiary recovery using fixed value of ω = 1.

Figure 6.5 shows the optimisation results for the slug size versus the total oil production (FOPT). For secondary recovery using the calibrated value of ω, it can be seen that the total oil production (FOPT) increases as the slug size decreases (<0.03 PV). This behaviour differs to that for the oil recovery using the fixed value of ω = 1, where it can be seen that the slug size has no trend to achieve higher oil recovery (FOPT) which is the opposite to what is observed at the calibrated value of ω. In the tertiary recovery using the calibrated value of ω, the slug size has increased to 0.075 PV to achieve high oil recovery (FOPT), while at the fixed value of ω there was some trend towards small slug sizes, however, it can be seen that larger slug sizes (0.13 PV) achieved higher recovery for the total oil produced (FOPT).

The slug size has no impact on the production of water and gas for all scenarios (Appendix D. 3 and Appendix D. 4).

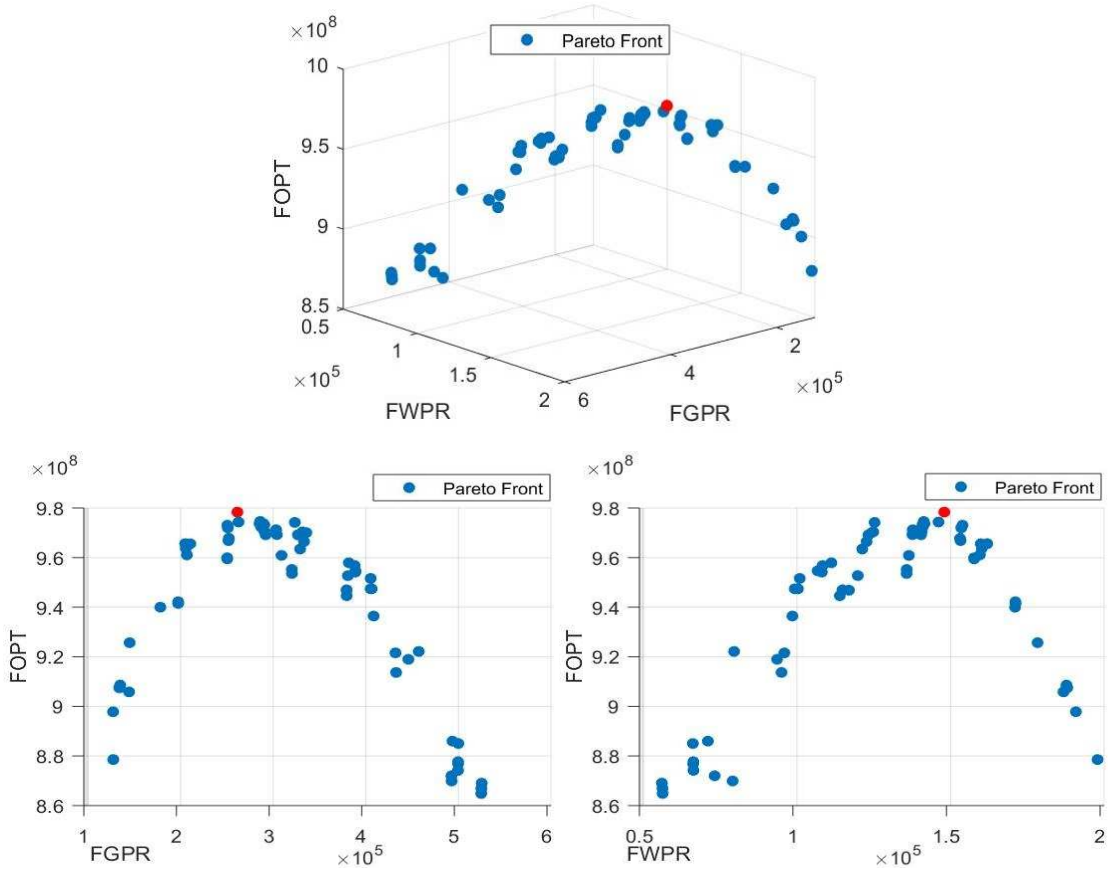

Figure 6.6 Pareto front for the results of MOPSO for the recovery at the calibrated value of ω. The Pareto front shows the trade-off in increasing the total oil recovery (FOPT) and minimising both gas (FGPR) and water (FWPR) production. The red circle represents the optimal solution for FOPT.

Figure 6.6 shows the Pareto front for the total field oil recovery (FOPT) using both 3D and 2D plots, because it is difficult to visualise the Pareto front solely on a 3D plot. The plots reveal a number of optimal solutions that represent the trade-off between maximum oil production (FOPT), and minimum production of gas (FGPR) and water (FWPR), demonstrating that careful selection of the optimal solution is required. It appears that the objectives FGPR and FWPR compete against each other to obtain the minimum value while FOPT is neutral (has no impact). The oil recovery is maximum on the middle of the curve (within the range 2.8×10^5 to 4×10^5 for FGPR and 1.2×10^5 to 1.5×10^5 for FWPR), outside of these ranges the oil recovery decreased with either increasing or decreasing gas or water production. Similar behaviour was observed in the rest of the optimisation scenarios.

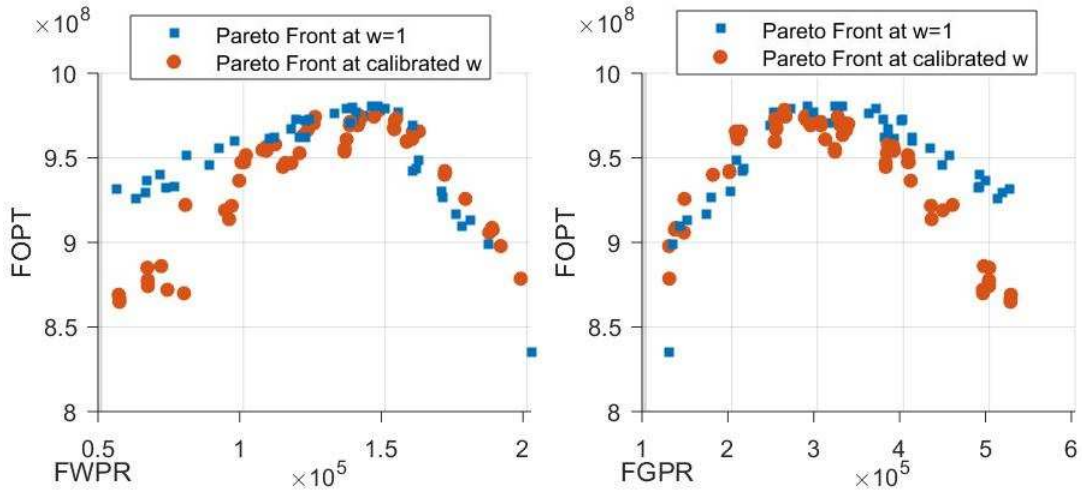

Figure 6.7 Comparison between the Pareto front for the results of MOPSO for the secondary recovery at the calibrated value of ω and at the fixed value of ω. The Pareto front show the trade-off in increasing the total oil recovery (FOPT) and minimising both gas (FGPR) and water (FWPR) production. The red circle represents the optimal solution for FOPT.

Figure 6.7 compares the Pareto front for secondary recovery using the calibrated value of ω and the fixed value of ω on a 2D plot. It shows that the calibrated value of ω had a significant impact on the oil recovery compared with the fixed value of ω. The oil recovery decreased significantly as the gas production increased. Therefore, the optimal solution for FOPT was chosen in order to compare the impact of ω on the optimisation results; the red circle in Figure 6.6 represents the chosen optimal solution. Figure 6.6 and Figure 6.7 are representative plots, similar behaviour was observed in the rest of the optimisation scenarios.

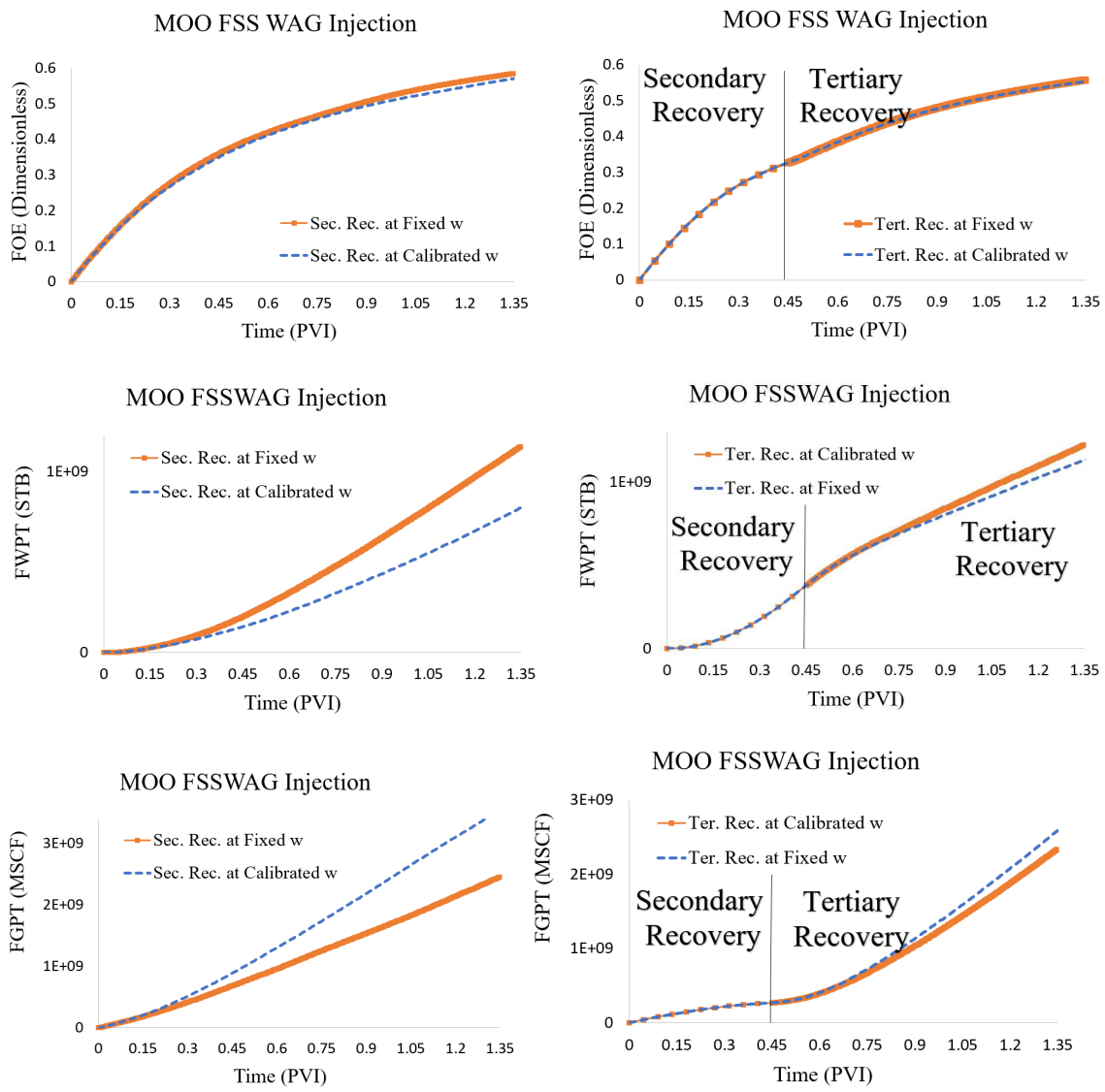

Figure 6.8 The reservoir performance of the optimal solution for both secondary and tertiary recovery. MOO is multi-objective optimisation. FOE represents field oil recovery. FWCT represents field water cut. FGPT represents field gas production total.

Figure 6.8 shows the comparison between the calibrated value of ω and the fixed value of ω for the reservoir performance from the optimal solution for FOPT for both secondary and tertiary recovery. The results are:

1. **For the secondary recovery:** the optimal solution for FOPT for the calibrated value of ω is a slug size of 0.014 PV and a WAG ratio of 3:4 (months) (in this case ω = 0.952), while the optimal solution for the fixed value of ω=1 is a slug size of 0.022 PV and WAG ratio of 7:5 (months). The results do not show a significant difference in the oil recovery, the field efficiency of oil recovery (FOE)

is 0.573 for the calibrated value of ω and 0.589 for the fixed value of $\omega = 1$. However, the results do show a larger impact on the water production and the gas production. The water production is lower at 8.127×10^8 STB (for the calibrated value of ω, FWCT = 0.786), compared with 1.169×10^9 STB (for the fixed value of $\omega = 1$, FWCT = 0.847). While the gas production total (FGPT) is larger at 3.58×10^9 MSCF (for the calibrated value of ω), compared with 2.51×10^9 MSCF (for the fixed value of $\omega = 1$).

2. **For the tertiary recovery**: different behaviour is observed compared with secondary recovery. The optimal solution for the calibrated value of ω is a slug size of 0.01 PV and WAG ratio of 2:3 (months) (in this case the $\omega = 0.931$), while the optimal solution for the fixed value of ω=1 is a slug size of 0.005 PV and WAG ratio of 1:2 (months). The results, again, do not show a significant difference in the oil recovery i.e. FOE = 0.602 for calibrated value of ω and the FOE = 0.608 for the fixed value of $\omega = 1$), which is similar to the secondary recovery. Additionally, the water production was slightly higher, 1.58×10^9 STB (for the calibrated value of ω, FWCT = 0.844) compared with, 1.47×10^9 STB (for the fixed value of $\omega = 1$, FWCT = 0.838). However, the results do show greater impact on the gas production. The gas production total (FGPT) was 3.7×10^9 MSCF (for the calibrated value of ω) and 4.25×10^9 MSCF (for the fixed value of ω=1).

6.5.1.2. Conclusion from optimising of the slug size and WAG ratio at the calibrated value of ω and at the fixed value of ω

From the results mentioned earlier, the following conclusions can be drawn:

1. As the slug size decreases below 0.025 PV the total oil production increases for all the scenarios (secondary and tertiary recovery, fixed and calibrated values of ω).
2. For secondary recovery, the optimal solution for the calibrated value of ω is a slug size smaller than the slug size using the fixed value of ω=1. The period of injection for the fixed value of ω=1 (7:5 months) was bigger than the period of injection for the calibrated value of ω (3:4 months), this shows that the value of ω impacts the optimisation results. This impact was negligible for the oil recovery; however,

the impact on the gas and water production was more significant. The produced gas was higher for the calibrated value of ω, and the opposite behaviour is seen for the water production with it being lower for the calibrated value of ω.

3. For the tertiary recovery, the optimal solution using the calibrated value of ω is a slug size of 0.01 PV, this is similar to that of the secondary recovery for the calibrated value of ω. The optimal solution has a small slug size bigger than the slug size for the fixed value of ω = 1 (0.005 PV). The period of injection is comparable in both cases (2:3 months for the calibrated value of ω, and 1:2 months for the fixed value of ω). This shows that the value of ω plays a role in the interaction between the WAG ratio and the slug size, leading to the achievement of higher recovery. Therefore, it can be concluded that the value of ω does not significantly impact the optimisation results for tertiary recovery.

6.5.2 Optimisation of WAG ratio and slug size during the optimisation of the WAG pattern injection when there is unlimited gas available to inject

To further investigate the impact of ω on the optimisation results, the optimisation of WAG pattern injection was added to the optimisation of WAG ratio and slug size.

Optimising the type of fluid to inject, also known as WAG pattern injection, is a method of determining which well will inject gas alternating with water and which well will inject water only during the whole period of injection. Therefore, instead of using all the wells to inject gas alternating water, some of the wells will inject water only. The advantage of WAG pattern optimisation is to allow a more efficient use of the gas available to inject in case there is limited amount of gas available to inject.

The optimisation parameters are:

1. FWINJ between 0.3 and 0.8
2. Slug size between 0.005 and 0.15
3. WAG pattern injection (injecting water or FSS WAG) for the injectors (1-8).

The workflow of the optimisation is shown in Figure 6.9, and is summarised:

1. The optimisation software provided Python code 2 (Appendix C.2) with the optimisation parameters, which is in this case were WAG ratio, slug size, and injection fluid type for each of the injection wells under the optimisation in a shape of numbers (1 for gas alternating water and 2 for water only). The Python code 2 was developed from Python code 1 to take into account the type of fluid to inject (gas or water) in addition to the interpolated values of ω for different slug size and WAG ratios.
2. The code takes the values of the fluid in each injection well and updated each injection well in the Eclipse deck with the type of fluid to inject, whether gas alternating water injection or water injection only. In addition, it interpolated the value of ω based on the optimised values of WAG ratio and slug size, and then updated the Todd and Longstaff mixing parameter value in the Eclipse deck with the interpolated value of ω. Moreover, it updated the time step and the number of cycles in the Eclipse data deck according to the slug size and the WAG ratio, as mentioned previously.
3. The optimisation software ran the Eclipse deck and returned the objective function values.

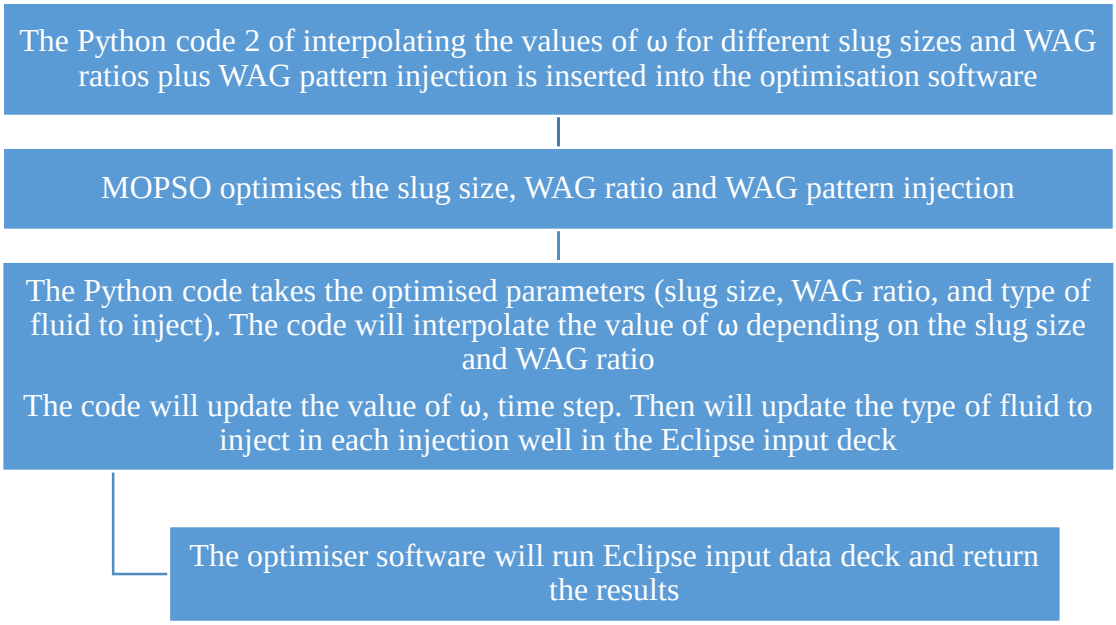

Figure 6.9 The workflow of the WAG pattern optimisation

6.5.2.1. Results of optimising the WAG ratio, slug size and WAG pattern while there is unlimited gas available to inject

The results of optimisation are obtained for both secondary and tertiary recovery of miscible FSS WAG injection for two cases, the calibrated value of ω and at the fixed value of ω. The aim was to compare the optimisation results that were obtained for the calibrated value of ω (that was modified in the Eclipse data file according to the value of the slug size and WAG ratio) with the optimisation results for a fixed value of ω = 1 (in the Eclipse data file).

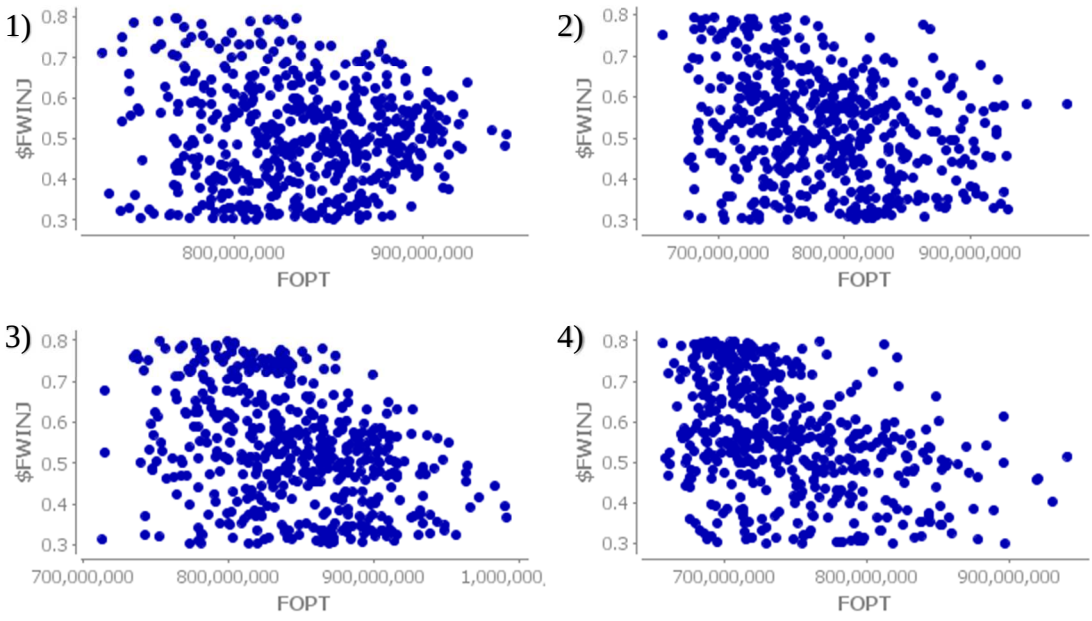

Figure 6.10 The optimisation results for the WAG ratio (i.e. FWINJ) vs the total oil production (FOPT), for: 1) secondary recovery at the calibrated value of ω, 2) secondary recovery at fixed value of ω = 1, 3) tertiary recovery at the calibrated value of ω, 4) tertiary recovery at fixed value of ω = 1.

Figure 6.10 shows the optimisation results for the WAG ratio (FWINJ) versus the total oil recovery (FOPT) for both secondary and tertiary recoveries, using the calibrated value of ω and the fixed value of ω. For secondary recovery with the calibrated value of ω (Figure 6.10, 1), the highest oil recovery occurred when the WAG ratio was between 0.5 and 0.6, which is similar to the scenario 1 optimisation. For the secondary recovery with ω = 1 (Figure 6.10, 2), the highest oil recovery was for the WAG ratio between 0.35 and 0.7, which was a wider range than values in scenario 1 of optimisation (FWINJ = 0.5 to 0.6).

For tertiary recovery with the calibrated value of ω, the highest oil recovery was when the WAG ratio ranged between 0.3 to 0.6, which was a wider range than for scenario 1 of optimisation (FWINJ = 0.4 to 0.6). While, the results of the tertiary recovery at the fixed value of ω = 1 were similar to the results of the tertiary recovery with the calibrated value of ω (FWINJ = 0.3 – 0.6) in this scenario, but different from the scenario 1 of optimisation (FWINJ = 0.3 to 0.4).

As for gas and water production, they behaved similarly to the gas and water production during optimising WAG ratio and slug size only. The gas production (FGPR) increased as the WAG ratio decreased (injecting gas more than water) for all the cases (Appendix E. 2), while the water production (FWPR) increased as the WAG ratio increased (injecting water more than gas) for all the cases (Appendix E. 2).

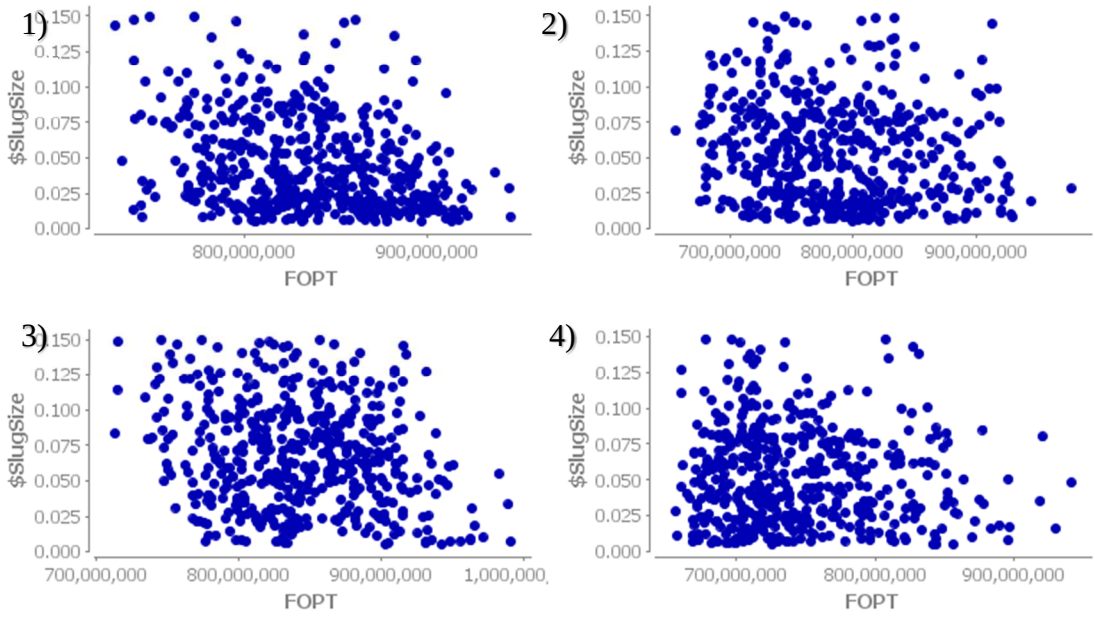

Figure 6.11 The optimisation results of the slug size vs the total oil production (FOPT), for: 1) secondary recovery at the calibrated value of ω, 2) secondary recovery at fixed value of ω=1, 3) tertiary recovery at the calibrated value of ω, 4) tertiary recovery at fixed value of ω=1.

Figure 6.11 shows the optimisation results for the slug size vs the total oil production (FOPT). In the secondary recovery at the calibrated value of ω, it can be seen that the oil recovery increases as the slug size decreases (<0.03 PV), similar to the scenario 1 optimisation. In the secondary recovery at the fixed value of ω, it can be seen that the highest oil recovery occurs for a wide range of slug sizes (0.005-0.14 PV), a wider range than the scenario 1 optimisation (<0.075 PV), however, the highest oil recovery is

obtained at slug size 0.04 PV. In the tertiary recovery at the calibrated value of ω, it can be seen that the oil recovery increases as the slug size decreases (<0.06 PV), which differs with the scenario 1 optimisation (slug size has no impact on the oil recovery). In the tertiary recovery at the fixed value of ω = 1, the oil recovery increases as the slug size decreases (<0.08 PV), which is less than what has been observed in the scenario 1 optimisation (0.13 PV). The slug size has no effect on the production of water and gas for all different scenarios, which was similar to what is observed for the optimisation of WAG ratio and slug size only.

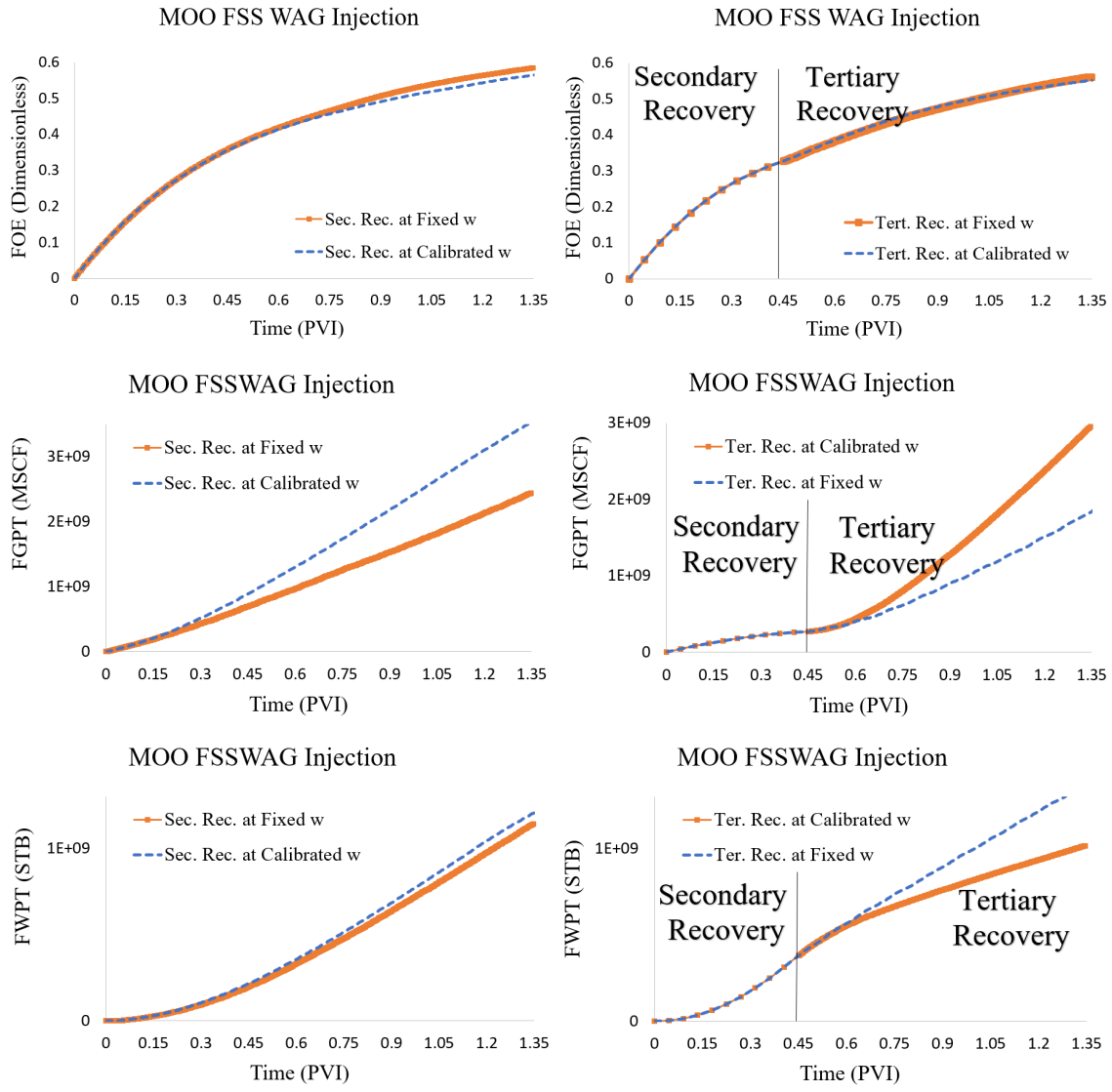

Figure 6.12 The reservoir performance of the optimal solution for both secondary and tertiary recovery. MOO is multi-objective optimisation. FOE represents field oil recovery. FWCT represents field water cut. FGPT represents field gas production total.

Figure 6.12 shows the comparison between the calibrated value of ω and the fixed value of ω for the reservoir performance from the optimal solution for both secondary and tertiary recovery. The results are:

1. **For the secondary recovery**: the optimal solution for the calibrated value of ω is a slug size of 0.008 PV. The WAG ratio at the calibrated value of ω (2:2 months= FWINJ is 0.5) (in this case the ω = 1). The optimal solution for the fixed value of ω=1 is a slug size of 0.028 PV. The WAG ratio for the fixed value of ω=1 is 10:7 months (FWINJ is 0.58). The results do not show a significant difference in the oil recovery, the field efficiency of oil recovery (FOE) is 0.567 for the calibrated value of ω and 0.587 for the fixed value of ω = 1. However, the results have a greater impact on the water production and the gas production. The water production was lower 1.162×10^9 STB (for the calibrated value of ω, FWCT = 0.837) compared with 1.228×10^9 STB (for the fixed value of ω = 1, FWCT = 0.851). The gas production total (FGPT) was lower 2.3×10^9 MSCF (for the calibrated value of ω) compared with 2.48×10^9 MSCF (for the fixed value of ω = 1).
2. **For the secondary recovery**: the WAG pattern injection for the calibrated value of ω is different from the WAG pattern injection for the fixed value of ω. For the calibrated value of ω, Injectors 1 and 7 injected only water throughout the whole period of injection, while the other injectors alternated between gas and water injection. For the fixed value of ω, all the injectors alternated gas and water injection for all of the period of injection. This shows that the calibrated value of ω plays a role in the optimisation results that decreasing the number of injection wells (to 6 injectors) that inject gas alternating with water.
3. **For the tertiary recovery**: similar behaviour is observed compared with secondary recovery. The optimal solution for the calibrated value of ω is a slug size of 0.007 PV, this is comparable with that of the secondary recovery for the calibrated value of ω. The WAG ratio at the calibrated value of ω is (1:3 months= FWINJ is 0.25) (in this case the ω = 0.938). While the optimal solution for the fixed value of ω=1 is a slug size of 0.048 PV. At the fixed value of ω=1, the optimal solution has a WAG ratio of (13:12 months=FWINJ is 0.52). The results show that the oil recovery i.e. FOE = 0.595 for calibrated value of ω is higher than

for the fixed value of ω = 1, FOE = 0.565. In addition, water production is lower, 1.278×10^9 STB (for the calibrated value of ω, FWCT = 0.822) compared with 1.38×10^9 STB (for the fixed value of ω = 1, FWCT = 0.825). The results do show an impact on the gas production. The gas production total (FGPT) is higher at 4.92×10^9 MSCF (for the calibrated value of ω) compared with 1.892×10^9 MSCF (for the fixed value of ω=1).

4. **For the tertiary recovery**: the WAG pattern injection for the calibrated value of ω is similar to the WAG pattern injection for the fixed value of ω=1. In both cases, all the injectors injected gas alternating with water throughout the whole period of injection. Compared to the secondary recovery of the scenario 2, the WAG pattern in the tertiary recovery was not influenced by the calibrated value of ω.

6.5.2.2. Conclusion for optimising the WAG ratio, slug size and WAG pattern while there is unlimited gas available to inject

Optimising the WAG pattern injection for secondary recovery using the calibrated value of ω resulted in improved reservoir performance compared with the fixed value of ω = 1 for both secondary and tertiary recovery. The calibrated value of ω changed the optimisation results, leading to a smaller slug size and to a short injection period. Therefore, using the calibrated value of ω for a specific WAG ratio and slug size, leads to an improvement of reservoir performance compared with using the fixed value of ω=1.

Based on the results presented earlier, the following conclusions can be drawn:

1. **For secondary recovery**, the slug size for the fixed value of ω (0.028 PV) is larger than the slug size of the calibrated value of ω (0.008 PV). The period of injection for the fixed value of ω (10:7 months) is greater than for the calibrated value of ω (2:2 months), meaning that the value of ω impacts the optimisation results.
2. **Comparison with scenario 1 optimisation**, the slug size is higher 0.014 PV (scenario 1) compared to 0.008 PV (scenario 2) using the calibrated value of ω. While the slug size slightly increased from 0.022 to 0.028 PV for the fixed value of ω=1. The WAG ratio was decreased for the calibrated value of ω from 3:4

months (scenario 1) to with 2:2 months (scenario 2). While the WAG ratio increased from 7:5 months for (scenario 1) to 10:7 months for (scenario 2) for the fixed value of ω = 1. The injection wells were reduced to six wells injecting FSS WAG injection and achieved a slightly lower recovery (FOE = 0.567) than scenario 1 (FOE = 0.573).

3. **For the tertiary recovery,** the slug size using the fixed value of ω = 1 was 0.048 PV, this is greater than the slug size for the calibrated value of ω (0.007 PV). Additionally, the period of injection was longer i.e. 1:3 months for the calibrated value of ω, and 13:12 months for the fixed value of ω. This shows that the calibrated value of ω plays a role in the interaction between the WAG ratio and the slug size for a higher recovery. It can therefore be concluded that the value of ω has a significant impact on the optimisation results for tertiary recovery.
4. **Comparison with scenario 1 for the tertiary recovery**, the slug size was decreased from 0.01 PV (scenario 1) to 0.007 PV (scenario 2) using the calibrated value of ω. While the slug size was increased from 0.005 to 0.048 PV for the fixed value of ω = 1. The WAG ratio was shortened by a month using the calibrated value of ω from 2:3 months (scenario 1) to 1:3 months (scenario 2). The WAG ratio was increased dramatically for the fixed value of ω = 1 (from 1:2 months to 13:12 months).

6.5.3 Optimisation of injection flow rate (Q_{inj}) in addition to the optimisation of WAG ratio, slug size and WAG pattern injection with unlimited injection gas supply

To further investigate the impact of the calibrated value of ω on the optimisation results, the optimisation of injection flow rate was added to the optimisation of WAG ratio, slug size and WAG pattern injection.

In the previous optimisation sections, it was assumed that the injection and the production amount were fixed and equal to maintain the average reservoir pressure. Here, the reservoir flow rate for the injectors was optimised in such a way that the FVIR (sum of all the injectors in reservoir barrel RB) was equal to FVPR to maintain the average reservoir pressure.

The optimisation parameters are:

1. FWINJ between 0.3 - 0.8
2. Slug size between 0.005 - 0.15
3. WAG pattern injection for the injectors 1-8
4. Amount of fluid to inject in each injection well is between 25,000 – 50,000.

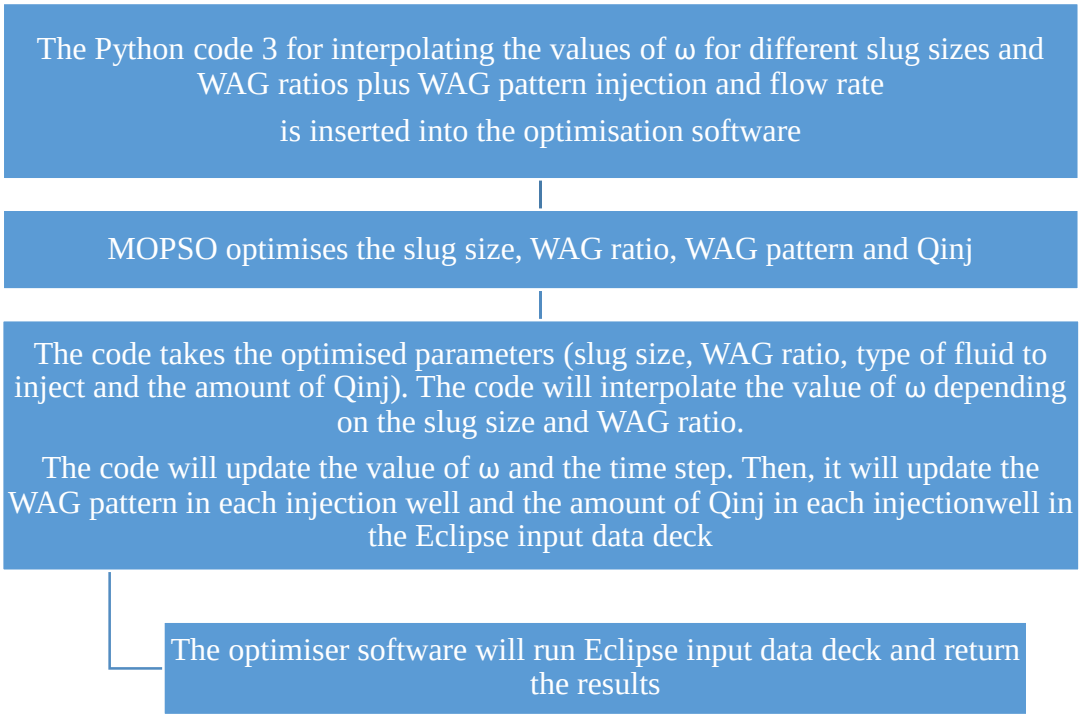

Figure 6.13 Workflow of the optimisation of the amount of flow rate to inject

The workflow of the optimisation is shown in the diagram below Figure 6.13, and is described:

1. Python code 3 was developed from Python code 2 to take into account the amount of fluid to inject and the WAG pattern injection in addition to the interpolated values of ω for different slug size and WAG ratios.
2. The optimisation software provided Python code 3 (Appendix C.3) with the optimisation parameters, which were WAG ratio, slug size, and type of injection for each injection well under the optimisation in a shape of numbers (1 for gas alternating water and 2 for water). The Python code 3 took the optimised parameters from the optimisation software, and then:
    - Updated the Todd and Longstaff mixing parameter value in the Eclipse deck, in addition it updated the time step and the number of cycles (similarly to the

previous optimisation section).

- It took the value of 1 for gas alternating water and 2 for water only, then, it updated each injection well in the Eclipse deck with the type of fluid to inject in each injection well, whether gas alternating water injection or water injection during the whole period of injection.
- It then updated each injection well with the amount of fluid to inject, and the sum of the amount was updated in the GCONPROD (Production rate controls/limits for groups or field).

3. The optimisation software ran the Eclipse data deck and then returned the results.

6.5.3.1. Results of optimising the WAG ratio, slug size, WAG pattern and amount of flow rate to inject while there is unlimited gas available to inject

The results of the optimisation were obtained for both secondary and tertiary recovery of miscible FSS WAG injection for the calibrated value of ω and the fixed value of ω=1.

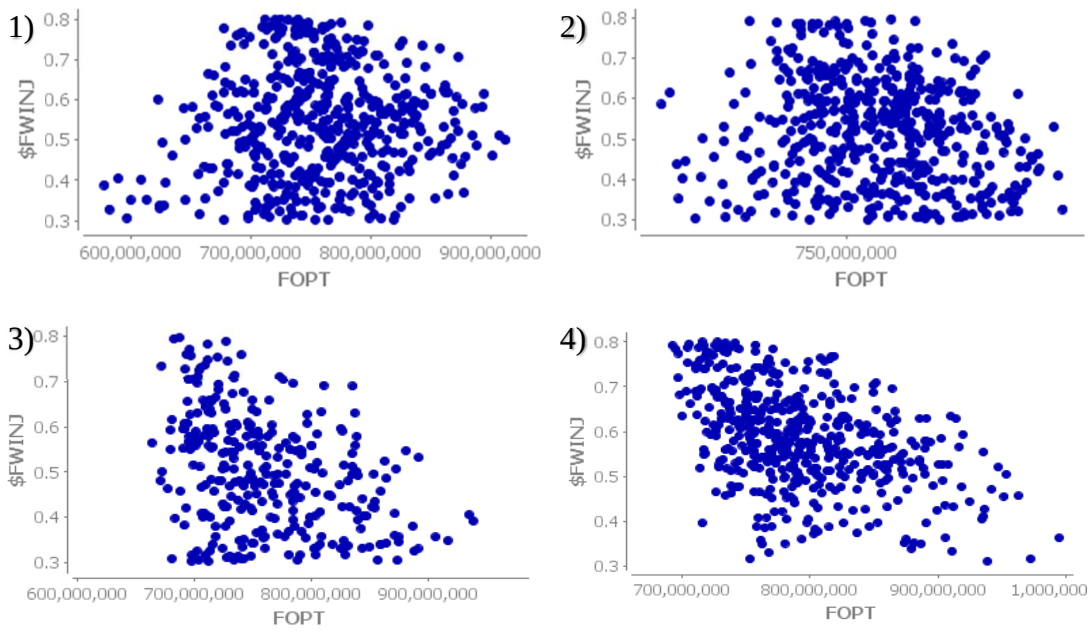

Figure 6.14 The optimisation results of the WAG ratio (i.e. FWINJ) vs the total oil production (FOPT), for: 1) secondary recovery at the calibrated value of ω, 2) secondary recovery at fixed value of ω = 1, 3) tertiary recovery at the calibrated value of ω, 4) tertiary recovery at fixed value of ω = 1.

Figure 6.14 shows the optimisation results of the WAG ratio (FWINJ) versus the total oil recovery (FOPT) for both secondary and tertiary recoveries, with the calibrated value of ω and the fixed value of ω. In the secondary recovery at the calibrated value of ω, it can

be seen that the highest oil recovery occurs when the WAG ratio ranged between 0.5 and 0.6, which is similar to the previous optimisations detailed above (scenario 1 and scenario 2). In the secondary recovery at the fixed value of ω (Figure 6.14, 2), the highest oil recovery occurred when the WAG ratio ranged between 0.3 and 0.6, which is a wider range than scenario 1 (0.35 to 0.7) and it is shifted and slightly narrower than scenario 2 (0.5 to 0.6).

In the tertiary recovery with the calibrated value of ω (Figure 6.14, 3), the highest oil recovery was when the WAG ratio was between 0.3 to 0.55, which is shifted and a slightly wider range than the scenario 1 optimisation (0.4 to 0.6) and is slightly narrower than the scenario 2 optimisation (0.3 to 0.6). The highest oil recovery in the tertiary recovery with the fixed value of ω = 1 was at WAG ratio 0.3, where the points have converged.

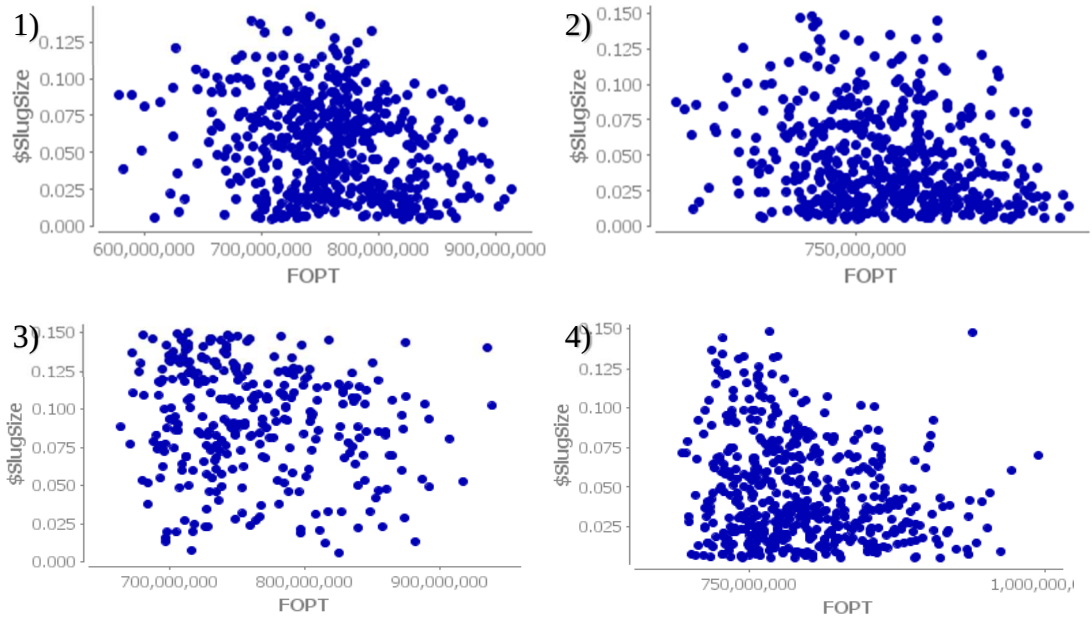

Figure 6.15 The optimisation results of the slug size vs the total oil production (FOPT), for: 1) secondary recovery at the calibrated value of ω, 2) secondary recovery at fixed value of ω = 1, 3) tertiary recovery at the calibrated value of ω, 4) tertiary recovery at fixed value of ω = 1.

Figure 6.15 shows the optimisation results of the slug size vs the total oil recovery (FOPT). In the secondary recovery at the calibrated value of ω, the oil recovery increases as the slug size decreases <0.075 PV, which is higher than previously seen in scenario 1 and 2 for the optimisation (<0.03 PV). In the secondary recovery at the fixed value of ω, the highest oil recovery occurs at slug sizes lower than 0.075 PV, this is similar to the calibrated value of ω and the scenario 1 optimisation (<0.075 PV), in comparison with

scenario 2 the range of slug sizes decreases (0.005-0.14 PV) for the higher achieved oil recover. In the tertiary recovery at the calibrated value of ω, the oil recovery increases as the slug size increases (>0.1 PV), which differs from scenario 1 optimisation (where slug size has no impact on the oil recovery) and is opposite to what is observed in the scenario 2 optimisation (<0.06 PV). For the tertiary recovery at the fixed value of ω = 1, the oil recovery increases as the slug size decreases (<0.08 PV), which is a decrease of what is observed in the scenario 1 optimisation (0.13 PV), but is similar to what occurs in the scenario 2 optimisation (<0.08 PV).

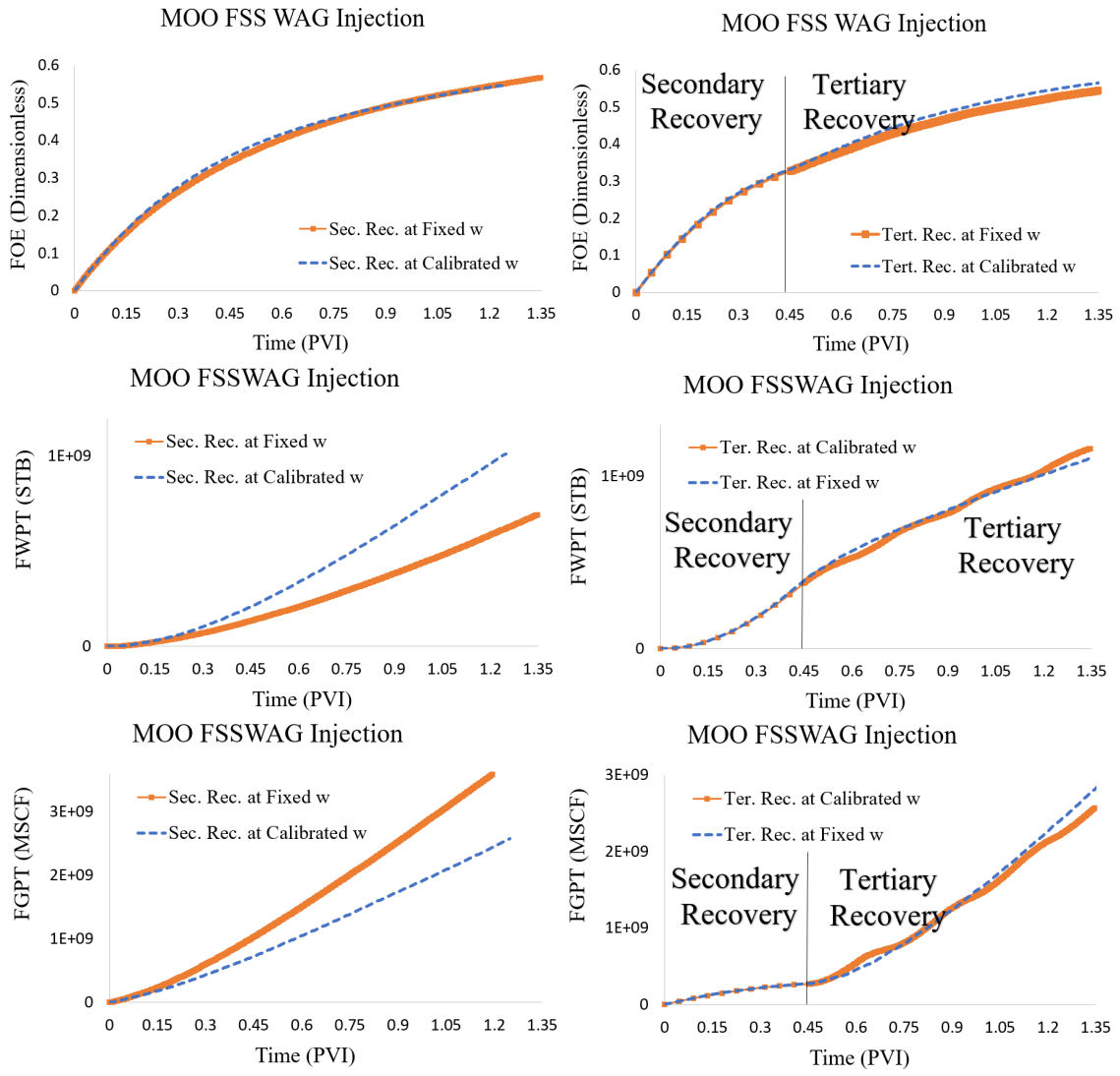

Figure 6.16 The reservoir performance of the optimal solution for both secondary and tertiary recovery. MOO is multi-objective optimisation. FOE represents field oil recovery. FWCT represents field water cut. FGPT represents field gas production total.

Figure 6.16 shows the comparison between the calibrated value of ω and the fixed value of ω, on the reservoir performance for the optimal solution for both secondary and tertiary recovery. The results are:

1. **For the secondary recovery**: the optimal solution for the calibrated value of ω is a slug size of 0.025 PV. The WAG ratio at the calibrated value of ω (6:6 months= FWINJ is 0.5) (in this case the ω = 0.924). The optimal solution for the fixed value of ω=1 is a slug size of 0.014 PV. The WAG ratio for the fixed value of ω is 3:7 months (FWINJ is 0.3). The results at the calibrated value of ω show that the oil recovery has declined to FOE equal to 0.539 compared to what is observed in the previous optimisation scenarios, but it is less than FOE (0.571) for the fixed value of ω = 1. The water production is higher at 1.048×10^9 STB (for the calibrated value of ω, FWCT = 0.849) compared with 7.12×10^8 STB (for the fixed value of ω = 1, FWCT = 0.765). The gas production total (FGPT) is lower 2.1×10^9 MSCF (for the calibrated value of ω) in contrast to 4.23×10^9 MSCF (for the fixed value of ω = 1). The total amount of fluid injected at the calibrated value of ω is 244,982 RB/day, which is less than the usual amount of fluid injected by an amount of 5,018 RB/day. In addition, it is less that total amount of fluid to inject at the fixed value of ω, 258,132 RB/day, which is greater than the usual amount of fluid injected by an amount of 8,132 RB/day.
2. **For the secondary recovery:** The WAG pattern injection for the calibrated value of ω had only Injector 7 injecting water only throughout the whole period of injection, while the other injectors injected gas alternating with water. In the previous scenario (scenario 2), there are two injectors injecting only water. For the WAG pattern injection for the fixed value of ω only Injector 1 was injecting water only throughout the whole period of injection, while the other injectors injected gas alternating with water. This did not happen in the previous scenario for optimising the WAG pattern injection, where all the injectors were injecting gas alternating with water. This shows that the optimisation of fluid volume to inject, plays a role in the optimisation results, leading to a reduction in the number of injection wells to 7 injectors that inject gas alternating with water for both cases (the calibrated value of ω and the fixed value of ω).

3. **For the tertiary recovery**: similar behaviour is observed compared with secondary recovery. The optimal solution for the calibrated value of ω is a slug size of 0.102 PV, which is significantly higher than what is been observed in the previous optimisations' scenarios. The WAG ratio for the calibrated value of ω is (26:41 months= FWINJ is 0.38) (in this case the ω = 0.812). The optimal solution for the fixed value of ω=1 is a slug size of 0.031 PV. At the fixed value of ω, the optimal solution is a WAG ratio of (7:16 months=FWINJ is 0.3). The results show that the oil recovery, for calibrated value of ω, FOE = 0.564, is smaller than for the fixed value of ω = 1, FOE = 0.606. In addition, water production is lower for the calibrated value of ω, 1.28×10^9 STB, FWCT = 0.834, than for the fixed value of ω = 1, FWCT = 0.819, 1.375×10^9 STB. The gas production total (FGPT) 3.02×10^9 MSCF for the calibrated value of ω is lower compared with the fixed value of ω=1, 4.386×10^9 MSCF. The total amount of fluid injected for the calibrated value of ω was 251,141 RB/day, which is an increase from the typical amount of fluid injected with an increase of 1,141 RB/day. The total amount of fluid injected for the fixed value of ω was 256,859 RB/day, which was greater than the typical amount of fluid injected by an amount of 6,859 RB/day.
4. **For the tertiary recovery**: the WAG pattern injection for the calibrated value of ω was similar to the WAG pattern injection for the fixed value of ω. In both cases, all the injectors injected gas alternating water throughout the whole period of injection. This shows that calibrated value of ω does not have a significant difference on the optimisation results of the tertiary recovery.

6.5.3.2. Conclusion of optimising the WAG ratio, slug size, WAG pattern and amount of flow rate to inject while there is unlimited gas available to inject

The addition of fluid flow rate of injection to the optimisation played a role in the optimisation results. From the results presented previously, the following conclusions can be drawn:

1. **Comparison between the calibrated value of ω and the fixed value of ω for secondary recovery:** the optimal solution for the calibrated value of ω is a slug size (0.028 PV) which is greater than the slug size (0.014 PV) at the fixed value of ω. The WAG ratio was 6:6 months (FWINJ =0.5) using the calibrated value

of ω, while the WAG ratio was 3:7 months (FWINJ = 0.3) for the fixed value of ω=1. The total amount of fluid to inject was decreased by 13,150 RB/day, the oil recovery at the calibrated value of ω was less than oil recovery at the fixed value of ω by approximately 4%. The total water and gas production was slightly higher for the calibrated value of ω. Meaning that the value of ω in combination with the amount of flow rate to inject shows a notable impact the optimisation results.

2. **Comparison with previous optimisation results for the secondary recovery at the calibrated value of ω**, the slug size (0.028 PV) is bigger than what have been observed in the previous optimisation scenarios (0.014 PV for scenario 1 and 0.008 PV for scenario 2). The period of injection 6:6 months (FWINJ=0.5) is longer than the period of injection that is observed for the previous optimisation scenarios (3:4 months (FWINJ=0.42) for scenario 1 and 2:2 month (FWINJ =0.5) for scenario 2). The injectors have been changed to seven injectors to inject FSS WAG injection (while previously it was 8 injectors for scenario 1, and 6 injectors for scenario 2). The total amount of fluid to inject was less than the previous scenarios of optimisation (250,000 RB/day) by 5,018 RB/day, there was little reduction in the oil recovery (approximately 3%). The total water production showed a minor increase compare with the total water production in scenario 2 and was had a negligible difference to the water production in scenario 1. The total gas production was less than the previous scenarios 1 and 2.
3. **Comparison with previous optimisation results for the secondary recovery at the fixed value of ω**, the slug size (0.014 PV) is smaller than what is observed in the previous optimisation scenarios (0.022 PV for scenario 1 and 0.028 PV for scenario 2). The period of injection (3:7 months, FWINJ = 0.3) is smaller than the period of injection observed in the previous optimisation scenarios (7:5 months (FWINJ = 0.58) for scenario 1 and 10:7 month (FWINJ =0.58) for scenario 2), and it is injecting greater amounts of gas compared with water similar to what has been observed in previous scenarios of optimisation. The number of injectors is reduced to seven injectors, injecting FSS WAG injection (in previous scenarios this is 8 injectors for both scenario 1 and scenario 2). The total amount of fluid to inject is more than the previous scenarios of optimisation (250,000 RB/day) by 8,132 RB/day, there was little increase in the oil recovery.

4. **Comparison between the calibrated value of ω and the fixed value of ω for tertiary recovery:** the optimal solution at the calibrated value of ω has a slug size (0.102 PV) bigger than the slug size (0.031 PV) at the fixed value of ω. The WAG ratio was 26:41 months (FWINJ =0.5) at the calibrated value of ω, while the WAG ratio was 7:16 months (FWINJ = 0.3) at the fixed value of ω. The total amount of fluid to inject at the calibrated value of ω was less than at the fixed value of ω by 5,718 RB/day, the oil recovery at the calibrated value of ω was less than oil recovery at the fixed value of ω by approximately 4%. The total water and gas production was slightly higher at the calibrated value of ω. Meaning that the value of ω impacted the optimisation results.
5. **Comparison with previous optimisation results for the tertiary recovery at the calibrated value of ω**, the slug size (0.102 PV) is bigger than what have been observed in the previous optimisation scenarios (0.011 PV for scenario 1 and 0.007 PV for scenario 2). The period of injection 26:41 months (FWINJ=0.38) is longer than the period of injection that have been observed in the previous optimisation scenarios (2:3 months (FWINJ=0.4) for scenario 1 and 1:3 month (FWINJ =0.25) for scenario 2) but within the same range of FWINJ. The total water and gas production was slightly higher compared to the previous optimisation scenarios by 1,141 RB/day.
6. **Comparison with previous optimisation results for the tertiary recovery at the fixed value of ω**, the slug size (0.31 PV) is bigger than what have been observed in the slug size of 0.005 PV for scenario 1 and smaller than the slug size of 0.048 PV for scenario 2. The period of injection 7:16 months is longer than the period of injection of 1:2 months for scenario 1 and smaller than the period of 13:12 month for scenario 2. The total water and gas production was slightly higher compared to the previous optimisation scenarios by 6,859 RB/day.

6.5.4 Adding a constraint on the gas availability while optimising the WAG ratio, slug size, WAG pattern and amount of flow rate to inject

In the previous optimisation sections, the assumption was unlimited supply of gas to inject. In this section, that assumption is removed, and the injectors injected water instead of gas once it was depleted.

The optimisation parameters are:

1. FWINJ between 0.3 and 0.8
2. Slug size between 0.005 and 0.15
3. Type of fluid to inject (wither water or gas) for the injectors (1-8).
4. Amount of fluid to inject in each injection well between 25,000 and 50,000.

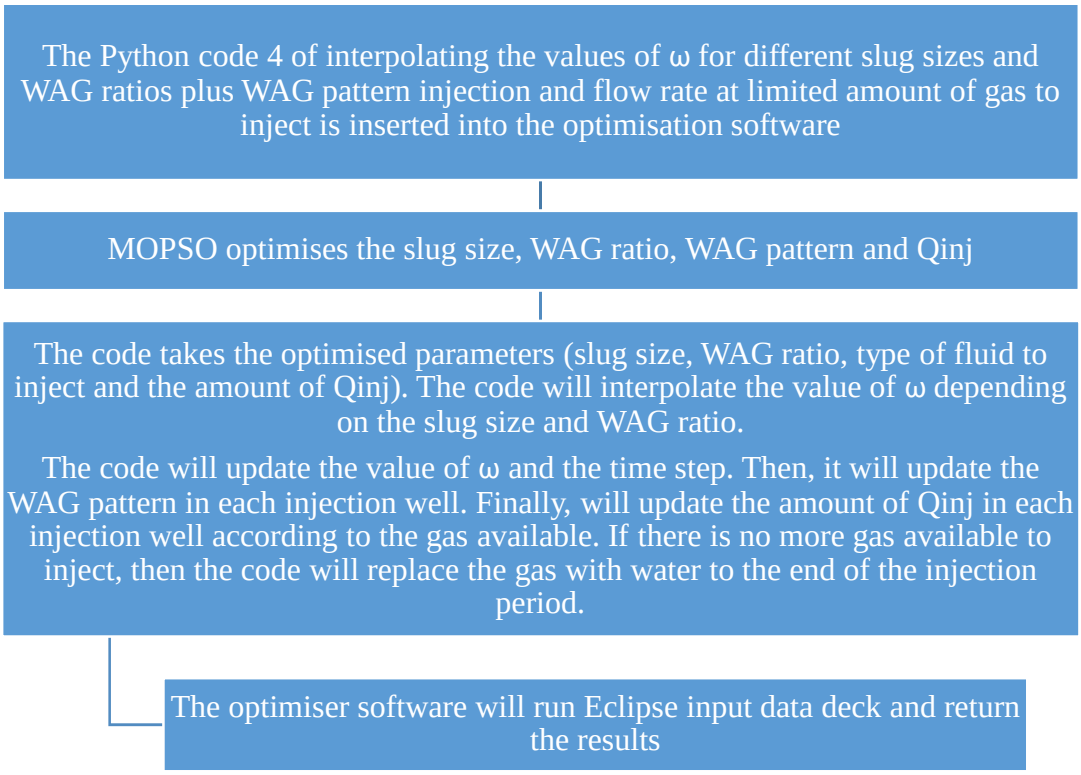

Figure 6.17 The optimisation workflow when there is a constraint on the gas available to inject

The workflow of the optimisation is shown in the diagram below Figure 6.17, and it is detailed below:

1. The optimisation software provided Python code 4 with the optimisation parameters, which is in this case were the WAG ratio, slug size, WAG pattern injection and the amount of fluid to inject. The python code 3 was further developed to Python code 4 (Appendix C.4) to consider the limited amount of the gas available to inject.
2. The Python code 4 took the optimised parameters and then:
   - Updated the Todd and Longstaff mixing parameter value in the Eclipse data

deck in addition it updated the time step and the number of cycles.

- Updated the WAG pattern injection in the injector wells.
- Updated each injection well with the amount of fluid to inject, and the sum of the amount was updated in the GCONPROD. However, the difference here was that the amount of gas injected in each injector was counted at each time step and was deducted from the total gas that was available for injection. If the amount of remaining gas could not be injected into all the injection wells during the same time step, then the code injected the remaining gas into the first injection well and then checked the quantity of the remaining gas. If sufficient gas was available, it proceeded to inject gas into the second injection well and continue this process of checking remaining gas and injecting into the next available well until no more gas was available. When the gas supply was depleted it was then replaced with water, even if it were within the same time step.

3. The optimisation software ran the Eclipse data deck and then returned the results.

6.5.4.1. Results of optimising the WAG ratio, slug size, WAG pattern and amount of flow rate to inject while adding a Constraint on the gas availability

The results of the optimisation were obtained for both secondary and tertiary recovery of miscible FSS WAG injection for the calibrated value of ω.

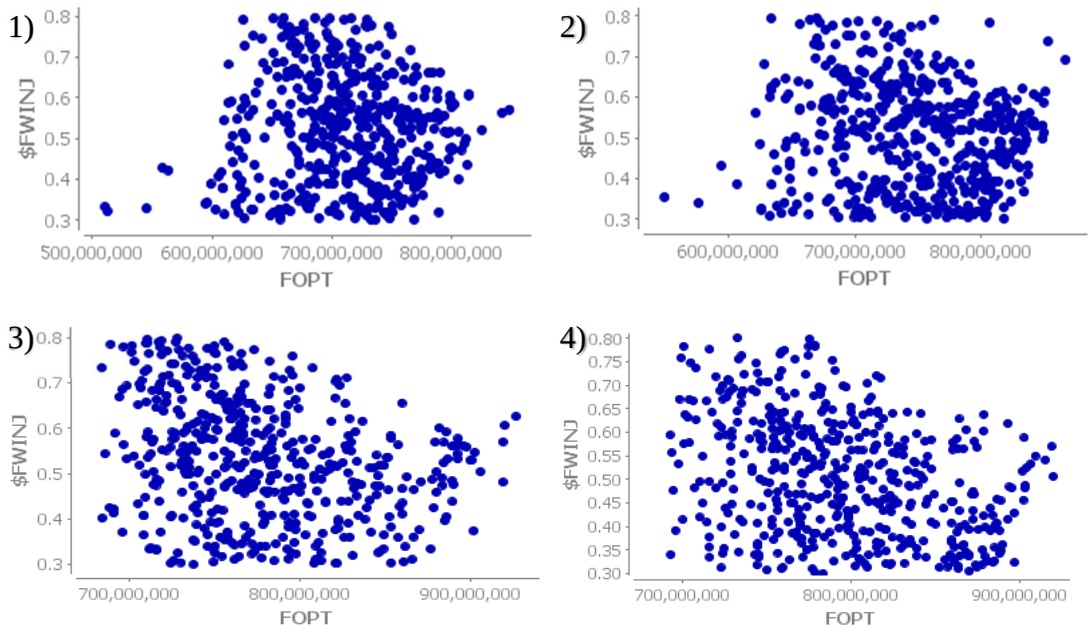

Figure 6.18 The optimisation results of the WAG ratio (i.e. FWINJ) vs the total oil production (FOPT), for: 1) secondary recovery at the calibrated value of ω, 2) secondary recovery at fixed value of ω = 1, 3) tertiary recovery at the calibrated value of ω, 4) tertiary recovery at fixed value of ω = 1.

Figure 6.18 shows the optimisation results of the WAG ratio (FWINJ) versus the total oil recovery for both secondary and tertiary recoveries, with the calibrated value of ω and the fixed value of ω. For secondary recovery with the calibrated value of ω, the highest oil recovery occurred when the WAG ratio was between 0.4 and 0.6 and convergence began at FWINJ = 0.57, differing from the results of previous optimisations' scenario. In the secondary recovery with the fixed value of ω (Figure 6.18, 2), the highest oil recovery occurred when the WAG ratio was in the region of 0.3 to 0.8, which is a wider range than that observed in the previous scenarios of optimisation, however it can be seen that convergence started at high WAG ratios (i.e. FWINJ = 0.7 – 0.75).

For the tertiary recovery with the calibrated value of ω, the highest oil recovery was for WAG ratios between 0.4 and 0.6, similar to the scenario 1 optimisation (FWINJ = 0.4 to 0.6), with a slightly narrower range than the scenario 2 optimisation (FWINJ = 0.3 to 0.6), and it is shifted and a slightly wider than the scenario 3 optimisation (FWINJ = 0.3 to 0.55). In the tertiary recovery with a fixed value of ω = 1, the highest oil recovery was at WAG ratio (FWINJ = 0.3 – 0.7), which is a wider range than those observed in the previous three scenarios.

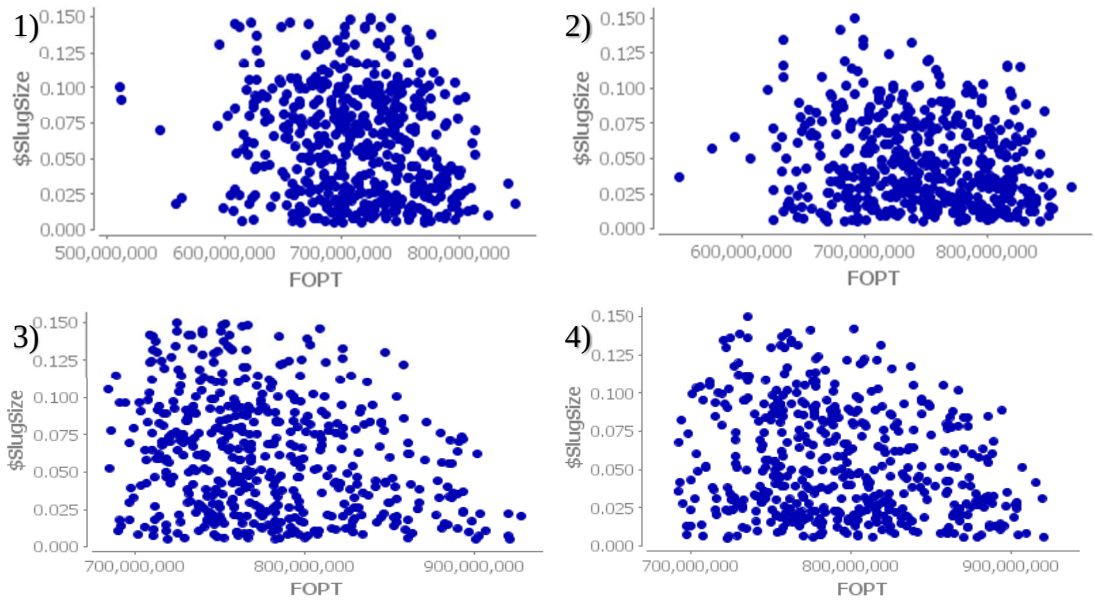

Figure 6.19 The optimisation results of the slug size vs the Total oil recovery (FOPT), for: 1) secondary recovery at the calibrated value of ω, 2) secondary recovery at fixed value of ω = 1, 3) tertiary recovery at the calibrated value of ω, 4) tertiary recovery at fixed value of ω = 1.

Figure 6.19 represents the optimisation results of the slug size vs the total oil production (FOPT). For the secondary recovery using the calibrated value of ω, the oil recovery increases as the slug size decreases <0.1 PV, this is higher than previously seen in scenarios 1 and 2 for the optimisation (<0.03 PV), and scenario 3 for the optimisation <0.075 PV. In the secondary recovery using the fixed value of ω, the highest oil recovery occurs for slug sizes lower than <0.1 PV, this is similar to the calibrated value of ω, but higher than that of scenario 1 for the optimisation (<0.075 PV), comparing with scenario 2 the range of slug sizes is narrower (0.005-0.14 PV) for the highest achieved oil recovery, and is opposite to what is observed from the scenario 3 results for the optimisation (>0.1 PV).

For the tertiary recovery with the calibrated value of ω, the oil recovery increases as the slug size decreases <0.08 PV, this differs from the scenario 1 optimisation (where slug size has no impact on the oil recovery) and is higher than what is observed in the scenario 2 optimisation (<0.06 PV) and is opposite to what occurs in scenario 3 where oil recovery increases with increasing slug size (>0.1 PV). For the tertiary recovery using the fixed value of ω = 1, the oil recovery increases as the slug size decreases (<0.08 PV), this is similar to the calibrated value of ω and to scenario 2 and 3 of optimisation but is less than what is observed for the scenario 1 optimisation (0.13 PV).

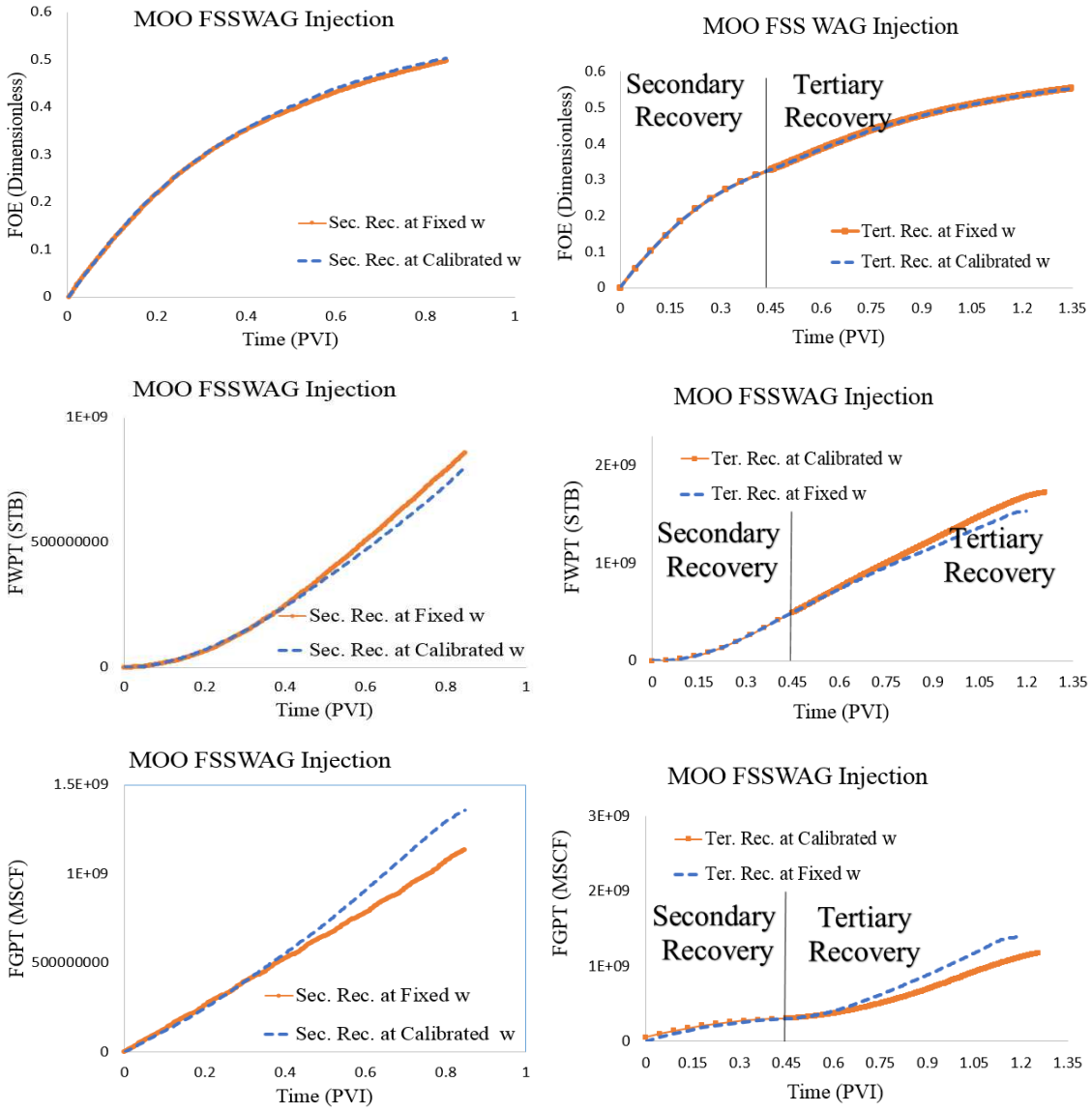

Figure 6.20 The reservoir performance of the optimal solution for both secondary and tertiary recovery. MOO is multi-objective optimisation. FOE represents field oil recovery. FWCT represents field water cut. FGPT represents field gas production total.

Figure 6.20 shows the comparison between the reservoir performance from the optimal solution of the calibrated value of ω and the fixed value of ω for both secondary and tertiary recovery are:

1. **For the secondary recovery**: the optimal solution for the calibrated value of ω is a slug size of 0.018 PV. The WAG ratio at the calibrated value of ω (5:4 months= FWINJ is 0.55) (in this case the ω = 0.958). The optimal solution for the fixed value of ω=1 is a slug size of 0.029 PV. The WAG ratio for the fixed value of ω is 15:7 months (FWINJ is 0.68). The results at the calibrated value of ω show that

the oil recovery has declined with the field efficiency of oil recovery (FOE) is 0.509 smaller than FOE (0.52) for the fixed value of $\omega = 1$. The water production is 8.47×10^8 STB (for the calibrated value of ω) which is less than compared with 1.035×10^9 STB (for the fixed value of $\omega = 1$). The gas production total (FGPT) is 1.37×10^9 MSCF (for the calibrated value of ω) which is higher than 1.28×10^9 MSCF (for the fixed value of $\omega = 1$). The total amount of fluid injected at the calibrated value of ω is 280,689 RB/day, which is less than the usual amount of fluid injected by an amount of 80,689 RB/day. In addition, it is more than that total amount of fluid to inject at the fixed value of ω, 276,677 RB/day, which is greater than the usual amount of fluid injected by an amount of 76,677 RB/day.

2. **For the secondary recovery:** The WAG pattern injection for the calibrated value of ω had only Injectors 3 and 7 injecting water only throughout the whole period of injection, while the other injectors injected gas alternating with water. While, the WAG pattern injection for the calibrated value of ω had only Injector 2 injecting water only throughout the whole period of injection, while the other injectors injected gas alternating with water.
3. **Comparison between the calibrated value of ω and the fixed value of ω for secondary recovery:** the optimal solution at the calibrated value of ω has a slug size (0.018 PV) smaller than the slug size (0.029 PV) at the fixed value of ω. The WAG ratio was 5:4 months (FWINJ =0.55) at the calibrated value of ω, while the WAG ratio was 15:7 months (FWINJ = 0.68) at the fixed value of ω. The total amount of fluid to inject at the calibrated value of ω was higher than at the fixed value of ω by 4,012 RB/day, however, it achieved lower oil recovery by approximately 2%. The total water production was lower at the calibrated value of ω, while total gas production was slightly higher at the calibrated value of ω. Meaning that the value of ω impacted the optimisation results.
4. **For the tertiary recovery**: the optimal solution for the calibrated value of ω is a slug size of 0.021 PV. The WAG ratio for the calibrated value of ω is (7:4 months= FWINJ is 0.63) (in this case the $\omega = 0.894$). The optimal solution for the fixed value of ω=1 is a slug size of 0.006 PV. At the fixed value of ω, the optimal solution is a WAG ratio of 1:1 months (FWINJ is 0.5). The results show that the oil recovery, for calibrated value of ω, FOE = 0.582, is bigger than for the

fixed value of ω = 1, FOE = 0.552. In addition, water production is lower for the calibrated value of ω, 1.44×10^9 STB, than for the fixed value of ω = 1, 1.5×10^9 STB. The gas production total (FGPT) 3.14×10^9 MSCF for the calibrated value of ω is higher compared with the fixed value of ω=1, 1.39×10^9 MSCF. The total amount of fluid injected for both the calibrated value of ω and the fixed value of ω to 300,000 RB/day, which is an increase from the typical amount of fluid injected with an increase of 100,000 RB/day.

5. **For the tertiary recovery**: the WAG pattern injection for the calibrated value of ω showed that injector 7 was injecting water only, while injectors 1 and 6 were injecting water only for the fixed value of ω.
6. **Comparison between the calibrated value of ω and the fixed value of ω for tertiary recovery:** the optimal solution at the calibrated value of ω has a slug size (0.021 PV) bigger than the slug size (0.006 PV) at the fixed value of ω. The WAG ratio was 7:4 months (FWINJ =0.63) at the calibrated value of ω, is longer than the WAG ratio of 1:1 months (FWINJ = 0.5) at the fixed value of ω. The total amount of fluid to inject at the calibrated value of ω was the same, however, it achieved higher oil recovery by approximately 3%. The total water production was lower at the calibrated value of ω, while total gas production was higher at the calibrated value of ω. Meaning that the value of ω impacted the optimisation results.

6.5.4.2. Conclusion of optimising the WAG ratio, slug size, WAG pattern and amount of flow rate to inject while there is limited gas available to inject

From the results mentioned earlier, the following conclusions can be drawn:

1. **Comparison between the optimisation results for the secondary recovery at the calibrated value of ω**, the slug size in scenario 4 (0.018 PV) is bigger than what have been observed in the previous optimisation scenarios (0.014 PV for scenario 1, 0.008 PV for scenario 2 and 0.025 PV for scenario 3). The slug size scenario 2 was very small compared to the other three scenarios. The period of injection 5:4 months (FWINJ=0.55) is varying (the difference is close, approximately 4 months) to what have been observed in the previous optimisation scenarios (3:4 months (FWINJ=0.42) for scenario 1, 2:2 month (FWINJ =0.5) for

scenario 2 and 6:6 for scenario 3 (FWINJ=0.5)) but within the same range of FWINJ (0.4-0.5). The injectors had been reduced to 6 injectors that inject FSS WAG injection (8 injectors in scenario 1, 6 injectors in scenario 2, and seven injectors in scenario 3). The total amount of fluid to inject increased in scenario 1 and 2 was 250,000 RB/day, in scenario 3 was 244,982 RB/day, and scenario 4 was 280,689 RB/ day. The oil recovery ranged between 0.573 for scenario 1, 0.567 for scenario 2, 0.539 for scenario 3, and 0.509 for scenario 4.

2. **Comparison between the optimisation results for the secondary recovery at the fixed value of ω**, the slug size in scenario 4 (0.029 PV) is within the same range that have been observed in the previous optimisation scenarios (0.022 PV for scenario 1, 0.028 PV for scenario 2 and 0.014 PV for scenario 3). The period of injection in scenario 4 is 15:7 months (FWINJ=0.68) is varying significantly to what have been observed in the previous optimisation scenarios (7:5 months (FWINJ=0.58) for scenario 1, 10:7 month (FWINJ =0.58) for scenario 2 and 3:7 months for scenario 3 (FWINJ=0.3)). The injectors had been reduced to 6 injectors that inject FSS WAG injection (8 injectors in scenario 1 and 2, and seven injectors in scenario 3). The total amount of fluid to inject increased in scenario 1 and 2 was 250,000 RB/day, 258,132 RB/day in scenario 3, and scenario 4 was 276,677 RB/ day. The oil recovery ranged between 0.589 for scenario 1, 0.587 for scenario 2, 0.571 for scenario 3, and 0.52 for scenario 4.
3. **Comparison between the optimisation results for the tertiary recovery at the calibrated value of ω**, the slug size in the optimisation scenarios is (0.01 PV for scenario 1, 0.007 PV for scenario 2, 0.102 PV for scenario 3 and 0.021 PV in scenario 4). The slug size in scenario 3 was very big compared to the other three scenarios. The period of injection in the optimisation scenarios is (2:3 months (FWINJ=0.4) for scenario 1, 1:3 month (FWINJ =0.25) for scenario 2, 26:41 for scenario 3 (FWINJ=38) and 7:4 months (FWINJ=0.63) for scenario 4). The period of injection in scenario 3 is very long compared to the other scenarios. The injectors had been reduced to 7 injectors that inject FSS WAG injection (8 injectors in scenario 1, 2, and 3). The total amount of fluid to inject is 250,000 RB/day in scenario 1 and 2, in scenario 3 was RB/day, and scenario 4 was 300,000

RB/ day. The oil recovery ranged between 0.602 for scenario 1, 0.595 for scenario 2, 0.564 for scenario 3, and 0.582 for scenario 4.

4. **Comparison between the optimisation results for the tertiary recovery at the fixed value of ω**, the slug size in optimisation scenarios is (0.005 PV for scenario 1, 0.048 PV for scenario 2, 0.031 PV for scenario 3, and 0.006 PV for scenario 4). The slug size scenario 1 and 3 was very small compared to the other scenarios. The period of injection in the optimisation scenarios is (1:2 months (FWINJ=0.33) for scenario 1, 13:12 month (FWINJ =0.52) for scenario 2, 7:16 for scenario 3 (FWINJ=0.3), and 1:1 months (FWINJ=0.5) for scenario 4). The injectors had been reduced to 6 injectors in scenario 4 that inject FSS WAG injection (8 injectors in scenario 1, 2, and 3). The total amount of fluid to inject in scenario 1 and 2 was 250,000 RB/day, in scenario 3 was 256,859 RB/day, and scenario 4 was 300,000 RB/ day. The oil recovery ranged between 0.608 for scenario 1, 0.565 for scenario 2, 0.606 for scenario 3, and 0.552 for scenario 4.

6.6 Summary of the chapter

In this chapter, the calibrated values of ω reported in Chapter 4 (Figure 4.50 for secondary recovery and Figure 4.51 for tertiary recovery) were interpolated for a wide range of slug size and WAG ratio using a Python code (a programming language), to enable the automatic generation of ω values for specific slug sizes and WAG ratios. The code was incorporated into an optimisation software used to optimise the slug size and WAG ratio for better use of the gas injected and for better oil recovery. When the optimisation software provided a value for slug size and WAG ratio, the code took those values and selected the value of the mixing parameter. The code then updated the mixing parameter value in the Eclipse data deck and the optimisation software ran the data deck and returned the results. Furthermore, the code was extended to the optimisation of the type of fluid to inject, so called WAG pattern optimisation. In this case, a code was developed that operated inside the optimisation software to update each well with the type of fluid to inject, whether injecting water only or alternating with gas. In addition to that, the slug size and WAG ratio was optimised, which aided in the WAG pattern optimisation and the pattern that will achieve the optimal recovery was identified. Also, the code was extended to take into account the optimisation of the flow rate. Finally, the code was extended to

take into account limited supply of gas to inject during the optimisation of WAG ratio, slug size, WAG pattern and flow rate.

The calibrated value of ω, in addition to each factor that has been used in the optimisation, plays a role in the optimisation results. From the results of the optimisation scenarios, the following conclusions can be drawn:

1. **Comparison between the optimisation results for the secondary recovery at the calibrated value of ω in all cases**. The slug size in the optimisation scenarios tends to be small (0.014 PV for scenario 1, 0.008 PV for scenario 2, 0.025 PV for scenario 3 and 0.018 PV for scenario 4). The slug size in scenario 2 was significantly smaller compared to the other three scenarios. The WAG ratio tends to be 1:1 of miscible FSS WAG injection. The period of injection in the optimisation scenarios (3:4 months (FWINJ=0.42) for scenario 1, 2:2 month (FWINJ =0.5) for scenario 2, 6:6 for scenario 3 (FWINJ=0.5) and 5:4 months (FWINJ=0.55) for scenario 4). The value of ω ranges between ω =0.924 for a slug size of 0.025 PV and a WAG ratio of 1:1 (period of injection is 6:6 months) to ω=1 for a slug size of 0.08 PV and a WAG ratio of 1:1 (period of injection is 2:2 months). The injectors were reduced to 6 injectors that inject FSS WAG injection in scenario 4 while the number of injectors in the other scenarios were: 8 injectors in scenario 1, 6 injectors in scenario 2, and 7 injectors in scenario 3. The total amount of fluid to inject changed depending on the scenario. In scenarios 1 and 2 this was 250,000 RB/day, in scenario 3 there was a decrease to 244,982 RB/day, and in scenario 4 increased to 280,689 RB/ day. The oil recovery was the highest for scenario 1 and with 0.573 at a slug size of 0.014 and a WAG ratio of 3:4 (period of injection is 3:4 months) where ω=0.952. The peak oil recovery for each scenario are 0.573 for scenario 1, 0.567 for scenario 2, 0.539 for scenario 3, and 0.509 for scenario 4. The highest total gas production was observed with scenario 1 and this was 3.58×10^9, while it was 2.3×10^9 for scenario 2, 2.1×10^9 for scenario 3, and 1.37×10^9 for scenario 4. The lowest total water production occurred in scenario 1 with 8.127×10^8, while it was 1.162×10^9 for scenario 2, 1.048×10^9 for scenario 3, and 8.47×10^8 for scenario 4.

2. **Comparison between the optimisation results for the secondary recovery at the fixed value of ω=1 in all cases**. The slug size in the optimisation scenarios tends to be small (0.022 PV for scenario 1, 0.028 PV for scenario 2, 0.014 PV for scenario 3 and 0.029 PV for scenario 4) but it was bigger than the slug size at the calibrated value of ω at the same scenario. The WAG ratio tends to inject water more than gas. The period of injection in the optimisation scenarios (7:5 months (FWINJ=0.58) for scenario 1, 10:7 month (FWINJ =0.58) for scenario 2, 3:7 months for scenario 3 (FWINJ=0.3) and 15:7 months (FWINJ=0.68) for scenario 4). The injectors were reduced to 6 injectors that inject FSS WAG injection in scenario 4 while the number of injectors in the other scenarios were: 8 injectors in scenario 1 and 2, and 7 injectors in scenario 3. The total amount of fluid to inject changed depending on the scenario. In scenarios 1 and 2 this was 250,000 RB/day, in scenario 3 there was an increase to 258,132 RB/day, and in scenario 4 increased to 276,677 RB/ day. The oil recovery was the highest for scenario 1 and with 0.589 at a slug size of 0.022 and a WAG ratio of 7:5 (period of injection is 7:5 months). The peak oil recovery for each scenario are 0.589 for scenario 1, 0.587 for scenario 2, 0.571 for scenario 3, and 0.52 for scenario 4. The highest total gas production was observed with scenario 3 and this was 4.23×109, while it was 2.51×109 for scenario 1, 2.48×109 for scenario 2, and 1.28×109 for scenario 4. The total gas production was the highest at scenario 3 and it was, while it was, it was, and it was for scenario 4. The lowest total water production occurred in scenario 3 with 7.12×108, while it was 1.169×109 for scenario 1, it was 1.228×109 for scenario 2, and it was 1.035×109 for scenario 4.
3. **Comparison between the optimisation results for the tertiary recovery at the calibrated value of ω in all cases.** The slug size in the optimisation scenarios has no trend (0.01 PV for scenario 1, 0.007 PV for scenario 2, 0.102 PV for scenario 3 and 0.021 PV in scenario 4). The slug size in scenario 3 was significantly higher compared to the other three scenarios. The period of injection in the optimisation scenarios (2:3 months (FWINJ=0.4) for scenario 1, 1:3 month (FWINJ =0.25) for scenario 2, 26:41 for scenario 3 (FWINJ=38) and 7:4 months (FWINJ=0.63) for scenario 4. The period of injection in scenario 3 is very long compared to the other scenarios. The value of ω was ω =0.931 for scenario 1, ω =0.938 for scenario 2,

ω =0.812 for scenario 3 and ω =0.894 for scenario 4. The injectors were reduced to 7 injectors that inject FSS WAG injection in scenario 4 while the number of injectors in the other scenarios were: 8 injectors in scenario 1, 2 and 3. The total amount of fluid to inject changed depending on the scenario. In scenarios 1 and 2 this was 250,000 RB/day, in scenario 3 there was a minor increase to 251,141 RB/day, and in scenario 4 increased to 300,000 RB/ day. The oil recovery was the highest for scenario 1 and with 0.602 at a slug size of 0.01 and a WAG ratio of 2:3 (period of injection is 2:3 months) where ω=0.931. The peak oil recovery for each scenario are 0.602 for scenario 1, 0.595 for scenario 2, 0.564 for scenario 3, and 0.582 for scenario 4. The highest total gas production was observed with scenario 2 and it was 4.92×109, while it was 3.7×109 for scenario 1, it was 3.02×109 for scenario 3, and it was 3.14×109 for scenario 4. The lowest total water production occurred in scenario 2 and it was 1.278×109, while it was 1.58×109 for scenario 1, it was 1.28×109 for scenario 3, and it was 1.44×109 for scenario 4.

4. **Comparison between the optimisation results for the secondary recovery at the calibrated value of ω in all cases**. The slug size in the optimisation scenarios has no trend (0.005 PV for scenario 1, 0.048 PV for scenario 2, 0.031 PV for scenario 3, and 0.006 PV for scenario 4). The slug size in scenario 1 and 3 were significantly smaller compared to the other scenarios. The WAG ratio has no specific trend. The period of injection in the optimisation scenarios (1:2 months (FWINJ=0.33) for scenario 1, 13:12 month (FWINJ =0.52) for scenario 2, 7:16 for scenario 3 (FWINJ=0.3), and 1:1 months (FWINJ=0.5) for scenario 4). The injectors were reduced to 6 injectors that inject FSS WAG injection in scenario 4 while the number of injectors in the other scenarios were 8 injectors in scenario 1, 2 and 3. The total amount of fluid to inject changed depending on the scenario. In scenarios 1 and 2 this was 250,000 RB/day, in scenario 3 there was an increase to 256,859 RB/day, and in scenario 4 increased to 300,000 RB/ day. The oil recovery was the highest for scenario 1 and with 0.608 at a slug size of 0.005 and a WAG ratio of 1:2 (period of injection is 1:2 months) where ω=0.952. The peak oil recovery for each scenario are 0.608 for scenario 1, 0.565 for scenario 2, 0.606 for scenario 3, and 0.552 for scenario 4. The highest total gas production was

observed with scenario 3 and it was 4.386×109, while it was 4.25×10^9 for scenario 1, it was 1.892×10^9 for scenario 2, and it was 1.39×10^9 for scenario 4. The lowest total water production occurred in scenario 3 and it was 1.375×109, while it was 1.47×109 for scenario 1, it was 1.38×109 for scenario 2, and it was 1.5×109 for scenario 4.

Overall, for the secondary recovery in the optimisation scenarios using the calibrated value of ω there is a trend toward small slug sizes (0.008-0.025 PV) with a WAG ratio was 1:1 (ω ranges between 0.924-1 depending on the slug size). The period of injection did not exceed six months for the either the gas or water injection and was not less than two months for either. For the secondary recovery in the optimisation scenarios using the fixed value of ω=1 the trend is toward small slug sizes (0.014-0.029 PV) but showed an increase compared with using the calibrated value of ω for the same scenario. The WAG ratio was to inject amounts of water compared to gas and the period of injection reached 15 months for water injection and 7 months for the gas injection.

For the tertiary recovery in the optimisation scenarios using the calibrated value of ω there is no specific trend for the slug sizes, similarly is the case for WAG ratio. As scenario 1 and 2 achieved similar oil recovery and the next greatest oil recovery was achieved in scenario 4 with a difference of only 0.02. The recommendation can be either to use a slug size of 0.01 PV and a WAG ratio of 2:3 (period of injection is 2:3 months) where ω= 0.931 or to use a slug size of 0.021 PV and a WAG ratio of 7:4 (period of injection is 7:4 months) where ω= 0.894. Similar behaviour has been observed in the optimisation scenarios of the tertiary recovery using the fixed value of ω=1 as there is no specific trend for the slug sizes, similarly is the case for WAG ratio.

Chapter 7

Conclusions and future work

7.1 Introduction

Todd and Longstaff (1972) model is the most commonly used model in black oil reservoir simulators to model the effects of viscous fingering on a field scale. The reason for that is, it requires the selection of a single parameter, namely the mixing parameter, ω also known as TLMIXPAR in black oil simulator such as Eclipse E100, the value of which includes the factors affecting viscous fingering. Additionally, it incorporates a method to calculate the effective viscosity when mixing occurs between oil and gas. Todd and Longstaff (1972) recommended a value of ω between ⅓ and ⅔ for simulating full scale secondary miscible gas injection.

Blunt and Christie (1993) showed that the value of ω should be increased to 1 when modelling simultaneous water and gas (SWAG) injection for secondary recovery and to 0.92 for tertiary SWAG injection. However, their work was limited to simultaneous WAG injection

This thesis demonstrated the calibration of ω for a specific slug size and WAG ratio for both secondary and tertiary recovery for miscible finite sized slug WAG injection. 1:1 WAG ratio at small slug sizes has a better apparent mixing between the solvent and the oil than at matched velocity WAG ratio. For secondary 1:1 WAG ratio, the mixing parameter at a slug size of 0.01 PV is ω=1, the mixing parameter at a slug size of 0.05 PV is ω=0.87, and the mixing parameter at a slug size of 0.1 PV is ω=0.84.

Then followed the calibration of ω by the implementation of the calibrated value of ω for a specific slug size and 1:1 WAG ratio in a black oil model to check the effect on the oil recovery in comparison to Todd and Longstaff's value and the full mixing value = 1. Finally, implementing the calibrated value of ω in the optimisation and comparing the results of the optimisation at fixed value of ω.

7.2 The key findings

Chapter 4 demonstrated the calibration of the mixing parameter, ω value for miscible finite sized slug WAG (FSS WAG) injection. This was a refinement and extension of previous work on the recalibration of ω for SWAG injection by Blunt and Christie (1993). Its innovation is the workflow of calculating the mixing parameter iteratively for a set of

WAG ratio, slug size, and different type of recovery. The results for the calibration of ω value using a 1D numerical model of detailed fingering in a line drive are:

1. A grid refinement study was performed on secondary miscible gas displacement to determine the effect of numerical diffusion in the 1D model on the fingering models used to calibrate the value of ω. Under grid refinement the mixing parameter's value returns to the Todd and Longstaff value and there is minimal effect of the numerical diffusion in the 1D model. Therefore, viscous fingering in the 1D model is triggered due to the viscosity ratio difference between the solvent and oil.
2. Using the same assumptions as Blunt and Christie, the results of the numerical model were validated against the analytical results in a manner to compare results obtained in two different ways and they were in a good agreement for SWAG injection both secondary and tertiary recovery. This gave confidence in our results for FSS WAG injection from the numerical model.
3. The values of ω increased beyond the value of ω = 0.92 for WAG ratios higher than the MVSWAG ratio. Blunt and Christie suggested the value of ω = 0.92 for the tertiary MV SWAG ratio and WAG ratios higher than the MVSWAG ratio. Even though the MV SWAG ratio gave a very small amount of fingering in the examples they considered, the viscous fingering decreased as the fractional flow increased. As a result, the values of ω increased as the fractional flow of water injected increased until the value of ω reached 1 for 2:1 SWAG injection (fractional flow of water injected = 0.67) and the value stabilised on 1 when the water injection increased.
4. For both secondary and tertiary finite-sized slug WAG injection, the results of calibrating the value of ω decreased as the slug size increased and this change depended on the WAG ratio.
5. The value of ω for secondary FSS WAG injection changed smoothly between the Koval (1963) value and the Todd and Longstaff (1972) value for secondary miscible gas injection and between Blunt and Christie's (1993) calibration for secondary SWAG injection. The value of ω returns to the Koval (1963) calibration for a secondary miscible injection at high slug sizes (0.25 to 0.3 PV) and at WAG ratio 1:6.5.

6. By plotting the values of ω at different slug sizes for FSS WAG injection as a function of the fractional flow of water injected along with the values of ω for SWAG injection for both secondary and tertiary recovery, it was seen that there was a significant difference between ω values using the numerical calibration method for FSS WAG injection and Blunt and Christie's analytical results for SWAG injection for secondary and tertiary recovery. At small slug sizes, the values of ω for FSS WAG injection are close to SWAG injection and for the tertiary FSS WAG injection are higher than the values of SWAG injection. Therefore, at small slug sizes the mixing between the injected gas and oil tends to act like SWAG injection. While for the other cases, as the slug size increases the mixing between solvent and oil decreases. At a slug size of 0.3 PV, there is no change in the value of ω at all and it is equal to ⅔ for both secondary and tertiary displacement and for different WAG ratios. Therefore, the miscible FSS WAG injection loses its benefit at high slug sizes.
7. Comparing between the results at viscosity ratio=10 and at viscosity ratio =50 for a secondary FSS WAG injection, there is a significant difference in the calibrated values of ω. The values of ω and the trend is quite different for the same WAG ratio and slug size. Therefore, to use the values of the calibrated ω on a field scale, the viscosity ratio should be considered and the values of ω should be calibrated considering the viscosity ratio.
8. Comparing between the results using a grid size =750×300 and at grid size = 375×150 for a secondary finite sized slug WAG injection, there was a slight difference in the calibrated values of ω. The values of ω at 750×300 were less than the values of ω using 375×150 by about 5-7%, but the trend was the same. Therefore, the values of ω using 375×150 were applicable for a wide range of grid blocks, since the values of ω converge at this level of refinement.

- **From Chapter 5:**

1. By applying the calibrated value of ω on quarter five-spot model, as the slug size in secondary miscible FSS WAG injection increased the oil recovery decreased. The oil recovery for the FSS WAG was greater than for the secondary SWAG injection, the secondary miscible gas injection and the water injection. As was seen, the oil recovery for the water injection method showed the highest recovery

at earlier time of the injection compared to the other types of injection, however, in the long term the oil recovery obtained was lower compared to the other methods. Secondary SWAG injection achieved almost the same recovery as secondary FSS WAG injection at slug size of 0.05 and 0.1 PV but was still lower than the FSS WAG injection for the slug sizes shown tested. This suggests that miscible FSS WAG injection improves oil recovery to a greater extent compared with the other types of injection.

2. Using the same injection techniques as previously used in the quarter five-spot model, it was seen that the oil recovery from the Watt field model behaves differently. The oil recovery was the highest for the FSS WAG injection with a slug size 0.01 PV and for the SWAG injection (both recoveries were equal). The oil recovery for the FSS WAG injection increased as the slug size decreased, which is similar to what was observed in the quarter five-spot model. The oil recovery from the water injection and the miscible gas injection at $\omega = 1$ were almost equal at the end of injection period, with both lower than the FSS WAG injections. While the SWAG and FSS WAG injection showed equal oil recovery, miscible FSS WAG is the preferred method, as SWAG has an operational complexity for implementation on a field scale.
3. Due to the complexity of the Watt Field, it was difficult to capture the three-phase region of the WAG zone and the impact of ω on it.
4. Using the quarter five spot model, it was seen that the three-phase flow of the WAG zone occurs considerably in the WAG injection and that the gas was fingering through the oil. Also, it was noted that the value of ω had an impact on the three-phase zone in the heterogeneous model but not in the homogeneous model. At the same grid block and time, the saturations vary significantly. It was observed that the fraction of three-phase-flow was considerably higher at $\omega = 1$ than at $\omega = 0.67$. It was also evident that the percentage of three-phase zone was higher at slug size 0.05 PV than at the slug size 0.1 PV. While, the three-phase zones were equal at the end of the injection of the slug size 0.05 PV between $\omega = 1$ and the calibrated value of ω, there was a difference at the end of the injection for a slug size 0.1 PV.

5. By applying the results of the calibrated value of ω on a homogeneous quarter five-spot model, it was seen that the different values of ω had no impact on the reservoir performance and/or the oil recovery.
6. The calibrated value of ω was tested on a heterogeneous model of the quarter five-spot model, with the value of ω having an impact on the oil recovery. The oil recovery at $\omega = 1$ was the highest, while the oil recovery at $\omega = 0.67$ was the lowest and the oil recovery at $\omega = 0.87$ was in between. This represents the reliable oil recovery that is going to be achieved from miscible FSS WAG injection. Similar results were obtained from the Watt field model. The impact of ω value on the oil recovery was very clear. At longer period of injection, the difference in the oil recovery should be even bigger.

- **From Chapter 6:**

The calibrated value of ω, in addition to each factor that has been used in the optimisation, played a role in the optimisation results.

For the secondary recovery in the optimisation scenarios using the calibrated value of ω there is a trend toward small slug sizes (0.008-0.025 PV) with a WAG ratio was 1:1 (ω ranges between 0.924-1 depending on the slug size). The period of injection did not exceed six months for the either the gas or water injection and was not less than two months for either. For the secondary recovery in the optimisation scenarios using the fixed value of ω=1 the trend is toward small slug sizes (0.014-0.029 PV) but showed an increase compared with using the calibrated value of ω for the same scenario. The WAG ratio was to inject amounts of water compared to gas and the period of injection reached 15 months for water injection and 7 months for the gas injection.

For the tertiary recovery in the optimisation scenarios using the calibrated value of ω there is no specific trend for the slug sizes, similarly is the case for WAG ratio. As scenario 1 and 2 achieved similar oil recovery and the next greatest oil recovery was achieved in scenario 4 with a difference of only 0.02. The recommendation can be either to use a slug size of 0.01 PV and a WAG ratio of 2:3 (period of injection is 2:3 months) where ω= 0.931 or to use a slug size of 0.021 PV and a WAG ratio of 7:4 (period of injection is 7:4 months) where ω= 0.894. Similar behaviour has been observed in the

optimisation scenarios of the tertiary recovery using the fixed value of ω=1 as there is no specific trend for the slug sizes, similarly is the case for WAG ratio.

7.3 Recommendations and future work

This thesis has focussed on using simple models to develop the understanding of the impact of the slug size, WAG ratio and type of recovery on the calibration of ω and its subsequent effect on a number of oil production metrics. It is vital that a step-wise addition of variables is maintained to ensure that the impact of each constituent part can be properly assessed and ranked.

The author would recommend that further research should be done to investigate:

1. The effect of gravity on the calibration of the mixing parameter value
2. The effect of capillary pressure on the calibration of the mixing parameter value
3. The effect of compressibility on the calibration of the mixing parameter value
4. The effect of physical diffusion and dispersion on the calibration of the mixing parameter value
5. The effect of sub-block heterogeneity (small and large scale) on the calibration of the mixing parameter (by including Koval factor)
6. Calibrate the mixing parameter value in quarter five spot (to consider the impact of the grid orientation on the calibration and comparing the results with the line drive results).
7. The effect of hysteresis on the calibration of the mixing parameter value

These elements reflect the cumulative increase in complexity described within this thesis and extend further into important factors that govern the flow in porous media that underpins successful reservoir simulation.

Appendix

Appendix A: 2D simulation input file - all dimensionless

TITLE of the input file
Title Secondary finite sized slug WAG injection

Number of grid blocks in the x and y directions
NGRID 375 150

The length of each grid block in the x and y direction
GSIZE 1.0 1.0

The matrix solve routine. This can be ICCGS for symmetric matrix of BANDP for non-symmetric matrices
SOLVER ICCGS
***SOLVER BANDP**

Water viscosity
VISCW 1.0

Oil viscosity
VISCO 4.0

Solvent viscosity
VISCS 0.4

Solvent density relative to water
DENSITYS 0.5

Oil density relative to water
DENSITYO 1.0

Initial water saturation
SINIT 0.2

Initial solvent saturation
CINIT 0.00

Critical water saturation
SWCRIT 0.2

Residual oil saturation
SORSDL 0.4

End point oil relative permeability
KROSWC 1.0

End point water relative permeability
KRWSOR 0.25

NW and NO are Powers to which normalized saturation is raised in the Corey equation to calculate the water and oil relative permeabilities.
* NW NO
RELPERM 2.0 2.0

Read in the dimensionless gravity component in the x and y directions
* GX GY
GRAV 0.0 0.0

Read permeability file
READPERM

Output the injection and production terms at the required intervals.
TOUT 0.100
TOUT 0.150
TOUT 0.250
TOUT 0.300
TOUT 0.400
TOUT 0.450
TOUT 0.550
TOUT 0.600
TOUT 0.600

Injection flow rate
QINJ 1.0

Specify the fractional flow of water injected VAL. The TIME keyword specifies the time when the injection is terminated. This should be the same the last value of the keyword TOUT. The following examples are for water flooding, gas injection and SWAG and slug WAG.
* VAL TIME
For gas injection
FWINJ 0.0 1.0

For water injection
FWINJ 1.0 1.0

For SWAG at WAG ratio of 1:1
FWINJ 0.5 1.0

For finite sized slug WAG injection of slug size10% PV and WAG ratio of 1:1 with gas as a first slug
FWINJ 0.0 0.100
FWINJ 1.0 0.150
FWINJ 0.0 0.250
FWINJ 1.0 0.300
FWINJ 0.0 0.400
FWINJ 1.0 0.450

FWINJ 0.0 0.550
FWINJ 1.0 0.600

The frequency at which the user specifies debug information
FRQDBG 10000

The restart data is written out to the restart file FRQST times
FRQRST 5000

The WELL data for horizontal wells is entered as follow
* BLX BLY TRX TRY TYPE BHP PI CINJ
WELL 1 1 1 NY INJN 1.0
* BLX BLY TRX TRY TYPE BHP PI
WELL NX 1 NX NY PROD 0.0 100000.0

The time step is determined according to the Courant, Priedrichs, Lewy condition using the keyword COUR
COUR 0.4

The fractional change in total velocity that must occur before the pressures are resolved can be controlled using the keyword CHANGEVT
CHANGEVT 0.05

Flux corrected transport scheme can be set when solving non-uniform flow matrix for both saturation and concentration using the following keywords
FCTS
FCTC

The level of output produced by subroutine OUTPUT can be set by the OUTLEVEL keyword. The lowest level is 1 and the highest level is 4
OUTLEVEL 1

The uncompressed real array output path in the OUTPUT subroutine can be selected using the following keyword
FULLSIZE

The END keyword must be entered at the end of the input file
END

Appendix B1: 1D model for calibrating the Todd and Longstaff's mixing Parameter

```
def fluxflow(S,c):   #water fractional flow
        mu_h  = ((1-c)*(mu_o**(-0.25)) + c*(mu_s**(-0.25)))**(-4)
        ans = 1-(((1-S-Sor)/(1-Swc-Sor))**2/mu_h)/(((0.25*((S-Swc)/(1-Swc-Sor))**2/mu_w)+((1-S-Sor)/(1-Swc-Sor))**2/mu_h))
        return ans

def fflow(S,c):   #Hydrocarbon fractional flow
        mu_h  = ((1-c)*(mu_o**(-0.25)) + c*(mu_s**(-0.25)))**(-4)
        ans = (((1-S-Sor)/(1-Swc-Sor))**2/mu_h)/(((0.25*((S-Swc)/(1-Swc-Sor))**2/mu_w)+((1-S-Sor)/(1-Swc-Sor))**2/mu_h))
        return ans

def fTL(c):
        mu_eff = (mu_o**(1-omega))/(mu_s**(1-omega))
        ans = c/(c+((1-c)/mu_eff))
        return ans

S = [Swc]*ngb
O = [0]*(ngb+1)
F = [0]*(ngb+1)
G = [0]*(ngb+1)
w = [0]*ngb
c = [0]*ngb
time = 0

for nstep in range (ntsteps+1):
        time=dt*nstep
        F[0] = FWINJ(time)
        G[0]=1-F[0]
        for i in range (ngb):
                F[i+1] = fluxflow(S[i],c[i])  #flux flow of water # F[i]=fluxflow(S[i-1])
                G[i+1] = (fflow(S[i],c[i]) * fTL(c[i]))    #flux flow of Solvent-Oil

                S[i] = S[i]- ((dt/dx) * (F[i+1] - F[i]))   #to calculate the water saturation
                O[i] += (1-F[i+1])* (1-fTL(c[i])) * dt   #Accumulation Oil prod= outlet fractional flow * dt
                w[i] = w[i] - ((dt/dx)  * (G[i+1] - G[i]))
                c[i] = w[i]/(1-S[i])      #to calculate the concentration
```

Appendix B2: Eclipse input deck used in the Watt field simulations (without the geological model)

```
RUNSPEC

NOECHO

TITLE

DIMENS

  112  30  40 /

OIL

WATER

GAS

DISGAS

MISCIBLE

   1   20    'NONE'   /

FAULTDIM

6000 /

-- Units

FIELD

WELLDIMS

        35     120      35       1 /

TABDIMS

 1  2  100 100 2 /

-- Memory allocation

NSTACK

 25 /

-- Unified output files
```

Appendix B2: Eclipse input deck used in the Watt field simulations (without the geological model)

```
UNIFOUT

START

 1 JAN 2011/

--============================================================

GRID

INCLUDE

 'G3_TS1_FM2_Grid' /

INCLUDE

  'INCLUDE\G3_CO1_OBJ_Perm.inc' /

INCLUDE

  'INCLUDE\G3_CO1_OBJ_Poro.inc' /

COPY

    PERMX  PERMY /

    PERMX  PERMZ /

/

MULTIPLY

         PERMZ 0.1 /

/

INCLUDE

  'G3_TS1_FM2_Faults' /

INCLUDE

   'FM2_MULT.inc' /

INIT

--============================================================

EDIT
```

Appendix B2: Eclipse input deck used in the Watt field simulations (without the geological model)

```
PROPS

STONE2

SWFN

0.20    0.000   0.0

0.25    0.004   0.0

0.30    0.016   0.0

0.35    0.035   0.0

0.40    0.063   0.0

0.45    0.098   0.0

0.50    0.141   0.0

0.55    0.191   0.0

0.60    0.250   0.0

0.80    0.563   0.0

1.00    1.000   0.0

/

SGFN

0.00    0.000   0.0

0.10    0.000   0.0

0.20    0.000   0.0

0.25    0.000   0.0

0.30    0.000   0.0

0.35    0.014   0.0

0.40    0.038   0.0

0.45    0.088   0.0

0.50    0.159   0.0

0.55    0.247   0.0
```

0.60 0.352 0.0

0.70 0.618 0.0

0.80 1.000 0.0

/

SOF3

0.20 0.0000 0.0000

0.25 0.0000 0.0000

0.30 0.0000 0.0000

0.35 0.0156 0.0136

0.40 0.0625 0.0378

0.45 0.1406 0.0882

0.50 0.2500 0.1591

0.55 0.3906 0.2472

0.60 0.5625 0.3517

0.70 0.7656 0.6182

0.80 1.0000 1.0000

/

SOF2

0.20 0.0000

0.25 0.0000

0.30 0.0000

0.35 0.0156

0.40 0.0625

0.45 0.1406

0.50 0.2500

0.55 0.3906

```
0.60     0.5625
0.70     0.7656
0.80     1.0000
/
SORWMIS
 0.25  0.002
 1.0  0.10 /
SGCWMIS
 0.0  0.0001
 1.0  0.05/
TLMIXPAR
0.85000 /
 PVTW
      3600     1.00001       3.0D-6         0.96           0  /
/
ROCK
      3600         4.0D-6   /
/
DENSITY
        45   63.02   0.0702  /
/
SDENSITY
                  0.0702  /
/
PVDG
400      0.47     0.076
```

800 0.46 0.077

1200 0.45 0.078

1600 0.44 0.079

2000 0.43 0.08

2400 0.42 0.081

2800 0.41 0.082

3200 0.40 0.083

3600 0.39 0.084

4000 0.38 0.085

4400 0.37 0.086

4800 0.36 0.087

5200 0.35 0.088

5600 0.34 0.089

6000 0.33 0.089

6400 0.32 0.089

6800 0.31 0.089

7200 0.30 0.089

/

/

PVTO

0.165 400 1.0120 1.170 /

0.335 800 1.0255 1.140 /

0.500 1200 1.0380 1.110 /

0.660 1600 1.0510 1.080 /

0.822 2000 1.0630 1.050 /

0.980 2400 1.0750 1.020 /

```
1.120   2800    1.0860 0.990   /
1.260   3200    1.0985 0.960   /
1.380   3600    1.1100 0.940   /
1.500   4000    1.1200 0.930   /
1.600   4400    1.1300 0.920   /
1.720   5000    1.1440 0.905   /
1.760   5200    1.1480 0.900   /
1.810   5600    1.1550 0.890
        6000    1.1500 0.890
        6400    1.1450 0.890
        6800    1.1400 0.890
        7200    1.1350 0.890   /
/
/
--=============================================================
REGIONS
INCLUDE
  'FIPNUM.inc' /
FILEUNIT
 FIELD /
FIPNUM
--=============================================================
SOLUTION
```

Appendix B2: Eclipse input deck used in the Watt field simulations (without the geological model)

```
EQUIL

5200 6000 5326 0.0 4160 0.0 1 1* 0 /

RSVD

  5000  0.5

  5362  0.5

/

RPTSOL

 FIP=1  /

--============================================================

SUMMARY

FOPR

FGPR

FWPR

/

--============================================================

SCHEDULE

RPTRST

 BASIC=2  FIP /

RPTSCHED

FIP=2/

DRSDT

0.005 /

ACTIONX

ACT1 6030 /
```

```
FPR > 6030 /

/

END

ENDACTIO

WELSPECS

        WELL1   TEMPL1  35  17  1*   OIL  2* 'SHUT' 1*  1    /

        WELL1A  TEMPL1  35  18  1*   OIL  2* 'SHUT' 1*  1    /

        WELL1B  TEMPL1  38  19  1*   OIL  2* 'SHUT' 1*  1    /

        WELL2   TEMPL1  20 21  1*   OIL  2* 'SHUT' 1*  1    /

        WELL2A  TEMPL1  20 25  1*   OIL  2* 'SHUT' 1*  1    /

        WELL3   TEMPL1  42 21  1*   OIL  2* 'SHUT' 1*  1    /

        WELL3A  TEMPL1  42 24 1*   OIL  2* 'SHUT' 1*  1    /

        WELL4   TEMPL1  49  17  1*   OIL  2* 'SHUT' 1*  1    /

        WELL4A  TEMPL1  52 19  1*   OIL  2* 'SHUT' 1*  1    /

        WELL5  TEMPL1  69 23  1*   OIL  2* 'SHUT' 1*  1    /

        WELL5A TEMPL1  19 18  1*   OIL  2* 'SHUT' 1*  1    /

        WELL6 TEMPL1  51 21  1*   OIL  2* 'SHUT' 1*  1    /

        WELL7 TEMPL1  48 12  1*   OIL  2* 'SHUT' 1*  1    /

        WELL8 TEMPL1  30 19  1*   OIL  2* 'SHUT' 1*  1    /

        WELL9 TEMPL1  42  14   1*   OIL  2* 'SHUT' 1*  1    /

        WELL10 TEMPL1  56  19  1*   OIL  2* 'SHUT' 1*  1    /

        WELL11 TEMPL1  105  21  1*   OIL  2* 'SHUT' 1*  1    /

        WELL12 TEMPL1  72  14  1*   OIL  2* 'SHUT' 1*  1    /

        WELL13 TEMPL1  39  19  1*   OIL  2* 'SHUT' 1*  1    /

        WELL14 TEMPL1  24  24  1*   OIL  2* 'SHUT' 1*  1    /

        WELL15 TEMPL1  55  24  1*   OIL  2* 'SHUT' 1*  1    /
```

Appendix B2: Eclipse input deck used in the Watt field simulations (without the geological model)

```
/

GCONPROD

 'TEMPL1' 'RESV' 225000 10* 250000 /

/

WELSPECS

   inj1     TEMPL2  46    9  1* LIQ 2* 'SHUT'/

   inj2     TEMPL2  50   23  1* LIQ 2* 'SHUT'   /

   inj3     TEMPL1  12   27  1* LIQ 2* 'SHUT'   /

   inj4     TEMPL2  34   14  1* LIQ 2* 'SHUT'   /

   inj5     TEMPL2  67   16  1* LIQ 2* 'SHUT'   /

   inj6     TEMPL2  62   9  1* LIQ 2* 'SHUT'   /

   inj7     TEMPL1  35   19  1* LIQ 2* 'SHUT'   /

   inj8     TEMPL1  46   15  1* LIQ 2* 'SHUT'   /

 /

--------------------------------------------------------------------------

ECHO

END
```

Appendix C.1: Python code 1 for optimising WAG ratio and slug size

```
if FWINJ <0.5:
    g=(1-FWINJ)/FWINJ
    w=1
else:
    w=FWINJ /(1-FWINJ)
    g=1

x = int(g*(SlugSize*PV/(gas))/(31)) ## tstep1 ##for PV of gas injected, 31 represents a month,
y = int(w*(SlugSize*PV/(wat))/(31)) ## tstep2 ##for PV of water injected

T=int(years/(x+y))

####interpolation TLMIXPAR value
tck = interpolate.bisplrep(xx, yy, zz, s=0)
def givemeomega(FWINJ,SlugSize):
        result = interpolate.bisplev(FWINJ,SlugSize,tck)
        return '{:.5f}'.format(min(1.0, result))

item = """WCONINJE
inj1    GAS OPEN    RESV    1*  40000   7000    /
inj2    GAS OPEN    RESV    1*  27000   7000    /
inj3    GAS OPEN    RESV    1*  42000   7000    /
inj4    GAS OPEN    RESV    1*  25000   7000    /
inj5    GAS OPEN    RESV    1*  27000   7000    /
inj6    GAS OPEN    RESV    1*  27000   7000    /
inj7    GAS OPEN    RESV    1*  27000   7000    /
inj8    GAS OPEN    RESV    1*  35000   7000    /
/

TSTEP
{}*31 /  ## will update the time step of gas injection

WCONINJE
inj1    WAT OPEN    RESV    1*  40000   7000    /
inj2    WAT OPEN    RESV    1*  27000   7000    /
inj3    WAT OPEN    RESV    1*  42000   7000    /
inj4    WAT OPEN    RESV    1*  25000   7000    /
inj5    WAT OPEN    RESV    1*  27000   7000    /
inj6    WAT OPEN    RESV    1*  27000   7000    /
inj7    WAT OPEN    RESV    1*  27000   7000    /
inj8    WAT OPEN    RESV    1*  35000   7000    /
/

TSTEP
{}*31 /   ## will update the time step of water injection

--end of cycle""".format(x, y)+"\n"
```

Appendix C.2: Python code 2 for optimising WAG ratio, slug size and WAG pattern

```
####interpolation data for TLMIXPAR
tck = interpolate.bisplrep(xx, yy, zz, s=0)
def givemeomega(FWINJ,SlugSize):
        result = interpolate.bisplev(FWINJ,SlugSize,tck)
        return '{:.5f}'.format(min(1.0, result))


####Updating teh Eclipse data deck with the type of fluid to inject
Ilist = []
for i in I:
        if i == 1.0:
                Ilist.append('GAS')
        else:
                Ilist.append('WAT')
col6 = [40000, 27000, 42000, 25000, 27000, 27000, 27000, 35000]
col7 = [7000, 7000, 7000, 7000, 7000, 7000, 7000, 7000]
item_dummy = 'WCONINJE' + '\n'
col4 =  ' ' + 'OPEN' + ' ' + 'RESV' + ' ' + '1*' + ' '
for i in range(8):
        col1 = 'inj' + str(i+1) + ' '
        col_end = '/' + '\n'
        string = col1 + Ilist[i] + col4 + str(col6[i]) + ' ' + str(col7[i]) + col_end
        item_dummy += string
item_dummy += """
/
TSTEP
{}*31 /
WCONINJE
inj1    WAT OPEN    RESV    1*  40000   7000    /
inj2    WAT OPEN    RESV    1*  27000   7000    /
inj3    WAT OPEN    RESV    1*  42000   7000    /
inj4    WAT OPEN    RESV    1*  25000   7000    /
inj5    WAT OPEN    RESV    1*  27000   7000    /
inj6    WAT OPEN    RESV    1*  27000   7000    /
inj7    WAT OPEN    RESV    1*  27000   7000    /
inj8    WAT OPEN    RESV    1*  35000   7000    /
/
TSTEP
{}*31 /

--end of cycle

"""

item_dummy = item_dummy.format(x, y)+"\n"
```

Appendix C.3: Python code 3 for optimising WAG ratio, slug size, WAG pattern and amount of fluid to inject

```
####interpolation data for TLMIXPAR
tck = interpolate.bisplrep(xx, yy, zz, s=0)
def givemeomega(FWINJ,SlugSize):
        result = interpolate.bisplev(FWINJ,SlugSize,tck)
        return '{:.5f}'.format(min(1.0, result))

#### Updating the Eclipse file data deck with the fluid to inject
Ilist = []
for i in I:
        if i == 1:
                Ilist.append('GAS')
        else:
                Ilist.append('WAT')

#### Updating the Eclipse file data deck with the amount fluid to inject
col6 = [Q1, Q2, Q3, Q4, Q5, Q6, Q7, Q8]
col7 = [7000, 7000, 7000, 7000, 7000, 7000, 7000, 7000]
item_dummy = 'WCONINJE' + '\n'
col4 =  ' ' + 'OPEN' + ' ' + 'RESV' + ' ' + '1*' + ' '
for i in range(8):
        col1 = 'inj' + str(i+1) + ' '
        col_end = '/' + '\n'
        string = col1 + Ilist[i] + col4 + str(int(col6[i])) + ' ' + str(col7[i]) + col_end
        item_dummy += string
item_dummy += """
/
TSTEP
{}*31 /
"""
item_dummy += 'WCONINJE' + '\n'
col4 =  ' ' + 'WAT' +' ' + 'OPEN' + ' ' + 'RESV' + ' ' + '1*' + ' '
for i in range(8):
        col1 = 'inj' + str(i+1) + ' '
        col_end = '/' + '\n'
        string = col1 + col4 + str(int(col6[i])) + ' ' + str(col7[i]) + col_end
        item_dummy += string
item_dummy +="""
/
TSTEP
{}*31 /
--end of cycle
"""
 item_dummy = item_dummy.format(x, y)+"\n"
```

Appendix C.4: Python code 4 for optimising WAG ratio, slug size, WAG pattern, amount of fluid to inject when the gas available to inject is limited

```
####interpolation data for TLMIXPAR
tck = interpolate.bisplrep(xx, yy, zz, s=0)
def givemeomega(FWINJ,SlugSize):
        result = interpolate.bisplev(FWINJ,SlugSize,tck)
        return '{:.5f}'.format(min(1.0, result))
####Updating Eclipse data deck with the type of fluid to inject
for i in I:
        if i == 1.0:
                Ilist.append('GAS')
        else:
                Ilist.append('WAT')
####Updating Eclipse data deck with the amount of fluid to inject
col6 = [Q1, Q2, Q3, Q4, Q5, Q6, Q7, Q8]
col7 = [7000, 7000, 7000, 7000, 7000, 7000, 7000, 7000]
####Putting a constraint on teh Gas availablity
Q_gas_avail = 5000000000 ##Reservoir barrel
def get_item_dummy():
        global Q_gas_avail

        Q_gas = [Qi for Qi,Ii in zip(Q,I) if Ii==1]
        Q_gas_injected = sum(Q_gas)*31*x

        item_dummy = 'WCONINJE' + '\n'
        col4 =  ' ' + 'OPEN' + ' ' + 'RESV' + ' ' + '1*' + ' '
        for i in range(8):
                coll = 'inj' + str(i+1) + ' '
                col_end = '/' + '\n'
                if Q_gas_injected < Q_gas_avail:
                        string = coll + Ilist[i] + col4 + str(int(col6[i])) + ' ' + str(col7[i]) + col_end
                        Q_gas_avail -= Q_gas_injected
##                        print (Q_gas_avail)
                else:
                        string = coll + 'WAT' + col4 + str(int(col6[i])) + ' ' + str(col7[i]) + col_end
                item_dummy += string

        item_dummy += """
/
TSTEP
{}*31 /
"""
        item_dummy += 'WCONINJE' + '\n'
        col4 =  ' ' + 'WAT' +' ' + 'OPEN' + ' ' + 'RESV' + ' ' + '1*' + ' '

        for i in range(8):
                coll = 'inj' + str(i+1) + ' '
                col_end = '/' + '\n'
                string = coll + col4 + str(int(col6[i])) + ' ' + str(col7[i]) + col_end
                item_dummy += string

        item_dummy +="""
/
TSTEP
{}*31 /
--end of cycle
"""
        item_dummy = item_dummy.format(x, y)+"\n"
        return item_dummy
```

Appendix D: Results of scenario 1 of optimising WAG ratio and slug size

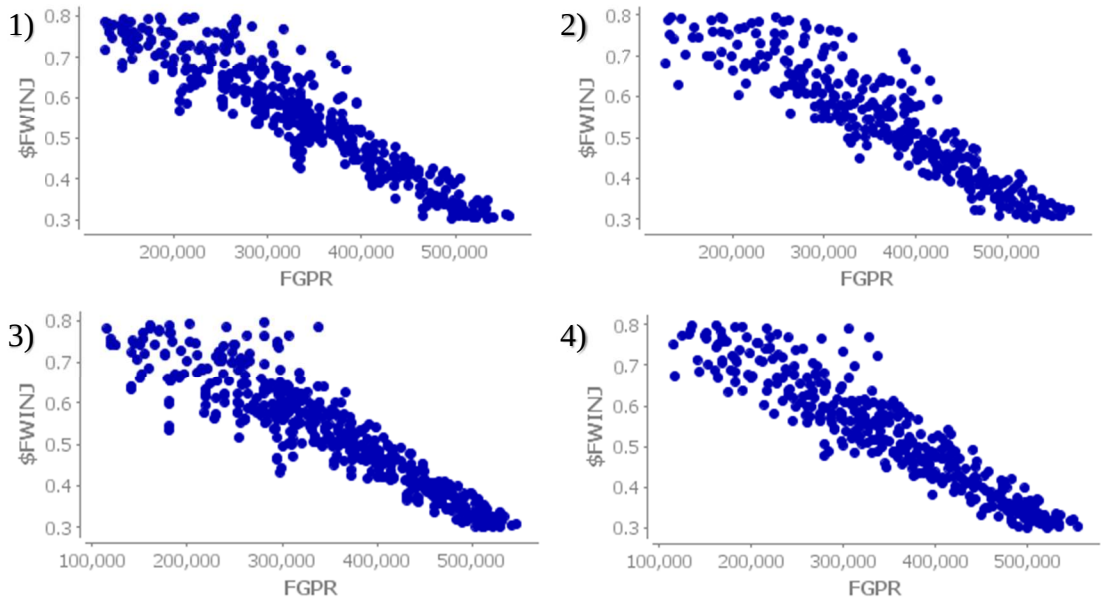

Appendix D. 1 The optimisation results of the WAG ratio (i.e. FWINJ) vs the field gas production (FGPR), for: 1) secondary recovery at the calibrated value of ω, 2) secondary recovery at fixed value of ω=1, 3) tertiary recovery at the calibrated value of ω, 4) tertiary recovery at fixed value of ω=1.

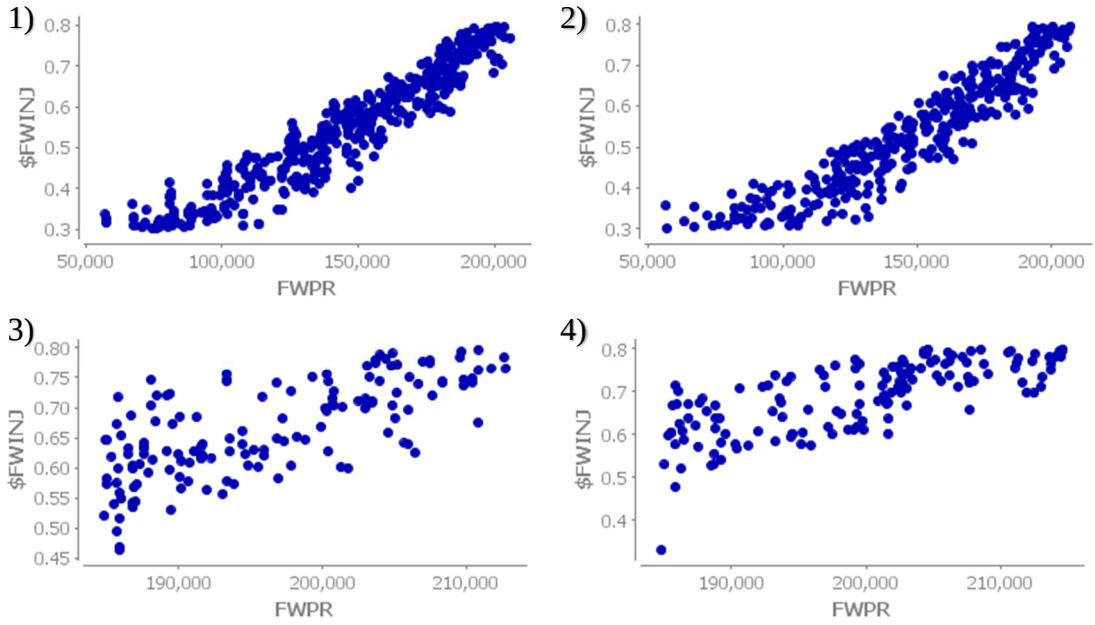

Appendix D. 2 The optimisation results of the WAG ratio (i.e. FWINJ) vs the field water production (FWPR), for: 1) secondary recovery at the calibrated value of ω, 2) secondary recovery at fixed value of ω=1, 3) tertiary recovery at the calibrated value of ω, 4) tertiary recovery at fixed value of ω=1.

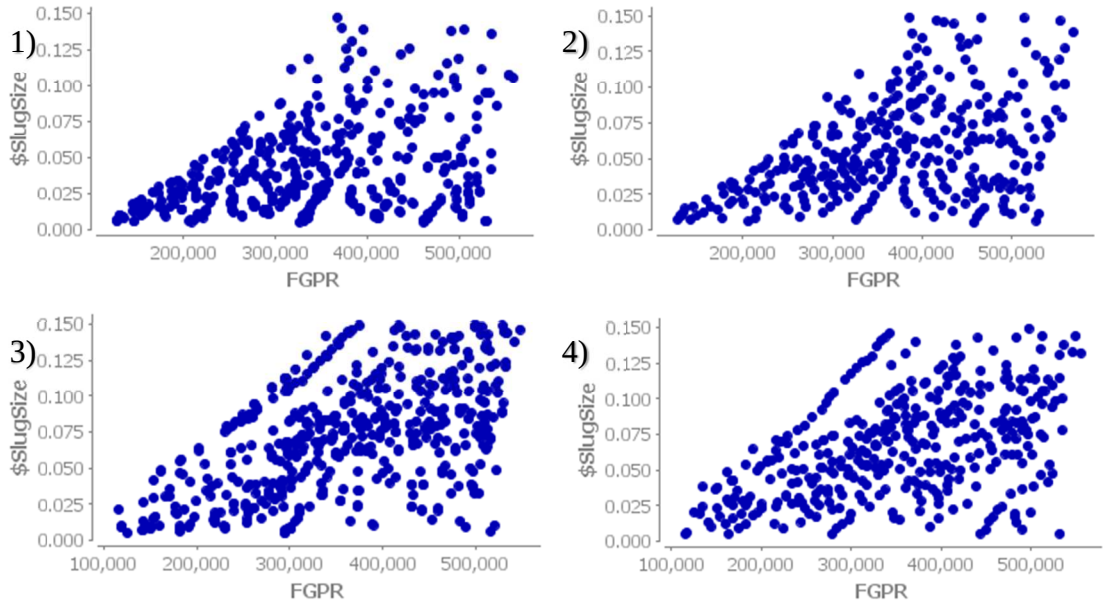

Appendix D. 3 The optimisation results of slug size vs field gas production (FGPR) for: 1) secondary recovery at the calibrated value of ω, 2) secondary recovery at fixed value of ω=1, 3) tertiary recovery at the calibrated value of ω, 4) tertiary recovery at fixed value of ω=1.

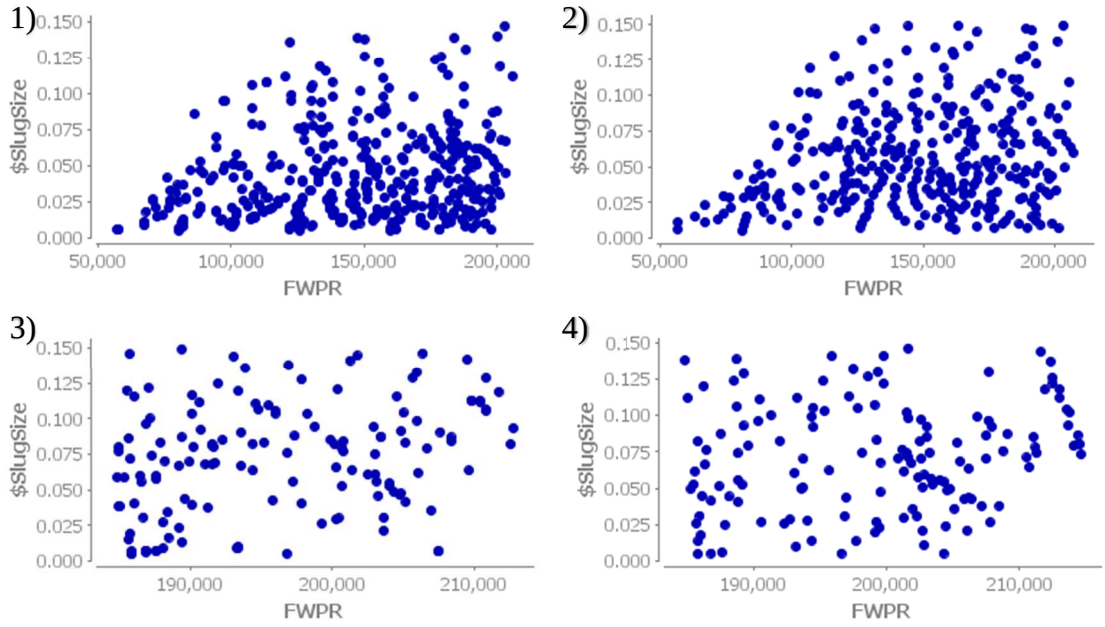

Appendix D. 4 The optimisation results of slug size vs field water production (FWPR) for: 1) secondary recovery at the calibrated value of ω, 2) secondary recovery at fixed value of ω=1, 3) tertiary recovery at the calibrated value of ω, 4) tertiary recovery at fixed value of ω=1.

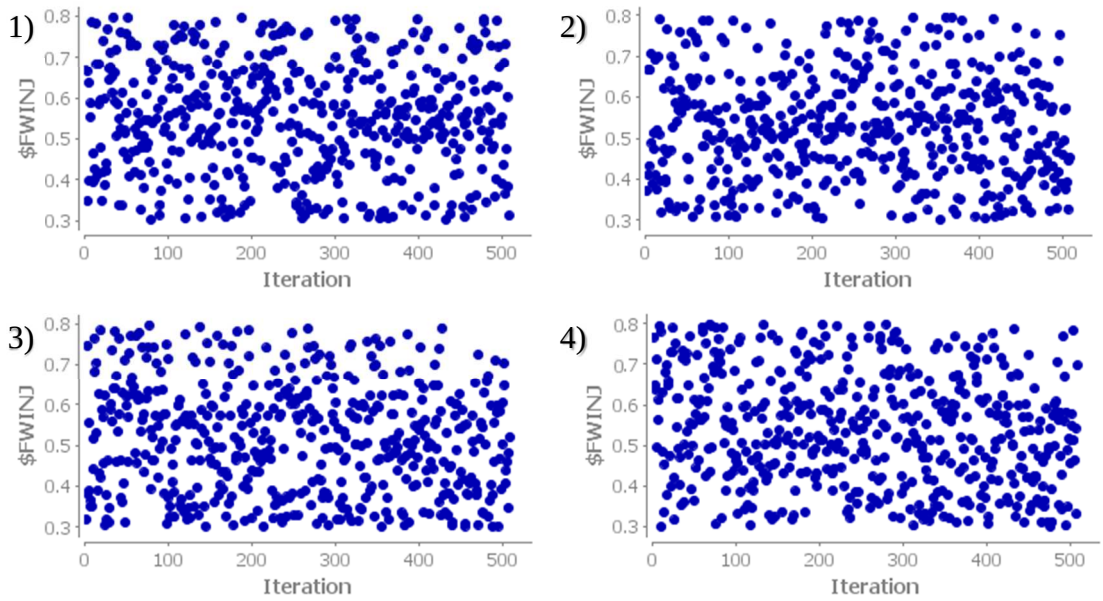

Appendix D. 5 The optimisation results of FWINJ vs iterations (particles) for: 1) secondary recovery at the calibrated value of *ω*, 2) secondary recovery at fixed value of *ω*=1, 3) tertiary recovery at the calibrated value of *ω*, 4) tertiary recovery at fixed value of *ω*=1

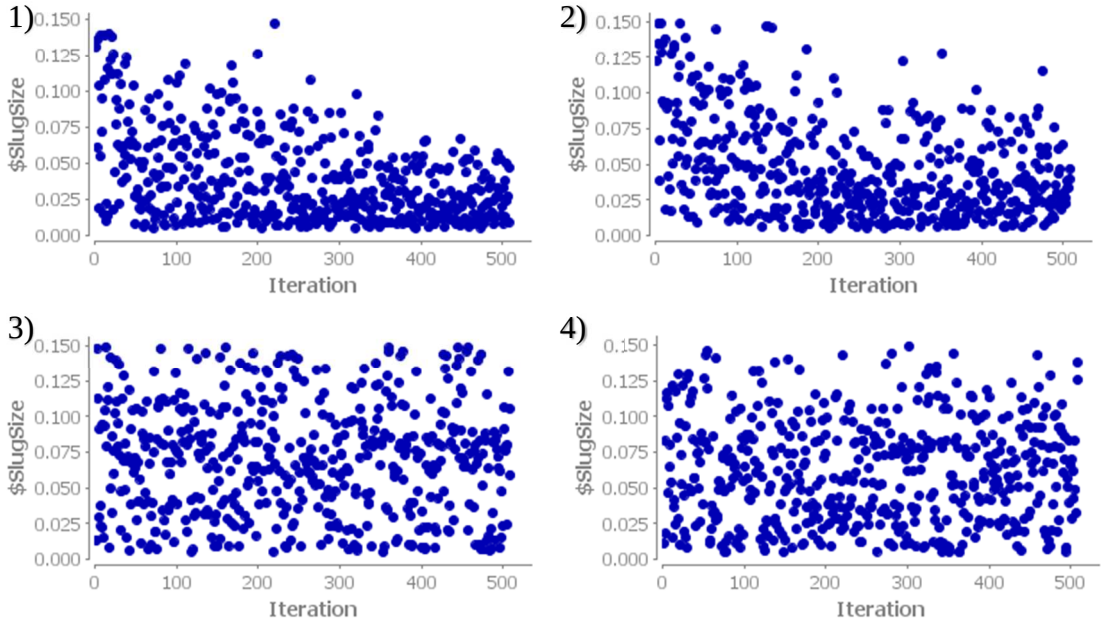

Appendix D. 6 The optimisation results of slug size vs iterations (particles) for: 1) secondary recovery at the calibrated value of *ω*, 2) secondary recovery at fixed value of *ω*=1, 3) tertiary recovery at the calibrated value of *ω*, 4) tertiary recovery at fixed value of *ω*=1.

Appendix D. 7 represents the interpolated values of ω (for the optimised slug size Appendix D. 5 and WAG ratio Appendix D. 6) versus iteration. The wide range of slug size's and WAG ratio's values led to a wide range of ω. Appendix D. 5 and Appendix D.

6 show the optimisation results of FWINJ and slug size vs iterations (particles). It can be seen that the MOPSO explored the FWINJ and slug size to maximise the FOPT and to minimise both the FGPR and the FWPR for all the cases.

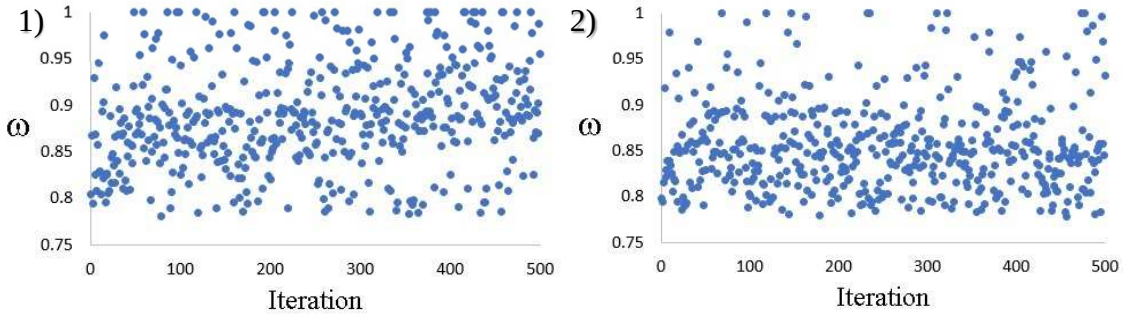

Appendix D. 7 The interpolated values of ω (for the optimised slug size and WAG ratio) vs iteration. The optimisation results of FWINJ vs iterations (particles) for: 1) secondary recovery at the calibrated value of ω, 2) tertiary recovery at the calibrated value of ω.

Appendix E: Results of scenario 2 of optimising WAG ratio and slug size during the optimisation of the WAG pattern

Appendix E. 1 represents the interpolated values of ω (for the optimised slug size and WAG ratio versus iteration, which is similar to Appendix D. 7. The wide range of slug size's and WAG ratio's values led to a wide range of ω.

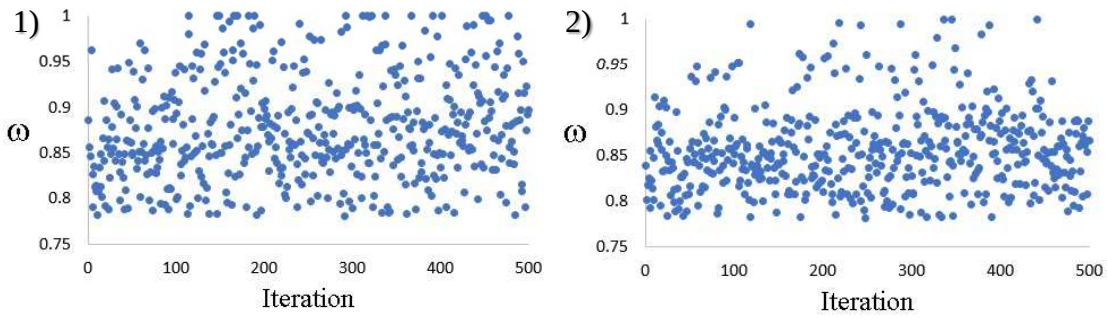

Appendix E. 1 Represents the interpolated values of ω (for the optimised slug size and WAG ratio) vs iteration. The optimisation results of FWINJ vs iterations (particles) for: 1) secondary recovery at the calibrated value of ω, 2) tertiary recovery at the calibrated value of ω.

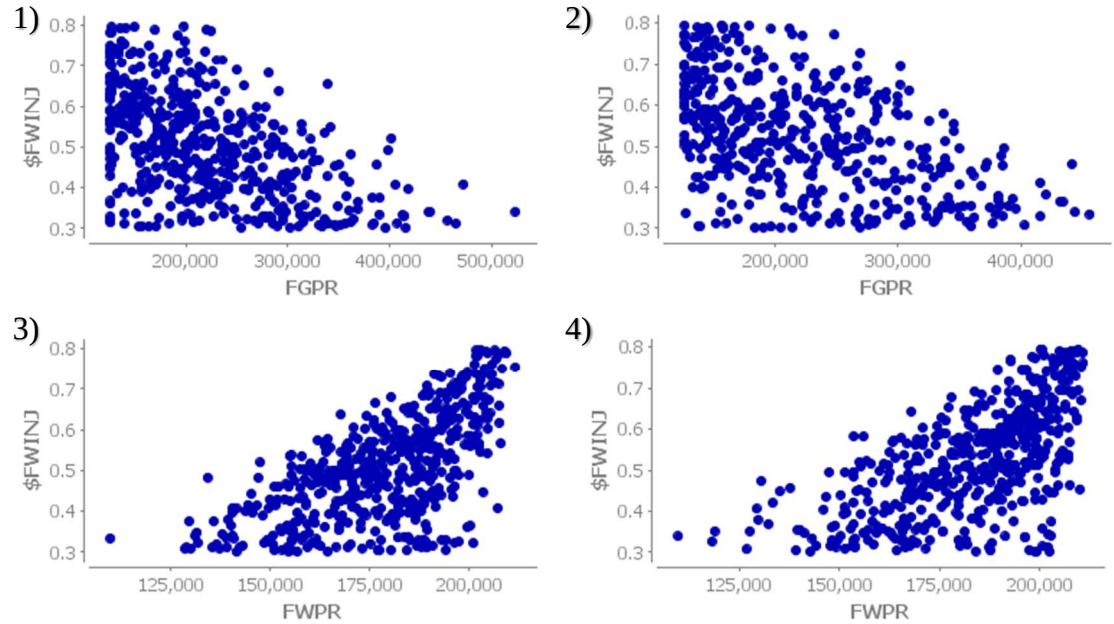

Appendix E. 2 The optimisation results of slug size vs field gas and water production (FGPR and FWPR, respectively) for: 1) secondary recovery at the calibrated value of ω, 2) secondary recovery at fixed value of ω=1, 3) secondary recovery at the calibrated value of ω, 4) secondary recovery at fixed value of ω=1

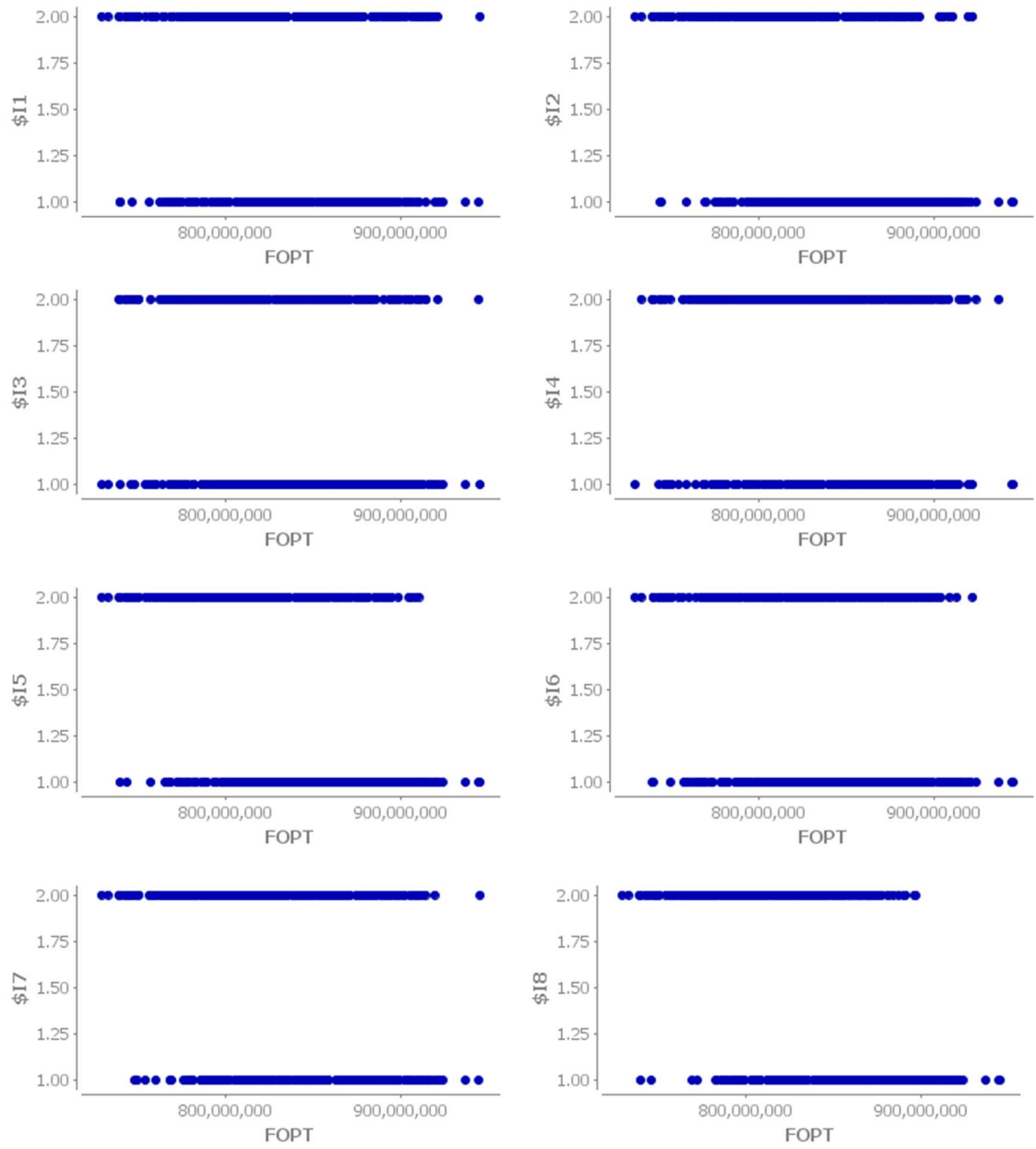

Appendix E. 3 The optimisation results of WAG pattern optimisation for tertiary recovery at calibrated value of ω=1

Appendix F: Results of scenario 3 of optimising WAG ratio, slug size, the WAG pattern and flow rate

Appendix F. 1 represents the interpolated values of ω (for the optimised slug size and WAG ratio versus iteration. The wide range of slug size's and WAG ratio's values led to a wide range of ω.

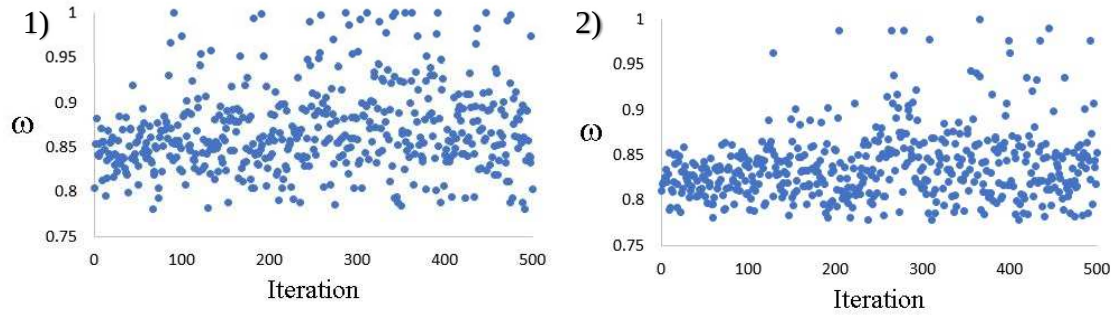

Appendix F. 1 Represents the interpolated values of ω (for the optimised slug size and WAG ratio) vs iteration. The optimisation results of FWINJ vs iterations (particles) for: 1) secondary recovery at the calibrated value of ω, 2) tertiary recovery at the calibrated value of ω.

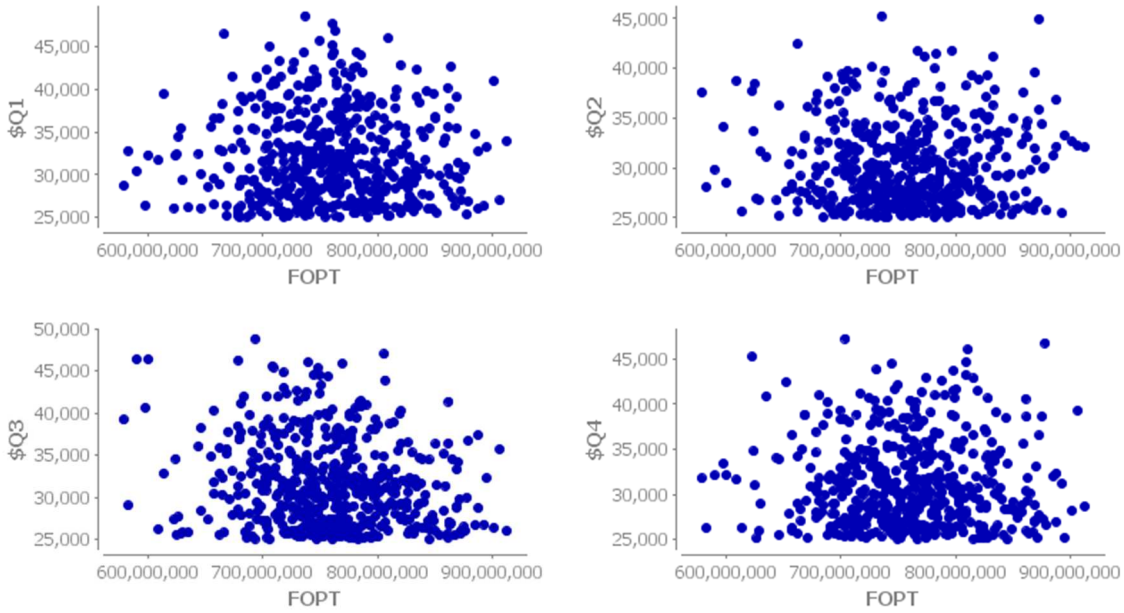

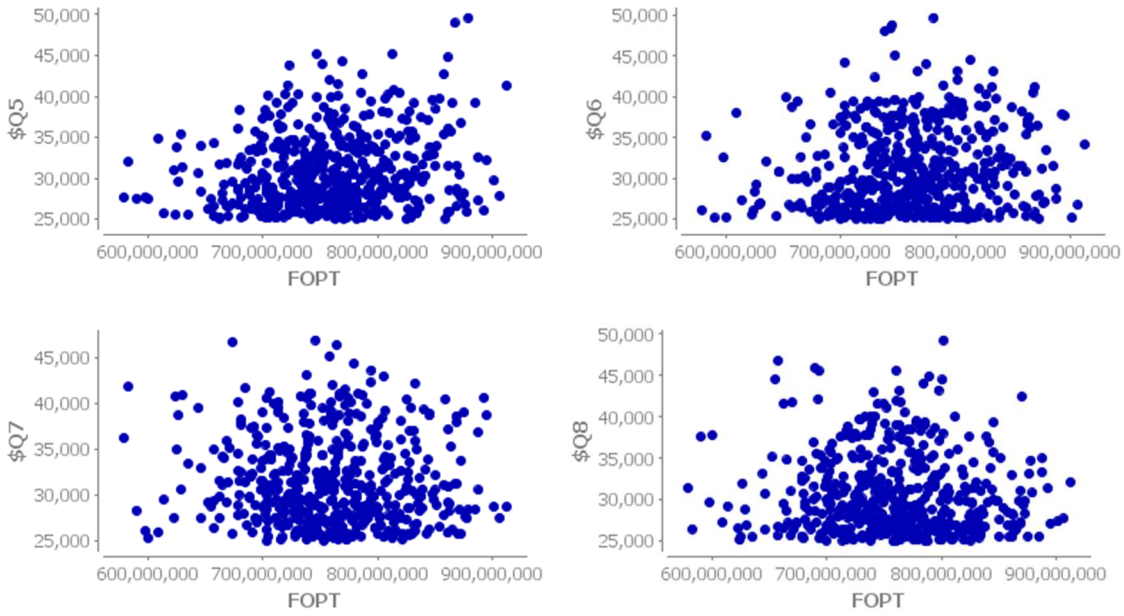

Appendix F. 2 Represents the optimisation results of flow rate for secondary recovery at calibrated value of ω=1

Appendix G: Results of scenario 4 of optimising WAG ratio, slug size, WAG pattern and flow rate at limited amount of gas to inject

Appendix G. 1 represents the interpolated values of ω (for the optimised slug size and WAG ratio versus iteration, which is similar to Appendix D. 7. The wide range of slug size's and WAG ratio's values led to a wide range of ω.

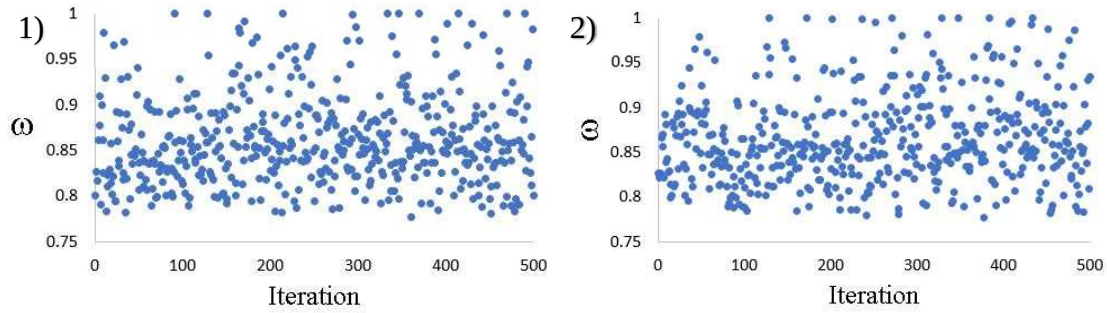

Appendix G. 1 Represents the interpolated values of ω (for the optimised slug size and WAG ratio) vs iteration. The optimisation results of FWINJ vs iterations (particles) for: 1) secondary recovery at the calibrated value of ω, 2) tertiary recovery at the calibrated value of ω.

Appendix H: Errors that have been encountered during the optimisation runs

500 simulations were run to provide the optimiser with a large number of points to analyse and find the optimal solution to meet the objective function. The reason for choosing 500 simulations was to provide an adequate number of points for meaningful results for the given computational cost and resulting simulation time. However, during the optimisation software runs, an Eclipse licence failure was encountered, ending the runs prematurely, and causing an error in the results. The objective function in one of the runs was equal to zero, as the simulation did not run at all and gave a zero result. For these results presented earlier in Chapter 6, the range given was for consistency with other figures presented. The results plotted below represent the complete data set including the errors from the incomplete runs. An attempt to re-run those simulations again has been made and an Eclipse licence failure was encountered again. Due to the time constraint in this research, it was not possible to re-run the simulations and work proceeded with the current results.

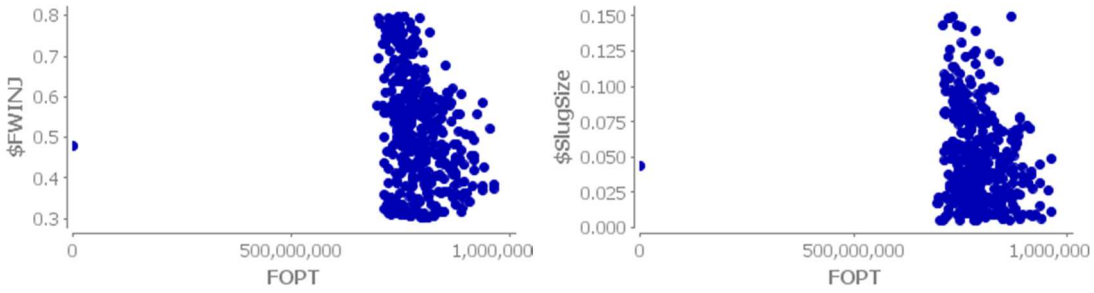

Appendix H. 1 Errors that have been encountered during scenario 3 of optimising WAG ratio, slug size, WAG pattern and flow rate for tertairy recovery at calibrated value *ω*

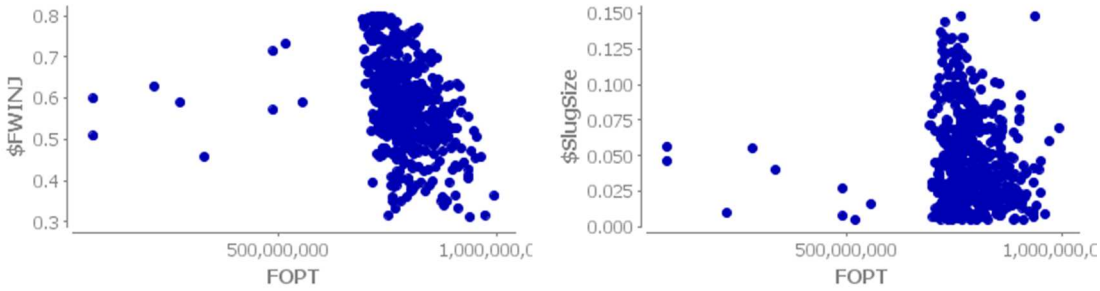

Appendix H. 2 Errors that have been encountered during scenario 3 of optimising WAG ratio and slug size during the optimisation of the WAG pattern and flow rate for tertairy recovery at fixed value of *ω*

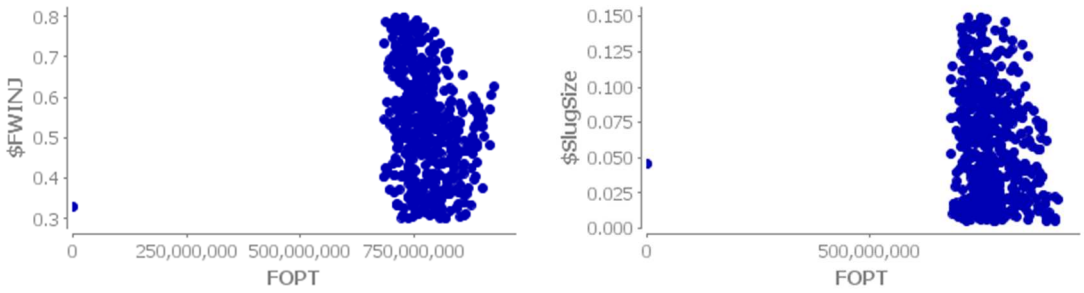

Appendix H. 3 Errors that have been encountered during scenario 4 of optimising WAG ratio and slug size during the optimisation of the WAG pattern and flow rate at limited gas constraint for tertiary recovery at calibrated value of *ω*

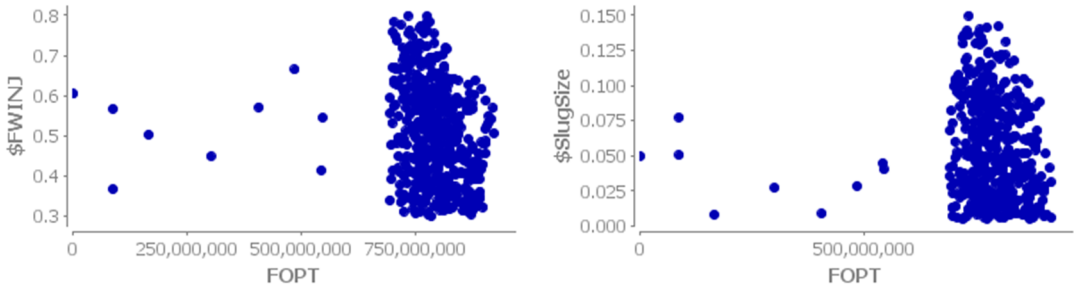

Appendix H. 4 Errors that have been encountered during scenario 4 of optimising WAG ratio and slug size, WAG pattern and flow rate at limited gas constraint for tertiary recovery at fixed value of *ω*

References

Aarnes, J. E., Gimse, T. and Lie, K. A. (2007) 'An introduction to the numerics of flow in porous media using Matlab', *Geometric modelling, numerical simulation, and optimization*: Springer, pp. 265-306.

Agada, S., Geiger, S., Elsheikh, A. and Oladyshkin, S. (2017) 'Data-driven surrogates for rapid simulation and optimization of WAG injection in fractured carbonate reservoirs', *Petroleum Geoscience,* 23(2), pp. 270-283.

Ahmed, T. (2006) *Reservoir engineering handbook.* Elsevier.

Al-Haboobi, Z. I., Christie, M. and Arnold, D. 'Calibration of the mixing parameter model for viscous fingering for varying water alternate gas WAG ratios and slug sizes'. *Paper SPE-185858-MS presented at the SPE Europec featured at 79th EAGE Conference and Exhibition (2017)*, Paris, France: Society of Petroleum Engineers.

Al-Shuraiqi, H. S. (2005) *Mechanisms of oil recovery via first contact miscible WAG injection.* Doctor of Philosophy Thesis, Imperial college London.

Alvarado, V. and Manrique, E. (2010) 'Enhanced oil recovery: an update review', *Energies,* 3(0), pp. 1529-1575.

Antoniou, A. (2016) *Practical optimization.* 1st Edition edn.: Cram101 Textbook Reviews, p. 72.

Araktingi, U. G. and Orr Jr, F. M. (1993) 'Viscous fingering in heterogeneous porous media', *SPE Advanced Technology Series,* 1(01), pp. 71-80. SPE-18095-PA.

Arnold, D., Demyanov, V., Christie, M., Bakay, A. and Gopa, K. (2016) 'Optimisation of decision making under uncertainty throughout field lifetime: A fractured reservoir example', *Computers and Geosciences,* 95, pp. 123-139.

Arnold, D., Demyanov, V., Tatum, D., Christie, M., Rojas, T., Geiger, S. and Corbett, P. (2013) 'Hierarchical benchmark case study for history matching, uncertainty quantification and reservoir characterisation', *Computers and Geosciences,* 50, pp. 4-15.

Arnold, R., Burnett, D. B., Elphick, J., Feeley, T. J. I. I. I., Galbrun, M., Hightower, M., Jiang, Z., Khan, M., Lavery, M., Luffey, F. and Verbeek, P. (2004) 'Managing water from waste to resource', *Oilfield Review,* 16(2), pp. 26-41.

Awan, A. R., Teigland, R. and Kleppe, J. (2008) 'A survey of North Sea enhanced-oil-recovery projects initiated during the years 1975 to 2005', *SPE Reservoir Evaluation and Engineering,* 11(3), pp. 497-512. SPE-99546-PA.

Aziz, K. and Settari, A. (1979) 'Petroleum reservoir simulation', *Applied Science Publishers,* 476.

Bandyopadhyay, S. and Saha, S. (2012) *Unsupervised classification: similarity measures, classical and metaheuristic approaches, and applications.* Springer Science & Business Media.

Batycky, R. P. (1997) *A three-dimensional two phase field scale streamline simulator.* Doctor of Philosophy Thesis, Stanford University.

Bear, J. (1972) *Dynamics of fluids in porous media.* Courier Corporation.

References

Blackwell, R. J., Rayne, J. R. and Terry, W. M. (1959) 'Factors influencing the efficiency of miscible displacement', *SPE General, Petroleum Transactions. AIME,* 217, pp. 1-8. SPE-1131-G.

Blunt, M. and Christie, M. A. (1993) 'How to predict viscous fingering in three component flow', *Transport in Porous Media, Kluwer Academic Publishers,* 12(3), pp. 207-236.

Blunt, M. J., Barker, J. W., Rubin, B., Mansfield, M., Culverwell, I. D. and Christie, M. A. (1994) 'Predictive theory for viscous fingering in compositional displacement', *SPE Reservoir Engineering,* 9(01), pp. 73-80. SPE-24129-PA.

Booth, R. (2008) *Miscible flow through porous media.* Doctor of Philosophy Thesis, University of Oxford.

Brodie, J. A., Jhaveri, B. S., Moulds, T. P. and Mellemstrand Hetland, S. 'Review of gas injection projects in BP'. *Paper SPE-154008-MS presented at the SPE Improved Oil Recovery Symposium (2012)*: Society of Petroleum Engineers.

Buckley, S. E. and Leverett, M. C. (1941) 'Mechanism of fluid displacement in sands', *SPE General, Petroleum Transactions. AIME,* 146(01), pp. 107-116. SPE-942107-G.

Caetano, R. P. L. (2017) *Optimization of a water alternating gas injection scheme evaluation of a miscible LPG injection with compositional fluid flow simulation in a Kazakhstan field.* Master of Science Thesis, Instituto Superior Técnico, Universidade de Lisboa.

Carlson, M. R. (2006) *Practical reservoir simulation: using, assessing, and developing results.* PennWell. Online version available at: http://app.knovel.com/hotlink/toc/id:kpPRSUADR3/practical-reservoir-simulation/practical-reservoir-simulation, p. 363-368.

Causon, D. M. and Mingham, C. G. (2010) *Introductory finite difference methods for PDEs.* Bookboon.

Chen, B. and Reynolds, A. C. (2016) 'Ensemble-based optimization of the water-alternating-gas-injection process', *SPE Journal,* 21(03), pp. 786-798. SPE-173217-PA.

Chen, B. and Reynolds, A. C. (2018) 'CO2 water-alternating-gas injection for enhanced oil recovery: Optimal well controls and half-cycle lengths', *Computers Chemical Engineering,* 113, pp. 44-56.

Chen, C. Y. and Meiburg, E. (1998) 'Miscible porous media displacements in the quarter five-spot configuration. Part 1. The homogeneous case', *Journal of Fluid Mechanics,* (371), pp. 233-268.

Chen, S., Li, H., Yang, D. and Tontiwachwuthikul, P. (2010) 'Optimal parametric design for water-alternating-gas (WAG) process in a CO2-miscible flooding reservoir', *Journal of canadian petroleum technology,* 49(10), pp. 75-82. SPE-141650-PA.

Christensen, J. R., Stenby, E. H. and Skauge, A. (2001) 'Review of WAG field experience', *SPE Reservoir Evaluation and Engineering*, pp. 1-10. SPE-71203-PA.

Christie, M. A. (1987) 'Application of high resolution simulation to modelling fluid instabilities', *Mathematics in oil production, S.F. Edwards and P.R. King (eds.), Clarendon Press, Oxford* pp. 269-284.

Christie, M. A. (1989) 'High resolution simulation of unstable flows in porous media', *SPE Reservoir Engineering,* 4, pp. 297-303. SPE-16005-PA.

Christie, M. A. and Bond, D. J. (1987) 'Detailed simulation of unstable processes in miscible flooding', *SPE Reservoir Engineering,* 2(4), pp. 514-522. SPE-14896-PA.

References

Christie, M. A., Muggeridge, A. H. and Barley, J. J. (1993) '3D simulation of viscous fingering and WAG schemes', *SPE reservoir engineering,* 8(1), pp. 19-26. SPE-21238-PA

Cobanoglu, M. 'A numerical study to evaluate the use of WAG as an EOR method for oil production improvement at B.Kozluca Field, Turkey'. *Paper SPE-72127-MS presented at the SPE Asia Pacific Improved Oil Recovery Conference (2001)*: Society of Petroleum Engineers.

Cunningham, R. E. and Williams, R. J. J. (1980) *Diffusion in gases and porous media.* New York: Plenum Press.

Dake, L. P. (1983) *Fundamentals of reservoir engineering.* Elsevier.

Dake, L. P. (2001) *The practice of reservoir engineering (revised edition).* Elsevier.

Dandekar, A. Y. (2013) *Petroleum reservoir rock and fluid properties.* CRC press.

Davies, D. 2016. Field development. *G11PT: Production Technology.* Unpublished: Heriot-Watt University, Institute of Petroleum Engineering.

De Wit, A. and Homsy, G. M. (1997) 'Viscous fingering in periodically heterogeneous porous media. II. Numerical simulations', *Journal of Chemical Physics,* 107(22), pp. 9619-9628.

Dumore, J. M., Hagoort, J. and Risseeuw, A. S. (1984) 'An analytical model for one-dimensional, three-component condensing and vaporizing gas drives', *SPE Journal,* 24(2), pp. 169-179. SPE-10069-PA.

Dutra, T. A., Pires, A. P. and Bedrikovetsky, P. G. 'Miscible EOR processes: existence of elliptic regions in gasflood modeling'. *Paper SPE-107886-MS presented at the SPE Latin American and Caribbean Petroleum Engineering Conference (2007)*, Buenos Aires, Argentina: Society of Petroleum Engineers, 1-8.

Eng, R. M. P. (2007) *Reservoir engineering for geologists.* Fekete Associates Inc.

Eymard, R., Gallouët, T. and Herbin, R. (2000) *Finite volume methods.* Handbook of numerical analysis.

Farzad, I. (2004) *Evaluating reservoir production strategies in miscible and immiscible gas-injection projects.* Master of Science Thesis Doctor of Philosophy Thesis, Texas A&M University.

Fayers, F. J. (1988) 'An approximate model with physically interpretable parameters for representing miscible viscous fingering', *SPE reservoir engineering,* 3(2), pp. 551-558. SPE-13166-PA

Fayers, F. J., Blunt, M. J. and Christie, M. A. 'Accurate calibration of empirical viscous fingering models'. *ECMOR II-2nd European Conference on the Mathematics of Oil Recovery 1990*, 1990.

Fayers, F. J. and Newley, T. M. J. (1988) 'Detailed validation of an empirical model for viscous fingering with gravity effects', *SPE reservoir engineering,* 3(2), pp. 542-550. SPE-15993-PA.

Fernández Martínez, J. L., Mukerji, T., García Gonzalo, E. and Suman, A. (2012) 'Reservoir characterization and inversion uncertainty via a family of particle swarm optimizers', *Geophysics,* 77(1), pp. M1-M16.

Ferziger, J. H. and Peric, M. (2012) *Computational methods for fluid dynamics.* Springer Science & Business Media.

References

Fonseca, C. M., Fleming, P. J., Zitzler, E., Deb, K. and Thiele, L. 'Evolutionary multi-criterion optimization'. *In Second International Conference, EMO 2003.*

Foroozanfar, M. and Aminshahidy, B. (2013) 'Efficiency evaluation of immiscible water alternating gas (IWAG) process in one of Iranian oil reservoirs', pp. 76-81.

Geoquest, S. 2014. Eclipse 100 reference manual. Schlumberger Geoquest.

Hassan, R., Cohanim, B., de Weck, O. and Venter, G. (2004) 'A copmarison of particle swarm optimization and the genetic algorithm', *American Institute of Aeronautics and Astronautics*.

Heinemann, Z. E. (2005) *Fluid flow in porous media.* Montanuniversität Leoben, Petroleum Engineering Department Textbook Series.

Hoffman, T. (2014) 'Modeling examines gas injection results for improving Bakken recovery', *The American Oil and Gas Reporter*.

Holm, L. W. (1987) 'Miscible displacement (1987 PEH Chapter 45)', *Petroleum Engineering Handbook*, pp. 1-15. SPE Chapter - 1987

Homsy, G. M. (1987) 'Viscous Fingering in Porous Media', *Annual Review of Fluid Mechanics,* 19(1), pp. 271-311.

Hutahaean, J. (2017) *Multi-objective methods for history matching, uncertainty prediction and optimisation in reservoir modelling.* Doctor of Philosophy Thesis, Heriot-Watt University.

Islam, M. R., Hossain, M. E., Mousavizadegan, S. H., Mustafiz, S. and Abou-Kassem, J. H. (2016) *Advanced petroleum reservoir simulation: towards developing reservoir emulators.* John Wiley & Sons.

Izadmehr, M., Daryasafar, A., Bakhshi, P., Tavakoli, R. and Ghayyem, M. A. (2018) 'Determining influence of different factors on production optimization by developing production scenarios', *Journal of Petroleum Exploration and Production Technology,* 8(2), pp. 505-520.

Jamaloei, B. Y., Kharrat, R. and Torabi, F. (2011) 'A mechanistic analysis of viscous fingering in low-tension polymer flooding in heavy-oil reservoirs', *Journal of Petroleum Science and Engineering,* 78(2), pp. 228–232.

Jensen, T. B., Harpole, K. J. and Østhus, A. 'EOR screening for Ekofisk'. *Paper SPE-65124-MS presented at the SPE European Petroleum Conference (2000)*: Society of Petroleum Engineers.

Jhaveri, B. S., Brodie, J. A., Zhang, P. and Daae, V. 'Review of BP's global gas injection projects'. *Paper SPE-171780-MS presented at the 21st World Petroleum Congress (2014)*: World Petroleum Congress.

John, F. O. (2015) *Optimization of a water alternating gas injection compositional fluid flow simulation with water alternating gas injection optimization on the upscaled synthetic reservoir CERENA-I.* Master of Science Thesis, Instituto Superior Técnico, Universidade de Lisboa.

Johns, R. T. and Dindoruk, B. (2013) 'Gas flooding in enhanced oil recovery field case studies', pp. 1-22.

Juanes, R. and Blunt, M. J. (2006) 'Impact of viscous fingering on the prediction of optimum WAG ratio', *SPE Journal,* 12(4), pp. 486-495. SPE-99721-PA.

Juanes, R. and Lie, K. A. 'A front-tracking method for efficient simulation of miscible gas injection processes'. *Paper SPE-93298-MS presented at the SPE Reservoir Simulation Symposium (2005)*: Society of Petroleum Engineers.

References

Kajishima, T. and Taira, K. (2016) *Computational fluid dynamics.* Springer International Pu.

Kang, P. S., Lim, J. S. and Huh, C. (2016) 'Screening criteria and considerations of offshore enhanced oil recovery', *Energies,* 9(1), pp. 44.

Karacaer, C. (2007) *Mixing issues in CO2 flooding: comparison of compositional and extended black-oil simulators.* Master of Science Thesis, Colorado School of Mines, Golden, CO.

Kathrada, M. (2009) *Uncertainty evaluation of reservoir simulation models using particle swarms and hierarchical clustering.* Doctor of Philosophy Thesis, Heriot-Watt University.

Kennedy, J. and Eberhart, R. 'Particle swarm optimization'. *Neural Networks, 1995. Proceedings., IEEE International Conference on*, Nov/Dec 1995, 1942-1948 vol.4.

Khatib, Z. and Verbeek, P. (2003) 'Water to value - produced water management for sustainable field development of mature and green fields', *Journal of Petroleum Technology,* 55(1), pp. 26-28. SPE-0103-0026-JPT.

Khu, S. T. and Madsen, H. (2005) 'Multiobjective calibration with Pareto preference ordering: an application to rainfall-runoff model calibration', *Water Resources Research,* 41(3).

Koval, E. J. (1963) 'A method for predicting the performance of unstable miscible displacement in heterogeneous media', *SPE Journal,* 3(2), pp. 145-154. SPE-450-PA.

Kulkarni, M. M. (2003) *Immiscible and miscible gas-oil displacements in porous media.* Master of Science Thesis, Louisiana State University and Agricultural and Mechanical College [Online] Available at: http://etd.lsu.edu/docs/available/etd-0709103-175151/unrestricted/Kulkarni_thesis.pdf (Accessed.

Lake, L. W. (1989) *Enhanced oil recovery.* Old Tappan, NJ; Prentice Hall Inc.

Lantz, R. B. (1971) 'Quantitative evaluation of numerical diffusion (truncation error)', *SPE Journal,* 11(3), pp. 315-320. SPE-2811-PA.

Lax, P. D. and Richtmyer, R. D. (1956) 'Survey of the stability of linear finite difference equations', *Communications on pure and applied mathematics,* 9(2), pp. 267-293.

Lepot, M., Aubin, J. B. and Clemens, F. H. (2017) 'Interpolation in time series: an introductive overview of existing methods, their performance criteria and uncertainty assessment', *Water,* 9(10).

LeVeque, R. J. (2002) *Finite volume methods for hyperbolic problems.* Cambridge university press.

Li, K. and Horne, R. N. (2006) 'Comparison of methods to calculate relative permeability from capillary pressure in consolidated water-wet porous media.', *Water resources research,* 42(6).

Mehos, G. J. and Ramirez, W. F. (1989) 'Use of optimal control theory to optimize carbon dioxide miscible-flooding enhanced oil recovery', *Journal of Petroleum Science and Engineering,* 2(4), pp. 247-260.

Minssieux, L. and Duquerroix, J.-P. 'WAG flow mechanisms in presence of residual oil'. *Paper SPE-28623-MS presented at the SPE Annual Technical Conference and Exhibition (1994)*: Society of Petroleum Engineers.

Mohagheghian, E. (2016) *An application of evolutionary algorithms for WAG optimisation in the Norne Field.* Doctor of Philosophy Thesis, Memorial University of Newfoundland.

References

Mohagheghian, E., James, L. A. and Haynes, R. D. (2018) 'Optimization of hydrocarbon water alternating gas in the Norne field: Application of evolutionary algorithms', *Fuel,* 223, pp. 86-98.

Mohamed, L. M. Y. (2011) *Novel sampling techniques for reservoir history matching optimisation and uncertainty quantification in flow prediction.* Doctor of Philosophy Thesis, Heriot-Watt University.

Moortgat, J. (2016) 'Viscous and gravitational fingering in multiphase compositional and compressible flow', *Advances in Water Resources,* 89, pp. 53-66.

Morais, H. L. (2012) *Application of WAG and SWAG injection techniques in Norne E-segment.* Master of Science Thesis, Norwegian University of Science and Technology [Online] Available at: http://www.diva-portal.org/smash/get/diva2:589680/FULLTEXT01.pdf (Accessed.

Muggeridge, A., Cockin, A., Webb, K., Frampton, H., Collins, I., Moulds, T. and Salino, P. (2014) 'Recovery rates, enhanced oil recovery and technological limits', *Philosophical Transactions of the Royal Society A: Mathematical, Physical and Engineering Sciences,* 372(2006).

Muggeridge, A. H., Jackson, M. D., Al-Mahrooqi, S., Al-Marjabi, M. and Grattoni, C. A. 'Quantifying bypassed oil in the vicinity of discontinuous shales'. *Paper SPE-77487-MS presented at the SPE Annual Technical Conference and Exhibition (2002)*: Society of Petroleum Engineers.

Nield, D. A. and Bejan, A. (2006) *Convection in porous media.* Springer.

Okandan, E. (1984) *Heavy crude oil recovery.* Springer.

Onwunalu, J. E. and Durlofsky, L. J. (2010) 'Application of a particle swarm optimization algorithm for determining optimum well location and type', *Computational Geosciences,* 14(1), pp. 183-198.

Panjalizadeh, H., Alizadeh, A., Ghazanfari, M. and Alizadeh, N. (2015) 'Optimization of the WAG injection process', *Petroleum Science Technology,* 33(3), pp. 294-301.

Peaceman, D. W. and Rachford, H. H. (1962) 'Numerical calculation of multidimensional miscible displacement', *SPE Journal,* 2(04), pp. 327-339. SPE-471-PA.

Perkins, T. K., Johnston, O. C. and Hoffman, R. N. (1965) 'Mechanics of viscous fingering in miscible systems', *SPE Journal,* 5(4), pp. 301-317. SPE-1229-PA.

Pritchard, D. W. L., Georgi, D. T., Hemingson, P. and Okazawa, T. 'Reservoir surveillance impacts management, of the Judy Creek hydrocarbon miscible flood'. *Paper SPE-20228-MS presented at the SPE/DOE Enhanced Oil Recovery Symposium (1990)*: Society of Petroleum Engineers.

Romero-Zerón, L. (2012) *Advances in enhanced oil recovery processes, introduction to enhanced oil*

recovery (EOR) processes and bioremediation of oil-contaminated sites. p. 318.

Saffman, P. G. and Taylor, G. (1958) 'The penetration of a fluid into a porous medium or Hele-Shaw cell containing a more viscous liquid', *Proceedings of the Royal Society of London A: Mathematical, Physical and Engineering Sciences,* 245(1242), pp. 312-329.

Sahimi, M. (2011) *Flow and transport in porous media and fractured rock: from classical methods to modern approaches.* John Wiley and Sons.

Sandrea, I. and Sandrea, R. (2007) 'Recovery factors leave vast target for EOR technologies', *Oil and Gas Journal,* 105(41), pp. 44-47.

References

Satter, A., Iqbal, G. M. and Buchwalter, J. L. (2008) *Practical enhanced reservoir engineering: assisted with simulation software.* Pennwell Books.

Sauer, T. (2016) *Numerical analysis.* 1st Edition edn.: Cram101 Textbook Reviews, p. 49.

Savic, D. (2002) 'Single-objective vs. multiobjective optimisation for integrated decision support', *Proceedings of the first biennial meeting of the international environmental modeling and software society,* 1, pp. 7–12.

Self, R. V., Atashnezhad, A. and Hareland, G. 'Use of a Swarm Algorithm to Reduce the Drilling Time through Measurable Improvement in Rate of Penetration'. *50th US Rock Mechanics/Geomechanics Symposium 2016*: American Rock Mechanics Association.

Shahverdi, H. (2012) *Characterization of three-phase flow and WAG injection in oil reservoirs.* Doctor of Philosophy Thesis Doctoral dissertation, Heriot-Watt University.

Shpak, R. (2013) *Modeling of miscible WAG injection using real geological field data.* Norwegian University of Science and Technology, Norway [Online] Available at: http://www.diva-portal.org/smash/get/diva2:644970/FULLTEXT01.pdf (Accessed.

Stalkup, F. I. (1983a) 'Miscible displacement', *Monograph Series, SPE of AIME,* 8, pp. 1-195.

Stalkup, F. I. (1983b) 'Status of miscible displacement', *Journal of Petroleum Technology*, pp. 815-826. SPE-9992-PA

Stone, H. L. (1970) 'Probability model for estimating three-phase relative permeability', *Journal of Petroleum Technology,* 22(2), pp. 214-218. SPE-2116-PA.

Stone, H. L. (1973) 'Estimation of three-phase relative permeability and residual oil data', *Journal of Canadian Petroleum Technology,* 12(4), pp. 53-61. SPE 73-04-06 PETSOC.

Tan, C. T. and Homsy, G. M. (1992) 'Viscous fingering with permeability heterogeneity', *Physics of Fluids A: Fluid Dynamics,* 4(6), pp. 1099-1101.

Tchelepi, H. A., Orr, F. M., Rakotomalala, N., Salin, D. and Wouméni, R. (1993) 'Dispersion, permeability heterogeneity, and viscous fingering: Acoustic experimental observations and particle-tracking simulations', *Physics of Fluids A: Fluid Dynamics*.

Thomas, S. 'Enhanced oil recovery-an overview', *Oil and Gas Science and Technology-Revue de l'IFP*: Oil and Gas Science and Technology, 9-19.

Todd, M. R. and Longstaff, W. J. (1972) 'The development, testing, and application of a numerical simulator for predicting miscible flood performance', *Journal of Petroleum Technology,* 24(7), pp. 874- 882. SPE-3484-PA

Vazquez, O., Young, C., Demyanov, V., Arnold, D., Fisher, A., MacMillan, A. and Christie, M. (2015) 'Produced-water-chemistry history matching in the Janice field', *SPE Reservoir Evaluation and Engineering,* 18(04), pp. 564-576. SPE-164903-PA.

Verma, M. K. (2015) 'Fundamentals of carbon dioxide-enhanced oil recovery (CO 2-EOR): a supporting document of the assessment methodology for hydrocarbon recovery using CO 2-EOR associated with carbon sequestration (No. 2015-1071)', *US Geological Survey*.

Waggoner, J. R., Castillo, J. L. and Lake, L. W. (1990) 'Simulation of EOR (enhanced oil recovery) processes in stochastically generated permeable media', *United States*.

References

Wilson, A. (2015) 'Magnus water alternating gas pattern optimization through data integration', *Journal of Petroleum Technology* 67(6), pp. 117-119. SPE-0615-0117-JPT.

Wu, X., Ogbe, D. O., Zhu, T. and Khataniar, S. (2004) 'Critical design factors and evaluation of recovery performance of miscible displacement and WAG process', *Petroleum Society of Canada*.

Zahoor, M. K., Derahman, M. N. and Yunan, M. H. (2011) 'WAG process design –an update review', *Brazilian Journal of Petroleum and Gas,* 5(2), pp. 109-121.

Zhang, P., Brodie, J. A., Daae, V., Erbas, D. and Duncan, E. 'BP North Sea Miscible Gas Injection Projects Review'. *Paper SPE-166597-MS presented at the SPE Offshore Europe Oil and Gas Conference and Exhibition (2013)*: Society of Petroleum Engineers.

Zuo, L., Chen, Y., Dengen, Z. and Kamath, J. (2014) 'Three-phase relative permeability modeling in the simulation of WAG injection', *SPE Reservoir Evaluation and Engineering,* 17(03), pp. 326-339. SPE-166138-PA.